SIMULATION OF THE SEISMIC PERFORMANCE OF NONSTRUCTURAL SYSTEMS

NEES Nonstructural

A NUMERICAL MODEL FOR CAPTURING THE IN-PLANE SEISMIC RESPONSE OF INTERIOR METAL STUD PARTITION WALLS

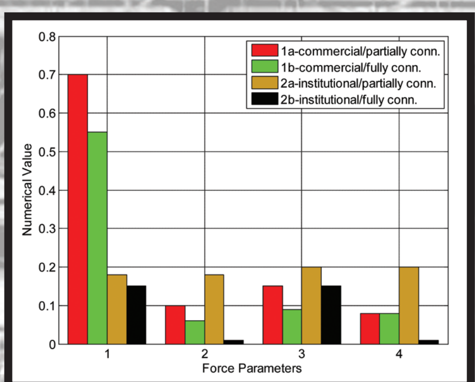

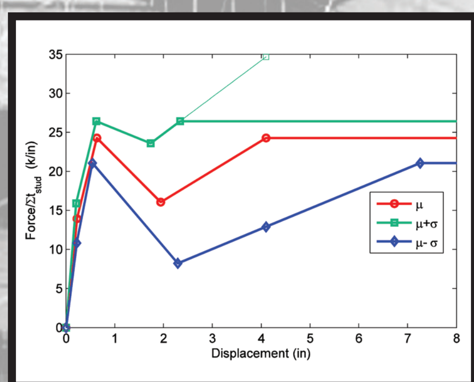

By

Richard L. Wood and Tara C. Hutchinson

Technical Report MCEER-12-0007 ▪ September 12, 2012

This research was conducted at the University of California, San Diego and was supported by the National Science Foundation under Grant No. CMMI-0721399.

Sponsored by the
National Science Foundation
NSF Grant Number CMMI-0721399

Project Title
Simulation of the Seismic Performance of
Nonstructural Systems

Project Team
University of Nevada Reno
University at Buffalo, State University of New York
Georgia Institute of Technology
Rutherford & Chekene
University of California, San Diego
Consortium of Universities for Research in Earthquake Engineering (CUREE)

Web Site
http://www.nees-nonstructural.org

DISCLAIMER

A Numerical Model for Capturing the In-Plane Seismic Response of Interior Metal Stud Partition Walls

by

Richard L. Wood[1] and Tara C. Hutchinson[2]

Publication Date: September 12, 2012
Submittal Date: November 8, 2011

Technical Report MCEER-12-0007

NSF Grant Number CMMI-0721399

1 Ph.D. candidate, Department of Structural Engineering, University of California, San Diego
2 Professor, Department of Structural Engineering, University of California, San Diego

MCEER
University at Buffalo, State University of New York
133A Ketter Hall, Buffalo, NY 14260
Phone: (716) 645-3391; Fax (716) 645-3399
E-mail: *mceer@buffalo.edu*; Website: *http://mceer.buffalo.edu*

Project Overview

NEES Nonstructural: Simulation of the Seismic Performance of Nonstructural Systems

Nonstructural systems represent 75% of the loss exposure of U.S. buildings to earthquakes, and account for over 78% of the total estimated national annualized earthquake loss. A very widely used nonstructural system, which represents a significant investment, is the ceiling-piping-partition system. Past earthquakes and numerical modeling considering potential earthquake scenarios show that the damage to this system and other nonstructural components causes the preponderance of U.S. earthquake losses. Nevertheless, due to the lack of system-level research studies, its seismic response is poorly understood. Consequently, its seismic performance contributes to increased failure probabilities and damage consequences, loss of function, and potential for injuries. All these factors contribute to decreased seismic resilience of both individual buildings and entire communities.

Ceiling-piping-partition systems consist of several components, such as connections of partitions to the structure, and subsystems, namely the ceiling, piping, and partition systems. These systems have complex three-dimensional geometries and complicated boundary conditions because of their multiple attachment points to the main structure, and are spread over large areas in all directions. Their seismic response, their interaction with the structural system they are suspended from or attached to, and their failure mechanisms are not well understood. Moreover, their damage levels and fragilities are poorly defined due to the lack of system-level experimental studies and modeling capability. Their seismic behavior cannot be dependably analyzed and predicted due to a lack of numerical simulation tools. In addition, modern protective technologies, which are readily used in structural systems, are typically not applied to these systems.

This project sought to integrate multidisciplinary system-level studies to develop, for the first time, a simulation capability and implementation process to enhance the seismic performance of the ceiling-piping-partition nonstructural system. A comprehensive experimental program using both the University of Nevada, Reno (UNR) and University at Buffalo (UB) NEES Equipment Sites was developed to carry out subsystem and system-level full-scale experiments. The E-Defense facility in Japan was used to carry out a payload project in coordination with Japanese researchers. Integrated with this experimental effort was a numerical simulation program that developed experimentally verified analytical models, established system and subsystem fragility functions, and created visualization tools to provide engineering educators and practitioners with sketch-based modeling capabilities. Public policy investigations were designed to support implementation of the research results.

The systems engineering research carried out in this project will help to move the field to a new level of experimentally validated computer simulation of nonstructural systems and establish a model methodology for future systems engineering studies. A system-level multi-site experimental research plan has resulted in a large-scale tunable test-bed with adjustable dynamic properties, which is useful for future experiments. Subsystem and system level experimental results have produced unique fragility data useful for practitioners.

In this study, a numerical model is developed to capture the in-plane seismic response of full-height gypsum board on cold-formed steel framed partition walls. OpenSees is used to develop a lumped model to capture

the behavior of the partition wall. The lumped model characteristics are determined by analyzing a large suite of experimental data on institutional and commercial type metal studs (see MCEER-11-0005). Two error metrics, based on calculation of the maximum force and half-cycle hysteretic energy, are introduced to assess the robustness of the model. The model's predictive capabilities are demonstrated via simulation of individual walls. The partition element is then integrated into numerical models of representative building types and the sensitivity of the building dynamic characteristics due to the presence of the partition wall are evaluated. The largest period shift was found in a model of a three story hospital, which considered the use of institutional partition walls.

Project Management Committee

Manos Maragakis, Principal Investigator, University of Nevada Reno, Department of Civil Engineering, Reno, NV 89557; *maragaki@unr.edu.*

André Filiatrault, Co-Principal Investigator, University at Buffalo, State University of New York, Department of Civil, Structural and Environmental Engineering, Buffalo, NY 14260; *af36@buffalo.edu.*

Steven French, Co-Principal Investigator, Georgia Institute of Technology, College of Architecture, P.O. Box 0695, Atlanta, GA 30332; *Steve.French@ arch.gatech.edu*.

William Holmes, Rutherford & Chekene, 55 Second Street, Suite 600, San Francisco, CA 94105; *wholmes@ruthchek.com.*

Tara Hutchinson, Co-Principal Investigator, University of California, San Diego, Department of Structural Engineering, 9500 Gilman Drive, #0085, La Jolla, CA 92093; *tara@ucsd.edu*.

Robert Reitherman, Co-Principal Investigator, CUREE, 1301 S. 46th Street, Bldg. 420, Richmond, CA 94804; *reitherman@curee.org*.

ABSTRACT

A commonly used nonstructural system representing significant investment in building construction is the ceiling-piping-partition (CPP) system. In this work, one of the subsystems within the CPP is given particular attention, namely the partition wall subsystem. Using data from experiments conducted at the State University of New York, University at Buffalo within the National Science Foundation and Network for Earthquake Engineering Simulation Grand Challenge Nonstructural project, a numerical model is developed for capturing the in-plane seismic response of full-height gypsum board on cold-formed steel-framed partition walls. It should be noted that the most common partition wall subsystem utilized in the United States for buildings other than houses is constructed of gypsum board on cold-formed steel framing and this is therefore the focus of this work.

The platform selected to model the partition walls is the Open System for Earthquake Engineering Simulation (OpenSees), developed by a community of researchers largely housed within the Pacific Earthquake Engineering Research Center (PEER). The behavior of the partition wall is captured using a lumped model localized within a zero-length element. The lumped material is developed with a pinching material used in a parallel configuration. It is characterized as a simple spring, which may easily be implemented in the longitudinal direction. A simplistic, lumped model is utilized to facilitate ease of implementation in beam-column type finite element analyses commonly adopted in design of building structures. The lumped model characteristics are determined by analyzing a large suite of experimental data on institutional and commercial type metal stud partition walls. Two error metrics based on calculation of the maximum force and half-cycle hysteretic energy are introduced to assess the model robustness. The model's predictive capabilities are demonstrated via simulation of individual walls. In particular, a normalized mean model is shown to capture the experimental hysteresis behavior of a fully connected partition wall with reasonable accuracy. The partition element is then integrated into numerical models of representative building types and the sensitivity of the building dynamic characteristics due to the presence of the partition wall evaluated. At most a period shift of 14% is noted for the shortest example building considered.

ACKNOWLEDGEMENTS

This project was supported by National Science Foundation Award #CMMI-0721399, “NEESR-Grand Challenge: Simulation of the Seismic Performance of Nonstructural Systems”, and IGERT Award #DGE-0966375, "Training, Research and Education in Engineering for Cultural Heritage Diagnostics." The input of the project management committee, namely Professors Manos Maragakis, André Filiatrault, and Steve French; Mr. Bill Holmes and Mr. Robert Reitherman are greatly appreciated.

Experimental data used in the model calibration was provided by SUNY-Buffalo. We particularly thank Professors André Filiatrault and Gilberto Mosqueda, Dr. Rodrigo Retamales, and Mr. Ryan Davies for providing this data and assisting with its interpretation.

Opinions, findings, and conclusions expressed in this report are those of the authors, and do not necessarily reflect those of the sponsoring organization. This report contributes to the doctoral dissertation of the first author at the University of California, San Diego, Department of Structural Engineering, where Professor Tara C. Hutchinson serves as the chair.

TABLE OF CONTENTS

Section	Title	Page
1	**INTRODUCTION**	**1**
1.1	Motivation	1
1.2	NEES Nonstructural Overview	3
1.3	Related Partition Wall Studies	4
1.3.1	Serrette et al. (1996, 1997)	5
1.3.2	NAHB Research Center, Inc. (1997)	5
1.3.3	Arnold et al. (2003, 2005)	6
1.3.4	Restrepo and Bersofsky (Restrepo et al., 2010; Bersofsky 2004)	7
1.3.5	Lang and Restrepo (2007)	8
1.3.6	Lee et al. (2007)	10
1.4	Related Modeling Studies	11
1.4.1	Ibarra et al. (2004)	11
1.4.2	Dinehart et al. (2000)	12
1.4.3	Van de Lindt and Walz (2003)	13
1.4.4	Fülöp and Dubina (2004a).	14
1.4.5	Folz and Filiatrault (2004a)	15
1.4.6	Judd and Fonseca (2005)	16
1.4.7	Kanvinde and Deierlein (2006).	16
1.4.8	Pang et al. (2007)	16
1.4.9	Baird et al. (2011)	17
1.4.10	Restrepo and Lang (2011)	17
1.4.11	Davies (2009)	18
1.5	Scope of this Work	19
1.6	Organization of the Report	20
2	**EXPERIMENTAL PROGRAM OVERVIEW**	**21**
2.1	Introduction	21
2.2	Observed Damage States	25
2.3	Example Specimen Response	28
2.4	Subgroup Classification Overview	30
2.5	Specimen Outliers in a Subgroup	32
2.5.1	Subgroup 1a.	32
2.5.2	Subgroup 1b	34
2.5.3	Subgroup 2a.	35
2.5.4	Subgroup 2b	35
3	**MODELING OVERVIEW**	**39**
3.1	Modeling Platform	39
3.2	Model Verification.	40
3.2.1	Partition Wall Backbone Characterization	40
3.2.2	Partition Wall Unloading and Reloading Behavior	42

TABLE OF CONTENTS (CONT'D)

Section	Title	Page
4	**REPRESENTATIVE SUBGROUP MODELS**	**45**
4.1	Subgroup Modeling Approach	45
4.1.1	Subgroup 1a Representative Model.	46
4.1.2	Subgroup 1b Representative Model	50
4.1.3	Subgroup 2a Representative Model	56
4.1.4	Subgroup 2b Representative Model.	61
4.2	Subgroup Model Discussion	68
5	**NORMALIZED MODELS**	**73**
5.1	Introduction	73
5.2	Force Normalization	73
5.3	Hysteretic Energy Normalization	76
5.4	Normalized Model Calibration	78
5.5	Normalized Model Verification	83
5.6	Normalized Model Discussion	87
5.7	Concluding Remarks	90
6	**ERROR METRICS ASSESSMENT**	**91**
6.1	Introduction	91
6.2	Average Error in Maximum Force	91
6.3	Total Half-Cycle Hysteretic Energy	94
6.4	Error Metrics and Modeling Assessment	97
6.5	Concluding Remarks	104
7	**PARTITION WALL IMPLEMENTATION**	**105**
7.1	Introduction	105
7.2	Partition Wall Implementation within a Building Model	105
7.3	Scaling Rules and Recommended Wall Lengths	107
7.3.1	Stiffness	108
7.3.2	Maximum Force (Yielding)	109
7.3.3	Post-Yield Degradation	110
7.3.4	Post-Yield Hardening and Capping Force.	110
7.3.5	Limitation in Wall Length	111
7.4	Example Building Suite Considered	111
7.5	Sample Building Sensitivity	112
7.6	Implementation, Conclusion and Further Studies	121
8	**CONCLUSIONS**	**123**
8.1	Motivation and Scope of Work	123
8.2	Model Summary	123
8.3	Model Use and Future Work	125

TABLE OF CONTENTS (CONT'D)

Section	Title	Page
9	**REFERENCES**	**127**
APPENDICES (Provided on attached CD)		
A	MODELING PERFORMANCE: SUBGROUP MODELS	A-1
B	MODELING PERFORMANCE: MEAN RESPONSE NORMALIZED MODELS	B-1
C	MODELING PERFORMANCE: MEAN PLUS ONE STANDARD DEVIATION RESPONSE NORMALIZED MODELS	C-1
D	MODELING PERFORMANCE: MEAN MINUS ONE STANDARD DEVIATION RESPONSE NORMALIZED MODELS	D-1
E	PARTITION WALL PROCEDURE FOR IMPLEMENTATION INTO OPENSEES	E-1

LIST OF FIGURES

Figure **Title** **Page**

1-1 Examples of nonstructural failures from the 2010 Baja California Earthquake (M_w=7.2). Partition wall and pipe failures at El Centro Regional Medical Center (upper) and ceiling fallout and HVAC system failure at Universidad Autónoma de Baja California in Mexicali, BC (lower) 2
1-2 Cost breakdown of typical office, hotel and hospital buildings (after Taghavi and Miranda, 2003) 3
1-3 NAHB shear wall configurations (right) and force-displacement results (left) (from NAHB 1997) 6
1-4 Damage state fragility functions for Bersofsky's experiment (from Bersofsky, 2004) 8
1-5 Plan view of test specimen for Lang's experiment (from Lang and Restrepo, 2007) 9
1-6 Testing protocols used in Lang's experiment (from Lang and Restrepo, 2007) 10
1-7 Hysteretic behavior of specimen 1 (left) and damage cost estimate vs story drift (from Lee et al., 2007) 11
1-8 Pinching hysteretic model shown for basic model rules (from Ibarra et al., 2005) 12
1-9 Model performance assessment for an example woodframe specimen considering a pinching model (from Ibarra et al., 2005) 12
1-10 Single hysteretic loop comparison for experimental result against theoretical result demonstrating the pinching effect (from Dinehart et al., 2000) 13
1-11 Hysteresis model considered with pinching behavior (from Van de Lindt and Walz, 2003) 14
1-12 Wall panel idealization through equivalent braced diagonal bars (from Fülöp and Dubina, 2004) 14
1-13 CASHEW model developed for woodframe shear walls (from Folz and Filiatrault, 2004a) 15
1-14 Shear wall backbone curve (courtesy Pang et al., 2007) 17
1-15 Proposed empirical backbone for gypsum board on light-gauge steel stud partition walls (from Restrepo and Lang, 2011) 18
1-16 Wayne-Stewart hysteretic model with strength degradation (from Carr, 2005) 19

2-1 In-plane partition wall setup: (a) parallel to shaking direction and (b) perpendicular to shaking direction, highlighting the shorter return walls (from Davies, 2009) 22
2-2 Typical cross section of partition wall (from Davies, 2009) 23
2-3 Typical in-plane partition wall setup (photo courtesy of Davies, 2009) 23
2-4 Dynamic nonstructural fragility testing protocol developed by Retamales et al. (2008) (from Davies, 2009) 24
2-5 Quasi-static drift sensitive protocol developed by Retamales et al. (from Davies, 2009) 25
2-6 Experimental force-displacement response for Specimen 20 28

LIST OF FIGURES (CONT'D)

Figure	Title	Page
2-7	Sheathing and framing connectivity details: (a-b) bottom and top track connections for partially connected specimens (slip track), (c-d) bottom and top track connections for fully connected specimens, (e) wall intersection details for commercial construction practices and (f) wall intersection details for institutional construction practices (from Davies, 2009)	31
2-8	Experimental load-displacement of specimen 10 (subgroup 1b). Note the anomalous dramatic reduction in load carrying capacity at 0.8% drift.	33
2-9	Photos of damage observed in specimen 10: (a) at 0.6% drift and (b) top track damage	33
2-10	Subgroup 1a experimental hysteretic behavior showing identified backbone and average subgroup backbone.	34
2-11	Subgroup 1b experimental hysteretic behavior showing identified backbone and average subgroup backbone.	36
2-12	Subgroup 2a experimental hysteretic behavior showing identified backbone and average subgroup backbone.	37
2-13	Subgroup 2b experimental hysteretic behavior showing identified backbone and average subgroup backbone.	38
3-1	Graphical description of the pinching4 material model (after Mazzoni et al., 2009).	40
3-2	Force-Displacement backbone for specimen 20 and the selected backbone points	41
3-3	Tangent stiffness demonstrating sudden changes in the force-displacement backbone curve for specimen 20	42
3-4	Experimental and numerical model comparison for specimen 20: (a) hysteretic behavior and (b) hysteretic area.	43
4- 1	Specimen 1 and 2 backbone curves, average backbone and selected backbone points for subgroup 1a.	46
4-2	Tangent stiffness demonstrating sudden changes in the force-displacement backbone curve for subgroup 1a.	47
4-3	Hysteretic area calculated from the average experimental subgroup average (target) compared to the model hysteretic area for subgroup 1a.	47
4-4	Hysteretic response of specimen 1 overlaid with the response of the representative subgroup model 1a.	48
4-5	Hysteretic response of specimen 2 overlaid with the response of the representative subgroup model 1a.	49
4-6	Comparison of the model hysteretic area to each of the specimens representing subgroup 1a	49
4-7	Percent error comparison showing the model hysteretic area to each of the specimens representing subgroup 1a	50
4-8	Specimen 4, 5, 6 and 8 backbone curves, average backbone and selected backbone points for subgroup 1b	51

LIST OF FIGURES (CONT'D)

Figure	Title	Page
4-9	Tangent stiffness demonstrating sudden changes in the force-displacement backbone curve for subgroup 1b	51
4-10	Hysteretic area calculated from the average experimental subgroup average (target) compared to the model hysteretic area for subgroup 1b.	52
4-11	Hysteretic response of specimen 4 overlaid with the response of the representative subgroup model 1b.	53
4-12	Hysteretic response of specimen 5 overlaid with the response of the representative subgroup model 1b.	53
4-13	Hysteretic response of specimen 6 overlaid with the response of the representative subgroup model 1b.	54
4-14	Hysteretic response of specimen 8 overlaid with the response of the representative subgroup model 1b.	54
4-15	Comparison of the model hysteretic area to each of the specimens representing subgroup 1b	55
4-16	Percent error comparison showing the model hysteretic area to each of the specimens representing subgroup 1b	55
4-17	Specimen 20-22 backbone curves, average backbone and selected backbone points for subgroup 2a.	56
4-18	Tangent stiffness demonstrating sudden changes in the force-displacement backbone curve for subgroup 2a.	57
4-19	Hysteretic area calculated from the average experimental subgroup average (target) compared to the model hysteretic area for subgroup 2a.	57
4-20	Hysteretic response of specimen 20 overlaid with the response of the representative subgroup model 2a.	58
4-21	Hysteretic response of specimen 21 overlaid with the response of the representative subgroup model 2a.	59
4-22	Hysteretic response of specimen 22 overlaid with the response of the representative subgroup model 2a	59
4-23	Comparison of the model hysteretic area to each of the specimens representing subgroup 2a	60
4-24	Percent error comparison showing the model hysteretic area to each of the specimens representing subgroup 2a	60
4-25	Specimen 23-28 backbone curves, average backbone and selected backbone points for subgroup 2b.	62
4-26	Tangent stiffness demonstrating sudden changes in the force-displacement backbone curve for subgroup 2b..	62
4-27	Hysteretic area calculated from the average experimental subgroup average (target) compared to the model hysteretic area for subgroup 2b.	63
4-28	Hysteretic response of specimen 23 overlaid with the response of the representative subgroup model 2b.	63
4-29	Hysteretic response of specimen 24 overlaid with the response of the representative subgroup model 2b.	64

LIST OF FIGURES (CONT'D)

Figure **Title** **Page**

4-30 Hysteretic response of specimen 25 overlaid with the response of the representative subgroup model 2b. 64
4-31 Hysteretic response of specimen 26 overlaid with the response of the representative subgroup model 2b. 65
4-32 Hysteretic response of specimen 27 overlaid with the response of the representative subgroup model 2b. 65
4-33 Hysteretic response of specimen 28 overlaid with the response of the representative subgroup model 2b. 66
4-34 Comparison of the model hysteretic area to each of the specimens representing subgroup 2b 66
4-35 Percent error comparison showing the model hysteretic area to each of the specimens representing subgroup 2b 67
4-36 Percent error comparison showing the model hysteretic area to each of the specimens representing subgroup 2b (clipped y-axis). 67
4-37 Overlay of each subgroup backbones shown demonstrating a large variability. 70
4-38 Unloading and reloading parameters (highlighted in red) within one element of the four parallel material model formulation. 70
4-39 Displacement parameters for each of the parallel materials for each subgroup 71
4-40 Force parameters for each parallel materials used for each subgroup 71

5-1 Partition wall backbones (force-displacement relations) for subgroups 1b and 2b. 74
5-2 Normalized partition wall backbones (force-displacement relations) for subgroups 1b and 2b. 75
5-3 Absolute valued normalized partition wall backbones considering positive and negative behavior 75
5-4 Absolute valued normalized backbones showing the mean, mean plus one standard deviation and mean minus one standard deviation. 76
5-5 Hysteretic energy for subgroups 1b and 2b for each of the specimens considered along with their respective subgroup averages. 77
5-6 Normalized hysteretic energy for subgroups 1b and 2b. 77
5-7 Selection of the mean response behavior of the partition wall model. Top shows normalized absolute valued hysteretic backbone while the bottom demonstrates the tangent stiffness of this backbone. 79
5-8 Selection of the mean plus one standard deviation response behavior of the partition wall model. Top shows normalized absolute valued hysteretic backbone while the bottom demonstrates the tangent stiffness of this backbone. 80
5-9 Selection of the mean minus one standard deviation response behavior of the partition wall model. Top shows normalized absolute valued hysteretic backbone while the bottom demonstrates the tangent stiffness of this backbone. 81
5-10 Hysteretic area of the mean model versus the target mean hysteretic area 82
5-11 Hysteretic area of the mean plus one standard deviation model versus the target mean plus one standard deviation hysteretic area 82

LIST OF FIGURES (CONT'D)

Figure **Title** **Page**

5-12 Hysteretic area of the mean minus one standard deviation model versus the target mean minus one standard deviation hysteretic area 83
5-13 Hysteretic behavior of the mean response shown with specimen 4 as an example 84
5-14 Hysteretic area of the mean model with specimen 4 as an example 84
5-15 Hysteretic behavior of the mean plus one standard deviation response shown with specimen 4 as an example 85
5-16 Hysteretic area of the mean plus one standard deviation model with specimen 4 as an example. 85
5-17 Hysteretic behavior of the mean minus one standard deviation response shown with specimen 4 as an example 86
5-18 Hysteretic area of the mean minus one standard deviation model with specimen 4 as an example 86
5-19 Overlay of each subgroup backbones shown demonstrating a large variability 87
5-20 Force parameters for each parallel material used for each subgroup. Note the fourth parameter of the mean minus one standard deviation model is zero.. 89
5-21 Displacement parameters for each parallel material used for each subgroup. 89

6-1 Hysteretic overlap comparison between specimen 23 and the 2b subgroup model ... 92
6-2 Captured maximum force envelope curve for specimen 23 and the 2b subgroup model 93
6-3 Difference in maximum attained force level when comparing specimen 23 and the 2b subgroup model. 93
6-4 Hysteretic energy (area) comparison between specimen 23 and the 2b subgroup model 95
6-5 Hysteretic energy (area) per half cycle comparison between specimen 23 and the 2b subgroup model shown against maximum achieved drift level. 95
6-6 Difference in hysteretic energy (area) per half cycle comparison for specimen 23 97
6-7 Overall average of the average force residual comparing the experimental to the developed models (subgroup, mean, mean plus one standard deviation and mean minus one standard deviation). 98
6-8 Average force residual comparing the experimental to the developed models by damage states: (a) no damage, (b) DS_1, (c) DS_2 and (d) DS_3. 99
6-9 Average force residual comparing the experimental to the developed models by damage states: (a) no damage, (b) DS_1, (c) DS_2 and (d) DS_3. Note just the subgroup model and mean model is presented. 100
6-10 Overall residual in half-cycle hysteretic energy comparing the experimental to the developed models (subgroup, mean, mean plus one standard deviation and mean minus one standard deviation) 101
6-11 Overall residual in half-cycle hysteretic energy comparing the experimental to the developed models by damage states: (a) $DS<DS_1$, (b) $DS_1 \leq DS<DS_2$, (c) $DS_2 \leq DS<DS_3$ and (d) $DS \geq DS_3$. 102

LIST OF FIGURES (CONT'D)

Figure	Title	Page
6-12	Overall residual in half-cycle hysteretic energy comparing the experimental to the developed models by damage states: (a) $DS<DS_1$, (b) $DS_1 \leq DS<DS_2$, (c) $DS_2 \leq DS<DS_3$ and (d) $DS \geq DS_3$. Note just the subgroup model and mean model is presented.	103
7-1	Partition wall implementation between two adjacent story levels.	106
7-2	Backbone of the normalized partition wall model as implemented in OpenSees.	106
7-3	Backbone of the Subgroup type partition wall model as implemented in OpenSees.	107
7-4	Example of partition wall scaling when the target wall is twice the length of the original wall with twice the number of vertical studs in the lateral direction. The four marked points highlight the points considered for scaling walls of different lengths.	108
7-5	Normalized plots demonstrating period and mass participations sensitivities for RC-2.	117
7-6	Normalized plots demonstrating period and mass participations sensitivities for RC-4	117
7-7	Normalized plots demonstrating period and mass participations sensitivities for RC-8	118
7-8	Normalized plots demonstrating period and mass participations sensitivities for RC-12	118
7-9	Normalized plots demonstrating period and mass participations sensitivities for RC-20.	119
7-10	Normalized plots demonstrating period and mass participations sensitivities for S-3	119
7-11	Normalized plots demonstrating period and mass participations sensitivities for S-3H.	120
7-12	Normalized plots demonstrating period and mass participations sensitivities for S-9.	120
7-13	Normalized plots demonstrating period and mass participations sensitivities for S-20	121
8-1	Example usage of light-gauge steel studding and gypsum board system during construction.	124

LIST OF TABLES

Table	Title	Page
1-1	Experimental configurations for Bersofsky's experiment (after Bersofsky et al., 2004)	7
2-1	Partition wall test configuration details (from Davies, 2009).	23
2-2	Damage state classification adopted for partition walls (photos courtesy of UB Experimental Team	26
2-3	Partition wall test specimens as considered for modeling and damage state summary herein.	27
2-4	Damage and corresponding hysteretic response report for Specimen 20	29
2-5	Partition wall classification by subgroup. Only subgroups with full height specimens are considered	30
4-1	Parameters for the subgroup models.	69
5-1	Parameters for the normalized partition wall model.	88
7-1	Partition wall indices for each building and corresponding wall lengths	109
7-2	Suite of buildings considered. (RC = reinforced concrete. NS=north-south direction, EW=east-west direction)	112
7-3	Modal periods and mass participation sensitivity for RC-2	113
7-4	Modal periods and mass participation sensitivity for RC-4	114
7-5	Modal periods and mass participation sensitivity for RC-8	114
7-6	Modal periods and mass participation sensitivity for RC-12	114
7-7	Modal periods and mass participation sensitivity for RC-20	115
7-8	Modal periods and mass participation sensitivity for S-3	115
7-9	Modal periods and mass participation sensitivity for S-3H	115
7-10	Modal periods and mass participation sensitivity for S-9	116
7-11	Modal periods and mass participation sensitivity for S-20	116

NOMENCLATURE

Symbol	Description	Units
DS_1	Damage state one; etc.	unitless
E_H	Hysteretic energy (area)	$F \cdot L$
$\sum E_{H_{DIFF}}$	Total half cycle hysteretic energy	$F \cdot L$
$\overline{F_{RES}}$	Average residual force	F
S_{D1}	Design spectral acceleration at period of 1.0 sec	L/T^2
S_{DS}	Design spectral acceleration at short periods	L/T^2
Σt_{stud}	Total thickness of wall studs in lateral direction	L
μ	Mean	unitless
σ	Standard deviation	unitless

SECTION 1
INTRODUCTION

1.1 Motivation

In recent earthquakes in the United States and some other developed countries, the damage to nonstructural components and systems (NCSs) has exceeded the cost of structural damage in buildings. Nonstructural systems and components are elements within a building either attached to the floors or walls that are not designed nor anticipated to contribute to the primary load bearing system of the building. Nonetheless, they will be subjected to the dynamic environment of the building undergoing seismic loading. Three broad categories of nonstructural components and systems are: 1) architectural elements, such as partition walls, suspended ceilings and lighting systems; 2) mechanical and electrical equipment, such as piping systems, fire protection systems, storage tanks, computer and data equipment, and power transformers; and 3) building contents, such as bookshelves, file cabinets and other furniture (BSSC 2000; Villaverde 2009). NCSs support the buildings functionality and as such their damage or loss of functionality can be more economically significant than that associated with structural damage. Furthermore, secondary damage associated with failure of NCSs has proven highly disruptive to businesses and their functionality. Some examples of failures in the past include water damage caused by failure of sprinkler systems for fire protection, lack of emergency power, failure of suspended ceilings and partition walls (see Figure 1-1). While many of these failures usually only affect the building performance after a seismic event, they are capable of causing serious injuries or death (Filiatrault et al., 2002; EERI, 2010a; EERI, 2010b).

NCSs within buildings often have complicated configurations and connections to a building making them susceptible to earthquake damage. The majority of NCSs are placed or distributed throughout a building, and therefore not subjected to the ground motion generated by the earthquake, but rather to an amplified and filtered motion transmitted by the building. The response of the NCS depends on its location within the structure, since the demands vary by floor level and location in plan. When compared to the structure itself, their mass, stiffness and damping characteristics are usually small. However, when the frequency of the NCSs and the building are similar, the NCSs are capable of experiencing severe resonance. The NCSs may be connected to multiple attachment locations within the building, inducing differential movements on the component. A good example of this situation is distributed piping systems or partition walls. When the NCS is stiff and heavy enough, it may modify the response of the building structure. As a result, the NCS and the building structure should be considered as a combined system to effectively predict response (Villaverde, 2009).

Figure 1-1 Examples of nonstructural failures from the 2010 Baja California Earthquake (M_w=7.2). Partition wall and pipe failures at El Centro Regional Medical Center (upper) and ceiling fallout and HVAC system failure at Universidad Autónoma de Baja California in Mexicali, BC (lower).

Given their many complexities, it is also unfortunate that the largest investment in the construction of buildings is associated with nonstructural components and systems. Studies of the cost breakdown of typical buildings have shown that NCSs are the largest investment for offices, hotels and hospitals, shown in Figure 1-2 (Taghavi and Miranda, 2003). The percent cost for nonstructural components vary from 48% in hospitals to 70% in hotels. While the building contents range from 17% to 44% of the total building cost, they are greatly influenced by the performance of the nonstructural systems. Examples of nonstructural components and systems include bookshelves, electronic equipment attached to partition walls and the piping systems capable of causing water damage to entire floors.

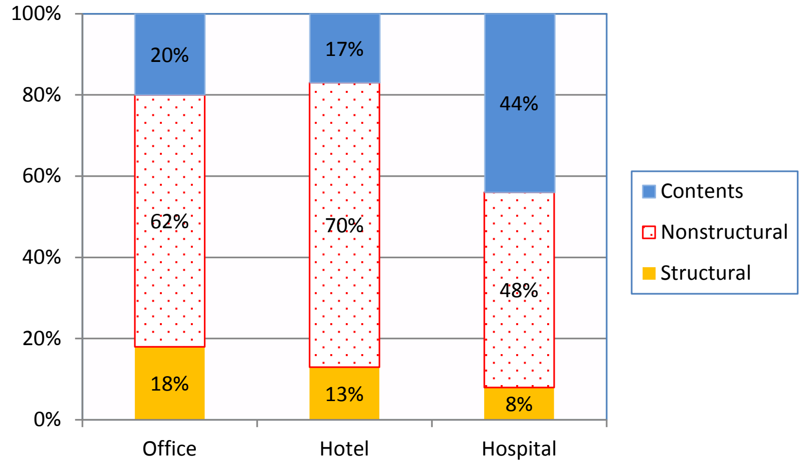

Figure 1-2 Cost breakdown of typical office, hotel and hospital buildings (after Taghavi and Miranda, 2003).

1.2 NEES Nonstructural Overview

The aforementioned discussion highlights the diverse nature of NCSs and as a result the complications with their response under seismic loading. Herein, this report presents a portion of a larger study whereby one widely used nonstructural system representing significant investment, the ceiling-piping-partition (CPP) system, is studied. This complicated system consists of several subsystems having complex geometries and boundary conditions, which interact with each other. In addition, multiple support attachments throughout the building impose acceleration and deformation demands on the various subsystems, which are dependent on their placement location. Due to a lack of system-level research on the CPP system, an NSF-NEES[1] Grand Challenge project was initiated by researchers across the United States. A key goal of the project is to understand the seismic performance of the CPP system as it contributes to economic loss, loss of functionality, and injury potential within a building. The NEES-Nonstructural[2] project

---

[1] NSF is the National Science Foundation, NEES is the Network for Earthquake Engineering Simulation
[2] In future reference, the NSF-NEES grand challenge project is referred to as the "NEES-Nonstructural" project

integrates a multi-disciplinary team of researchers to examine the system level performance of the CPP utilizing and developing experimental and simulation tools. A comprehensive experimental program is conducted at the University at Buffalo (UB) and the University of Nevada, Reno (UNR) and to perform subsystem and system-level full-scale experimental studies, respectively. Using data from the experimental studies conducted at UNR and UB, a detailed numerical simulation program is undertaken at the University of California, San Diego (UCSD), Cornell and North Carolina State University (NCSU). The goal of the numerical simulation program is to generate experimentally verified analytical models, establish system and subsystem level fragility functions and develop visualization tools for engineering educators, researchers and practitioners.

In this report, the focus is on the development and calibration of a numerical model, for use in capturing the in-plane seismic response of partition walls. It is envisioned to be easily integrated with the other components of the CPP, and into building models to support coupled numerical analysis. As part of the overall NEES-GC project, a 50-specimen test program was conducted at UB (Davies, 2009). The wall specimens were placed in the upper level of the Nonstructural Component Simulator (UB-NCS), which is a full-scale two-story frame mechanism capable of producing realistic floor motions in terms of acceleration, velocity, and displacement (Mosqueda et al, 2009). Using these experimental results, an experimentally verified partition wall modeling scheme is outlined. It should be noted that the most common institutional and commercial partition wall subsystem utilized in the United States is constructed of metal studs sheathed with gypsum board, therefore this is the type studied herein.

1.3 Related Partition Wall Studies

The following discusses past efforts relevant to studying the experimental performance of gypsum partition walls. This literature review covers the basics of previously tested gypsum partition walls on both light-gauge steel and wood studs. Particular focus is directed towards the behavior of the gypsum partition walls and key findings from each study. The review is not exhaustive and interested readers are encouraged to review the citations within the mentioned literature.

1.3.1 Serrette et al. (1996, 1997)

Serrette et al. tested thirteen full-size walls of 8.0 feet square constructed of light-gauge cold-formed steel stud walls, with the objective of studying the contribution of flat strap tension x-bracing, gypsum sheathing, and gypsum wall board to the in-plane shear resistance. For the frame setup, 20 gauge studs (30 mil) were placed at 24 inches center-to-center (c/c) with drywall screws at 6 inches (c/c) in the perimeter and 12 inches (c/c) in the field. The specimens were then loaded in plane incrementally to 25%, 50% and 75% of the estimated maximum load and then to failure. The general failure mechanism was breakage of the paper cover of the gypsum sheathing and the underlying gypsum. Prior to failure, the drywall screws rotated and pulled through the surface of the gypsum. Notable observations included: each of the gypsum panels behaved independently of each other, the shear strength of the wall decreased when the edges of the panel broke at the screw locations, and the screw edge distance did not have a significant effect on shear strength. The main strength of the wall was suggested to be governed by the penetration of the screw head.

In the follow up study in 1997, Serrette et al. tested twenty small-scale tests of 24 inches square walls to assess the shear behavior of screw connections along the edge of the panels for plywood, oriented strand board, gypsum wallboard and FiberBond wallboard. These smaller panels were loaded in tension until failure occurred. The normalized shear strength of these walls was comparable to the full-scale specimens, demonstrating that small scale tests provide a simple method for estimating the shear resistance.

1.3.2 NAHB Research Center, Inc. (1997)

A research program developed at the National Association of Home Builders (NAHB) Research Center was set up to assess the shear behavior of 40 foot long, cold-formed steel walls with openings. Four 8.0 feet by 40 feet shear wall specimens with 33-mil studs at 24 inches on center were tested. Oriented strand board (OSB) (7/16" thick) was placed on the exterior and 1/2 inch gypsum was oriented vertically in the interior with No. 6 screws at 7 inches (c/c) along the perimeter with 10 inches (c/c) in the field. The test frame for their study is shown in Figure 1-3. Variations explored in the study, included: openings due to doors and windows, percent sheathing, anchor bolt spacing and hold downs. The specimens were loaded monotonically until failure. The observations from the test sequence included: initial loading was linear until screw pull- through occurred, which reduced the stiffness, and near the ultimate capacity the OSB experienced cracking in the perimeter screw connections and usually tore the top track. Additionally weak axis bending of the studs approximately 12 inches from the top of the specimen was observed, and was followed by OSB tear-out around the screw connections at the top of the wall.

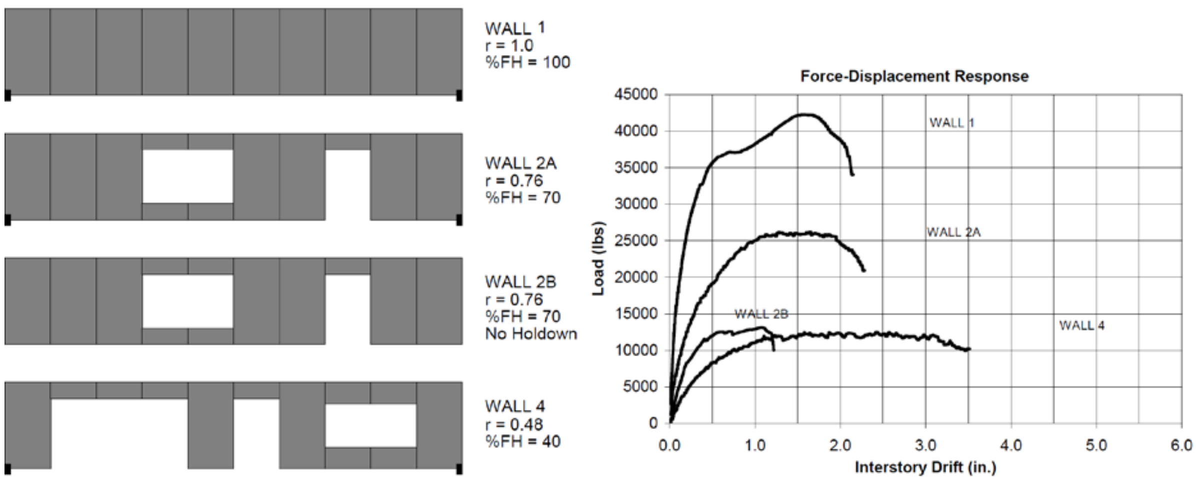

Figure 1-3 NAHB shear wall configurations (right) and force-displacement results (left) (from NAHB, 1997).

1.3.3 Arnold et al. (2003, 2005)

Arnold et al. tested 12 walls for the California Earthquake Authority (CEA)/Consortium of Universities for Research in Earthquake Engineering (CUREE) Woodframe Wall Testing Project. The first four walls were for phase I which correspond to walls within the first level of a two-story structure with the last eight walls (phase II) representative of a single-story structure. The wall specimens were approximately 8.0 feet by 16.0 feet long with either two window openings or one window and one door opening using 1/2 inch gypsum sheathing wood studs. The loading protocol was the CUREE Abbreviated Loading History for Ordinary Ground Motions developed by Krawinkler et al. (2000) for the testing of woodframe structures. This protocol was applied to the testing frame in one stage (no repair to the damaged wall specimens) and in a staged approach to allow for the repair of the structure between the testing sequence. A key observation from the experimental program included the observation that the wall strength of the single story structures (phase II) was approximately 25% less than the two-story structure idealization tested in phase I, indicating that the boundary conditions were significant. The gypsum experienced little damage at 0.20% drift with small hairline cracks and a few screw popping out. At a drift level of 0.40%, the gypsum started to deteriorate which was shown by the tearing of the joint tape, corner bead damage and fastener popping. With drift levels up to 0.70%, the gypsum sustained significant damage with wider cracks, more significant deterioration and screw popping.

1.3.4 Restrepo and Bersofsky (Restrepo et al., 2010; Bersofsky 2004)

In this experimental program, 16 walls were built to determine the seismic fragility of gypsum wallboard partitions on cold-formed steel studs. The specimens were 8.0 feet by 16.0 feet long and considered different connector spacing, gypsum heights (full height vs. partial height), track connections, gypsum thickness, stud mil and stud spacing (see Table 1-1). These wall specimens were set up to simulate the interstory drift experienced during a seismic event for a typical office building. The loading protocol selected for the study was based on the CUREE Abbreviated Loading History for Ordinary Ground Motions protocol for the testing of wood frame structures (Krawinkler et al, 2000).

Table 1-1 Experimental configurations for Bersofsky's experiment (after Bersofsky et al., 2004).

Test No.	Door	Connector Spacing (in)	Gypsum Height (ft)	Slip Track	Gypsum Thickness (in)	Stud Thickness (mil)	Stud Spacing (in)
1	Y	8.0	8.0	N	5/8	18	24
2	Y	8.0	8.0	N	5/8	18	24
3	**N**	8.0	8.0	N	5/8	18	24
4	Y	**12.0**	8.0	N	5/8	18	24
5	Y	8.0	**6.5**	N	5/8	18	24
6	Y	8.0	8.0	**Y**	5/8	18	24
7	Y	8.0	8.0	N	**1/2**	18	24
8	Y	8.0	8.0	N	5/8	**30**	**16**

To develop the fragility curves, three damage states were defined. Damage state 1 was minimal damage repairable by gypsum board joint compound ("mud"), tape and paint. Damage state 2 was characterized by superficial damage requiring replacement of gypsum sections and damage state 3 required full replacement of the wall. The observed drift levels associated with these damage states are shown in Figure 1-4. It is noted that, damage state 2 was not always obtained, as some specimens progressed directly from DS_1 to DS_3.

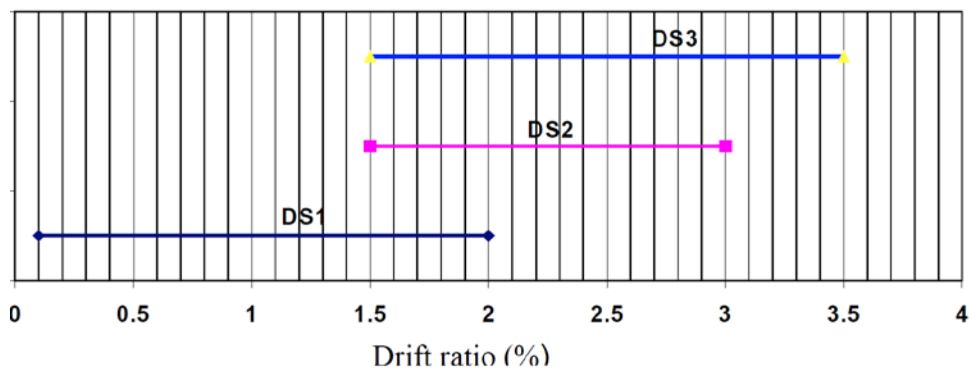

Figure 1-4 Damage state fragility functions for Bersofsky's experiment (from Bersofsky, 2004).

1.3.5 Lang and Restrepo (2007)

Continuing the work of Bersofsky et al. (2004), Lang and Restrepo (2007) constructed two identical specimens with light-gauge cold-formed steel stud gypsum wallboard to represent a typical office room. Both rooms had dimensions of 12 feet by 15 feet with additional features of a utility cutout, two t-wall (cantilever) configurations and a column wrap (Figure 1-5). The specimens were constructed using 20 gauge (30 mil) studs 3-5/8 inch at 24 inches on center. The gypsum thickness was 5/8 inch. Specimen 1 used the recommended loading protocol from ATC-58 and specimen two used a modified version, which reduced the low amplitude cycles while increasing the amplitude rate (Figure 1-6).

This study revealed that the seismic performance of light gauge metal stud construction was sensitive to loading protocol. The failure mechanism of the specimens was characterized by track slip. Once the track slip occurred, the partition walls were no longer subjected to the imposed drift demands and consequently the damage was greatly reduced. The failure of the top track is not a defined damage state noted by Bersofsky. The main issue of the track slip is that this damage is likely to go unnoticed, since minimal visible wall damage occurred.

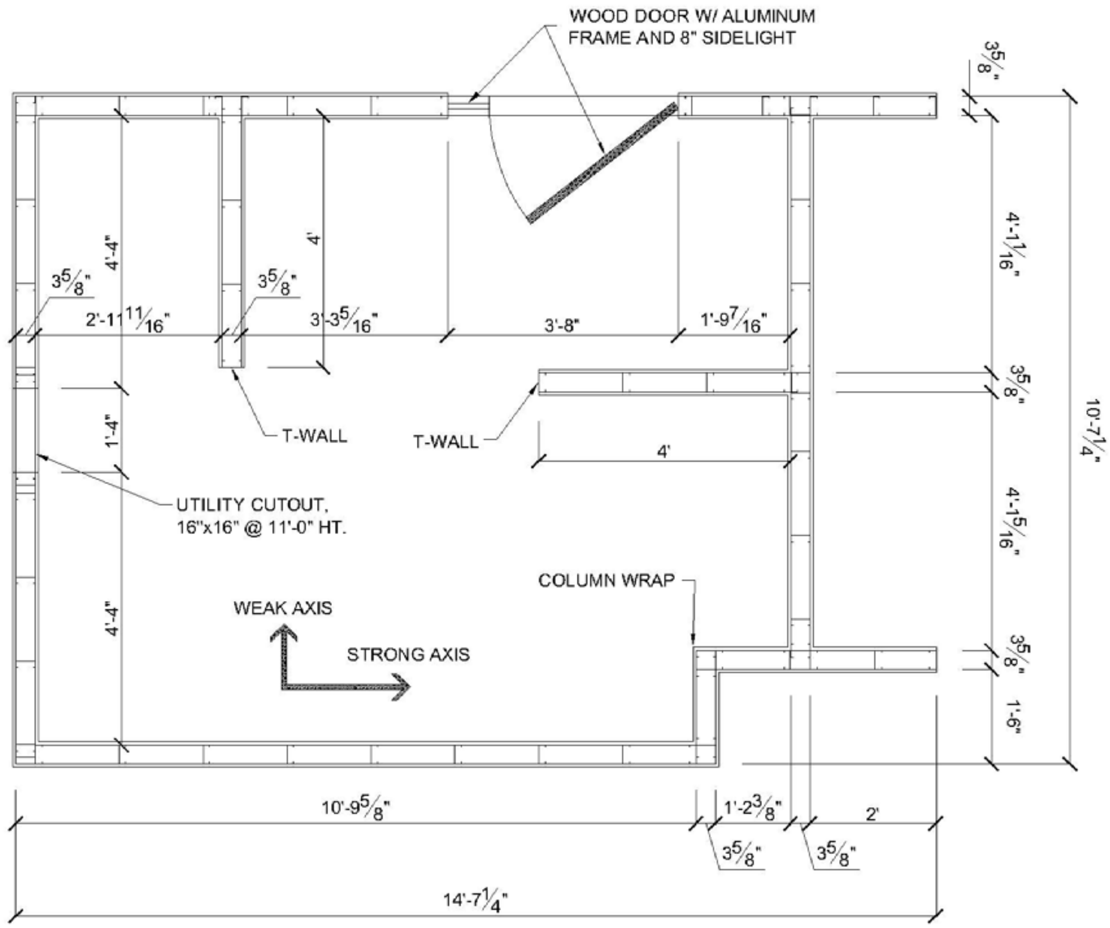

Figure 1-5 Plan view of test specimen for Lang's experiment (from Lang and Restrepo, 2007).

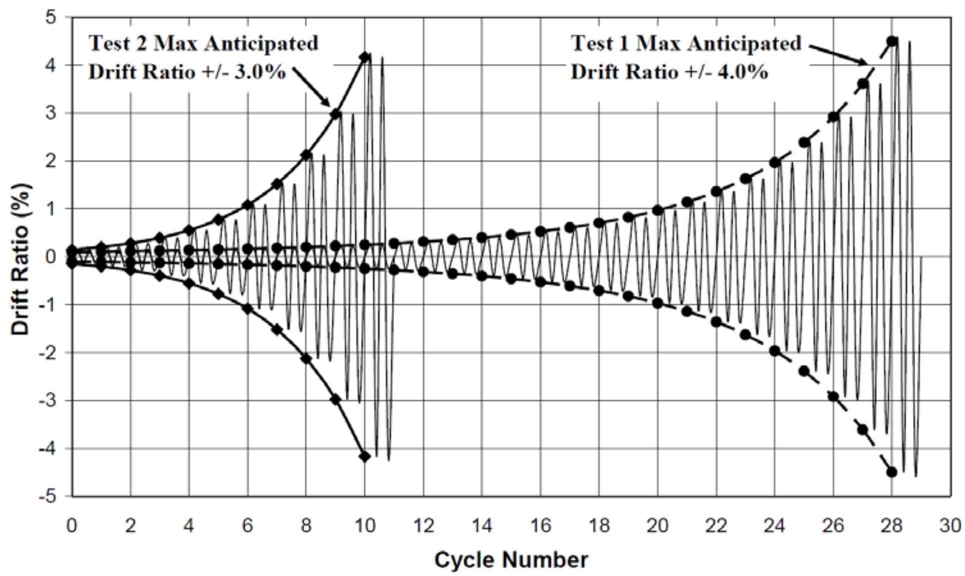

Figure 1-6 Testing protocols used in Lang's experiment (from Lang and Restrepo, 2007).

1.3.6 Lee et al. (2007)

Lee et al. (2007) tested four light gauge cold-formed steel framed walls with gypsum board to assess the performance and the repair costs associated with seismic demand of typical Japanese buildings. Three similar specimens (approximately 9 feet by 13 feet long) were constructed with typical installation techniques to assess the sensitivity of quasi-static verses dynamic loading protocols and the effect of a window cutout. A common installation technique different from US practice is a vertical gap of 0.39 – 0.59 inches (10-15 mm) at the partition and return wall connection. This gap is provided to reduce the damage of the partition, since the partition is unrestrained by a return wall or column for small deformations. The fourth specimen was approximately 9 feet by 9.75 feet with return walls longer than 5.0 feet. The walls saw no damage initially due to the gap at the partition ends, however when the partition wall bore on the boundary element (return walls), the partition wall sustained damage along the perimeter. When the two load protocols were compared, the dynamic loading effect was negligible. When the wall drift was less than 1%, the damage was found to be minimal, however with drift values larger than 2% the cost of damage was equal to the initial cost (Figure 1-7). The resistance of these tested walls was approximately 20% of the structural resistance of a steel moment frame, a value which is significant for design and analysis.

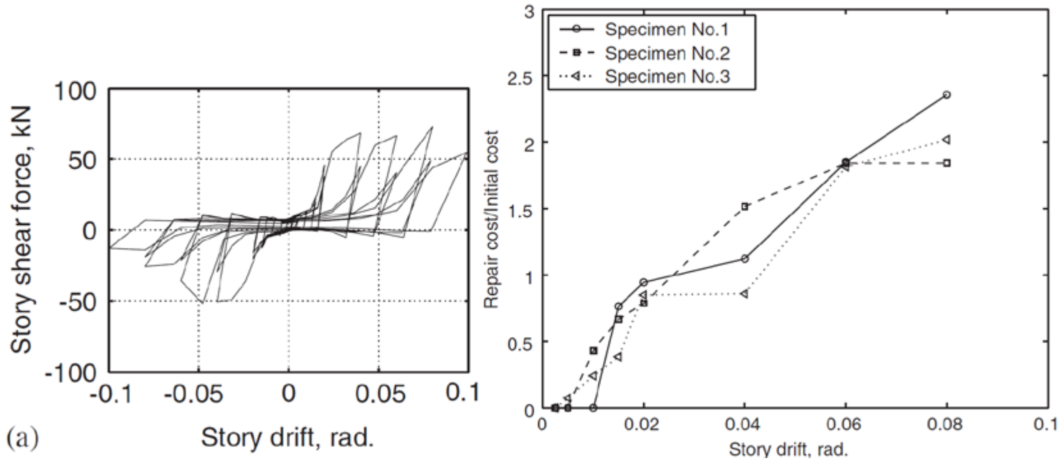

Figure 1-7 Hysteretic behavior of specimen 1 (left) and damage cost estimate versus story drift (right) (from Lee et al., 2007).

1.4 Related Modeling Studies

The following discusses the discrete hysteretic behavior modeling of wall elements. The focus is directed towards idealizing the hysteretic behavior with rules to define loading and unloading characteristics in a straight forward strategy to facilitate models readily implementable in design-oriented analyses. In what follows, a number of related efforts adopting such a strategy are discussed. In this modeling introduction, walls built with both wood and steel studs are explored to gather a broad scope of techniques. The review is not exhaustive and interested readers are encouraged to review the citations within the mentioned literature.

1.4.1 Ibarra et al. (2004)

Ibarra et al. postulate that lumped hysteretic models are capable of simulating the main characteristics of an experimental specimen. For example, an ideal model selected for capturing the hysteretic behavior of a plywood shear wall is a pinching model (Figure 1-8). The authors describe the pinching model in two main parts. The reloading branch is directed towards a “break point”, which is defined as a function of the maximum permanent deformation and maximum load experienced in the direction of loading. The critical break point, where the reloading stiffness increases, occurs when the reloading stiffness is directed towards the prior maximum deformation experienced earlier for that direction of loading. The pinching model matches the global hysteretic behavior and hysteretic energy for an example woodframe shear wall specimen (Figure 1-9). The pinching effect is noted in these example specimens.

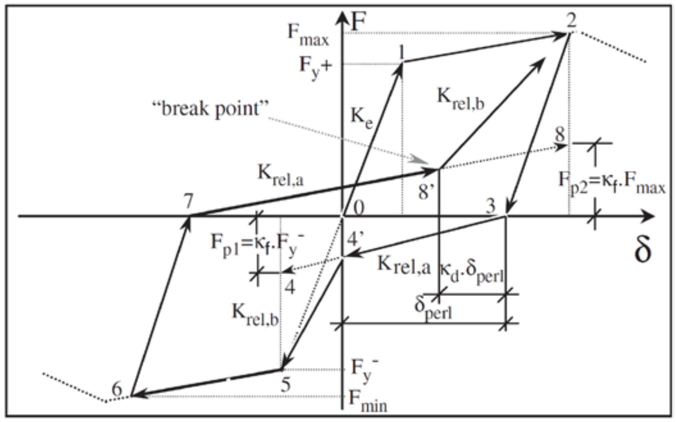

Figure 1-8 Pinching hysteretic model shown for basic model rules (from Ibarra et al., 2005).

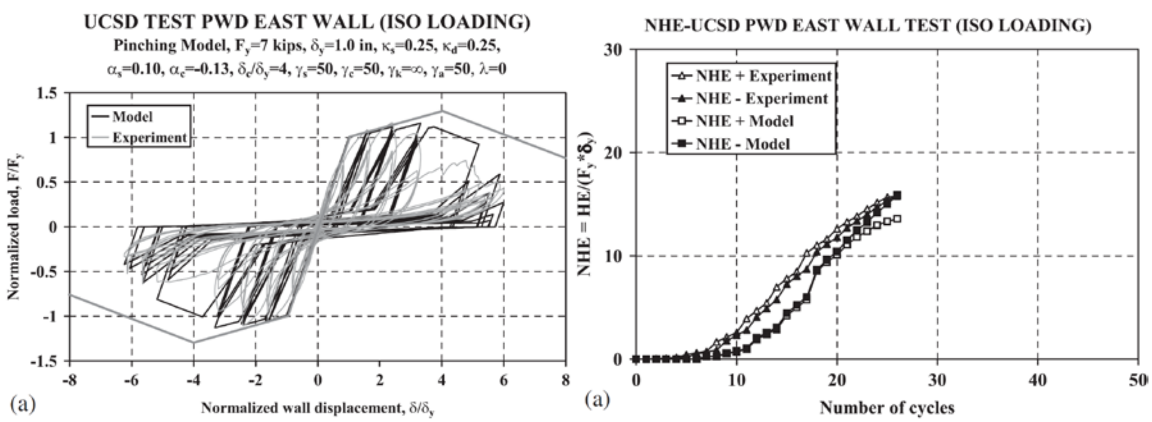

Figure 1-9 Model performance assessment for an example woodframe specimen considering a pinching model (from Ibarra et al., 2005).

1.4.2 Dinehart et al. (2000)

Dinehart et al. derived equations of motion governing the behavior of woodframe shear walls. In their approach, a discrete three degree-of-freedom model is developed capable of capturing the dominant features of the wall response including the racking, rotation, and translation. The model reasonably predicts the low to moderate displacement results, while at larger deformation fails to predict the pinched hysteretic behavior (Figure 1-10). In addition, the governing equations are cumbersome due to the nature of solving differential equations.

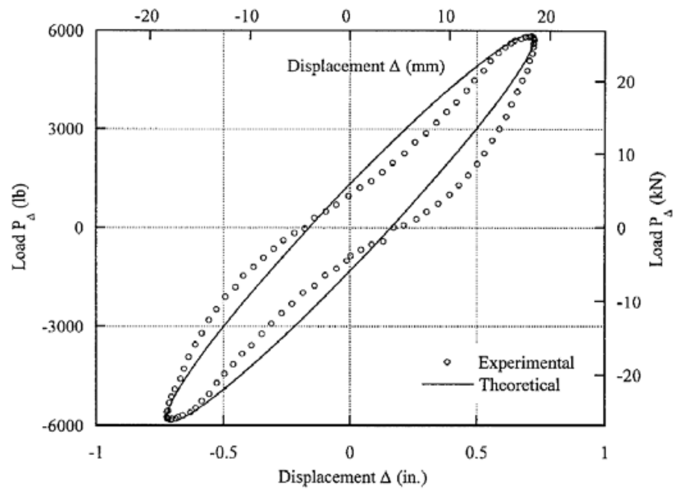

Figure 1-10 Single hysteretic loop comparison for experimental result against theoretical result demonstrating the pinching effect (from Dinehart et al., 2000).

1.4.3 Van de Lindt and Walz (2003)

Van de Lindt and Walz developed a hysteretic model for the dynamic analysis of wood shear walls to estimate the seismic reliability of such walls for various sites throughout the US. The model was developed using results from testing of ten shear wall specimens. The model was developed by applying a displacement at the top of the shear wall through a single degree-of-freedom oscillator, a piece-wise approximation of the hysteresis, an idealized constant valued pinching behavior, and the hysteretic response enveloped by the backbone curve (Figure 1-11).

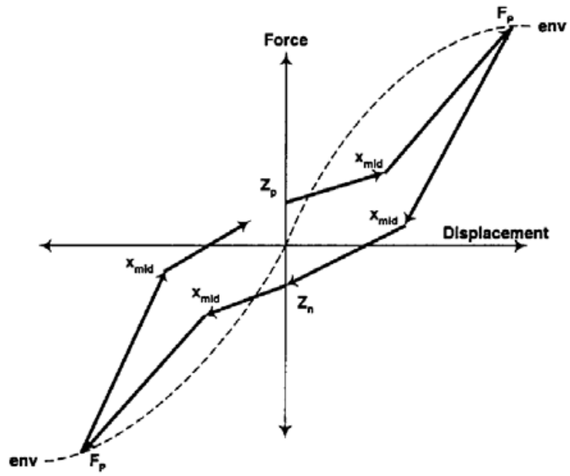

Figure 1-11 Hysteresis model considered with pinching behavior (from Van de Lindt and Walz, 2003).

1.4.4 Fülöp and Dubina (2004a)

Fülöp and Dubina (2004b) examined fifteen experimental wall-stud cold-formed shear panels under monotonic and cyclic loading. Using the experimental result, a full nonlinear fiber hinge within a single degree-of-freedom bar captured the behavior of shear-wall panels. These bars were installed in the model as an equivalent brace, diagonal member connecting beam-column nodes (Figure 1-12).

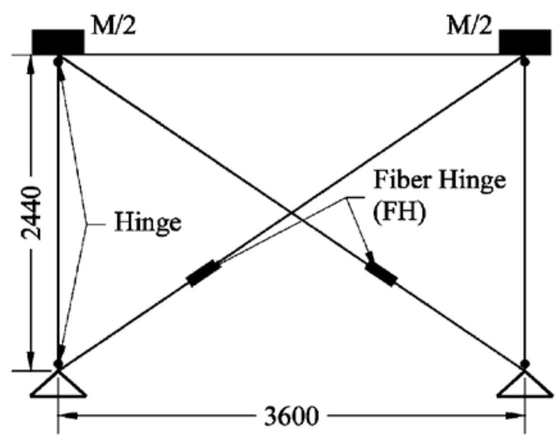

Figure 1-12 Wall panel idealization through equivalent braced diagonal bars (from Fülöp and Dubina, 2004).

1.4.5 Folz and Filiatrault (2004a)

Folz and Filiatrault developed a numerical model to predict the quasi-static and dynamic reversed cyclic response of woodframe buildings. In their approach, model reduction was ideal to reduce the computational demands associated within a finite-element model. This simplification lead to a shear wall spring element calibrated to represent the strength and stiffness degradation characteristics of the shear wall. Their study noted that the global deformation of the wood shear wall is very much dominated by the individual sheathing-to-framing connectors used in the construction of the wall. The cyclic analysis of shear walls (CASHEW) model utilized ten parameters to predict the behavior, a modified version of the Wayne-Stewart hysteresis model (Stewart 1987) (Figure 1-13). This model takes into account reduced load capacity (strength degradation), failure of the wall at a prescribed maximum displacement, strength degradation based on the loading history, and the pinching effect. Use of the model requires specifications of wall geometry, shear stiffness of the sheathing panels, and hysteretic properties of the sheathing-to-framing connections, all outlined in its development (Folz and Filiatrault, 2004b).

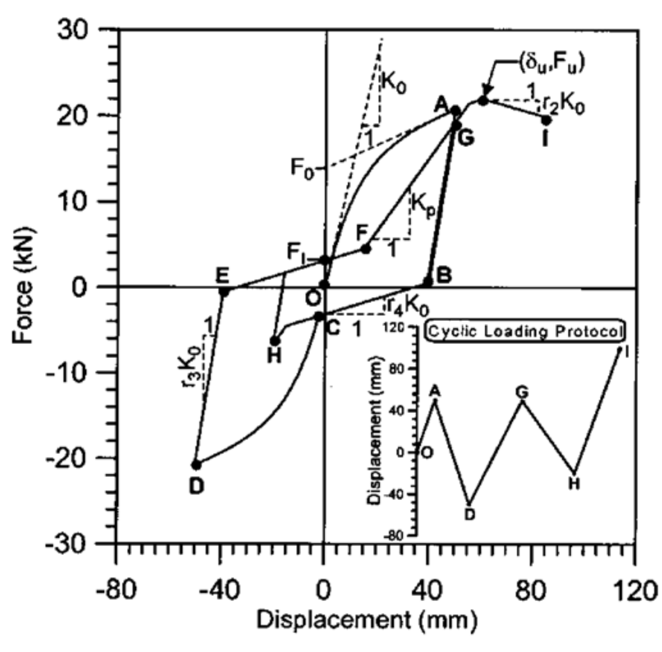

Figure 1-13 CASHEW model developed for woodframe shear walls (from Folz and Filiatrault, 2004a).

1.4.6 Judd and Fonseca (2005)

Judd and Fonseca provided a new analytical model representing the sheathing-to-framing connections within a wood shear wall as a pair of oriented orthogonal nonlinear springs. When a simplified sheathing-to-framing connection is idealized as one nonlinear spring, the displacement trajectory of the connection is primarily considered unidirectional. Drawbacks of using only one nonlinear spring include a potential displacement trajectory that is bidirectional under reversed cyclic loading or highly nonlinear loading and numerical difficulties around the ultimate load. Using the oriented spring pair model, the actual connection behavior is more accurately represented.

1.4.7 Kanvinde and Deierlein (2006)

Kanvinde and Deierlein proposed numerical models to determine the strength and stiffness of wood-framed gypsum partition walls accounting for the effects of wall geometry, door or window openings, connector type and spacing, and boundary conditions. Their focus was limited to partition walls constructed of gypsum board on wood framing, while recommending broader extension to partition walls framed with light-gauge steel studs. Their study provided three relationships to determine the lateral strength and stiffness, the coefficients to describe the piecewise linear curve of the nonlinear response, and the coefficients for a peak-oriented hysteretic model to detail the nonlinear hysteretic behavior.

1.4.8 Pang et al. (2007)

Pang et al. outlined an evolutionary parametric hysteretic model (EPHM) based on development of the CASHEW model (Folz and Filiatrault, 2001). The CASHEW model includes a built-in shear wall parameter estimation tool to develop the parameters needed for the nonlinear backbone curve and the linear line segments that control the hysteretic behavior. The EPHM model retains the parameter estimation tools while using exponential functions for the backbone, the loading path, and the unloading path. This model requires definition of 17 parameters, where seven of these parameters are required to define the two exponential functions for the backbone curve (Figure 1-14). The loading and unloading curves are modeled using one exponential function each with evolutionary parameters and the remaining ten parameters are used in the degradation process by updating the evolutionary parameters. Examples of types of degradation considered include backbone force, force-intercept (pinching effect), unloading stiffness, and reloading stiffness values. In comparison of the EPHM to the CASHEW model, the EPHM performed better for cumulative energy dissipation.

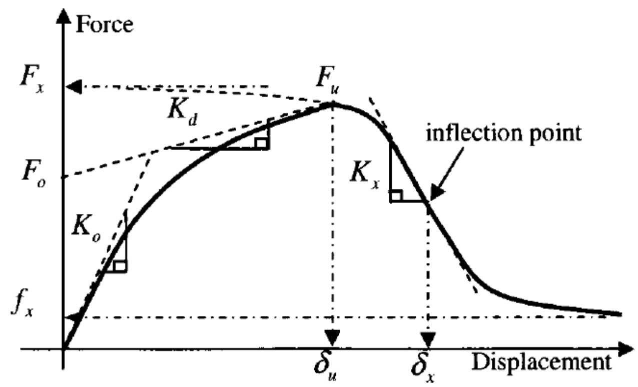

Figure 1-14 Shear wall backbone curve (from Pang et al., 2007).

1.4.9 Baird et al. (2011)

Baird et al. presented the preliminary results of a combined model system of precast concrete cladding systems and moment resisting frame buildings. In the study, diagonal springs representing compressive struts are used in a lumped fashion; similar to the modeling technique applied to infill masonry frames. The hysteretic behavior was modeled using the Crisafulli hysteresis rule, a rule validated to model the stiffness and strength degradation of masonry infill panels. This simplified methodology demonstrates the effect of the inclusion of cladding systems, a strength increase of 10-20%.

1.4.10 Restrepo and Lang (2011)

Restrepo and Lang examined the influence of two reversed cyclic loading protocols on the response of cold-formed light-gauge partition walls. Gypsum board partition response was characterized in a linear piecewise function, where the lateral force value of the wall was normalized by the wall length (Figure 1-15). These empirical formulae were developed by considering the individual components of the backbone responses in their test and a previous test conducted by Restrepo and Bersofsky (2010).

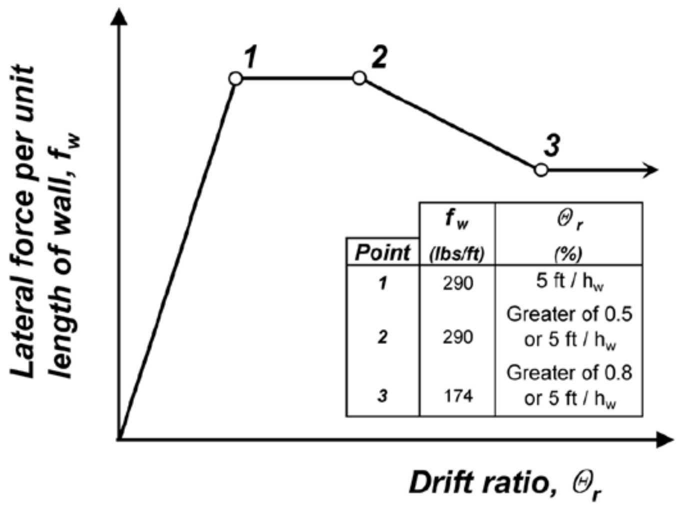

Figure 1-15 Proposed empirical backbone for gypsum board on light-gauge steel stud partition walls (from Restrepo and Lang, 2011).

1.4.11 Davies (2009)

Davies used regression analysis to analyze 35 partition wall specimens to develop representative hysteretic models of the in-plane partition walls. Model parameters were determined from each partition wall specimen to represent the Wayne-Stewart model, noted as the best fit model within the nonlinear software suite RUAUMOKO (Figure 1-16). Nine parameters were characterized to represent this model: initial stiffness, post yield stiffness factor, post capping stiffness factor considering strength degradation, unloading stiffness factor, yield strength, capping strength, intercept strength, reloading or pinch power factor, and the beta or softening factor. In addition, no gap distance was set, and this rule was run with a modified loop allowing the post yield stiffness to have a negative value. Hysteretic behavior of the specimens followed a tri-linear relationship where the ratcheting effect, noted later as post-peak hardening, was not considered in the modeling technique. The post-peak hardening was not considered because it was noted to generally occur beyond 2% drift and after strength degradation. Two modeling sets were developed, one based on the mean values for each of the individual subgroups considered in the experimental program and a second set requiring only the mean initial stiffness and capping strength with the remaining seven parameters assigned via statistical ratios. Using representative models, a coupled dynamic analysis was conducted for an example hospital building with and without partition walls. The partition wall was implemented into the building model via a shear spring.

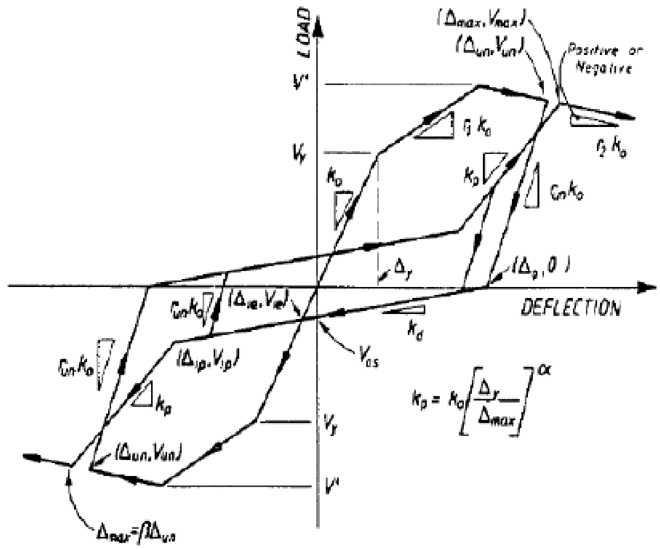

Figure 1-16 Wayne-Stewart hysteretic model with strength degradation (from Carr, 2005)

1.5 Scope of this Work

The aforementioned experimental and numerical studies provide key insights into the behavior and modeling of partition wall subsystems. However, a systematic experimental study of these subsystems, when adopting metal studs overlaid by gypsum, considering the broad range of details encountered in practice, is lacking. Data from such a test program would be valuable for further refinement of modeling tools. A different modeling approach is undertaken in this study whereby a strength degrading pinched hysteretic model is sought. Importantly, design-oriented numerical tools, which can be readily integrated in building structural analysis software, which generally utilize beam-column "line-type" finite elements, would be valuable to design practitioners and researchers conducting an extensive number of simulations. In this work, such an approach is sought. Modeling the partition wall is undertaken via a strength degrading pinched hysteretic model, which can be lumped at strategic locations within a building. The calibrated partition wall model provides pinching characteristics as a function of displacement, capturing the post-peak hardening experienced in the experimental setup, and uses a set of four springs in a parallel configuration to closely capture the cumulative hysteretic energy.

To this end, the results of a large experimental program conducted by the University at Buffalo, State University of New York (UB) are utilized to calibrate a simplified numerical model of the in-plane behavior of the metal stud-type partition walls. The model of the partition wall focuses on the in-plane behavior of full-height specimens. While this is a subset of the partition walls tested, this group of walls is characterized as the stiffest set which is most sensitive when placed into realistic building models. The set of partition wall models developed are grouped at first by their installation technique as either commercial or institutional grade construction and considering either a partial or a fully connected specimen. In this report, an overview of the partition wall modeling is presented along with an error assessment of the accuracy of the developed models.

1.6 Organization of the Report

This report is organized as follows. Section 1 provides background to the work presented. Section 2 presents an overview of the experiments used in the model development and outlines the subgroup classification. Section 3 presents the modeling formulation and determination of model parameters. Section 3 also provides a demonstration of the modeling technique applied to a single specimen. Section 4 outlines the representative subgroup models. Section 5 presents the normalized partition wall models and representative models capturing the input parameter statistics. Section 6 demonstrates the effectiveness of the developed models using both a force and energy error assessment. Section 7 of this report demonstrates the partition wall implementation into numerical building models, including an example of how the walls might be scaled when considering different wall lengths. Section 8 provides an overview of the accomplished work with some concluding remarks. Appendices A-D illustrate the individual comparisons for each of the calibrated models against associated experimental specimens. In these appendices, the error metrics for each specimen are presented in full detail. Appendix E provides the example script for implementing the partition wall model in OpenSees.

SECTION 2
EXPERIMENTAL PROGRAM OVERVIEW

2.1 Introduction

The experiments used in the model development are part of a NEES grand challenge project led by the University of Nevada, Reno (UNR). Fifty wall specimens were tested at the State University of New York, University at Buffalo (UB). These partition walls were approximately 11.5 feet tall by 12 feet long with return walls (perpendicular to the loading direction) of either 2.0 feet or 4.0 feet (Davies, 2009). The wall specimens were placed in the upper level of the Nonstructural Component Simulator (UB-NCS), shown in Figure 2-1 through Figure 2-3, which is a full scale two story frame mechanism capable of producing realistic floor motions in terms of acceleration, velocity and displacement (Retamales et al., 2008). The variables considered in the various wall configurations included: connectivity of the sheathing and studs to the top and bottom tracks (slip track or full connection), spacing of the track-concrete fasteners (12 or 24 inches on center), presence of return walls, wall intersection detailing, attachments of weights to the partition walls (bookshelves, equivalent ceiling), height of the partition wall, stud and track thickness (30 mil or 18 mil), spacing of the steel studs, direction of testing (in-plane or out-of-plane) and test type (quasi-static or dynamic) (Davies, 2009). The various specimen details are shown in Table 2-1.

The loading protocols chosen for this project were developed by Retamales et al. (2008). An upward and downward sweeping dynamic protocol was developed specifically for the testing of nonstructural components allowing both representative acceleration and drift sensitive loading history in the same load sequence. This protocol was developed particularly for the UB-NCS allowing for the simulation of two adjacent floors within a building. In the context of this study, the seismic demands imposed on the partition walls are consistent with a generic site with spectral accelerations of S_{DS} = 1g, S_{D1} = 0.6g, and a nonstructural component located at the roof level. The maximum interstory drift imposed is 3% to ensure all damage stares are observed (Figure 2-4). To evaluate the drift sensitive components partition walls in the test program, without attached masses, a quasi-static protocol was developed and selected (Figure 2-8). In this figure, the donuts identify the locations where detailed inspections were carried out.

During testing, extensive instrumentation was employed for the measuring of load and response characteristics of the setup. For the in-plane wall setups, load cells were placed underneath the wall specimens to measure the forces acting on the wall, while potentiometers were used to measure in-plane deformations which include relative displacements between the tracks and attached concrete slabs, vertical studs and tracks, perpendicular walls and any diagonal wall deformation (Davies, 2009).

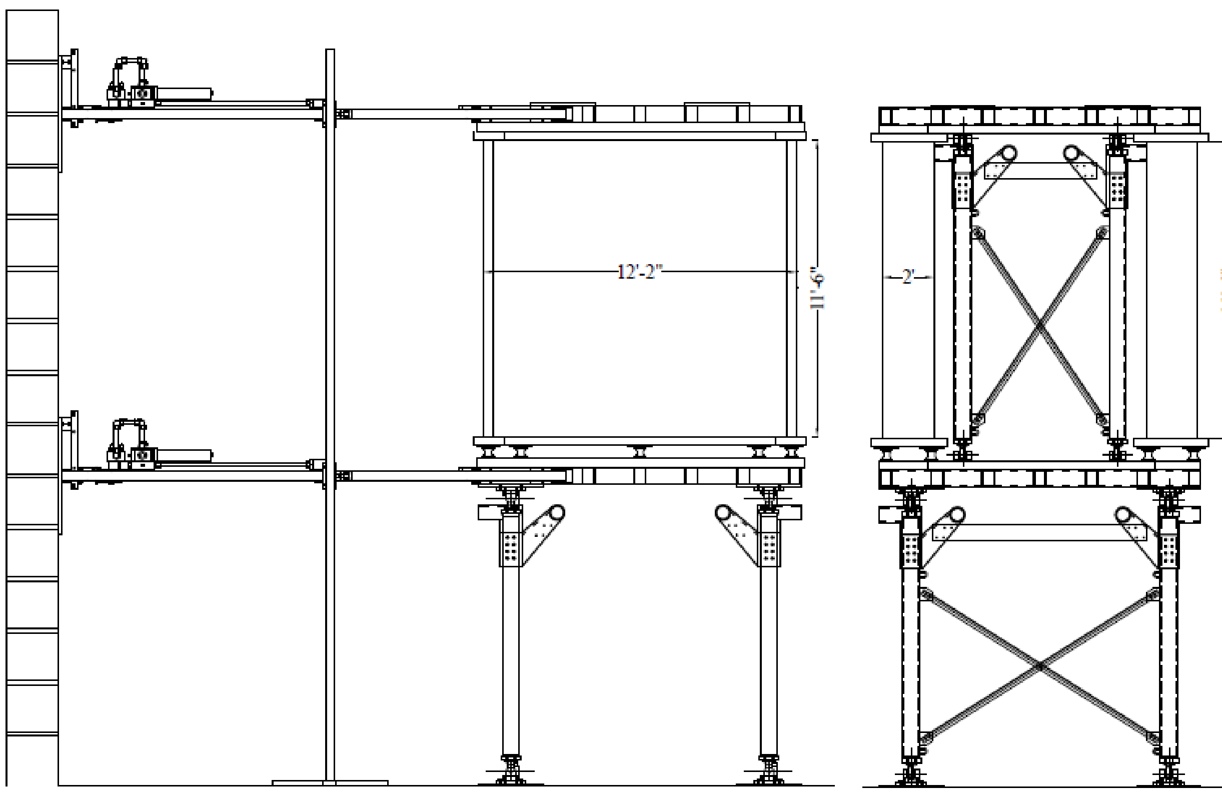

(a) (b)

Figure 2-1 In-plane partition wall setup: (a) parallel to shaking direction and (b) perpendicular to shaking direction, highlighting the shorter return walls (from Davies, 2009).

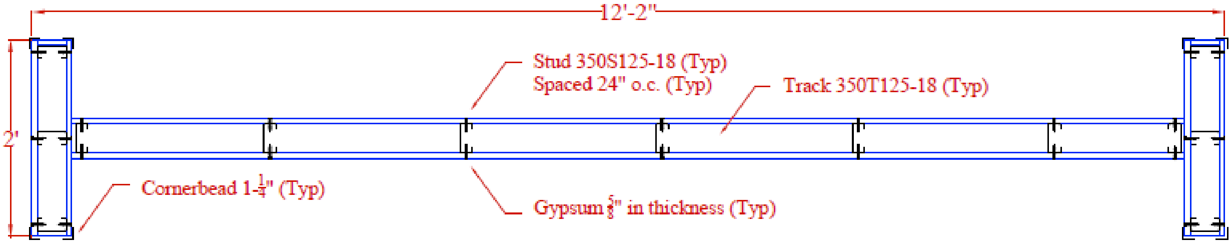

Figure 2-2 Typical cross section of partition wall (from Davies, 2009).

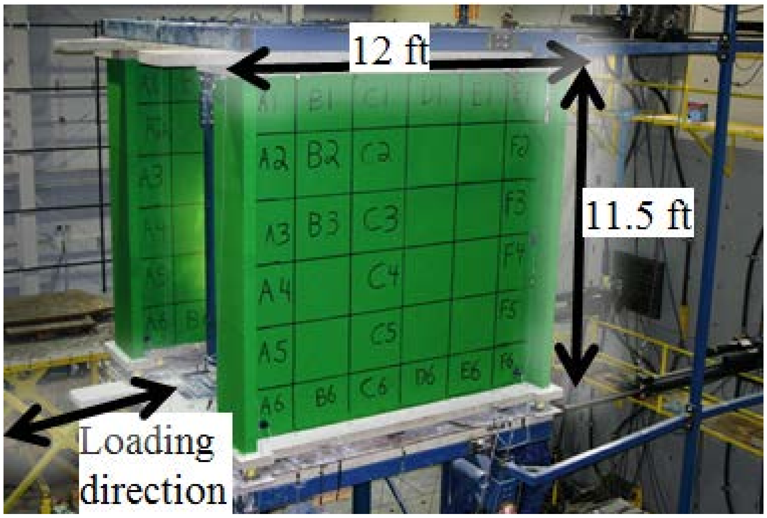

Figure 2-3 Typical in-plane partition wall setup (photo courtesy of Davies, 2009).

Table 2-1 Partition wall test configuration details (from Davies, 2009).

Config	Specimen ID	Specimen Description	Loading Direction/Rate	Steel Stud Type	Steel Frame and Sheathing Connectivity: Stud to Bottom Track	Stud to Top Track	Gypsum to Bottom Track	Gypsum to Top Track	Return Walls	Attached Mass	Ceiling Connected
1	1, 2 & 3	Basic (slip track)	In Plane/Static	350S125-18	No	No	Yes	No	Yes	No	No
2	4	Gypsum connected to top track	In Plane/Static	350S125-18	No	No	Yes	Yes	Yes	No	No
3	5, 6 & 10	No Return	In Plane/Static	350S125-18	No	No	Yes	Yes	No	No	No
4	7, 8 & 9	Full connection	In Plane/Static	350S125-18	Yes	Yes	Yes	Yes	Yes	No	No
5	11, 12 & 13	Bookshelf	In Plane/Dynamic	350S125-18	No	No	Yes	No	No	Yes	No
6	14, 15, & 16	Equivalent Ceiling	In Plane/Dynamic	350S125-18	Yes	No	Yes	No	No	Yes	Yes
7	17, 18 & 19	Partial height braced wall	In Plane/Static	350S125-18	Yes	Yes	Yes	Yes	Yes	No	No
8	20, 21 & 22	Institutional const./slip track	In Plane/Static	350S125-30	Yes	No	Yes	No	Yes	No	No
9	23, 24 & 26	Institutional const./Full Connection@24"	In Plane/Static	350S125-30	Yes	Yes	Yes	Yes	Yes	No	No
10	25, 27 & 28	Institutional const./Full Connection@12"	In Plane/static	350S125-30	Yes	Yes	Yes	Yes	Yes	No	No
11	29 & 30	No Return/Dynamic	In Plane/Dynamic	350S125-18	No	No	Yes	No	No	Yes	No
12	31 & 32	C-Shaped Walls	In Plane/Static	350S125-18	Yes	No	Yes	No	Yes	No	No
13	33	Solution to T corner damage/corner gaps	In Plane/Static	350S125-18	Yes	No	Yes	No	Yes	No	No
14	34	Solution to T corner damage/double slip track	In Plane/Static	350S125-18	No	No	No	No	Yes	No	No
15	35	Solution to L corner damage/corner gaps	In Plane/Static	350S125-18	Yes	No	Yes	No	Yes	No	No
16	36	Solution to T corner damage/slip track	In Plane/Static	350S125-18	Yes	No	Yes	No	Yes	No	No
17	37	Unloaded Wall w/ Returns	Out of Plane/Dynamic	350S125-18	No	No	Yes	No	Yes	No	No
18	38	Unloaded Wall w/o Returns	Out of Plane/Dynamic	350S125-18	No	No	Yes	No	No	No	No
19	39, 45 & 47	Bookshelf wall w/ returns	Out of Plane/Dynamic	350S125-18	No	No	Yes	No	Yes	Yes	No
20	40, 41 & 43	Bookshelf wall w/o returns	Out of Plane/Dynamic	350S125-18	No	No	Yes	No	No	Yes	No
21	42, 44 & 46	Equivalent Ceiling wall w/ returns	Out of Plane/Dynamic	350S125-18	Yes	No	Yes	No	Yes	Yes	Yes
22	48, 49 & 50	Partial height braced wall	Out of Plane/Dynamic	350S125-18	Yes	Yes	Yes	Yes	Yes	No	No

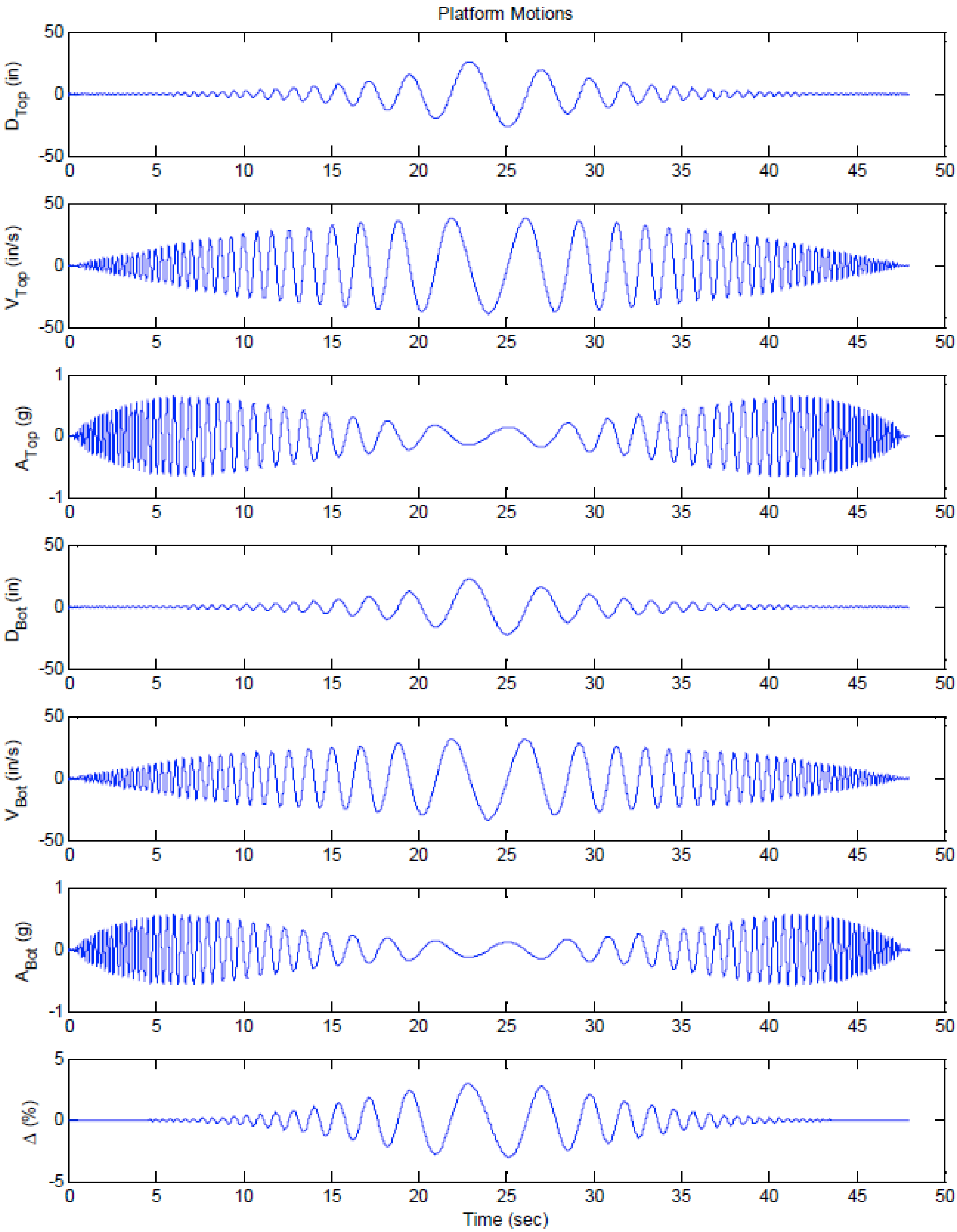

Figure 2-4 Dynamic nonstructural fragility testing protocol developed by Retamales et al. (2008) (from Davies, 2009).

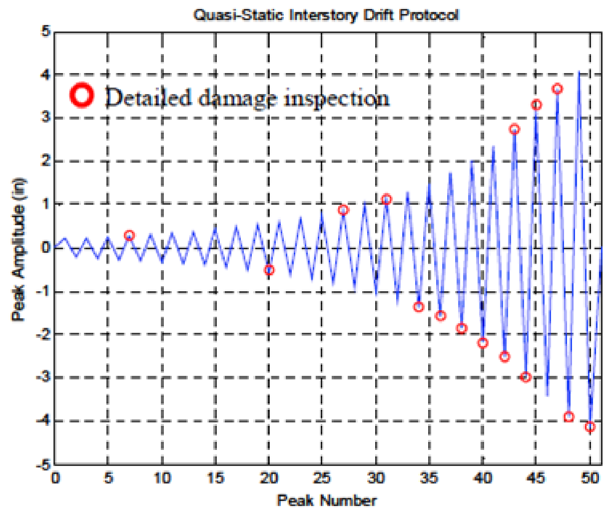

Figure 2-5 Quasi-static drift sensitive protocol developed by Retamales et al.
(from Davies, 2009).

2.2 Observed Damage States

Damage states (DS) were defined by UB (Davies, 2009) to describe the physically observed damage and the required repair techniques (Tables 2.2 and 2.3**)**. In the classification of damage, three damage states were proposed: DS_1 referring to light damage, DS_2 to moderate damage and DS_3 to complete or severe damage. Damage within DS_1 can be repaired such that the wall appears new. DS_2 is moderate damage, where the damage is localized, including crushing in the wall corners, out-of-plane bending of the wallboard at wall intersections, or damaged boundary studs. DS_2 can be repaired in local damaged regions with gypsum and boundary stud replacement. DS_3 is the most severe damage, characterized by track damage or hinging of the studs. Walls reaching DS_3 would require full replacement. These damage states were adopted by the experimental team at the University at Buffalo (UB) in the experimental stages of the project. It is noted that similar damage state classifications have been identified by others (e.g. Bersofsky, 2004; Restrepo and Lang, 2011). The damage state classification identified at UB has been adopted here in the simulation program. Consistent with the approach of the UB experimental team, if a higher class damage state was identified before a lower class damage state, then the two damage states are set equal. For example, if DS_2 occurred at 1.0% interstory drift and DS_1 occurred at 1.5%, DS_1 and DS_2 are then both defined at 1.0%. It should also be noted that select specimens (for reasons described later) are noted to be outliers (gray specimens in Table 2-3). In this table, the last column "normalized model" indicates for Chapter 5 which specimens are considered for the normalized model development.

Table 2-2 Damage state classification adopted for partition walls (photos courtesy of UB Experimental Team)

Damage State	Description and Repair	Example
1 Light	Light damage to walls, cracks along cornerbeads and joint tape,along with screw pullout. Repair requires cornerbead and screw replacement with some refinishing techniques.	
2 Moderate	Crushing in wall corners, out of plane bending, damaged boundary studs. Localized repairs of gypsum and replacement of boundary studs.	
3 Severe	Track damage (tear, bent), hinges in studs. Full replacement.	

Table 2-3 Partition wall test specimens as considered for modeling and damage state summary herein.

Specimen No.	Subgroup	Construction Grade	Connection Type	Damage State (drift ratio, %)			Normalized Model[3]
				1	2	3	
1	1a	Commercial	Partial	0.2	0.62	0.62	
2	1a	Commercial	Partial	0.2	0.62	1	
3[4]	1a	Commercial	Partial	0.4	0.62	0.62	
4	1b	Commercial	Full	0.4	0.62	1.16	X
5	1b	Commercial	Full	0.2	0.4	2.32	X
6	1b	Commercial	Full	0.4	0.62	2.66	
7	1b	Commercial	Full	0.2	0.62	1	
8	1b	Commercial	Full	0.4	1	1	X
9	1b	Commercial	Full	0.2	0.4	0.62	
10	1b	Commercial	Full	0.2	0.81	0.81	
20	2a	Institutional	Partial	0.2	1	2.32	
21	2a	Institutional	Partial	0.4	0.81	--	
22	2a	Institutional	Partial	0.62	0.62	1	
23	2b	Institutional	Full	0.4	0.81	1	X
24	2b	Institutional	Full	0.4	0.4	1.16	X
25	2b	Institutional	Full	0.4	0.4	0.62	X
26	2b	Institutional	Full	0.4	1	1	X
27	2b	Institutional	Full	0.4	0.62	0.81	X
28	2b	Institutional	Full	0.4	0.81	0.81	X

[3] Normalized model refers to whether or not the test specimen is utilized in the model described in Chapter 5.
[4] Gray rows are identified as outliers to the subgroup behavior.

2.3 Example Specimen Response

In order to explore typical damage progression and response of an in-plane wall setup, specimen 20 is presented. This specimen corresponds to the first experimental partition wall tested from group 2a, institutional style construction with a partially connected boundary condition. Subgroup introduction and classification immediately follows in 2.4. Specimen 20 is illustrated here as it is used later in section 3 to verify the modeling procedure. Figure 2-6 presents the experimental hysteretic force-displacement response while Table 2-2 summarizes the damage observed as noted by the UB experimental team and its corresponding hysteretic response characteristics. The final state of this specimen is characterized by damage located primarily in the return walls and its intersection with the longitudinal in-plane walls.

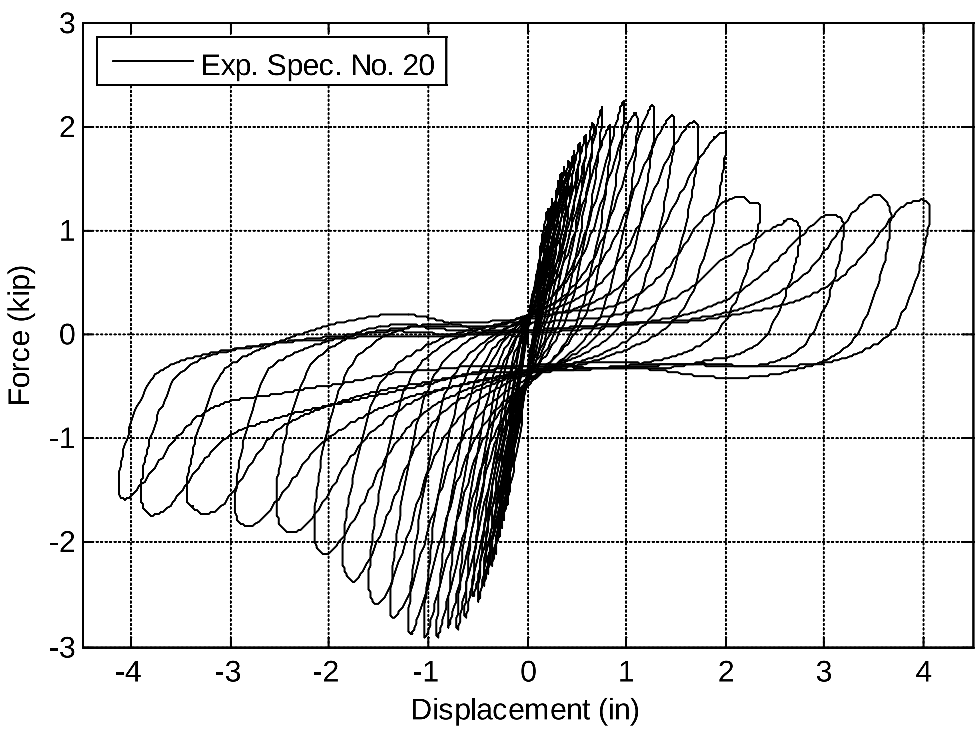

Figure 2-6 Experimental force-displacement response for Specimen 20.

Table 2-4 Damage and corresponding hysteretic response report for Specimen 20.

Drift (in)	Drift (%)	Load Step	Observed Damage[5]	Hysteretic Response
0.000	0.00	0	-	-
0.279	0.20	7	Slight crack in paint (1' long) in wall corner. No additional damage observed	Initially very stiff corresponding to the uncracked stiffness, load cycling is primarily elastic. Loading and unloading stiffness are similar.
0.559	0.40	20	Crushing of gypsum board in one corner of longitudinal wall. 2' long crack in joint paper tape at wall intersection	Specimen cracks, stiffness degradation initiated, load cycle begins to dissipate energy, unloading stiffness degrades.
0.858	0.62	27	Crack along top 4' in joint paper tape at wall intersection. 1/16-1/8" gap (approx.) under bottom track	Continued response with greater energy dissipation.
1.120	0.81	31	Large gap observed at longitudinal and transverse wall intersection. Joint paper tape destroyed in top 4' at wall intersection. Increased gap under longitudinal wall bottom track. Out of plane bending of transverse wall	Specimen dissipates greater energy than previously, wall strength value plateaus at the peak value.
1.384	1.00	34	Damage of top 6' of joint paper tape at wall intersection. Screws pulled out from webs of studs located in wall corners. Closed gap under longitudinal wall bottom track	Similar to previous.
1.601	1.16	36	Crushing of gypsum board in one corner of longitudinal wall. Increased out of plane bending of transverse walls	Similar to previous.
1.861	1.35	38	Vertical crack along the center of the return wall. Horizontal crack along paper tape covering joints between transverse wall gypsum boards	Specimen continues to dissipate greater energy (per cycle) and strength begins to degrade.
2.171	1.57	40	No new damage states triggered	Similar to previous.
2.537	1.84	42	No global rocking of walls observed, presumably due to nails passing through longitudinal wall bottom track web	Similar to previous.
2.743	1.99	43	No new damage states triggered	Extensive strength degradation is experienced.
2.963	2.15	44	Longitudinal wall boundary studs twisted. Bending of flanges of transverse wall top track observed.	Strength degradation plateaus, initiation of post-peak hardening due to 'gap closing' demonstrated slightly on the positive side. Continued increase in energy dissipation.
3.196	2.32	45	One nail in the connection of the transverse wall top track pulled out of concrete. Global twist of transverse wall observed	Similar to previous.
3.673	2.66	47	Longitudinal wall gypsum board detached from boundary stud. Transverse wall top track flanges completely bent	Similar to previous.
3.893	2.82	48	No new damage states triggered	Similar to previous.
4.140	3.00	50	No new damage states triggered	Similar to previous.
Final condition			Severe damage in transverse walls and along intersection between the longitudinal and transverse walls.	-

[5] Observed damage reports provided by the UB experimental research team, taken from Davies, 2009.

2.4 Subgroup Classification Overview

Building occupancy will certainly affect the materials and details used for its partition walls. For example, commercial grade partition walls have thinner gauge studs, spaced at larger intervals, when compared with partition walls installed in institutional buildings. Likewise, stronger connections are required for the institutional configuration (Figure 2-7). Consequently four types of partition wall are identified as predominant, namely: 1) commercial, 2) institutional, 3) partial height and 4) remedial design (Table 2.5). It is noted that the details adopted in these tests were identified via consultation with practicing engineers, architects, and construction industry representatives familiar with the most common configurations. Accordingly, numerical models are developed for the subgroups 1a, 1b, 2a and 2b. Groups 3 and 4, not shown here, are not selected for modeling. Group 3 refers to partial height specimens, in which the failure mechanism was governed by brace buckling. Due to the buckling nature of the braces, the unrestrained length of the studs is critical, and to reasonably capture this, one needs to explicitly model the brace. These details may vary substantially in practice. Nonetheless, knowledge of the brace characteristics would allow for modification of the developed models herein by altering the top boundary condition. Group 4, remedial designs, is also not considered, since these are not typical construction practices.

Table 2-5 Partition wall classification by subgroup. Only subgroups with full height specimens are considered.

Subgroup	Name	Description
1a	Commercial partially connected	Full-height specimens constructed using commercial practice and slip track connections
1b	Commercial fully connected	Full-height specimens constructed using commercial practice and full connections
2a	Institutional partially connected	Full-height specimens constructed using institutional practice and slip track connections
2b	Institutional fully connected	Full-height specimens constructed using institutional practice and full connections

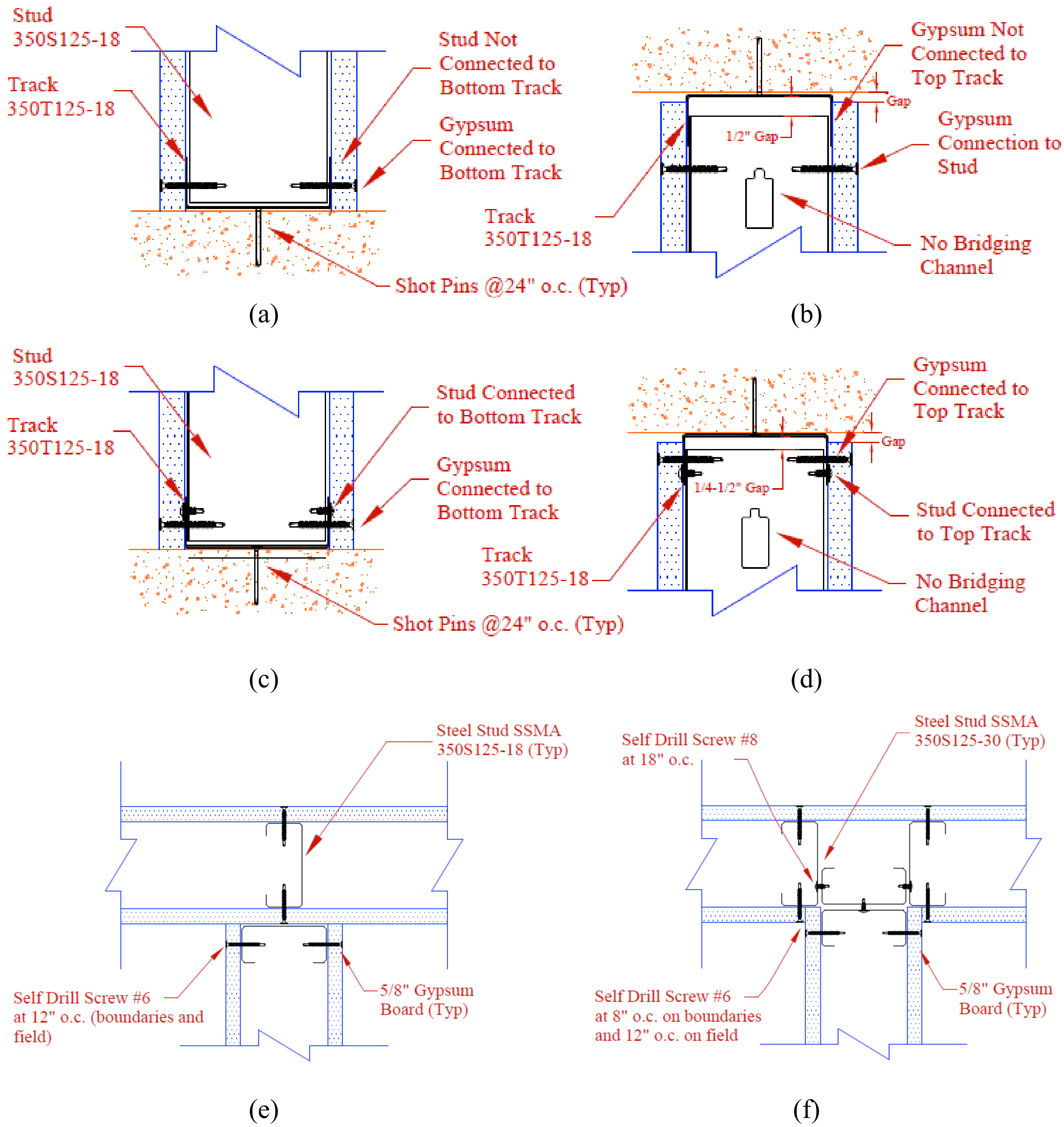

Figure 2-7 Sheathing and framing connectivity details: (a-b) bottom and top track connections for partially connected specimens (slip track), (c-d) bottom and top track connections for fully connected specimens, (e) wall intersection details for commercial construction practices and (f) wall intersection details for institutional construction practices (from Davies, 2009).

While the partition walls are grouped according to their installation techniques, specimen-to-specimen variation does exist. The largest contribution for specimen variability lies within the installation procedure, and this variation does exist in practice. Accepting this variability, initially representative models for each subgroup are targeted for the mean behavior and later models developed target an overall group model of all the fully connected specimens. The subgroup representative force-displacement curves are averaged before the backbone selection procedure is conducted.

2.5 Specimen Outliers in a Subgroup

In the analysis of the experimental response of all walls, one observes specimens that are outliers with respect to other specimens within their subgroup. These may be due to uncharacteristic failures. Examples of uncharacteristic failures include connection separation where the screws pulled through the partition wall and top track failures including: wall sliding, track tearing, and crushing/bending. An example is shown for specimen 10 in Figures 2-8 and 2-9. For specimen 10, the screws pulled through at a displacement less than 0.86 inches (0.6% drift) and crushing/bending of the top track occurred before 1.12 inches (0.8% drift). While this behavior is realistic, it is not observed in other specimens within the subgroup 1b and resulted in significantly lower lateral load carrying capacity. In identifying this specimen as an outlier to the subgroup 1b, it is removed from the averaging of results.

2.5.1 Subgroup 1a

Subgroup 1a is classified as commercial grade construction, partially connected specimens. This subgroup utilizes 18 mil track, 18 mil vertical studs at 24 inches (c/c) with partially connected, commercial details illustrated in Figure 2-7. Subgroup 1a originally consisted of specimens 1, 2 and 3 for the static in-plane configurations. In a detailed specimen-to-specimen inspection of the hysteretic behavior of this subgroup, Specimen 3 is considered an outlier. In the damage report of specimen 3 at 1.34 inches, the gypsum panels at the top of the wall detached from the studs at the wall boundaries (Davies, 2009). Consequently specimen 3 is not considered for the subgroup representative modeling. In Figure 2-10, each of the specimens making up subgroup 1a is shown. The dark blue hysteretic curves shown are considered for modeling, while the lighter gray curve is characterized as an outlier. The dashed curve shown on the specimens considered for modeling shows that individual specimen backbone while the thicker black curve demonstrates the overall subgroup average (mean) backbone, neglecting the specimen (3) considered as an outlier.

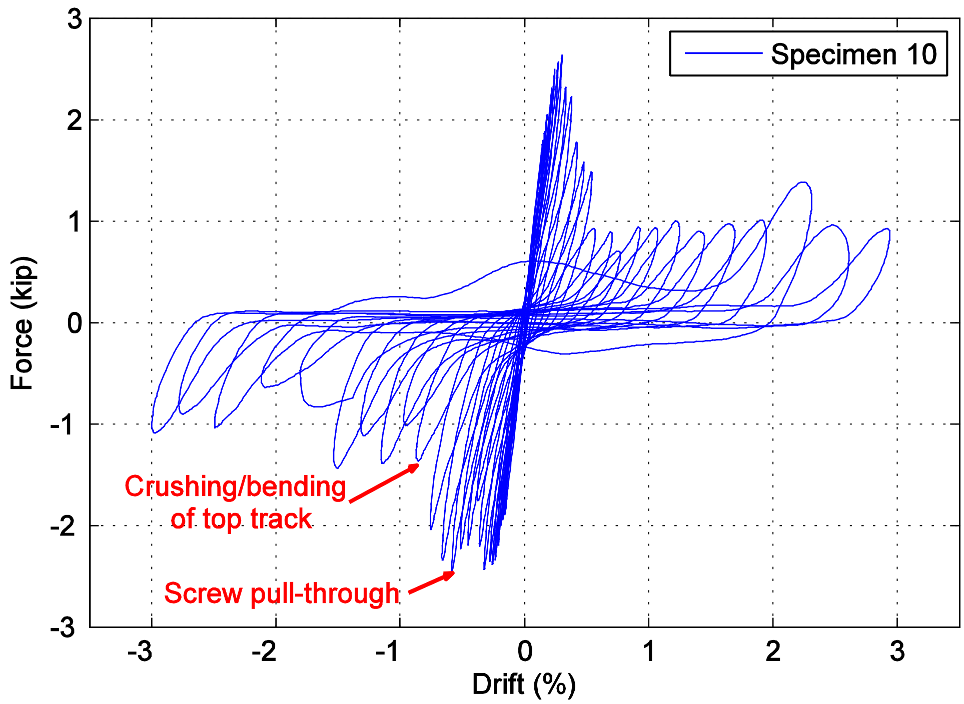

Figure 2-8 Experimental load-displacement of specimen 10 (subgroup 1b). Note the anomalous dramatic reduction in load carrying capacity at 0.8% drift.

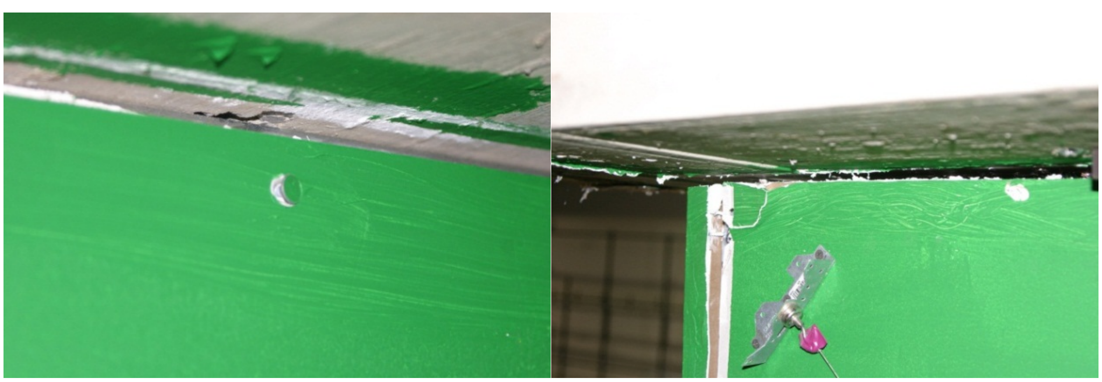

(a) (b)

Figure 2-9 Photos of damage observed in specimen 10: (a) at 0.6% drift and (b) top track damage.

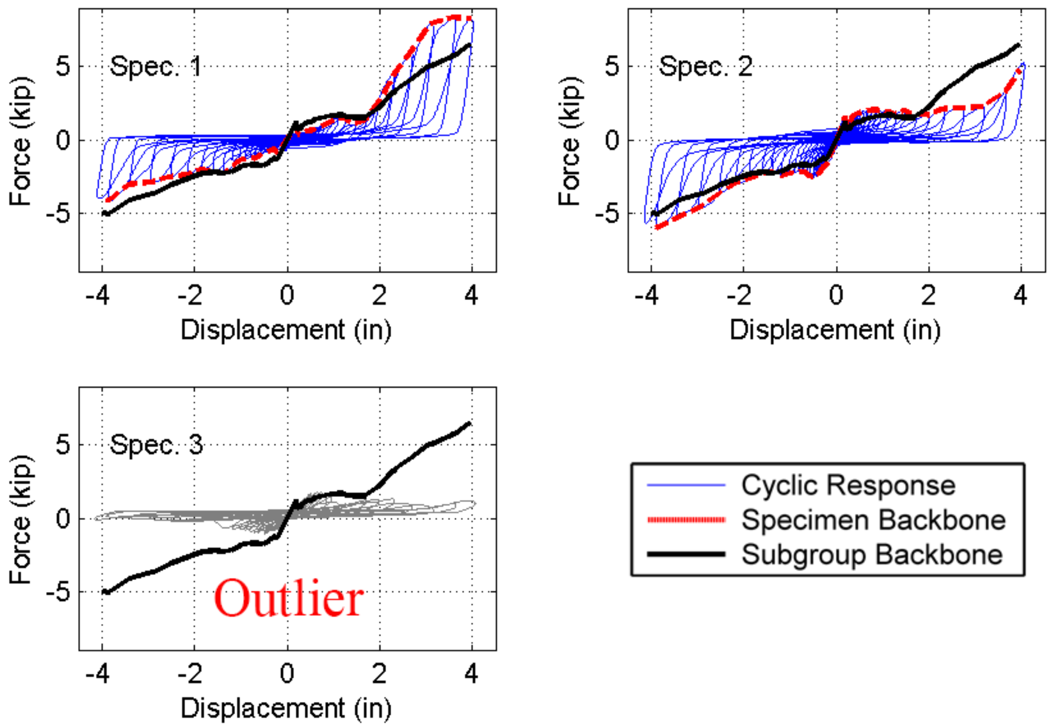

Figure 2-10 Subgroup 1a experimental hysteretic behavior showing identified backbone and average subgroup backbone.

2.5.2 Subgroup 1b

Subgroup 1b is classified as commercial grade construction with fully connected detailing. This subgroup utilizes 18 mil track, 18 mil vertical studs at 24 inches (c/c) with fully connected, commercial details illustrated in Figure 2-7. Subgroup 1b originally consisted of specimens 4 – 10. In a detailed specimen-to-specimen inspection, specimens 7, 9 and 10 are characterized as outliers. The main difference in these specimens in the damage report was top track tearing. While removing three out of the original 7 specimens seem significant, the removal of these specimens will result in a more conservative model neglecting any installation variance resulting in lower strength characteristics. In Figure 2-11, each of the specimens making up subgroup 1b is shown. The dark blue hysteretic curves shown are considered for modeling, while the lighter gray curves (7, 9 and 10) are characterized as outliers. The dashed curve shown on the specimens considered for modeling shows that individual specimen backbone while the thicker black curve demonstrates the overall subgroup average backbone, neglecting the specimens (7, 9 and 10) considered as an outliers.

2.5.3 Subgroup 2a

Subgroup 2a is classified as institutional grade construction with partially connected detailing. This subgroup utilizes 30 mil track, 30 mil vertical studs at 16 inches (c/c) with partially connected institutional details illustrated in Figure 2-7. Subgroup 2a consists of specimens 20-22. In a detailed specimen-to-specimen inspection, no specimens are characterized as outliers. In Figure 2-12, each of the specimens making up subgroup 2a is shown. The dark blue hysteretic curves shown are considered for modeling, the dashed curve shows the individual specimen backbone while the thicker black curve demonstrates the overall subgroup average backbone.

2.5.4 Subgroup 2b

Subgroup 2b is classified as institutional grade construction with fully connected detailing. This subgroup utilizes 30 mil track, 30 mil vertical studs at 16 inches (c/c) with partially connected, institutional details illustrated in Figure 2-7. Subgroup 2b consists of specimens 23-28. In a detailed specimen-to-specimen inspection, no specimens are characterized as outliers. In Figure 2-13, each of the specimens making up subgroup 2b is shown. The hysteretic curves shown in dark blue are considered for modeling, the dashed curve shows that individual specimen backbone while the thicker black curve demonstrates the overall subgroup average backbone. It is noted that very consistent hysteretic behavior is observed among the group of six specimens forming this subgroup.

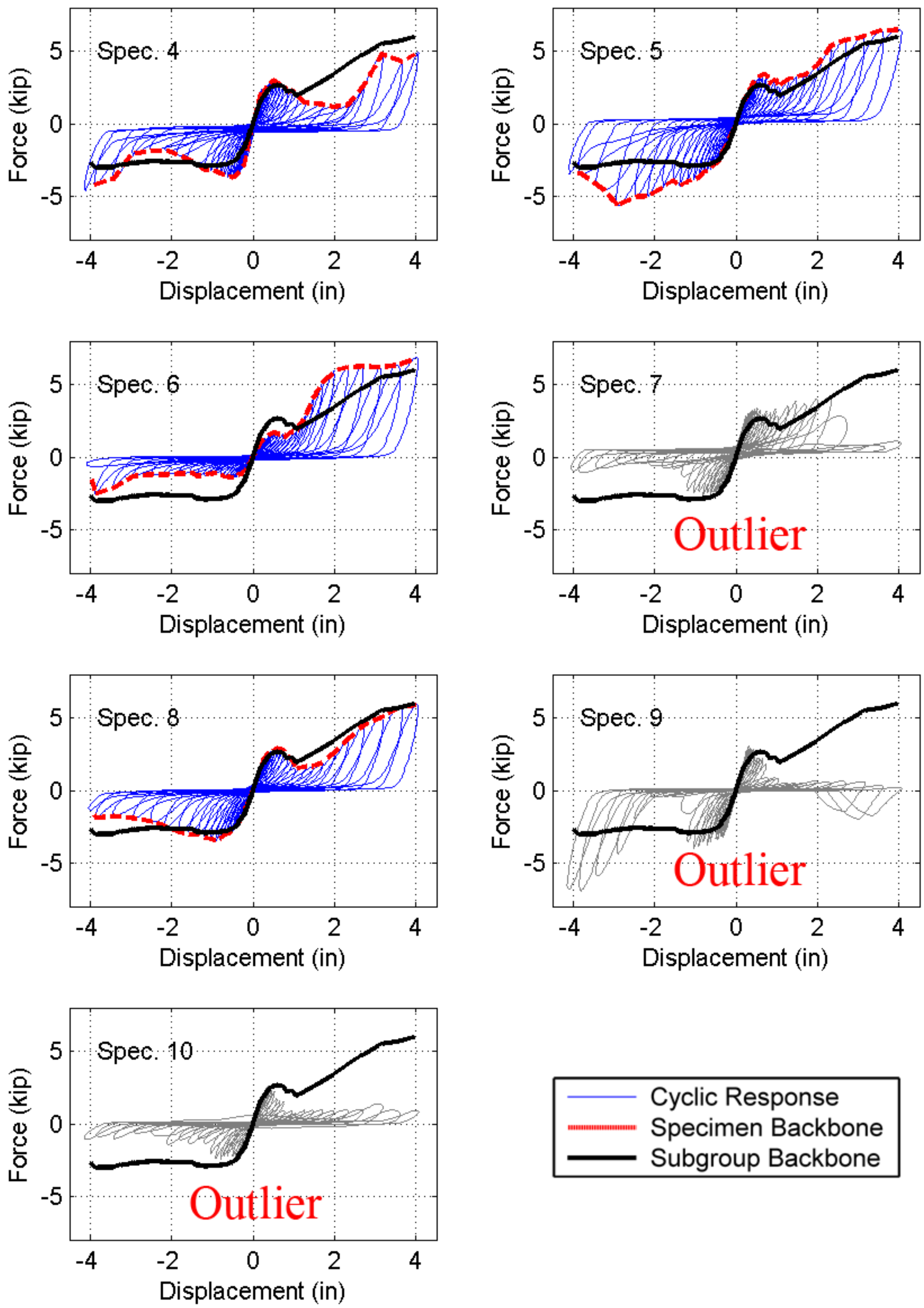

Figure 2-11 Subgroup 1b experimental hysteretic behavior showing identified backbone and average subgroup backbone.

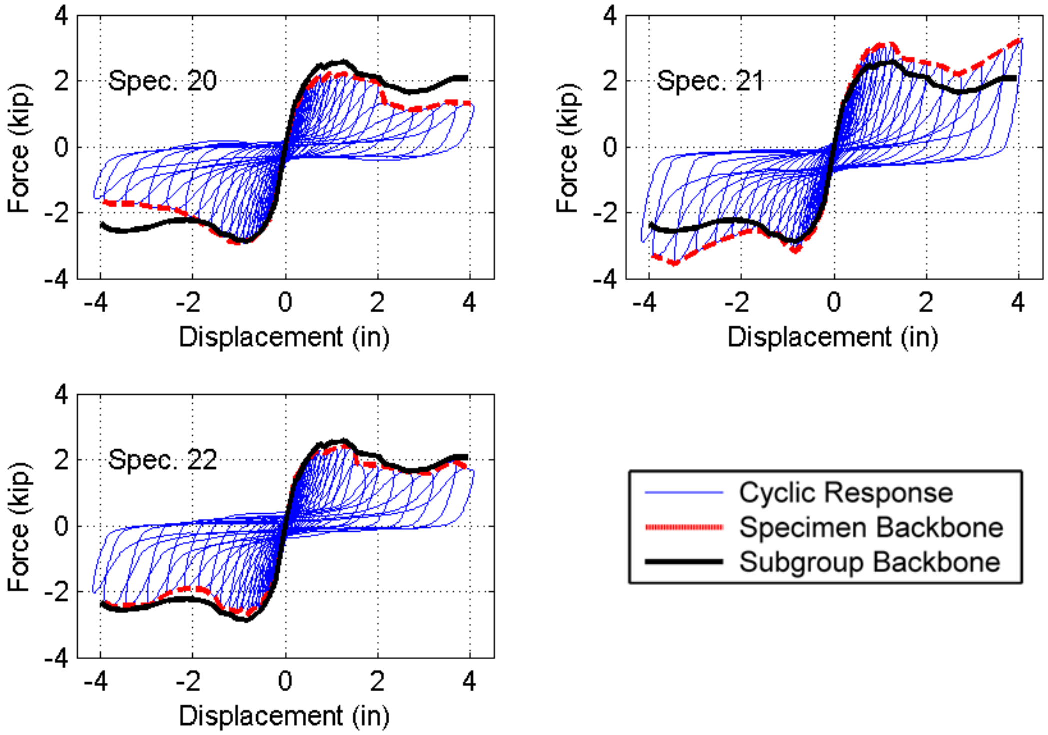

Figure 2-12 Subgroup 2a experimental hysteretic behavior showing identified backbone and average subgroup backbone.

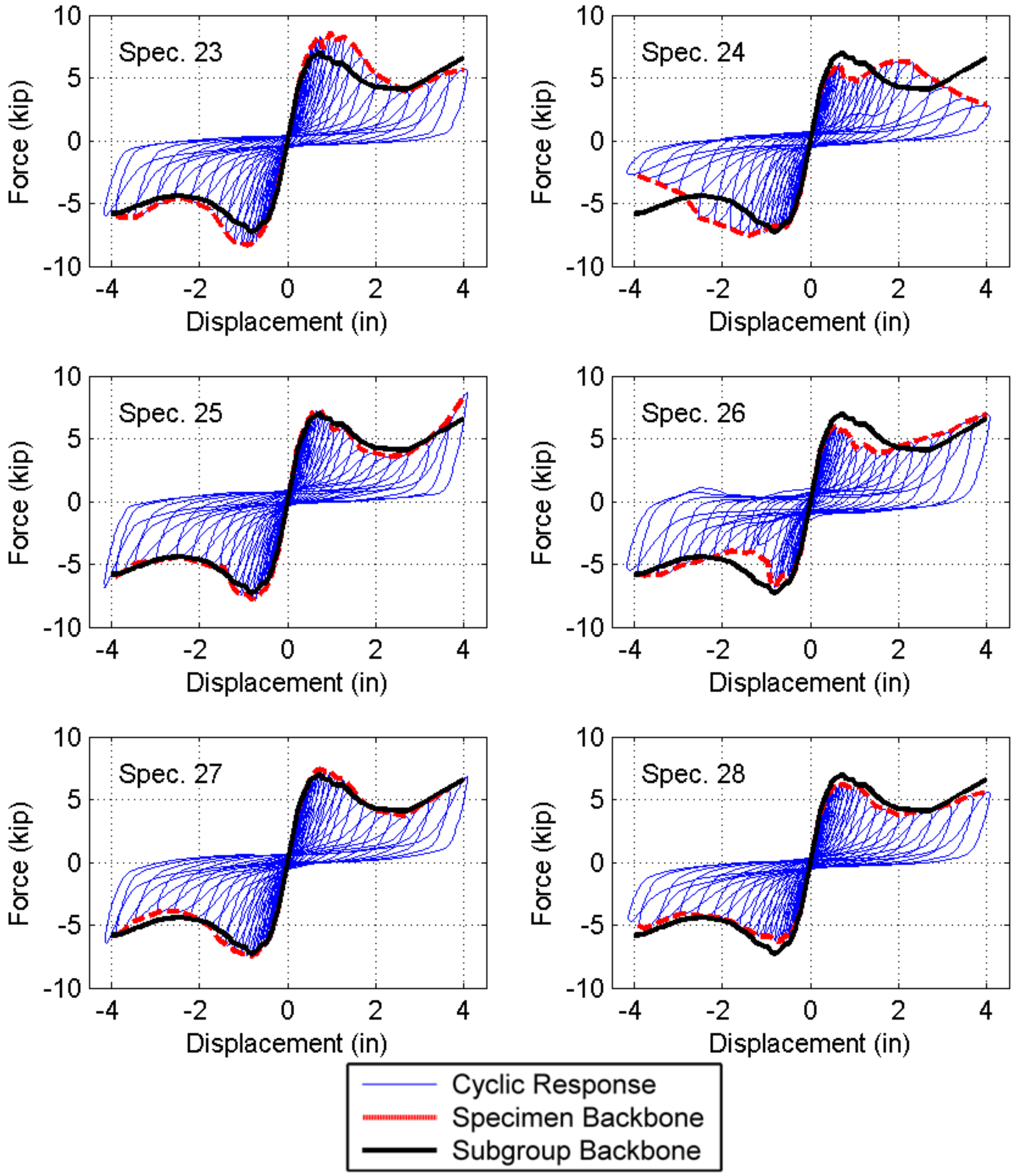

Figure 2-13 Subgroup 2b experimental hysteretic behavior showing identified backbone and average subgroup backbone.

SECTION 3
MODELING OVERVIEW

3.1 Modeling Platform

The platform selected to model the partition walls is OpenSees, developed by the Pacific Earthquake Engineering Research (PEER) Center (Mazzoni et al., 2009). OpenSees is an open-source numerical platform based on finite element modeling that provides the capabilities to perform advanced nonlinear time history analysis of buildings, bridges and other structural systems. However to date, it does not have tools available for modeling nonstructural components and systems. Nonetheless, one advantage of OpenSees is its open-source nature and freely available tools. To capture the nonlinear hysteretic behavior of the various partition wall models, a lumped material is created. The motivation for doing so is primarily simplification and computational efficiency, as one may envision that partition subsystems are to be distributed throughout a building model, and a finely discretized model of partition wall would be cumbersome in the computation of larger building-partition system response calculations. Moreover, the use of lumped hysteresis is highly compatible with finite element models readily used by building analysts in design practice. To this end, the lumped material model is assigned to a zero-length one degree-of-freedom, element. The lumped material behavior is created using the *pinching4* material, which is available in OpenSees (Figure 3-1). *Pinching4* is a uniaxial material model that allows for a “pinched” load-deformation response with an optional degradation contribution. As can be seen in Figure 3-1, the model is flexible enough to capture a broad range of backbone and hysteretic characteristics.

To represent the experimental specimens, this *pinching4* material is used in a parallel configuration providing better control of the unload and reload parameters as a function of the displacement range. As a result, the number of parameters for the partition wall element model is 24. The first 16 parameters describe the force-displacement envelope or backbone of the model, while the remaining eight parameters control the unloading and reloading behavior. By placing the materials in a parallel formulation, three additional unloading and reloading relationships are required, as compared to the original *pinching4* material model.

In the use of the material, the partition wall is characterized as a simple spring. This spring would be implemented only in the longitudinal direction whereas the out-of-plane behavior of the partition walls is not characterized numerically herein. The out-of-plane stiffness of the walls is approximately 10% of the in-plane partition wall stiffness and therefore provides negligible contribution to the behavior of a building-partition wall system.

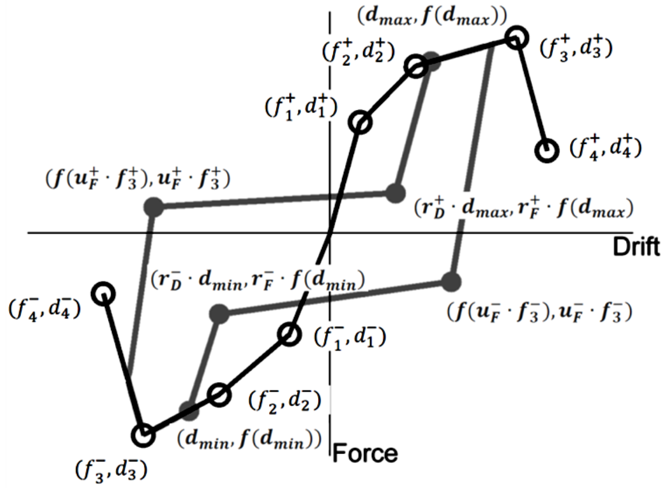

Figure 3-1 Graphical description of the pinching4 material model.
(after Mazzoni et al., 2009)

3.2 Model Verification

Ideally, each experimental specimen should have a detailed numerical model. However this would be impractical, alternatively representative groups based on their mechanical configuration, which drives their physical behavior. To test this methodology, the evaluation of the performance of an individual specimen is first conducted. Specimen 20, specimen within group 2a, institutional style construction with a partially connected boundary condition, is selected for this exercise.

3.2.1 Partition Wall Backbone Characterization

The initial step in the modeling approach is to determine the force-displacement backbone from the experimental data. This is done by taking the force associated with each maximum displacement excursion (Figure 3-2). The idealized force-displacement backbone is characterized by a total of eight points, four positive and four negative (denoted as “backbone points” in Figure 3-2). The selection of these points is based upon capturing the overall shape of the backbone curve, with some guidance provided by calculating the first derivative of the backbone (tangent stiffness, Figure 3-3). The first derivative illustrates the slope of the backbone curve and identifies significant changes at given displacements. The selected points for specimen 20 are shown in Figure 3-2. Note the backbone points are located near sudden changes in the slope of the backbone curve (Figure 3-3).

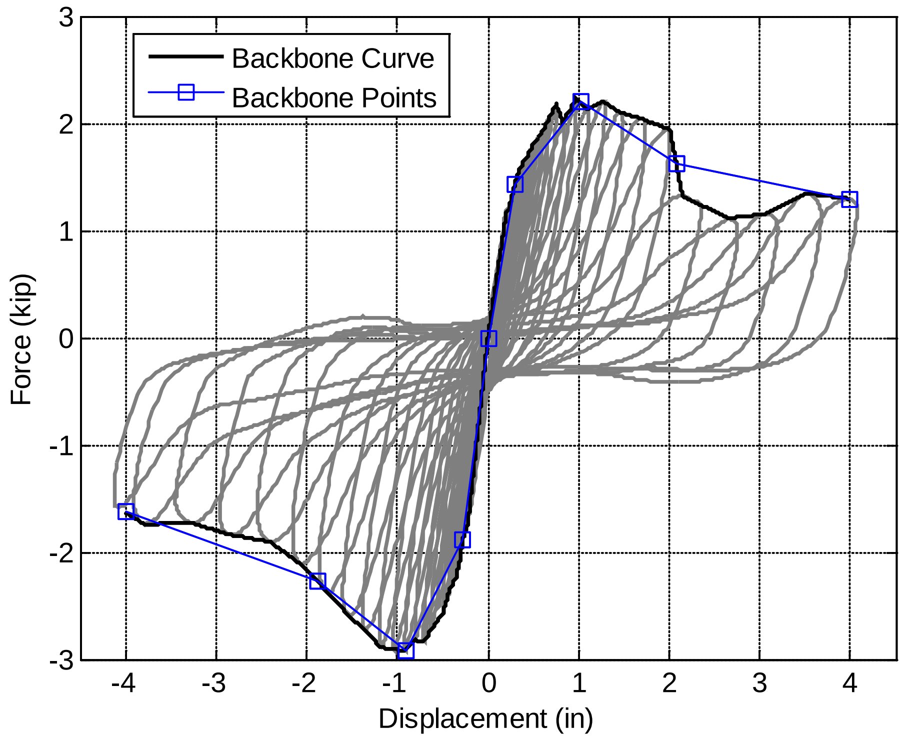

Figure 3-2 Force-Displacement backbone for specimen 20 and the selected backbone points.

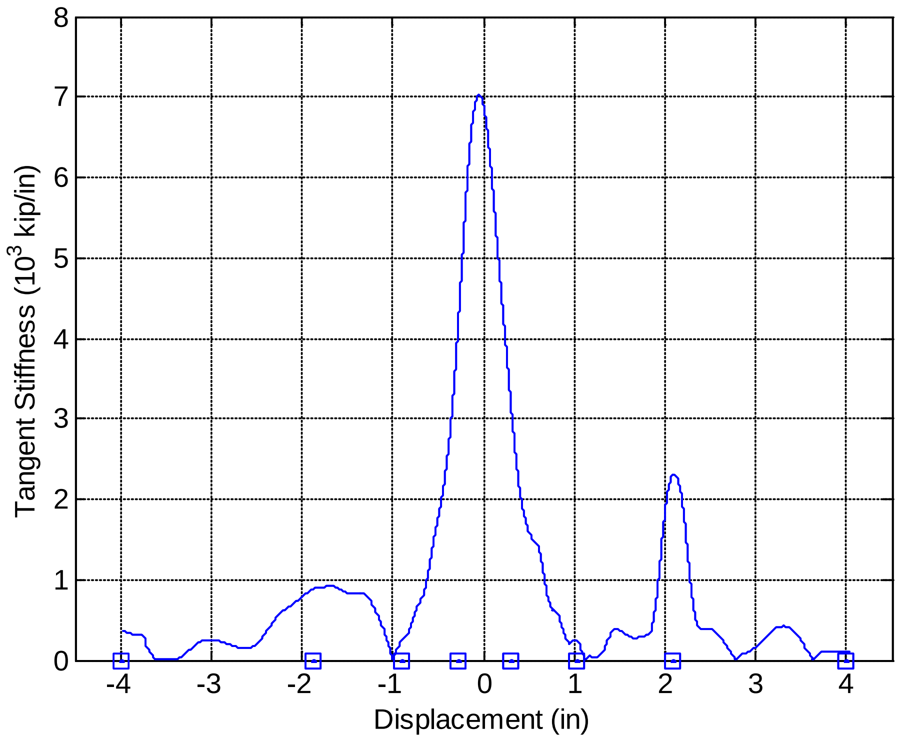

Figure 3-3 Tangent stiffness demonstrating sudden changes in the force-displacement backbone curve for specimen 20.

3.2.2 Partition Wall Unloading and Reloading Behavior

After selection of the backbone points, a calibration procedure is executed to determine the unloading and reloading parameters. Recall in Figure 3-1, that the numerical values of the unload and reload parameters are ratios of force or displacement values as governed in the material model. For simplicity in the unloading and reloading parameters, this behavior is assumed to be symmetrical, that is for each of the parallel materials, only one force and one displacement value is determined and this is the same in positive and negative regions (Figure 3-1). The remaining eight parameters (two for each individual material) are iterated such that the difference in the cumulative hysteretic area (between the model and experiment) is minimized. For specimen 20, the final hysteretic model overlay and hysteretic area (energy plots) are shown in Figure 3-4 against pseudo-time, representing the time sequence of the quasi-static test. The resultant hysteretic behavior and hysteretic area agree well. The comparison of the cumulative hysteretic energy provided demonstrates upon the discrete calibration, the numerical model reasonably captures the experimental behavior across the range of damage states until the end of test. Consequently, this technique for modeling is utilized throughout.

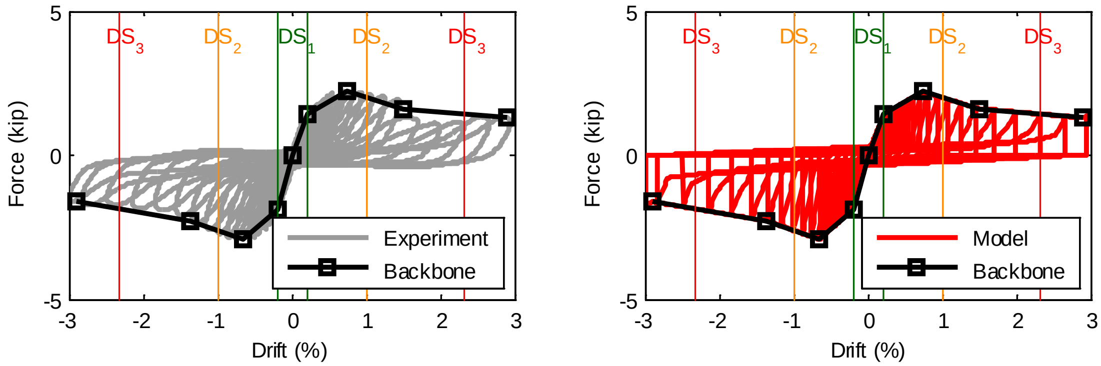

(a)

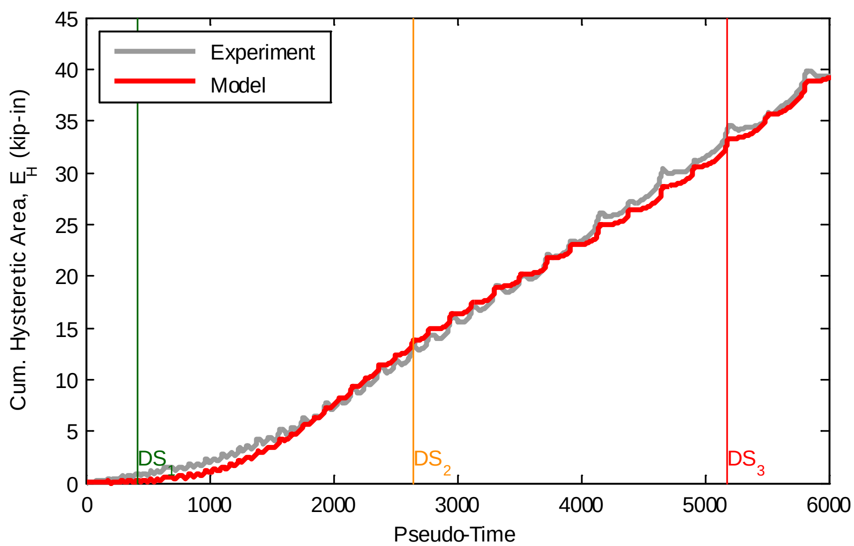

(b)

Figure 3-4 Experimental and numerical model comparison for specimen 20: (a) hysteretic behavior and (b) hysteretic area.

SECTION 4
REPRESENTATIVE SUBGROUP MODELS

4.1 Subgroup Modeling Approach

After removing the subgroup outliers, an average (mean) model representing each subgroup can be developed. As a result, four subgroup models are developed: 1) 1a commercial partial connection, 2) 1b commercial full connection, 3) 2a institutional partial connection and 4) 2b institutional full connection. Each of these models is based on the mean response of the specimens within the subgroup. To develop the representative models, two details are required: (1) force-displacement backbone points and (2) unload and reload parameters. To determine the force-displacement backbone points, the mean backbone is calculated from the experimental setups. In this calculation, the backbone points are sampled throughout the entire displacement range, including the individual dips and valleys from each test. To capture the average force-displacement backbone, the mean behavior is calculated using each of the specimens in the subgroup. Using this average force-displacement backbone curve, the eight backbone points are selected to idealize it in a piece-wise function (Figure 4-1). The selection of the backbone points is guided by examining the first derivative of the backbone, the tangent stiffness, to demonstrate where significant changes occur in the response. Using these displacement values the corresponding force values are used in the idealization.

The second required detail for the subgroup model involves unload and reload parameters. These parameters are critical to capture the hysteretic behavior, as they control the hysteretic loops using ratios of force or displacement values as governed in the material model. Using the 4 materials in a parallel formulation, 16 unload and reload parameters exist. However for simplification, the unload and reload parameters are considered to be identical in the positive or negative region. Using equal positive and negative unload and reload parameters, a total of eight parameters need to be calibrated. Four parameters each relate to force and displacement, as a result of considering a four material parallel formulation. These parameters are calibrated to match the average experimental hysteretic energy (area) of the subgroup. In what follows, this modeling calibration is demonstrated for each of the subgroups of interest.

4.1.1 Subgroup 1a Representative Model

The first subgroup described is subgroup 1a – commercial grade, partially connected specimens. Subgroup 1a is developed using the response of test specimens 1 and 2. Figure 4-1 demonstrates the average backbone calculation and the idealization of this backbone. Figure 4-2 shows the tangent stiffness of the average backbone, demonstrating the significant changes in slopes. Figure 4-2 is used solely as a guide because to capture the overall slope changes, smoothing of the average backbone is conducted using a moving average method. After the backbone points are identified, the unload and reload parameters are determined such that the average hysteretic area between the experimental hysteretic energy average of the subgroup and its model are well matched (Figure 4-3).

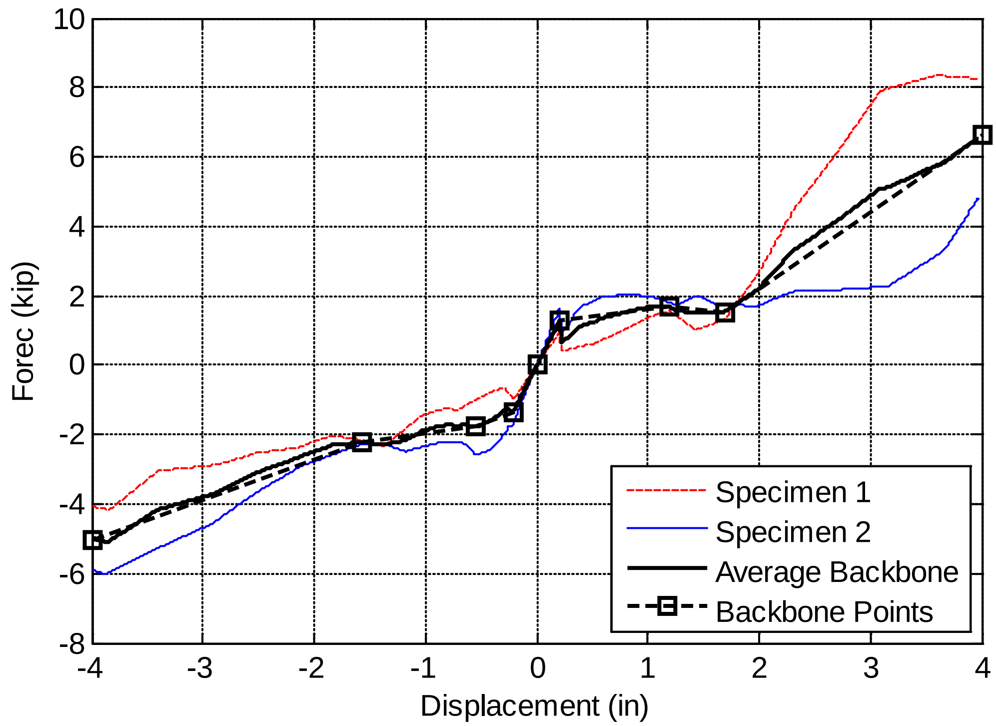

Figure 4-1 Specimen 1 and 2 backbone curves, average backbone and selected backbone points for subgroup 1a.

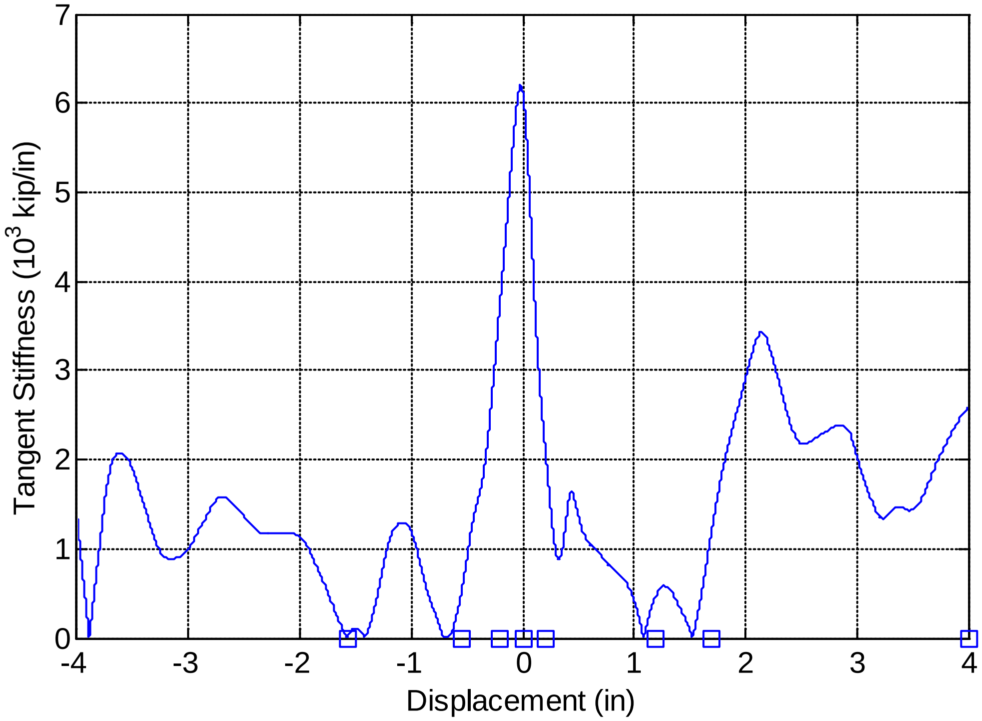

Figure 4-2 Tangent stiffness demonstrating sudden changes in the force-displacement backbone curve for subgroup 1a.

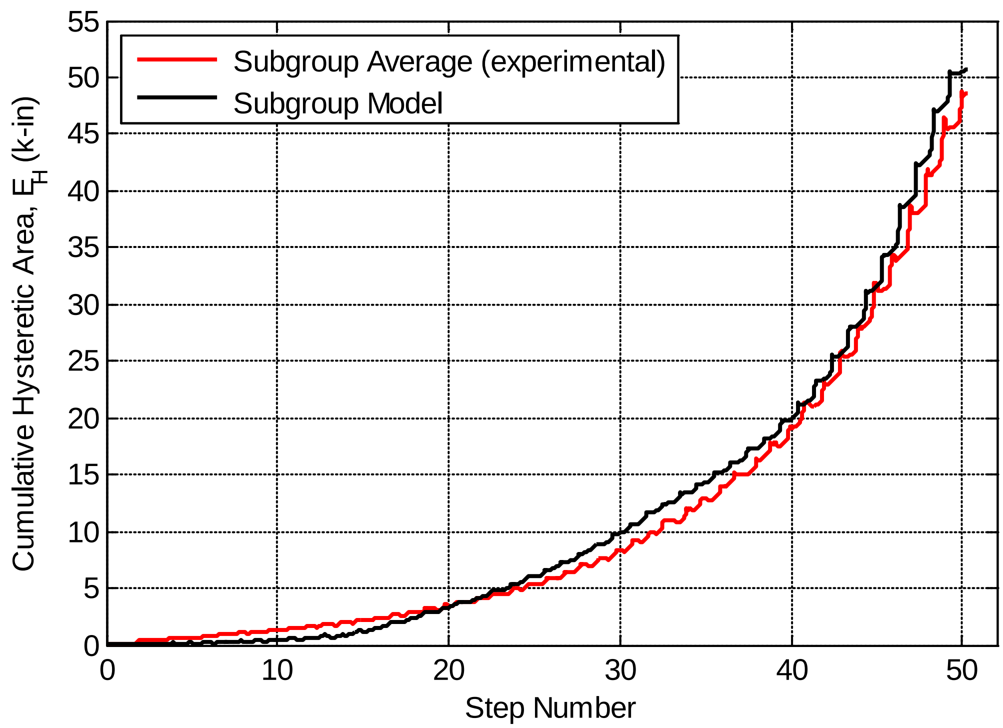

Figure 4-3 Hysteretic area calculated from the average experimental subgroup average (target) compared to the model hysteretic area for subgroup 1a.

To assess the robustness of the subgroup model, an individual comparison is made of the model to each of the specimens in the subgroup. Figures 4-4 and 4-5 overlay the hysteretic behavior of the subgroup model to specimens 1 and 2 respectively. The model behaves as expected in terms of the hysteretic response, with some minor discrepancies associated with specimen-to-specimen variability between specimens 1 and 2. The second comparison to each individual specimen is the ability of the model to capture the hysteretic energy (Figures 4-6 and 4-7). As expected, the model is sought to capture the subgroup average, thus a specimen level differences exist. Figure 4-7 identifies the percent error of the hysteretic area. Initially the model performs poorly, however it rebounds to have a percent error within 20% for specimen 1. The reason for the seemingly poor performance is in the percent error metric: when the denominator is a small value, a large percent error results. The error metric is studied further in Section 6.

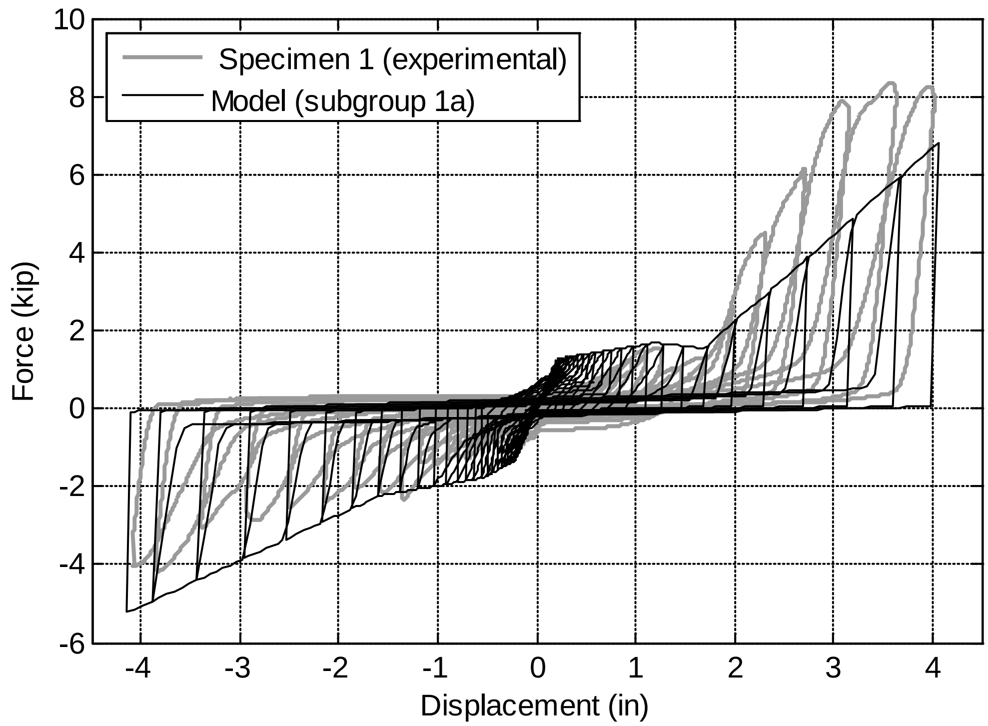

Figure 4-4 Hysteretic response of specimen 1 overlaid with the response of the representative subgroup model 1a.

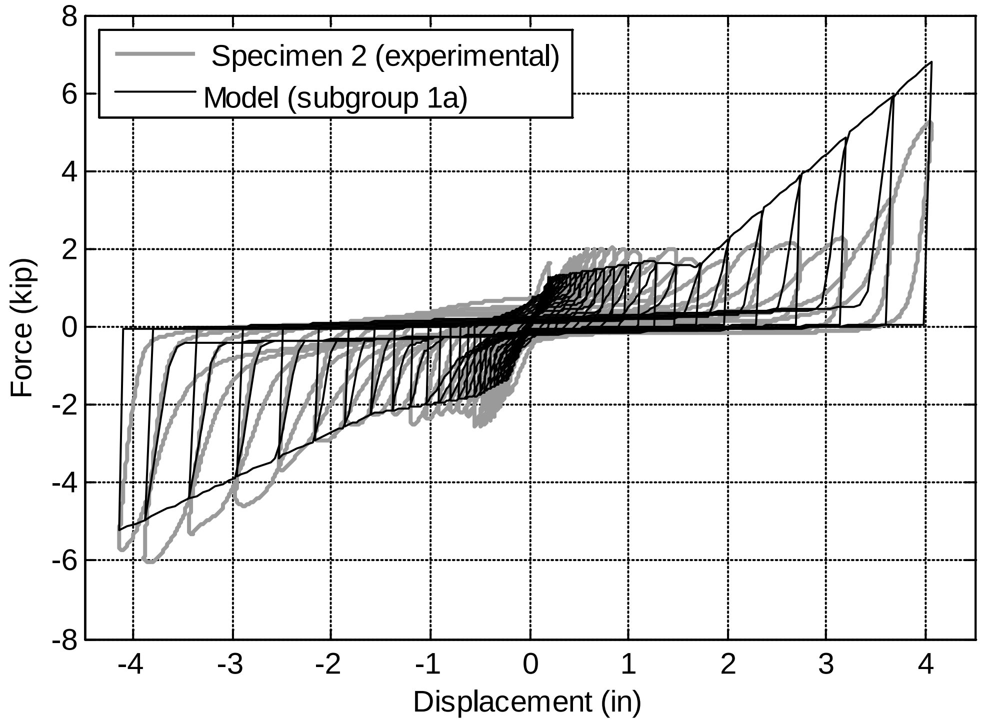

Figure 4-5 Hysteretic response of specimen 2 overlaid with the response of the representative subgroup model 1a.

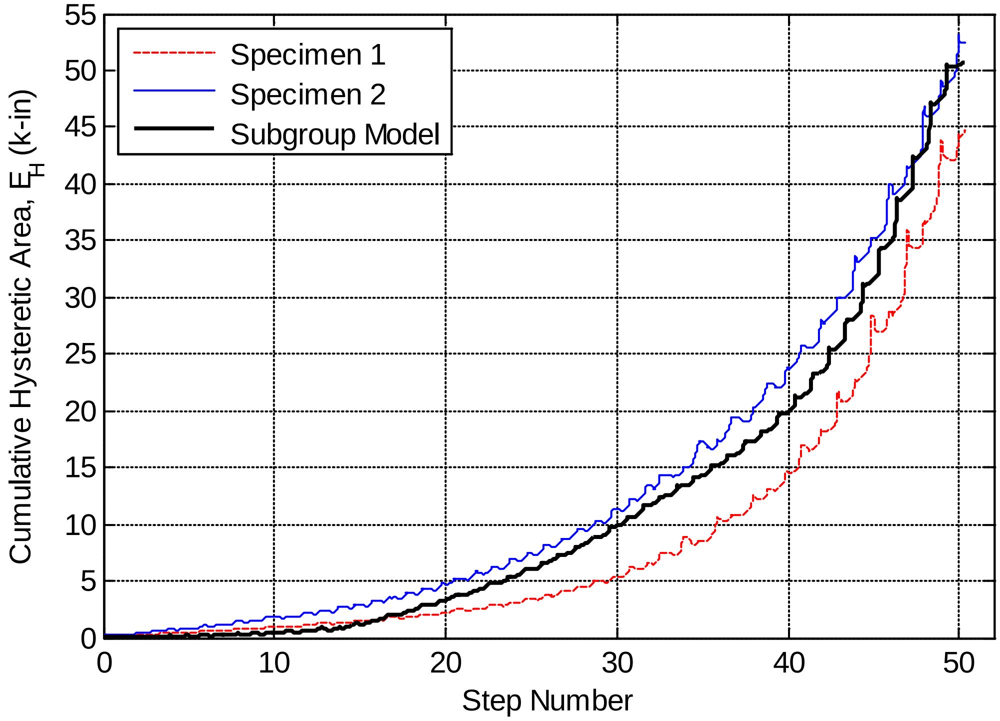

Figure 4-6 Comparison of the model hysteretic area to each of the specimen representing subgroup 1a.

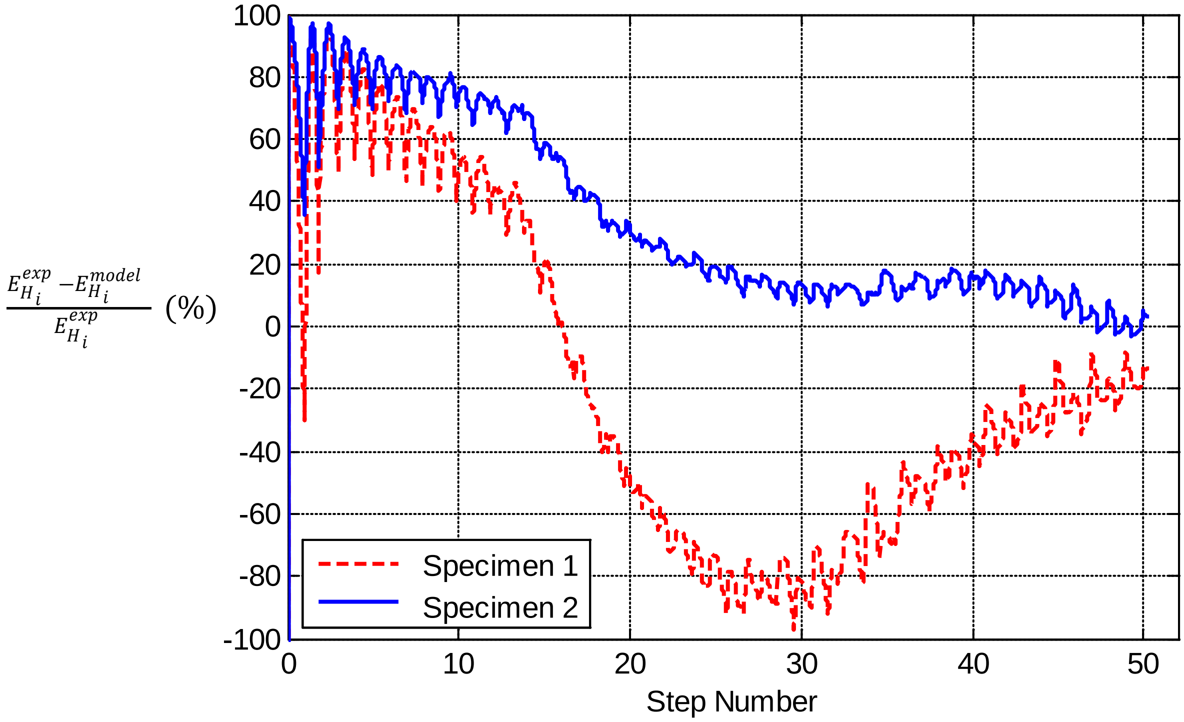

Figure 4-7 Percent error comparison showing the model hysteretic area to each of the specimens representing subgroup 1a.

4.1.2 Subgroup 1b Representative Model

The second subgroup described is subgroup 1b – commercial grade, fully connected specimens. Subgroup 1b is developed using the response of test specimens 4, 5, 6 and 8. Figure 4-8 demonstrates the average backbone calculation and the idealization of this backbone. Figure 4-9 shows the tangent stiffness of the average backbone, identifying the significant slope changes. After the backbone points are identified, the unload and reload parameters are determined such that the average hysteretic area between the experimental hysteretic energy average of the subgroup and its model are well matched (Figure 4-10).

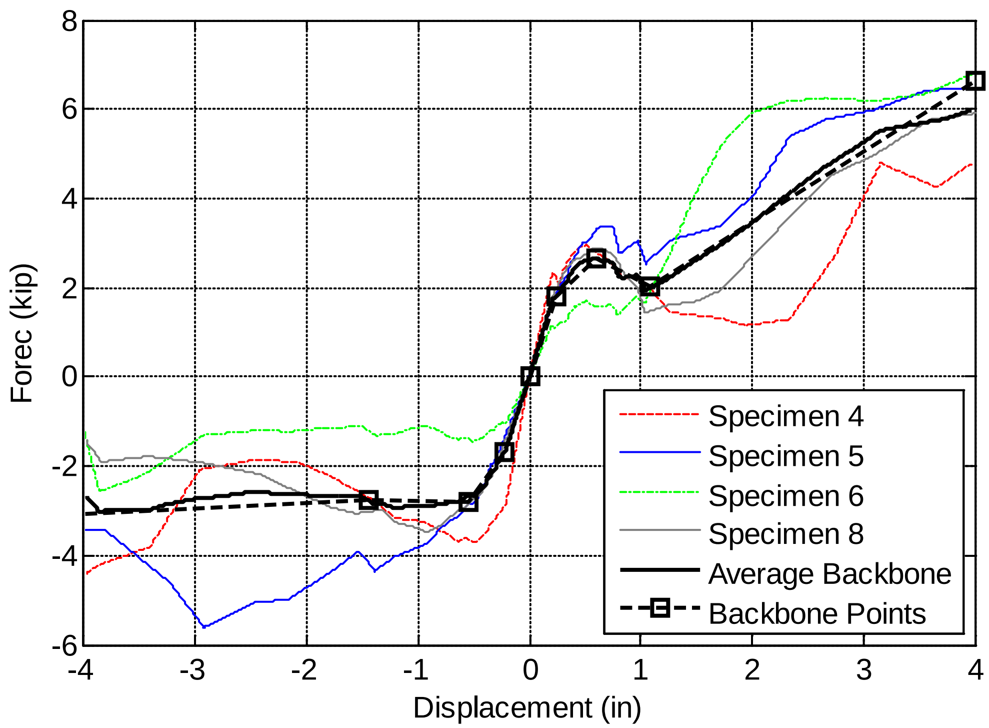

Figure 4-8 Specimen 4, 5, 6 and 8 backbone curves, average backbone and selected backbone points for subgroup 1b.

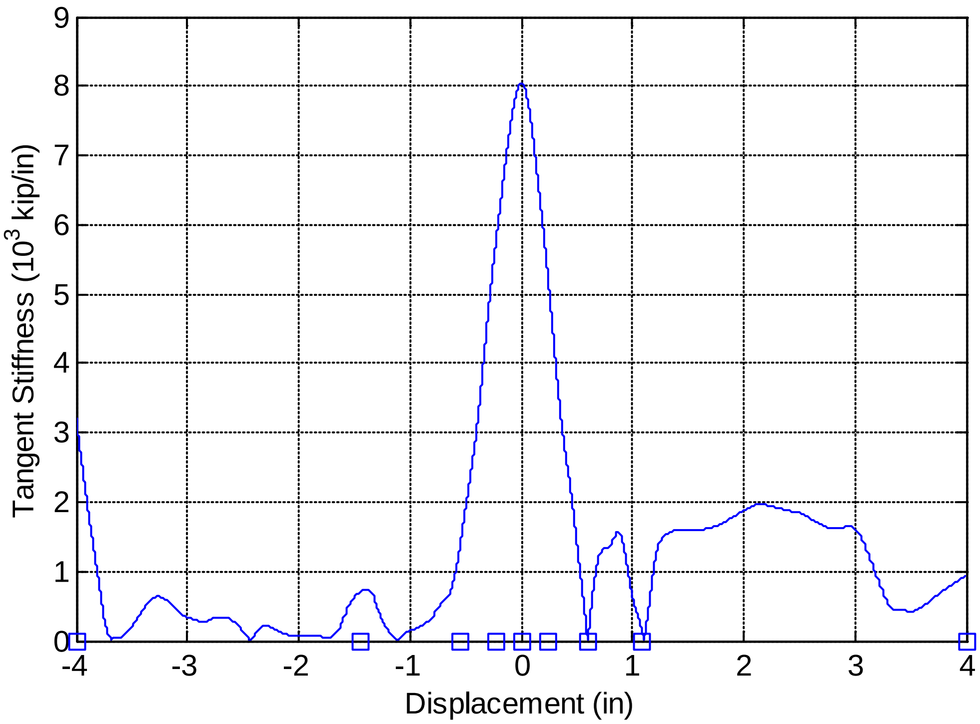

Figure 4-9 Tangent stiffness demonstrating sudden changes in the force-displacement backbone curve for subgroup 1b.

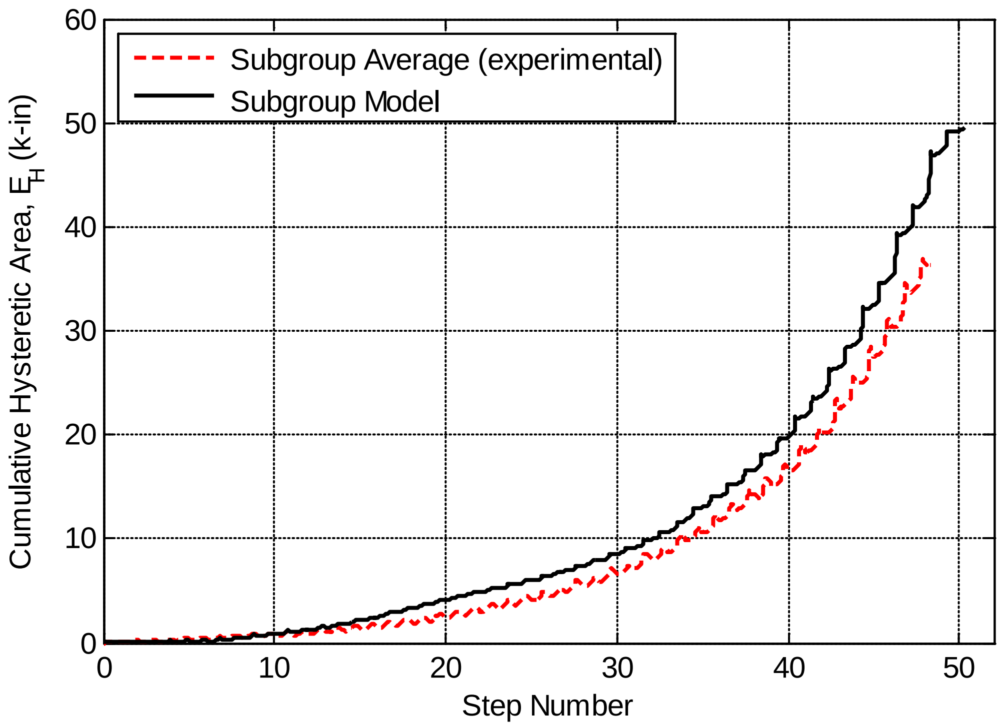

Figure 4-10 Hysteretic area calculated from the average experimental subgroup average (target) compared to the model hysteretic area for subgroup 1b.

To assess the robustness of the subgroup model, an individual comparison is made of the model to each of the specimens in the subgroup. Figure 4-11 through Figure 4-14 overlay the hysteretic behavior of the subgroup model to specimens 4, 5, 6 and 8 respectively. The model behaves as expected in terms of the hysteretic response, with some minor discrepancies associated with specimen-to-specimen variability. The second comparison for each specimen is the ability of the model to capture the hysteretic energy (Figures 4-15 and 4-16). As expected, the model is sought to capture the subgroup average, thus a specimen level differences exist. Figure 4-16 identifies the percent error of the hysteretic area. As in subgroup 1a, for subgroup 1b large variance exists in the hysteretic energy between specimens. Specimen 6 seemingly performs poorly when compared with the representative average model. This might be due to the fact that this specimen was a reused specimen. In other words, specimen 6 was subject to existing damage from an earlier experiment and consequently could not dissipate energy as well as a virgin un-damaged specimen.

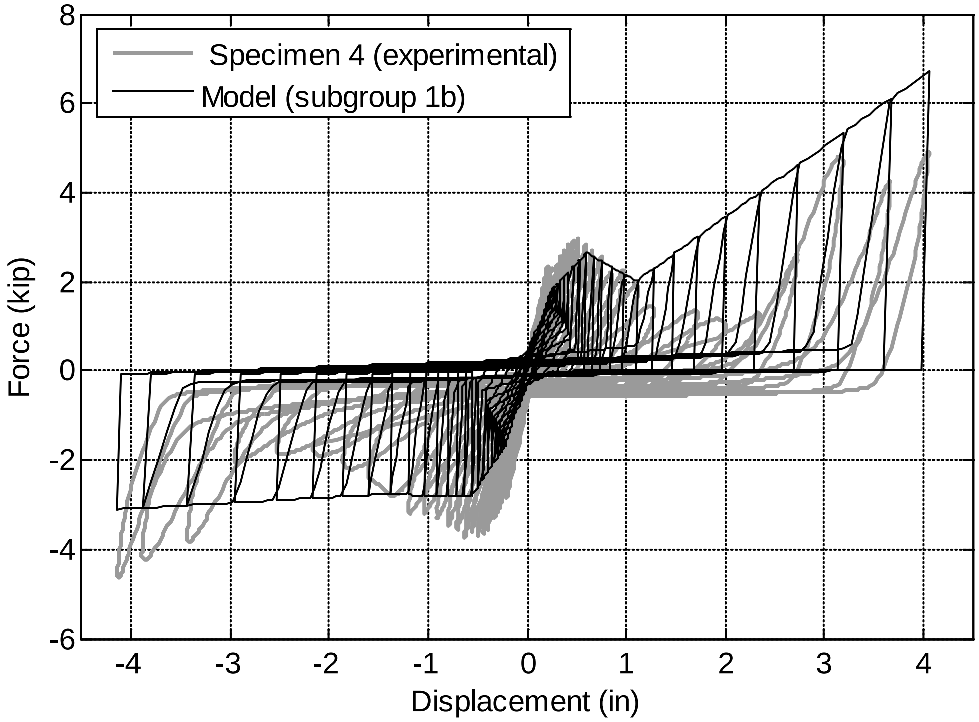

Figure 4-11 Hysteretic response of specimen 4 overlaid with the response of the representative subgroup model 1b.

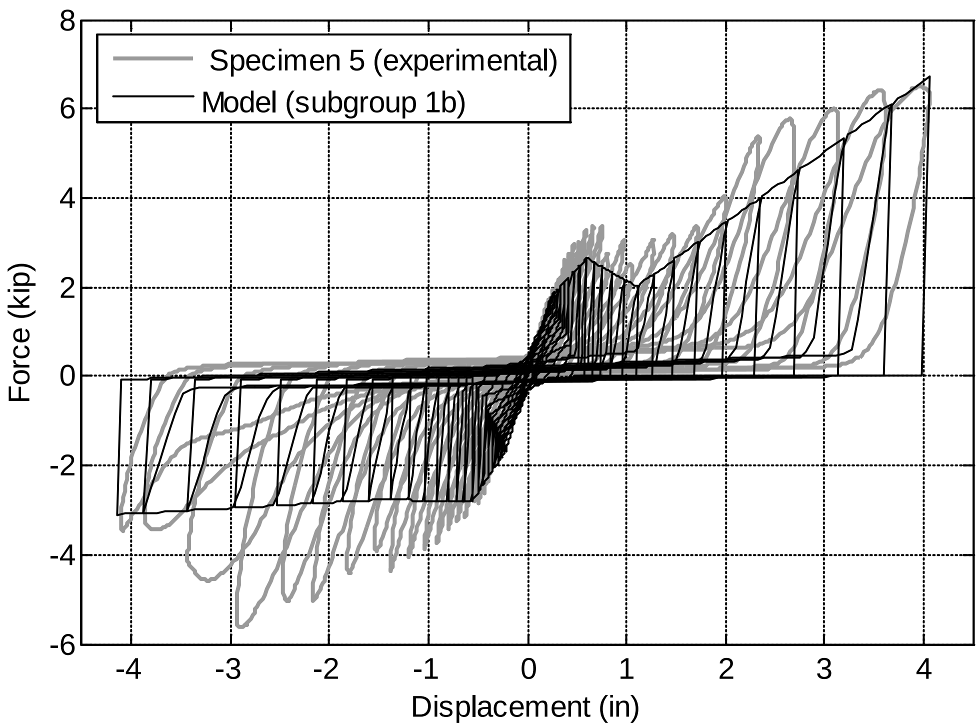

Figure 4-12 Hysteretic response of specimen 5 overlaid with the response of the representative subgroup model 1b.

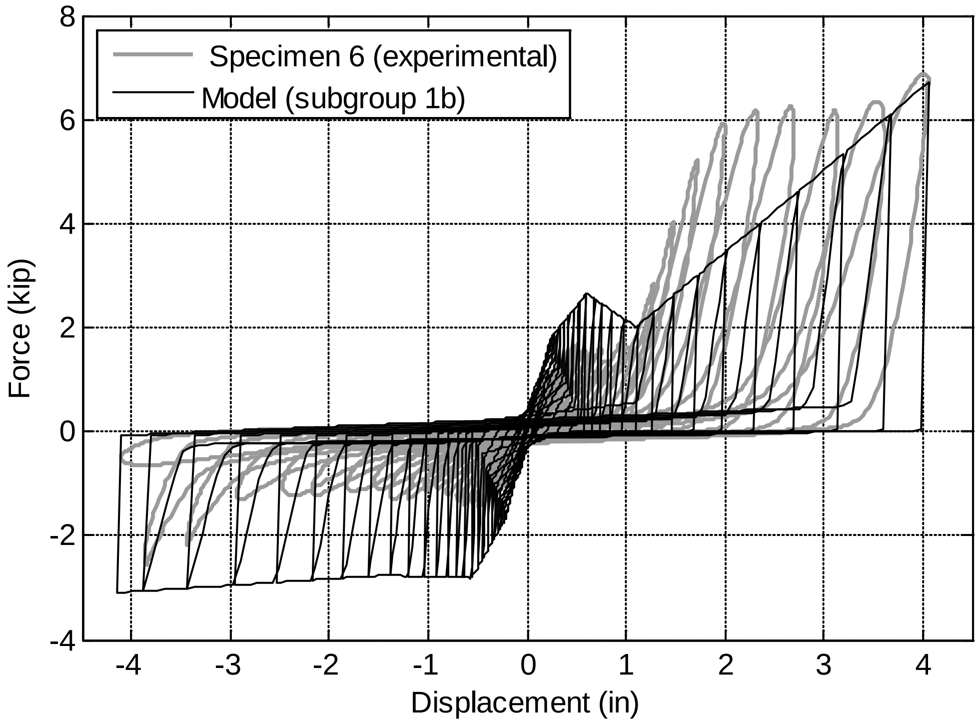

Figure 4-13 Hysteretic response of specimen 6 overlaid with the response of the representative subgroup model 1b.

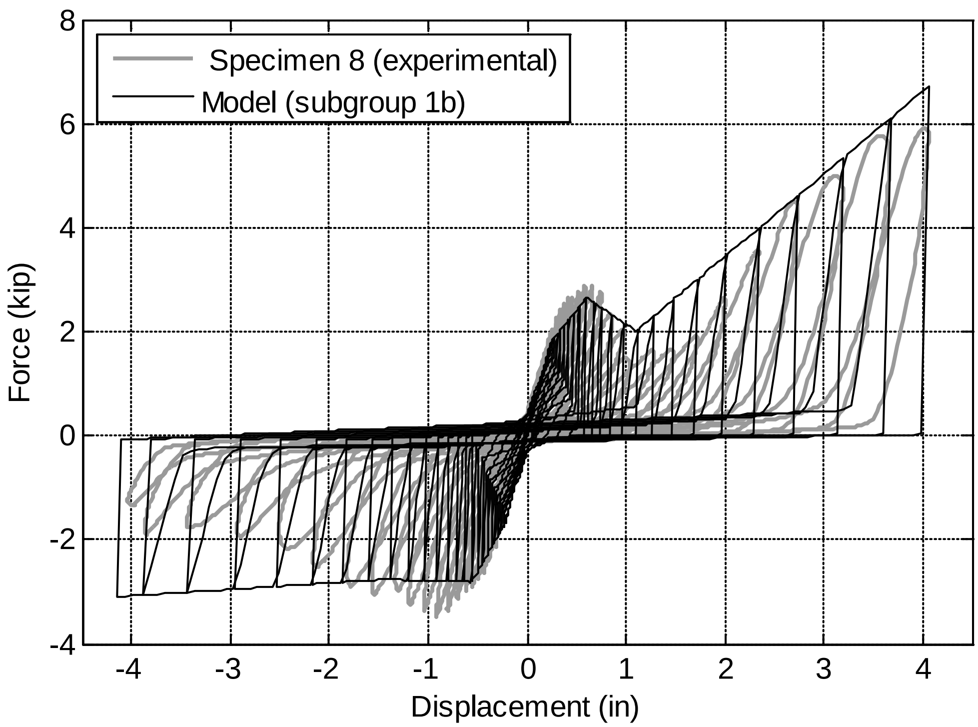

Figure 4-14 Hysteretic response of specimen 8 overlaid with the response of the representative subgroup model 1b.

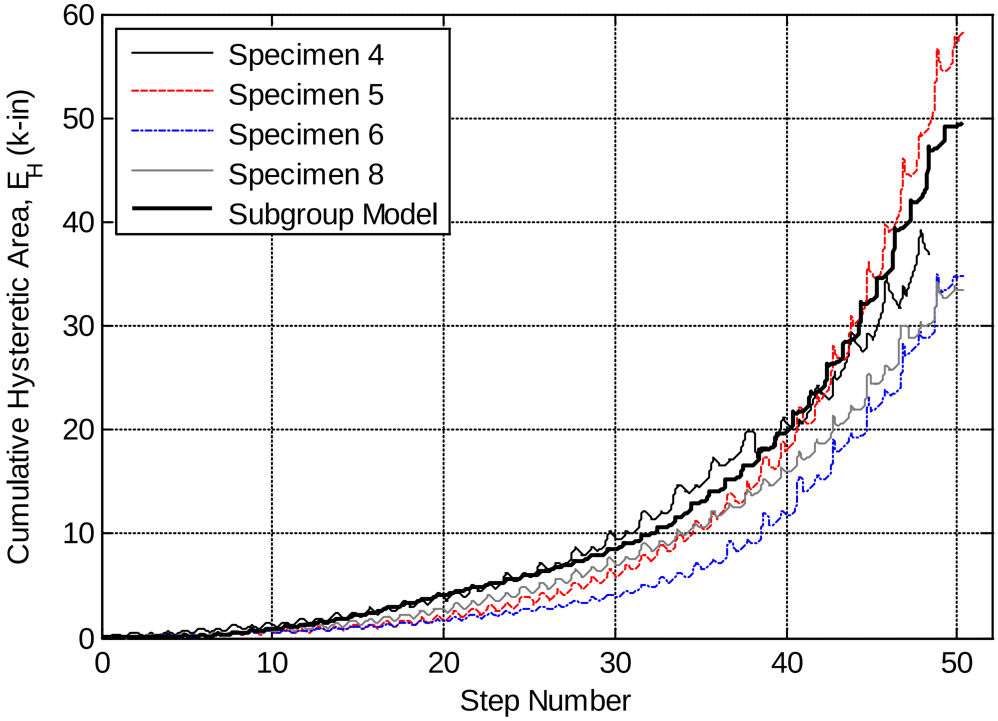

Figure 4-15 Comparison of the model hysteretic area to each of the specimen representing subgroup 1b.

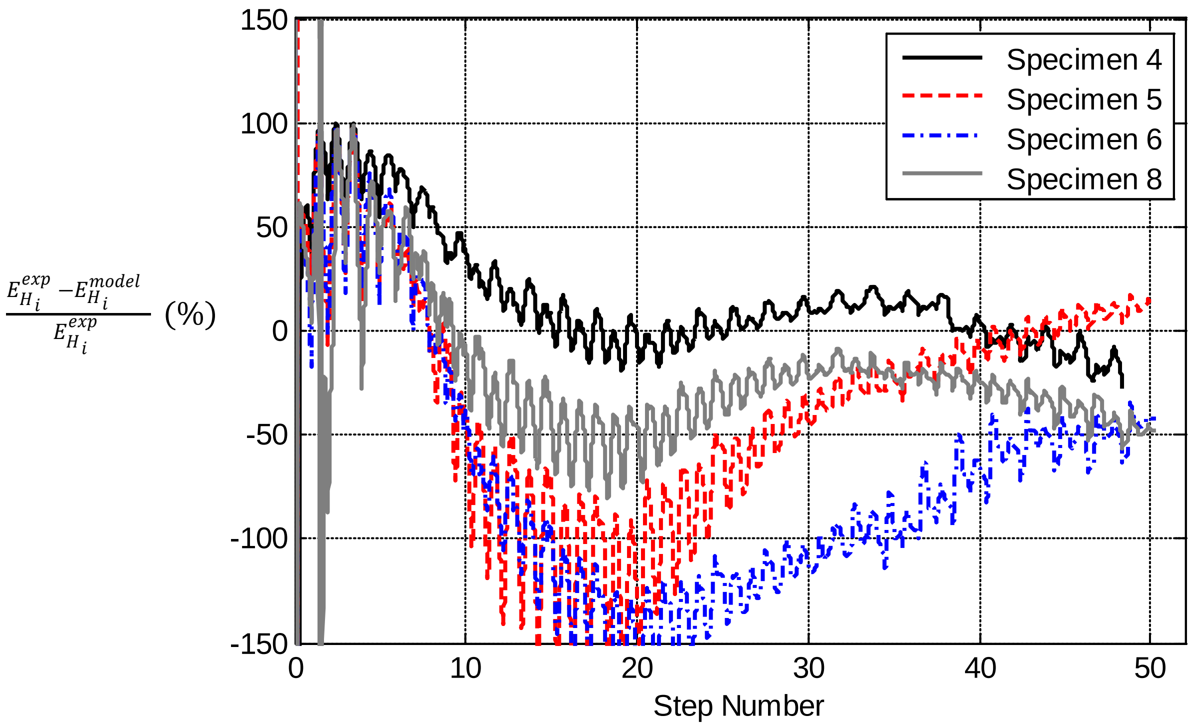

Figure 4-16 Percent error comparison showing the model hysteretic area to each of the specimens representing subgroup 1b.

4.1.3 Subgroup 2a Representative Model

The third subgroup described is subgroup 2a – institutional grade, partially connected specimens. Subgroup 2a is developed using the response of test specimens 20-22. Figure 4-17 demonstrates the average backbone calculation and the idealization of this backbone. Figure 4-18 shows the tangent stiffness of the average backbone, identifying the significant slope changes. After the backbone points are identified, the unload and reload parameters are determined such that the average hysteretic area between the experimental hysteretic energy average of the subgroup and its model are well matched (Figure 4-19).

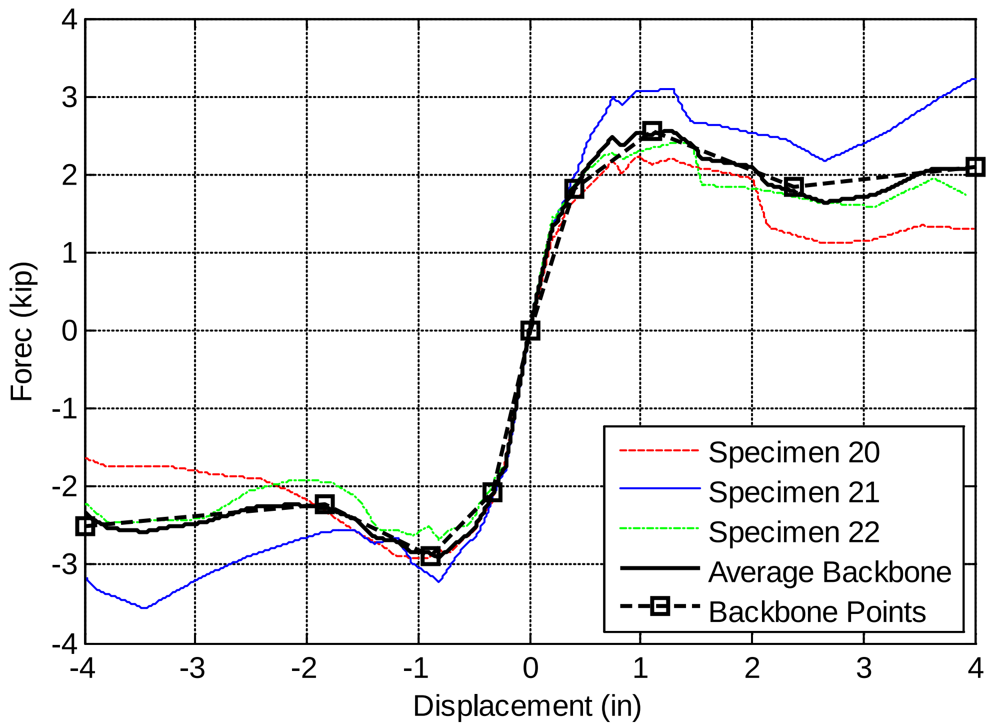

Figure 4-17 Specimen 20-22 backbone curves, average backbone and selected backbone points for subgroup 2a.

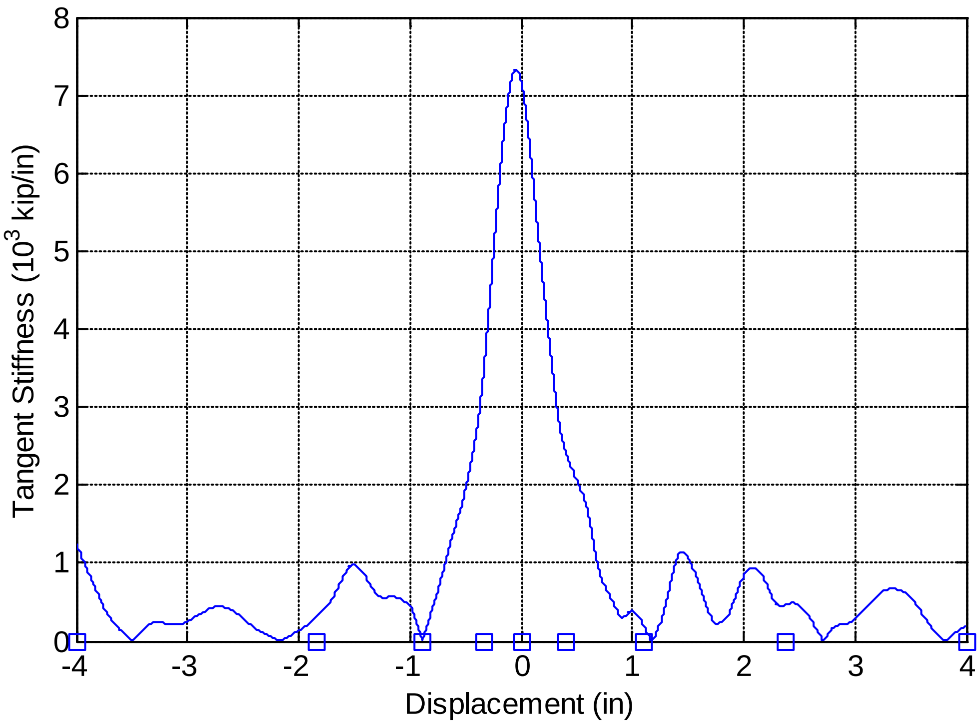

Figure 4-18 Tangent stiffness demonstrating sudden changes in the force-displacement backbone curve for subgroup 2a.

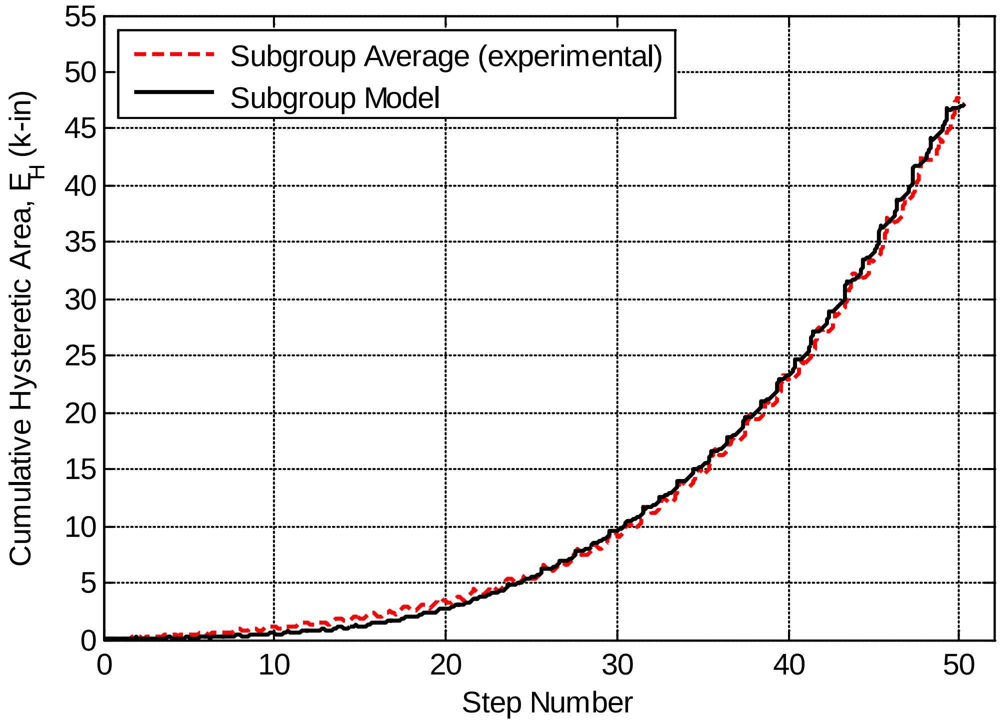

Figure 4-19 Hysteretic area calculated from the average experimental subgroup average (target) compared to the model hysteretic area for subgroup 2a.

To assess the robustness of the subgroup model, an individual comparison is made of the model to each of the specimens in the subgroup. Figure 4-20 through Figure 4-22 overlay the hysteretic behavior of the subgroup model to specimens 20-22, respectively. The model behaves as expected in terms of the hysteretic response, with some minor discrepancies associated with specimen-to-specimen variability between specimens. The second comparison for each specimen is the ability of the model to capture the hysteretic energy (Figures 4-23 and 4-24). As expected, the model is sought to capture the subgroup average, thus a specimen level differences exist. Figure 4-24 identifies the percent error of the hysteretic area with an overall percent error, where a large variance exists in the hysteretic energy between specimens.

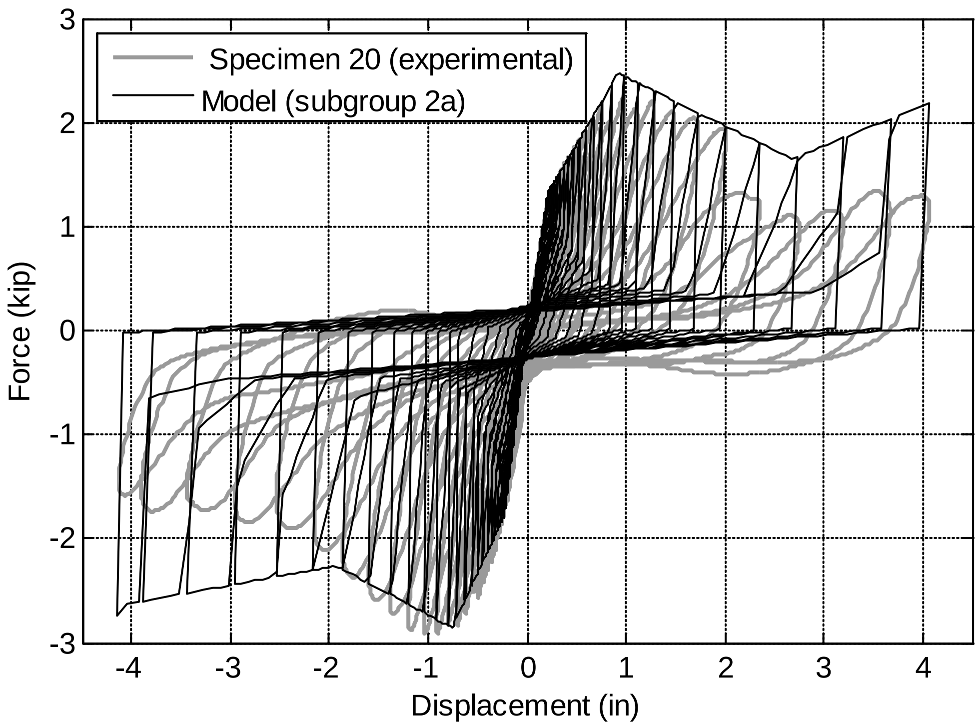

Figure 4-20 Hysteretic response of specimen 20 overlaid with the response of the representative subgroup model 2a.

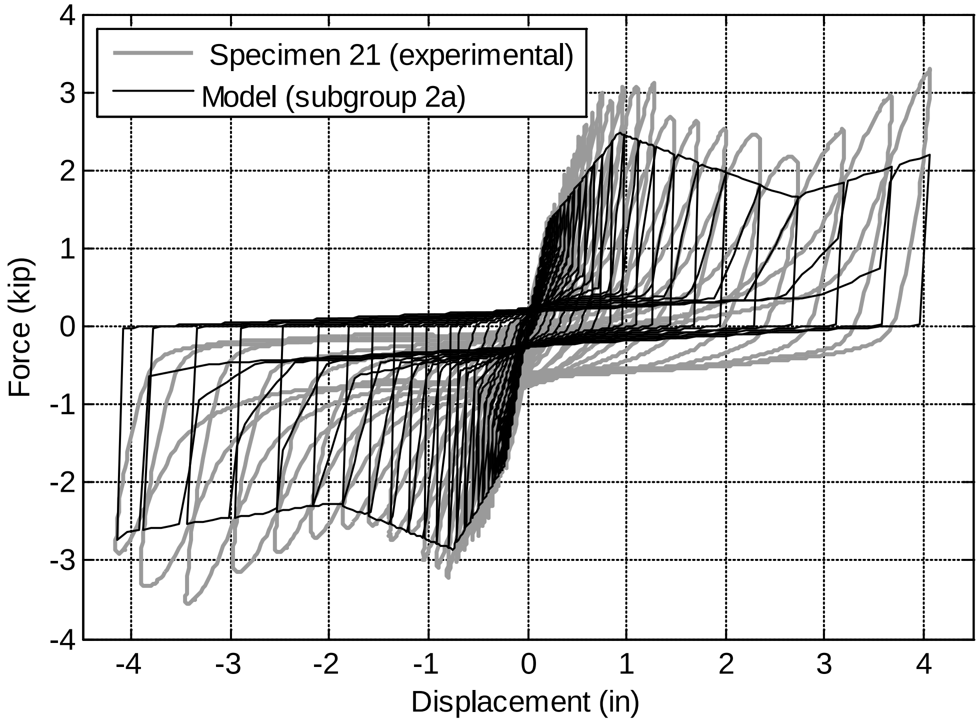

Figure 4-21 Hysteretic response of specimen 21 overlaid with the response of the representative subgroup model 2a.

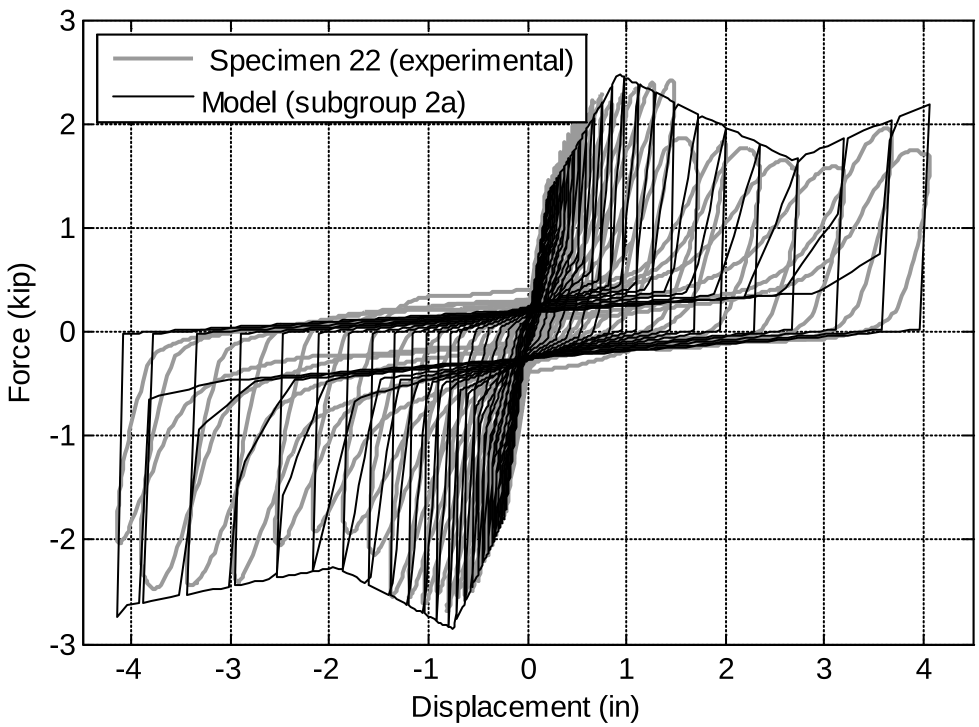

Figure 4-22 Hysteretic response of specimen 22 overlaid with the response of the representative subgroup model 2a.

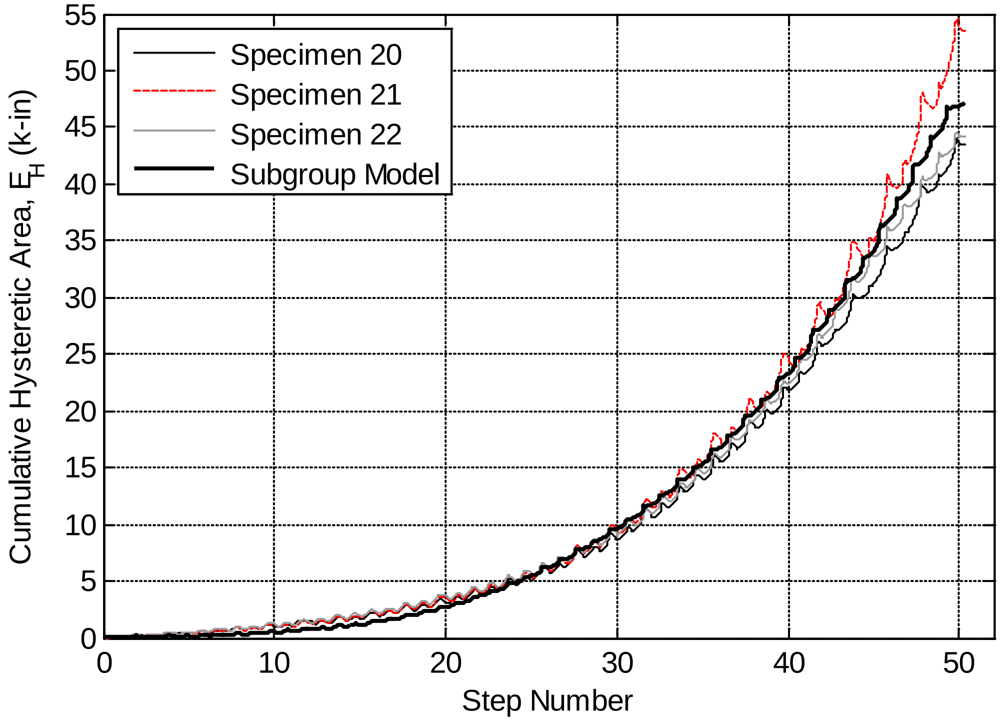

Figure 4-23 Comparison of the model hysteretic area to each of the specimen representing subgroup 2a.

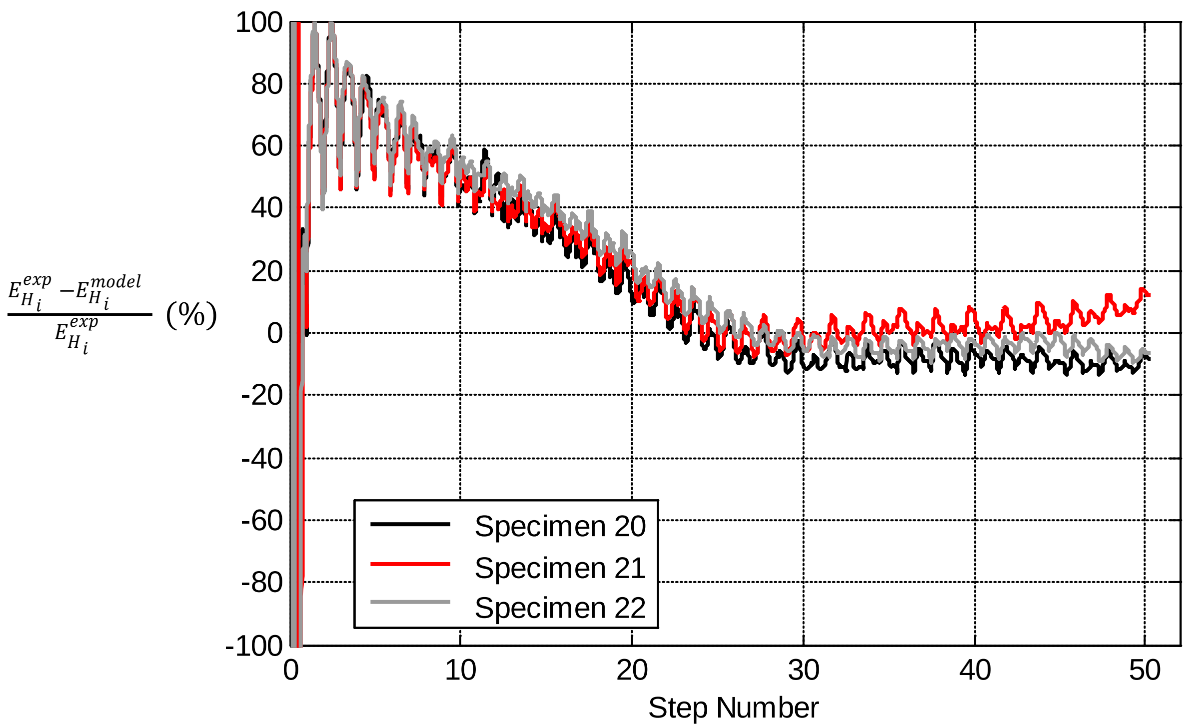

Figure 4-24 Percent error comparison showing the model hysteretic area to each of the specimens representing subgroup 2a.

4.1.4 Subgroup 2b Representative Model

The last subgroup described is subgroup 2b – institutional grade, fully connected specimens. Subgroup 2b is developed using the response of test specimens 23-28. Figure 4-25 demonstrates the average backbone calculation and the idealization of this backbone. Figure 4-26 shows the tangent stiffness of the average backbone, identifying the significant slope changes. After the backbone points are identified, the unload and reload parameters are determined such that the average hysteretic area between the experimental hysteretic energy average of the subgroup and its model are well matched (Figure 4-27).

To assess the robustness of the subgroup model, an individual comparison is made of the model to each of the specimens in the subgroup. Figure 4-28 through Figure 4-33 overlay the hysteretic behavior of the subgroup model to specimens 23-28, respectively. The model behaves as expected in terms of the hysteretic response, with some minor discrepancies associated with specimen-to-specimen variability between specimens. The second comparison for each specimen is the ability of the model to capture the hysteretic energy (Figures 4-34 through 4-36). As expected, the model is sought to capture the subgroup average, thus a specimen level differences exist. Figures 4-35 and 4-36 identify the percent error of the hysteretic area with a percent error within 2% after the first 10 cycles (20 steps). The first few cycle steps experience large spikes in the percent error associated with the small denominators, particularly in specimens 23, 26 and 28. This is due to the specimen-to-specimen variability in which these specimens have lower hysteretic energies than compared to the average response. However after the first few excursions, the model rebounds and the hysteretic area percent area behaves better despite the large variance that exists in hysteretic energy between specimens.

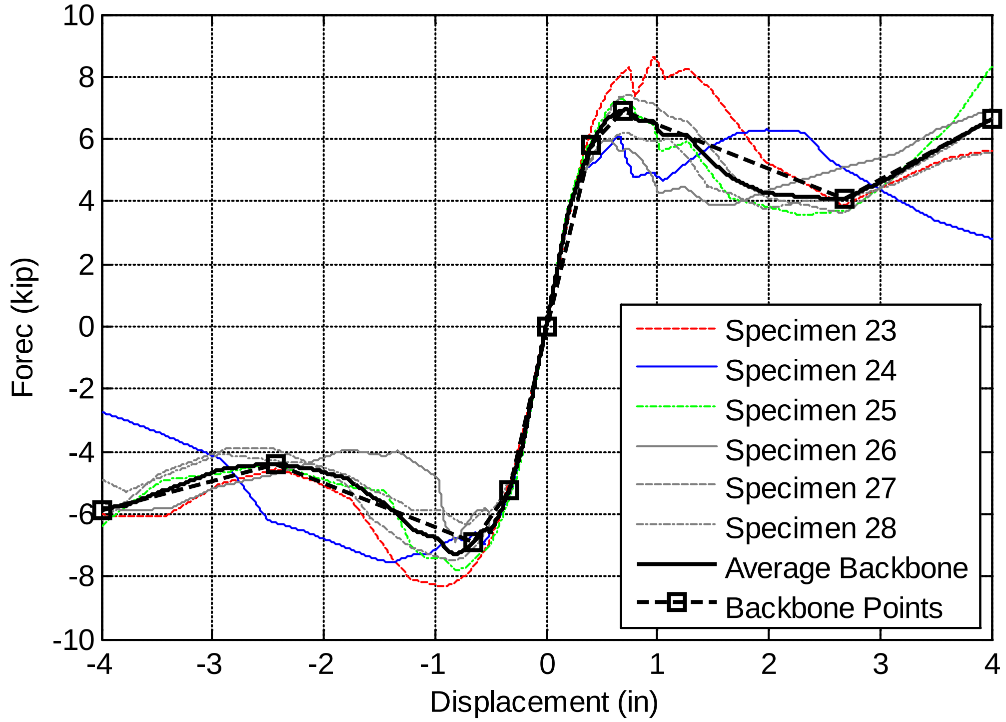

Figure 4-25 Specimen 23-28 backbone curves, average backbone and selected backbone points for subgroup 2b.

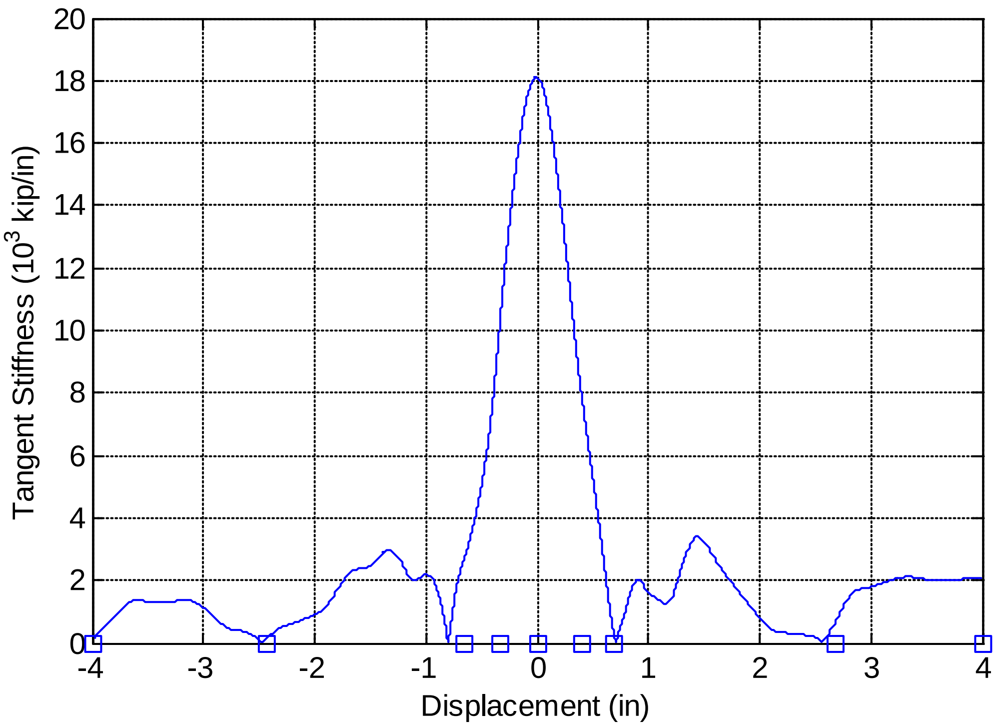

Figure 4-26 Tangent stiffness demonstrating sudden changes in the force-displacement backbone curve for subgroup 2b.

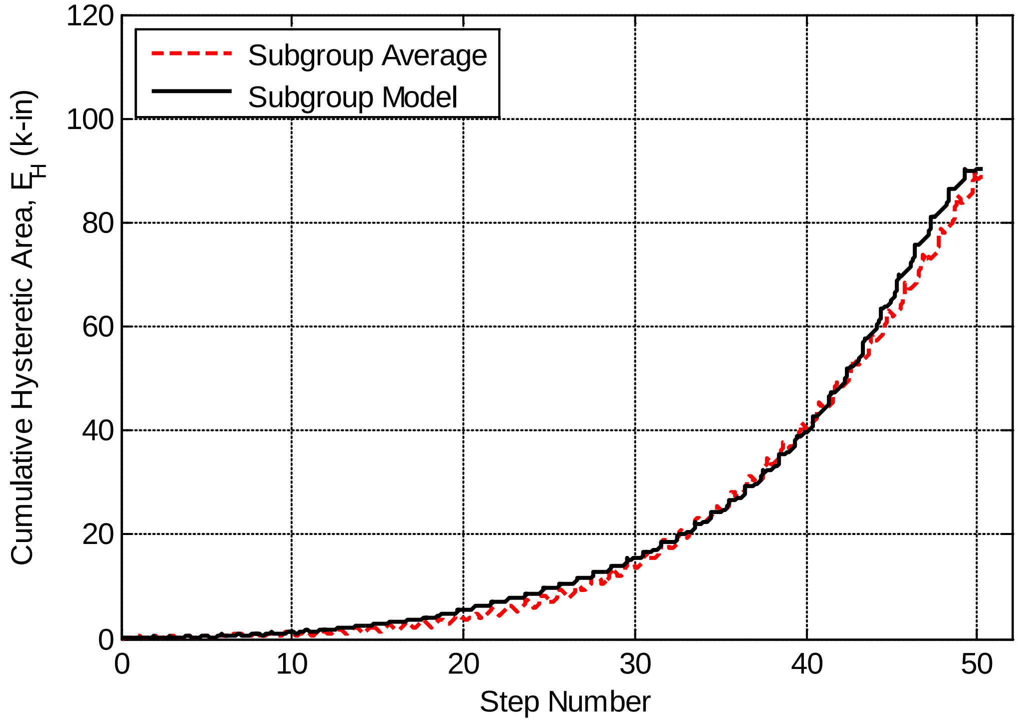

Figure 4-27 Hysteretic area calculated from the average experimental subgroup average (target) compared to the model hysteretic area for subgroup 2b.

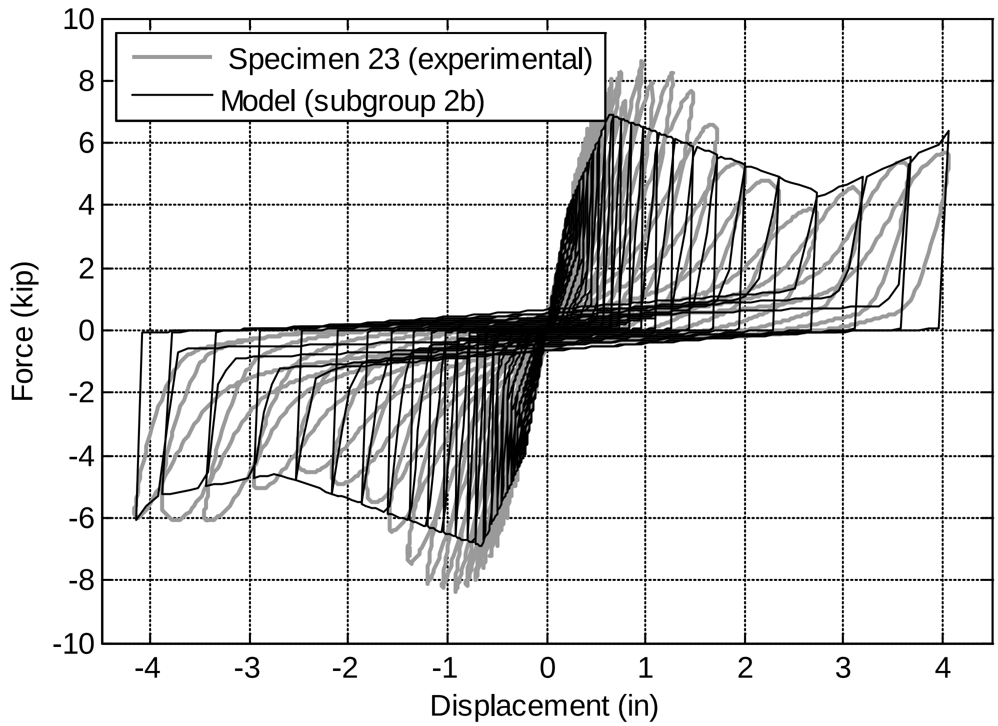

Figure 4-28 Hysteretic response of specimen 23 overlaid with the response of the representative subgroup model 2b.

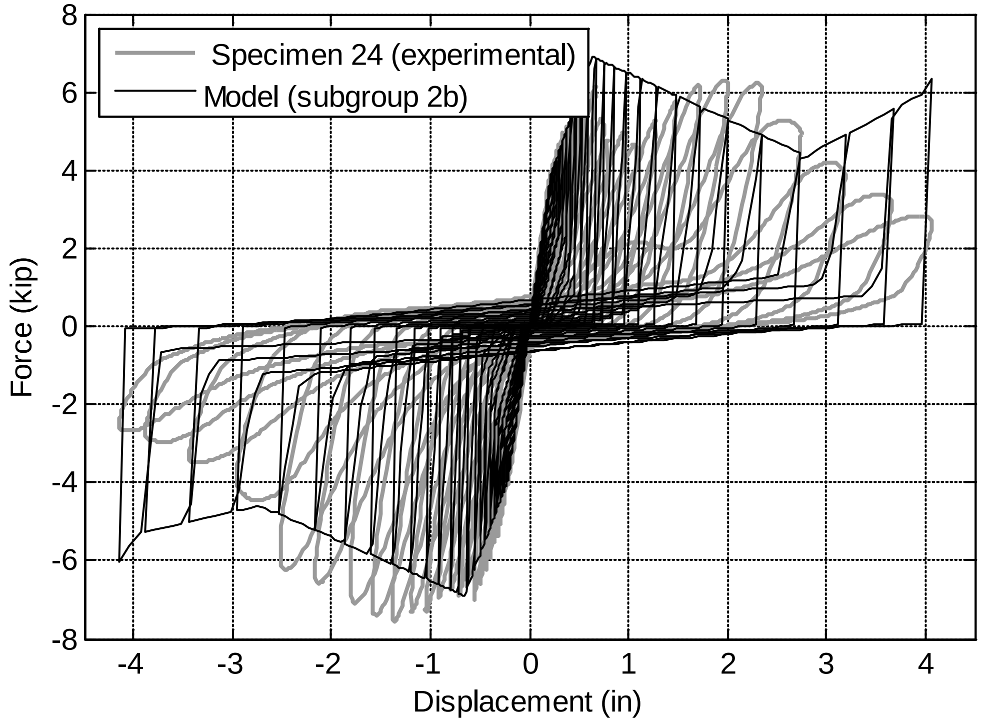

Figure 4-29 Hysteretic response of specimen 24 overlaid with the response of the representative subgroup model 2b.

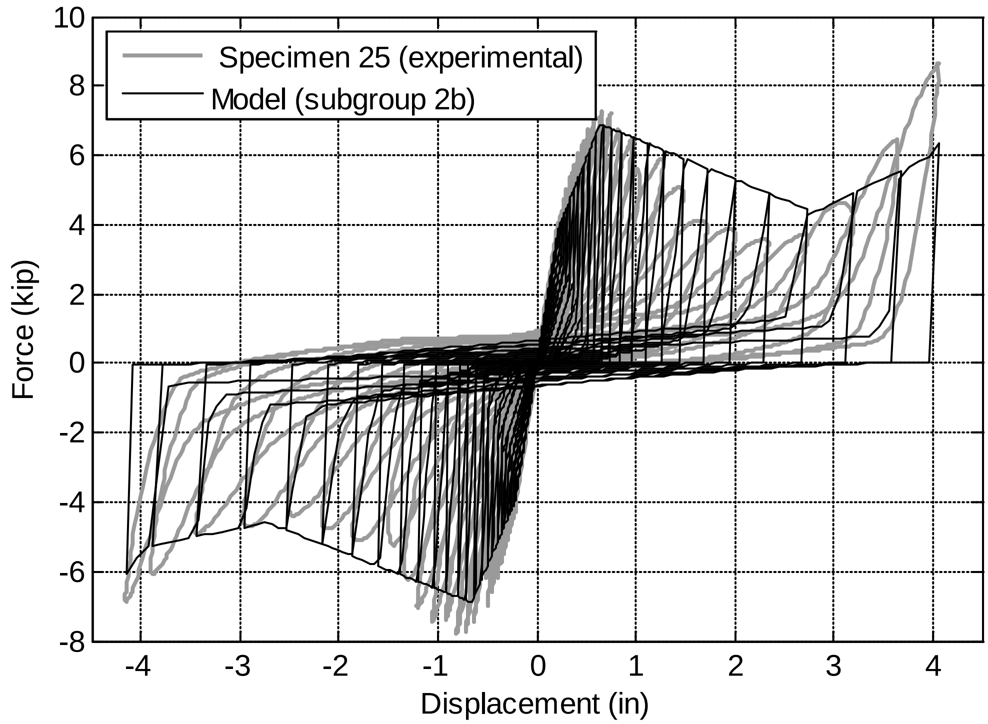

Figure 4-30 Hysteretic response of specimen 25 overlaid with the response of the representative subgroup model 2b.

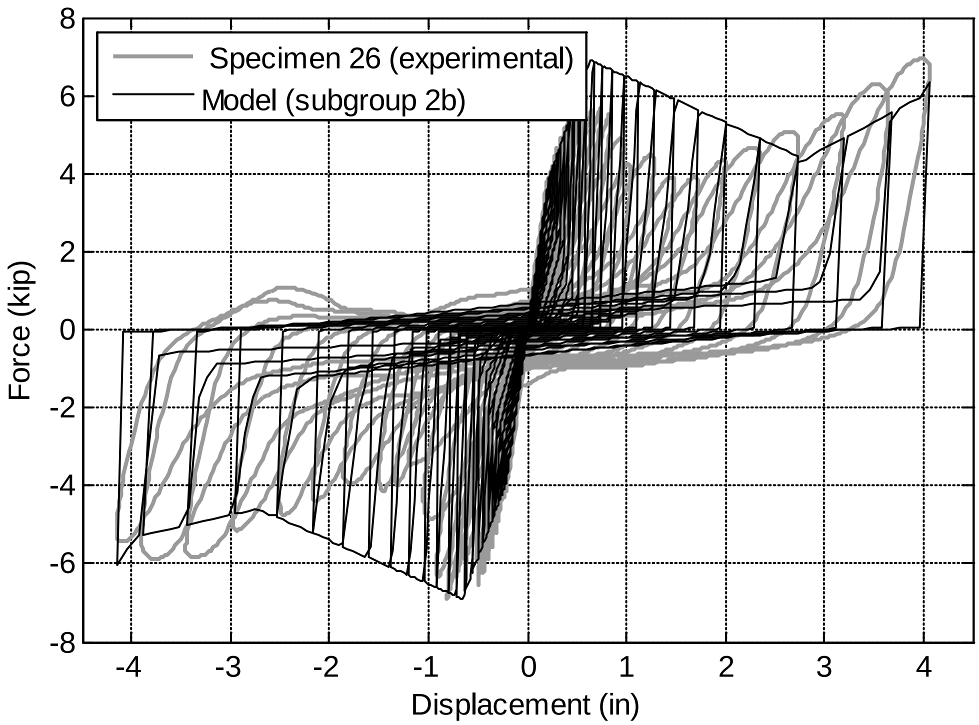

Figure 4-31 Hysteretic response of specimen 26 overlaid with the response of the representative subgroup model 2b.

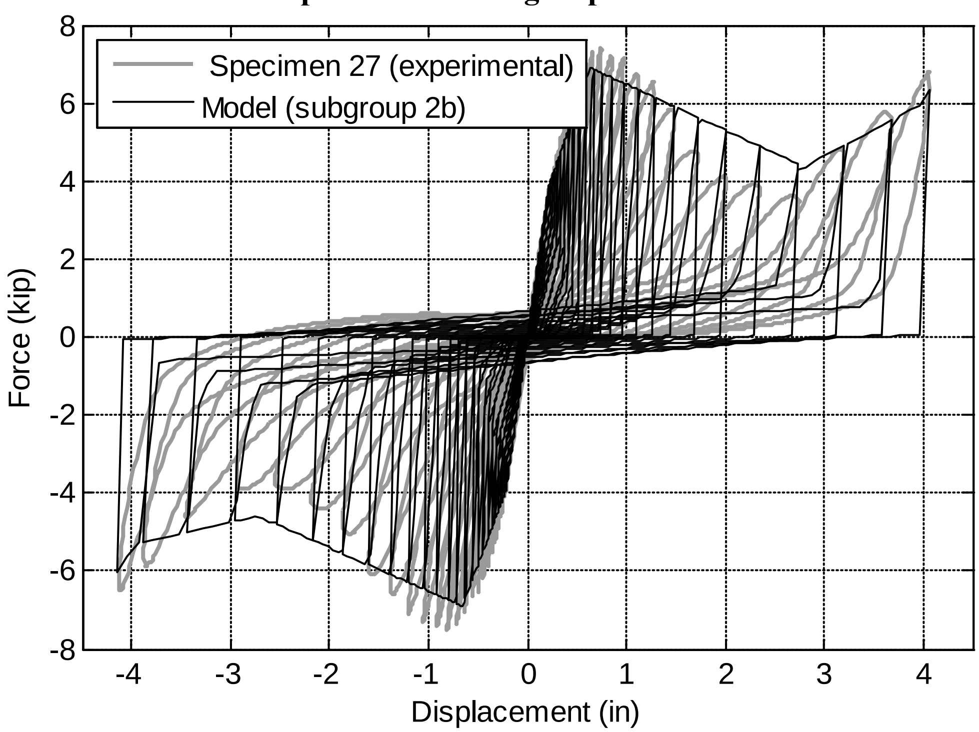

Figure 4-32 Hysteretic response of specimen 27 overlaid with the response of the representative subgroup model 2b.

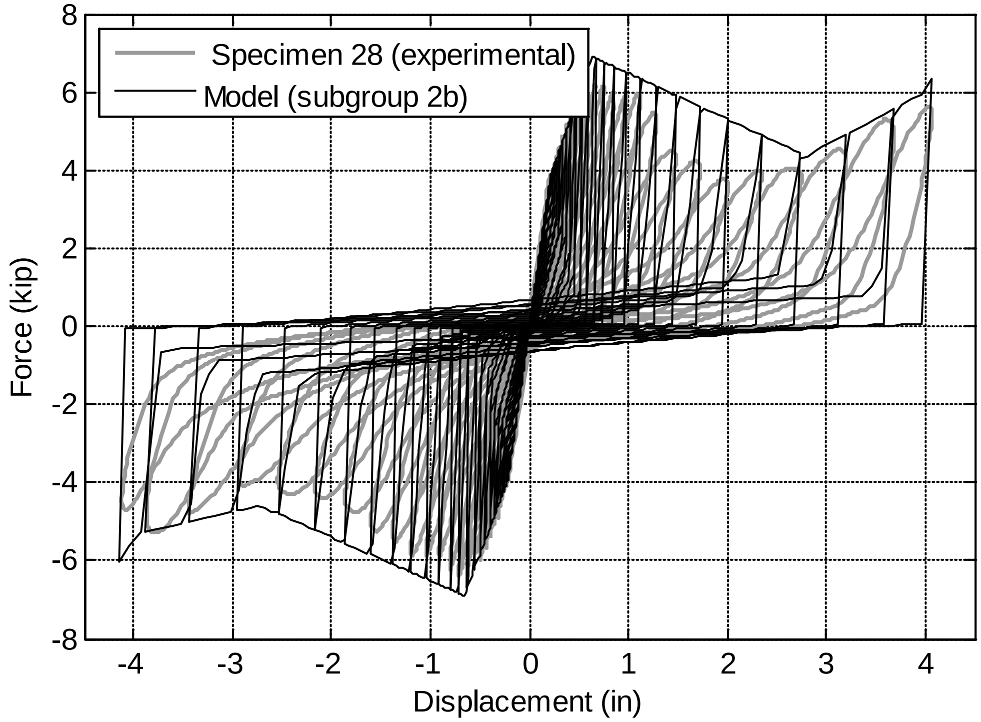

Figure 4-33 Hysteretic response of specimen 28 overlaid with the response of the representative subgroup model 2b.

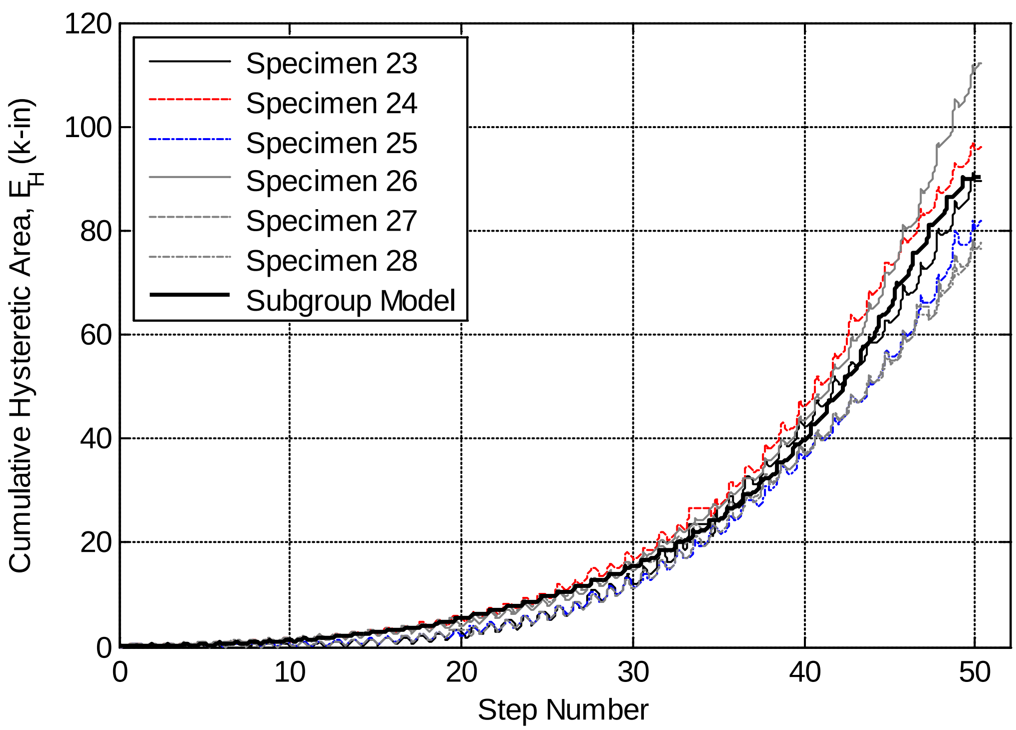

Figure 4-34 Comparison of the model hysteretic area to each of the specimen representing subgroup 2b.

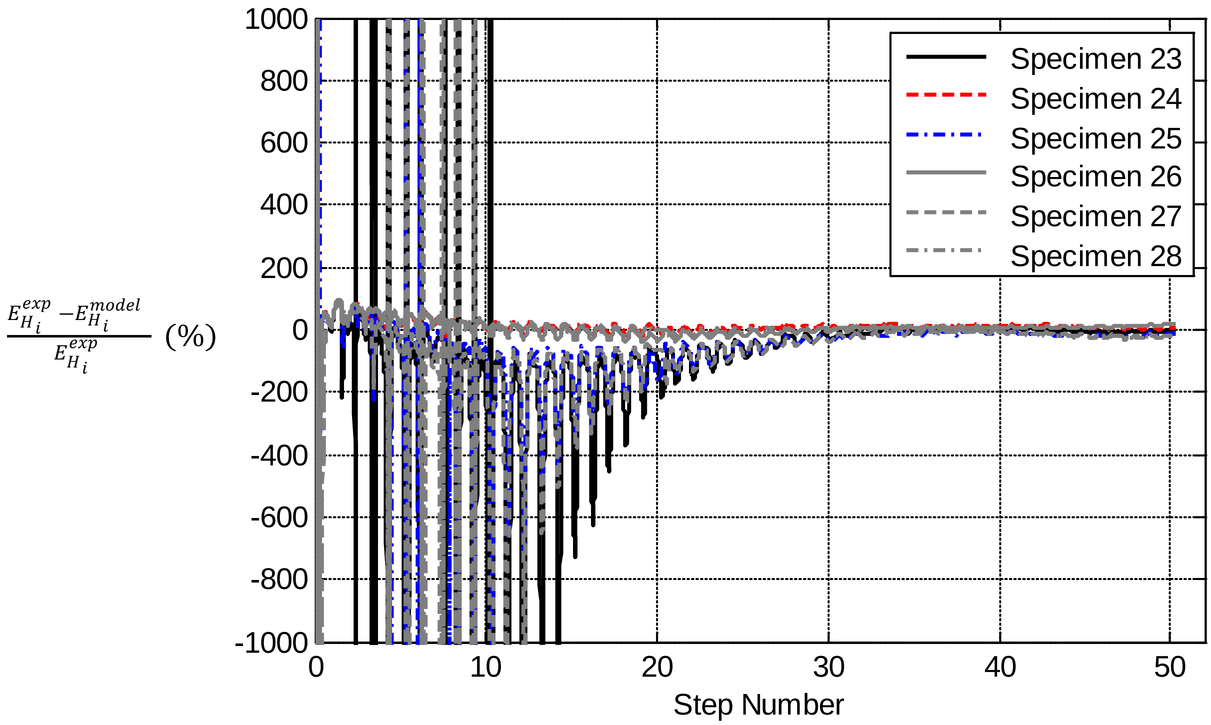

Figure 4-35 Percent error comparison showing the model hysteretic area to each of the specimens representing subgroup 2b.

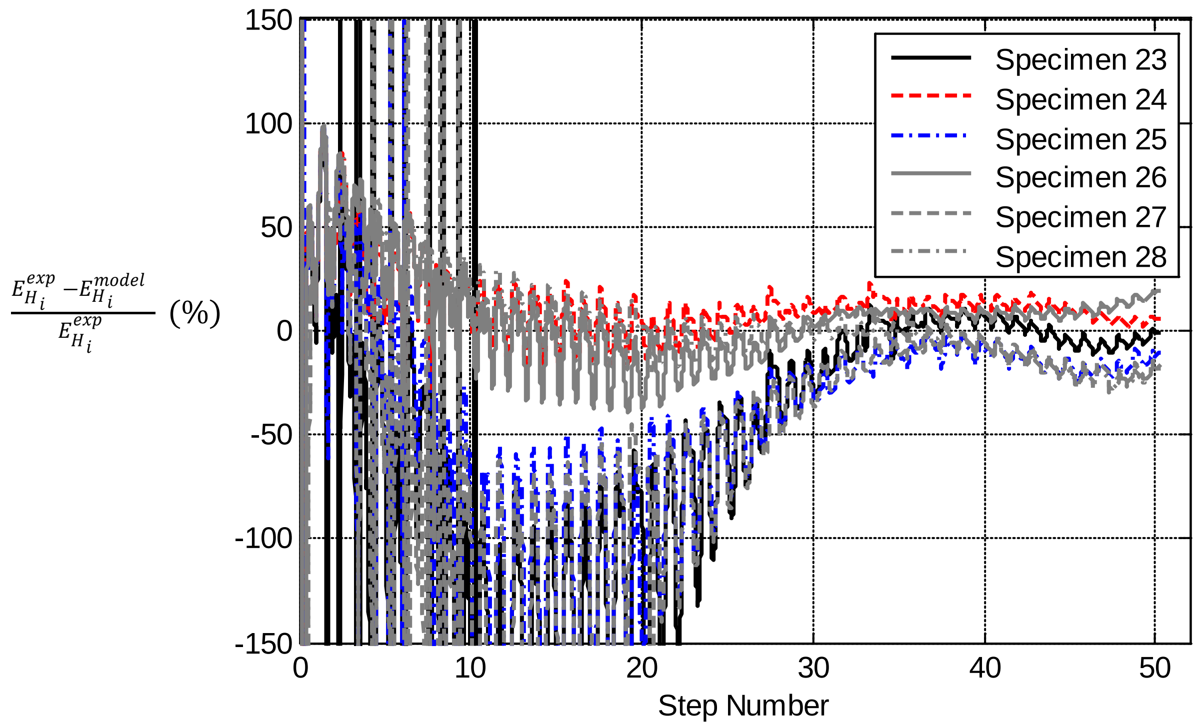

Figure 4-36 Percent error comparison showing the model hysteretic area to each of the specimens representing subgroup 2b (clipped y-axis).

4.2 Subgroup Model Discussion

In the development of the four representative subgroup models, a comparison is made between the groups. First, the subgroup backbones are compared in Table 4-1 and Figure 4-37. In this figure, subgroups 1a, 1b and 2a are somewhat similar in their force-displacement characteristics. However subgroup 2b stands out as the strongest and stiffest type of wall subsystem. One reason subgroup 2b is the strongest and stiffest wall is related to the institutional installation details and the thicker vertical studs used. One may also note to that subgroups 1a, 1b and 2b exhibit a post-peak hardening at around 1% drift (in general). This may be attributed to closure of a gap between the wall and the top track. This behavior is not significantly noted in the response of specimens within subgroup 2a, moreover it is less pronounced in the negative drift direction of subgroup 1b. The second comparison between the representative subgroup models lies within the calibrated unload and reload parameters, highlighted in Figure 4-38. Figures 4-39 and 4-40 identify the numerical values (ratio values) calibrated for force and displacement parameters, respectively. Considerable variability exists when comparing the numerical value of a given parameter for the various subgroups. One notes that the largest variation for the subgroup type is within the displacement and force parameter which controlls the pre-peak behavior, relating to the initial stiffness of the various subgroups as well. When connection detailing, subgroup 1a to 2a and 1b to 2b, the relationship is strong for the full connection specimens, this is perhaps due to more uniform detailing techniques.

Backbone response for subgroups 1a, 1b, 2a and 2b are created using data from two, four, three and six specimens, respectively. With the number of specimens at most under six per subgroup, a variability assessment is difficult to justify due to the low specimen count. Therefore, only the mean (average) response is characterized. In the next section, a normalized approach is adopted with the goal of capturing the variability inherent in the partition wall response.

Table 4-1 Parameters for the subgroup models.

Model	Backbone Points					Unload/Reload	
		Disp (in)	Force (kip)	Disp (in)	Force (kip)	Force	Disp
1a	1	0.204	1.270	-0.214	-1.328	0.70	0.10
	2	1.196	1.680	-0.549	-1.770	0.10	0.70
	3	1.695	1.538	-1.572	-2.218	0.15	0.90
	4	4.000	6.650	-4.000	-5.060	0.08	0.93
1b	1	0.237	1.790	-0.216	-1.666	0.55	0.30
	2	0.599	2.645	-0.555	-2.810	0.06	0.92
	3	1.098	2.008	-1.451	-2.756	0.09	0.86
	4	4.000	6.620	-4.000	-3.080	0.08	0.90
2a	1	0.400	1.810	-0.356	-2.060	0.18	0.40
	2	1.100	2.550	-0.930	-2.900	0.18	0.85
	3	2.370	1.840	-1.984	-2.220	0.20	0.80
	4	4.000	2.100	-4.000	-2.510	0.20	0.99
2b	1	0.412	5.807	-0.336	-5.265	0.15	0.40
	2	0.694	6.912	-0.650	-6.900	0.01	0.90
	3	2.676	4.080	-2.433	-4.389	0.15	0.55
	4	4.000	6.650	-4.000	-5.850	0.01	0.99

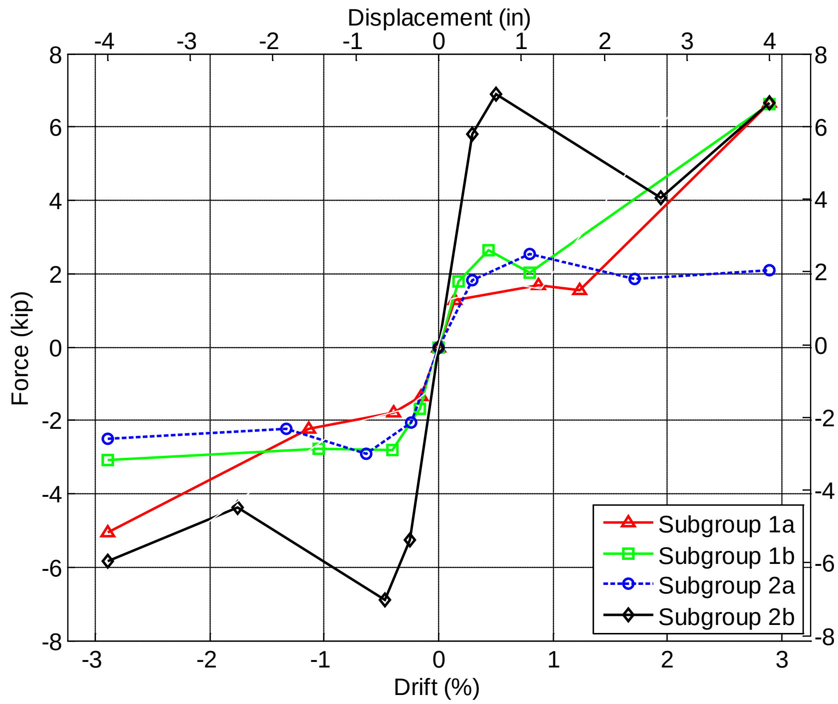

Figure 4-37 Overlay of each subgroup backbones shown demonstrating a large variability.

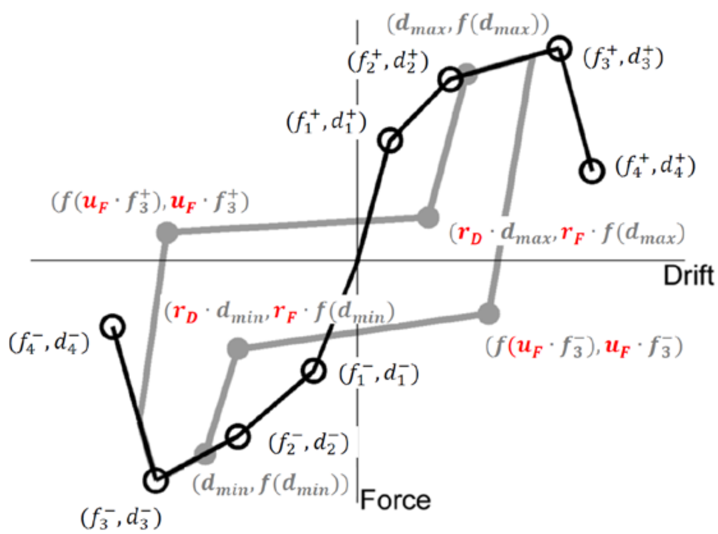

Figure 4-38 Unloading and reloading parameters (highlighted in red) within one element of the four parallel material model formulation.

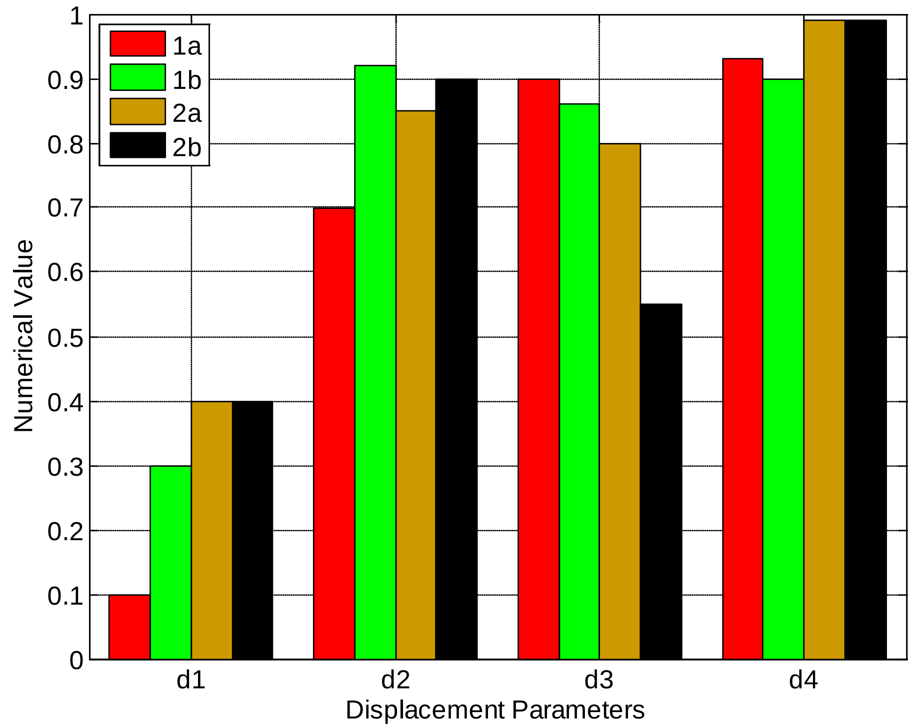

Figure 4-39 Displacement parameters for each of the parallel materials for each subgroup.

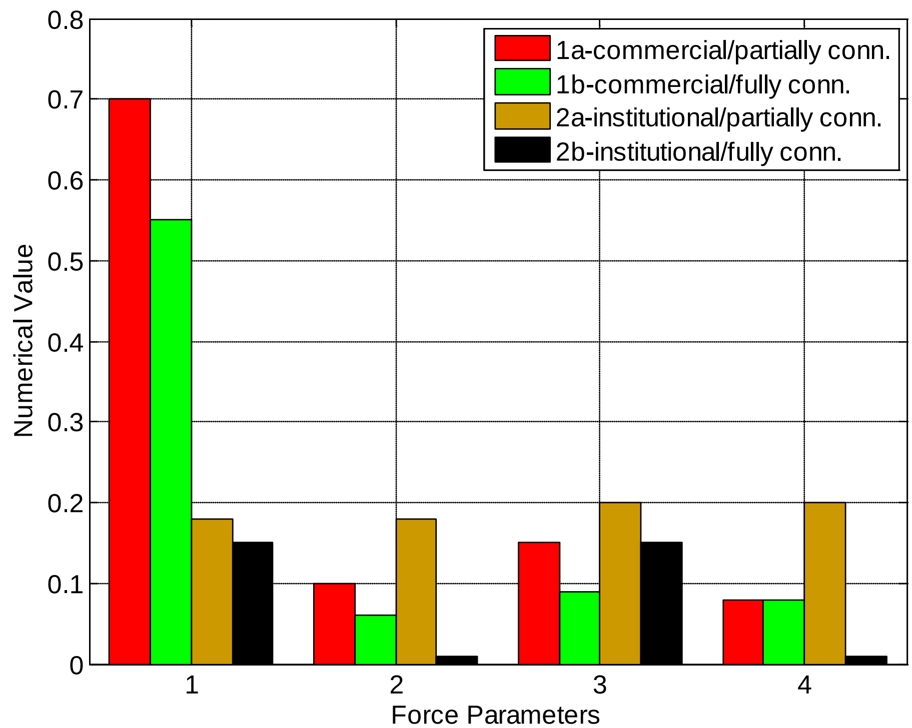

Figure 4-40 Force parameters for each parallel materials used for each subgroup.

SECTION 5
NORMALIZED MODELS

5.1 Introduction

To further simplify the modeling approach, subgroups 1b and 2b are combined and used to develop the normalized models. These subgroups involved only the fully connected specimens. Subgroups 1a and 2a, partially connected specimens, are not considered for the normalized models due to different failure mechanisms developed during testing. Namely, since the gypsum board was not connected to the top track resulting in damage primarily in the return walls. One may note that the strength of the walls in subgroup 2b is much greater than that for walls in subgroup 1b (Figure 4-37). For this reason, wall strength is normalized and hence removed as a variable in the following analyses. By characterizing a normalized model, the analyst need only provide wall length and building occupancy (commercial or institutional). With knowledge of the building occupancy, the selected wall stud type and spacing will dictate the performance of the wall, by characterization into the respective subgroup.

5.2 Force Normalization

Using the plan details of each wall specimen, the sum of the thickness of the stud webs in the in-plane direction, denoted as Σt_{stud} is calculated. The actual value used for the thickness of the studs is the minimum required thickness as determined by the manufacturing standards. The commercial studs are SSMA 350S123-18, which corresponds to a stud thickness of 18 mil with a design thickness of 0.0188 inches. The institutional studs are SSMA 350S125-30 which corresponds to a stud thickness of 30 mil with a design thickness of 0.0312 inches (S,SMA, 2010). Seven studs were used for the commercial configuration resulting in a total thickness of 0.1316 inches, while 10 studs were used in the institutional configuration for a total thickness of 0.3120 inches. In Figure 5-1, the backbones are repeated prior to normalization. In this figure, it is clearly visible that the institutional specimens are stiffer and stronger than those of the commercial specimens. By normalizing the force at each displacement by the sum of the stud thickness Σt_{stud}, the backbones collapse to a similar range as shown in Figure 5-2. After the normalization has been conducted on the backbone, variability is less significant within the less than 1% drift range. Considering the normalized partition wall model, it is feasible to consider the model as symmetric in push and pull directions, since there is no physical justification for different positive and negative values. Consequently, Figure 5-3 shows the specimens in subgroups 1b and 2b with the absolute valued normalized backbones. One may note that only those specimens used in the subgroup model development are considered here (i.e. excluding the outliers). One difference from the subgroup model is noted where, specimen 6 is excluded from this analysis due to the lower energy dissipation associated with a reused specimen. Using the nine specimens of subgroups 1b and 2b, 18 backbone curves (one positive and one negative per specimen) are then used to characterize (μ) and standard deviation (σ) of the specimens (Figure 5-4). The mean, mean plus one standard deviation and mean minus one standard deviation of the normalized backbone curves provides a mechanism to characterize the variability experienced in the experiments.

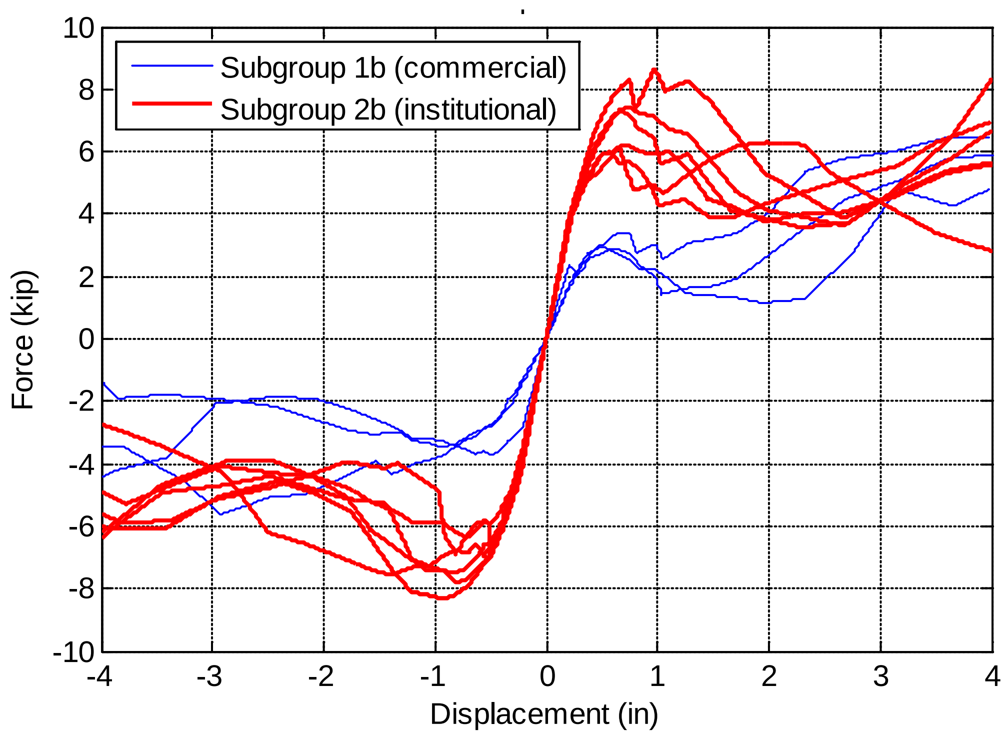

Figure 5-1 Partition wall backbones (force-displacement relations) for subgroups 1b and 2b.

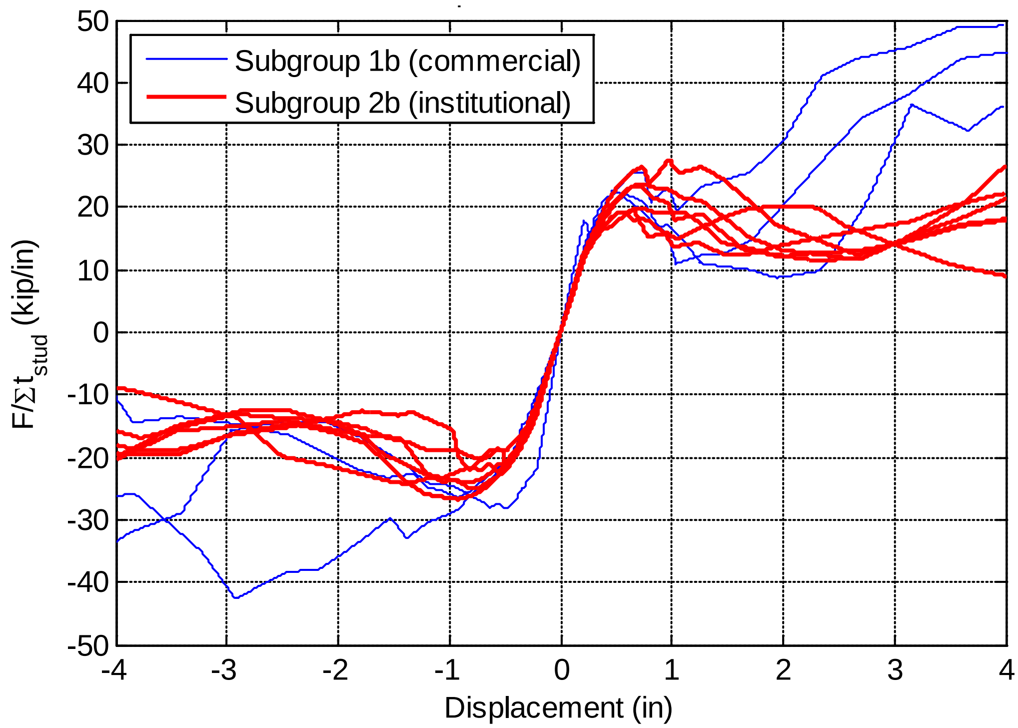

Figure 5-2 Normalized partition wall backbones (force-displacement relations) for subgroups 1b and 2b.

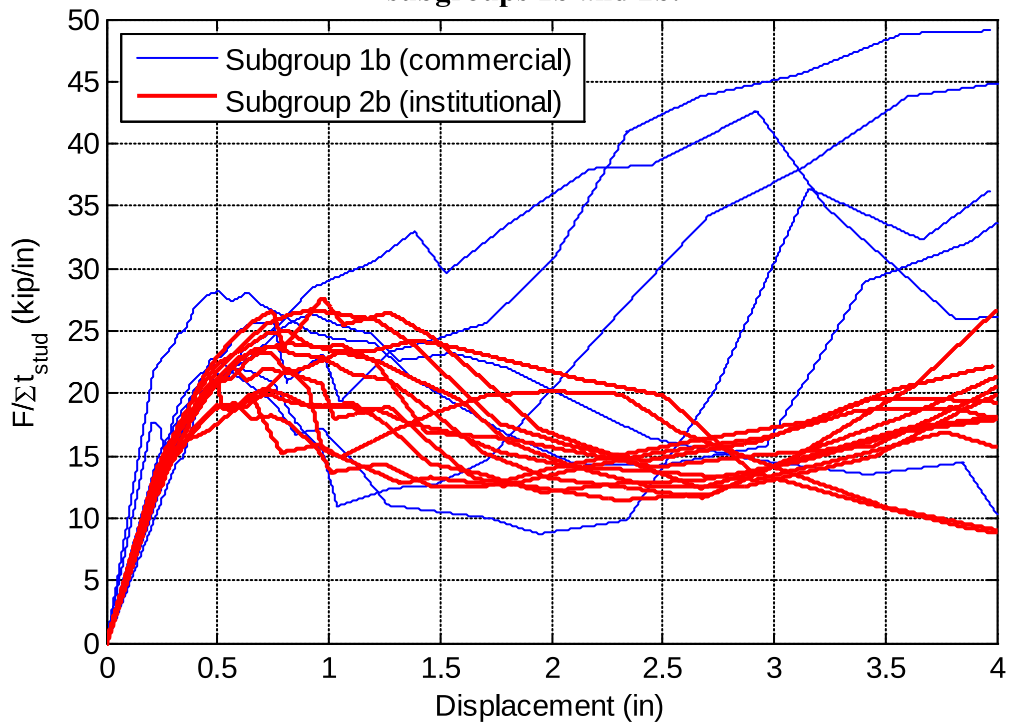

Figure 5-3 Absolute valued normalized partition wall backbones considering positive and negative behavior.

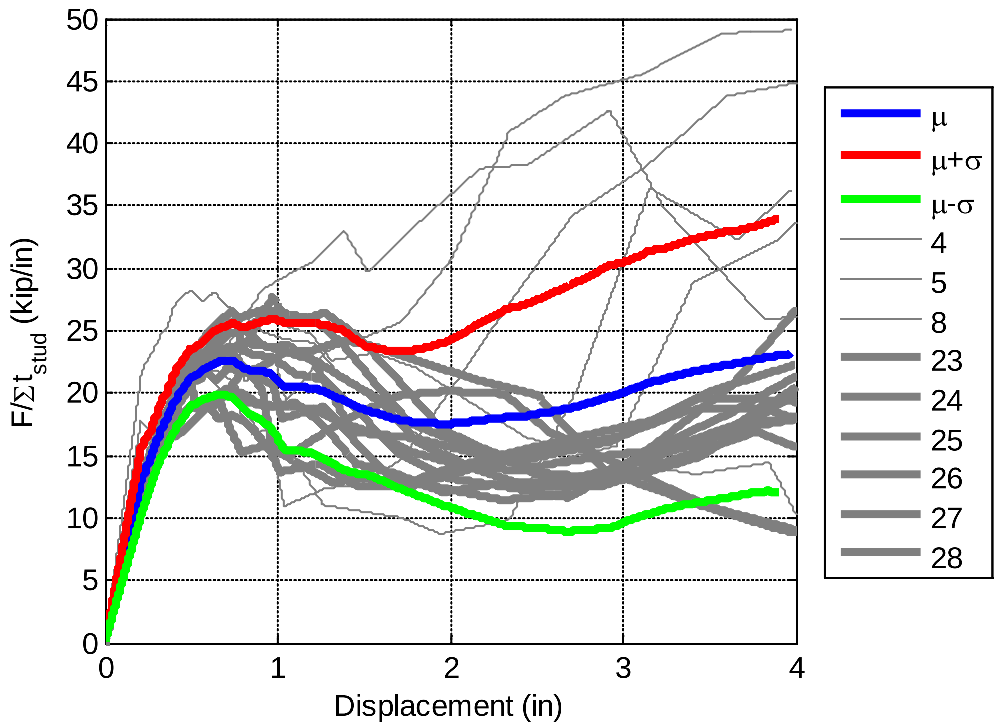

Figure 5-4 Absolute valued normalized backbones showing the mean, mean plus one standard deviation and mean minus one standard deviation.

5.3 Hysteretic Energy Normalization

In like fashion, the calculated hysteretic area should agree in a normalized fashion (Figure 5-5) with that of the experimental model. In the same approach as the force-normalization, the hysteretic area (energy) is also normalized by the sum of the thickness of the studs in the lateral direction. When the normalization is conducted, agreement in the normalized hysteretic energy supports the normalization procedure (Figure 5-6). The hysteretic area showing the mean plus one standard deviation and the mean minus one standard deviation will be provided later during the calibration exercise.

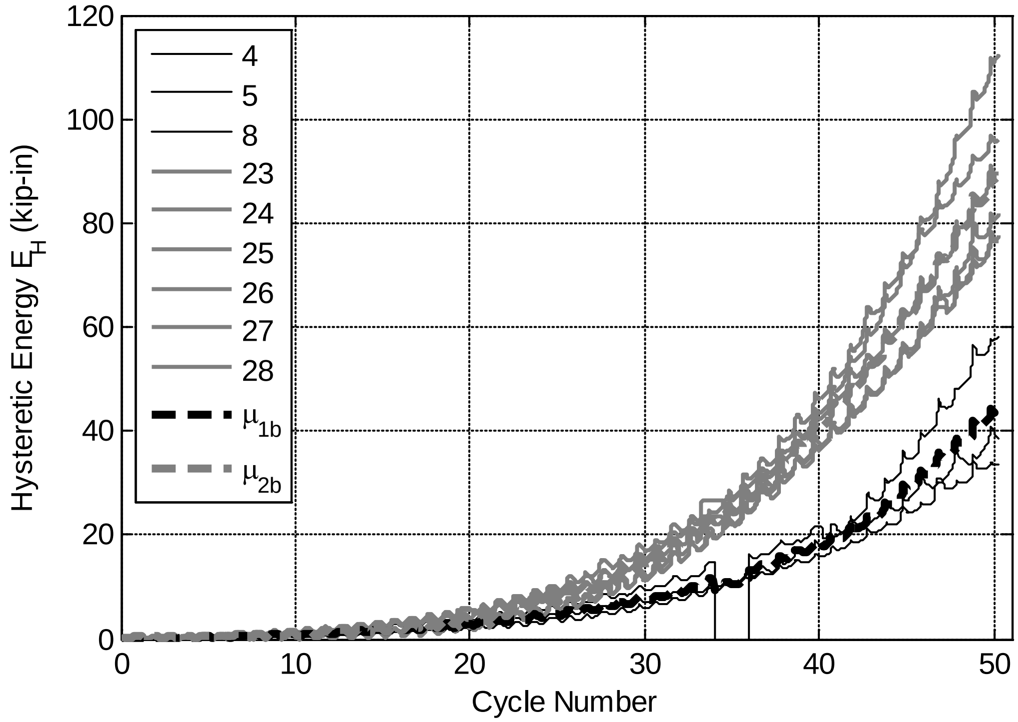

Figure 5-5 Hysteretic energy for subgroups 1b and 2b for each of the specimens considered along with their respective subgroup averages.

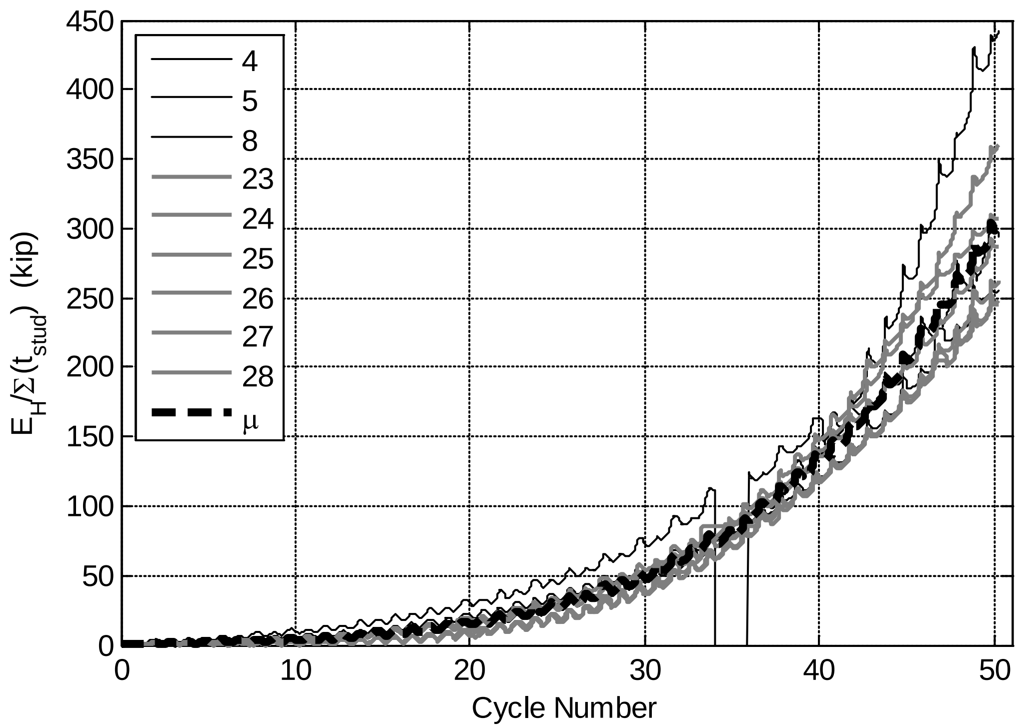

Figure 5-6 Normalized hysteretic energy for subgroups 1b and 2b.

5.4 Normalized Model Calibration

Similar to the subgroup model characterization, two key parameters involved in developing the representative models are the idealized backbone curve and unload and reload parameters. Each of these is calibrated such that the hysteretic energy of the model matches that of the target experimental specimens. In this approach three representative models are sought, namely: 1) mean response, 2) mean response plus one standard deviation and 3) mean response minus one standard deviation, where the standard deviation responses are considered to explore the experimental variability. The force-displacement backbone idealization is shown in Figure 5-7 through Figure 5-9. In this procedure, the backbone points are selected based on significant backbone slope changes shown in the tangent stiffness plots. Identifying the locations of significant slope change, the corresponding y-value pertaining to the normalized force quantity is iterated to minimize the difference between the target backbone and the idealized piece-wise backbone curve. Consequently, for the (x-values) displacement, the selected normalized force quantity is the closest match to the curve. The downside of this method sometimes is overestimation or underestimation of values than what was experimentally determined. For the selection of the unload and reload parameters, these are calibrated for each of the normalized models (Figure 5-10 through Figure 5-12).

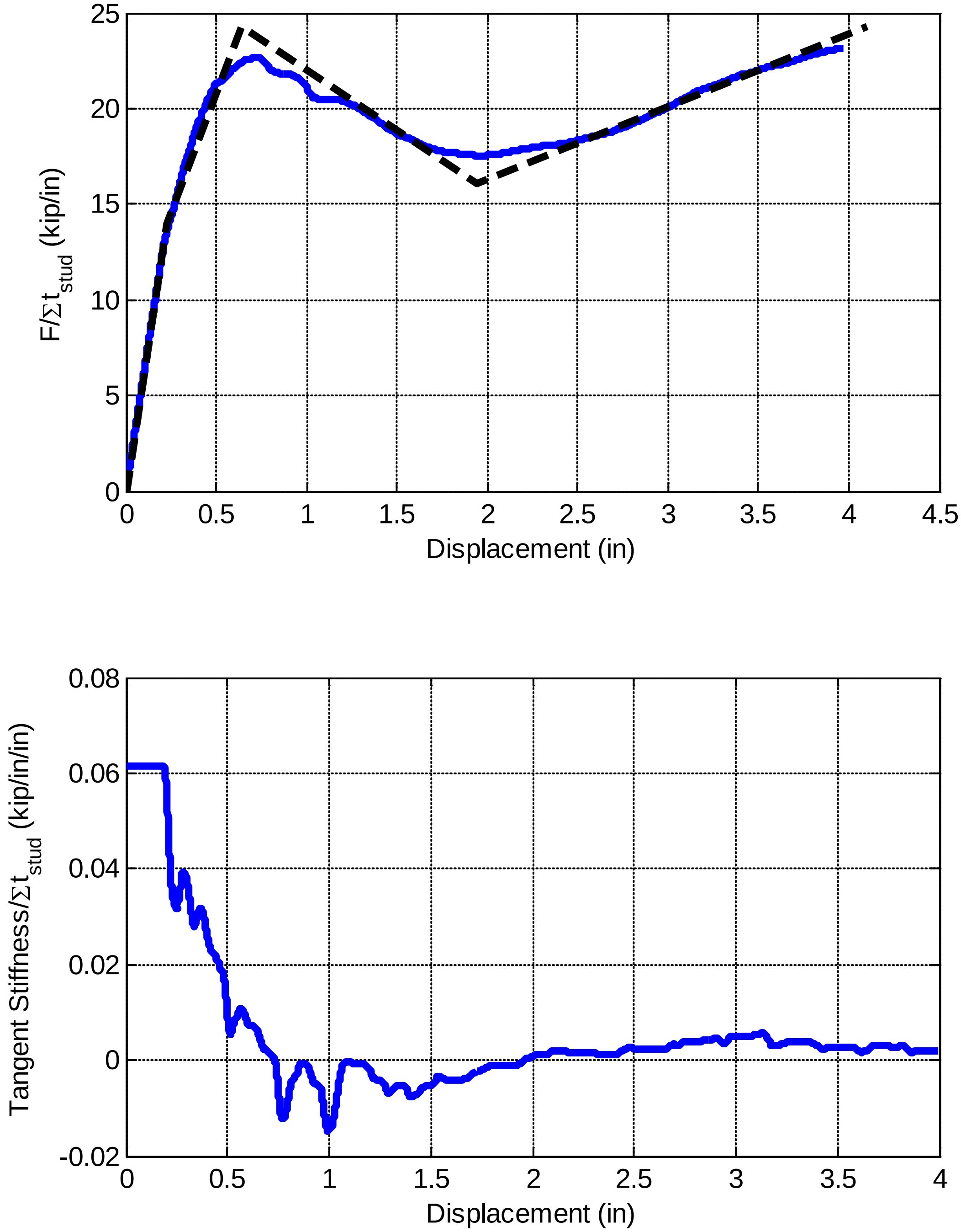

Figure 5-7 Selection of the mean response behavior of the partition wall model. Top shows normalized absolute valued hysteretic backbone while the bottom demonstrates the tangent stiffness of this backbone.

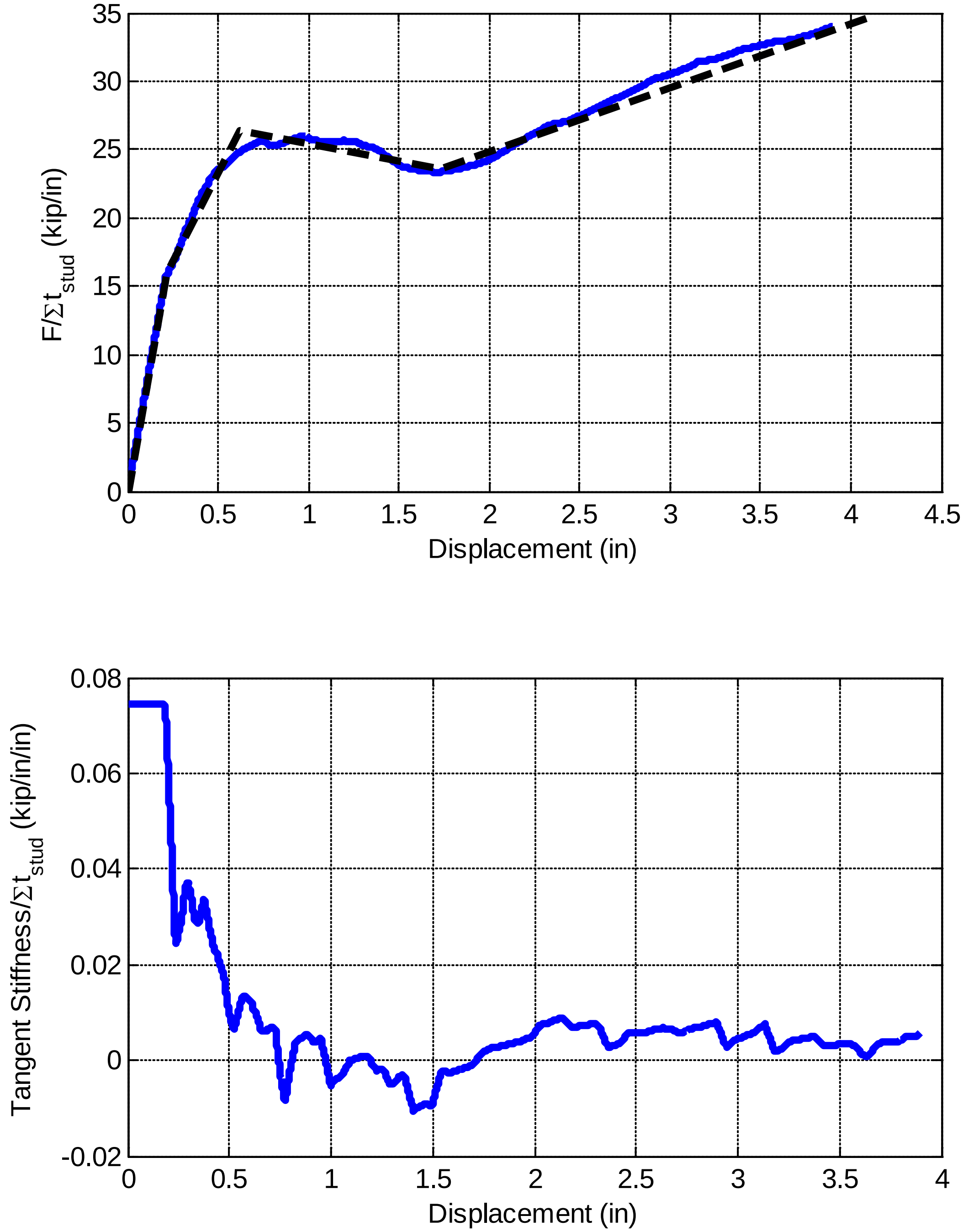

Figure 5-8 Selection of the mean plus one standard deviation response behavior of the partition wall model. Top shows normalized absolute valued hysteretic backbone while the bottom demonstrates the tangent stiffness of this backbone.

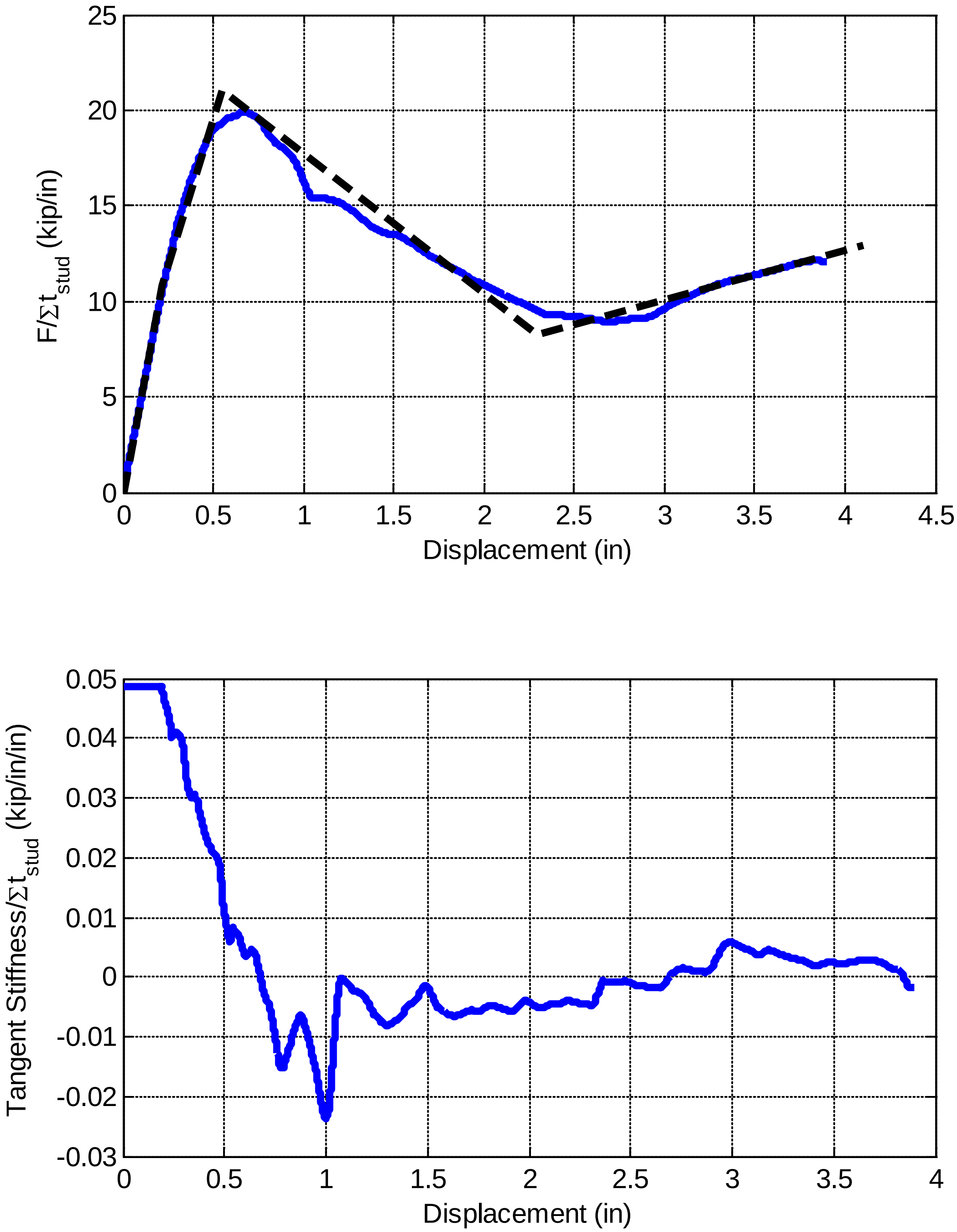

Figure 5-9 Selection of the mean minus one standard deviation response behavior of the partition wall model. Top shows normalized absolute valued hysteretic backbone while the bottom demonstrates the tangent stiffness of this backbone.

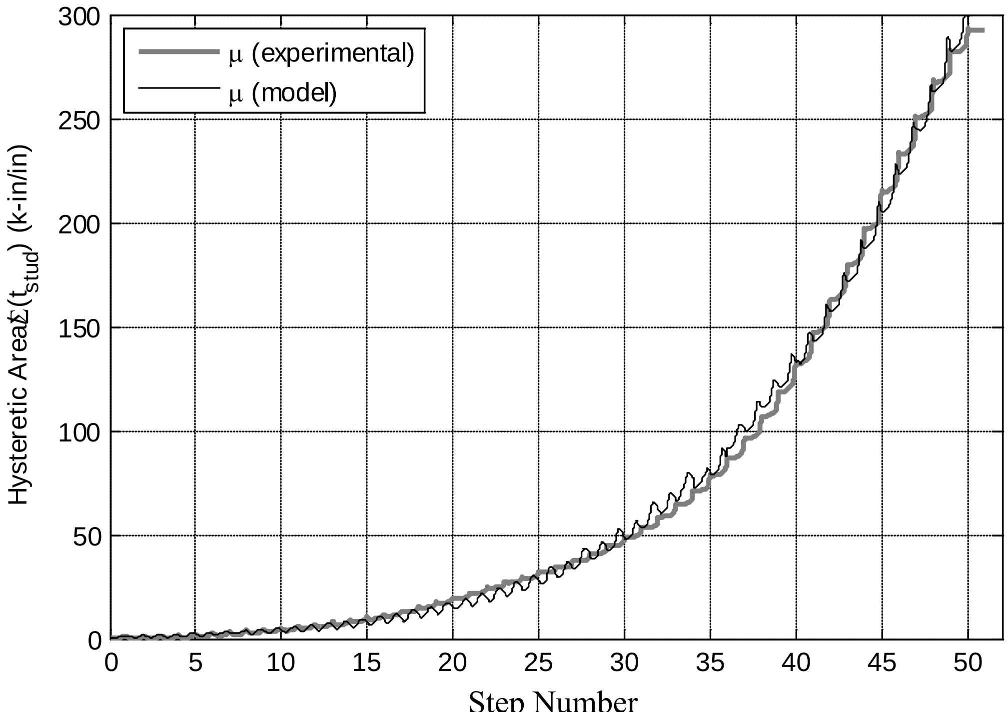

Figure 5-10 Hysteretic area of the mean model versus the target mean hysteretic area.

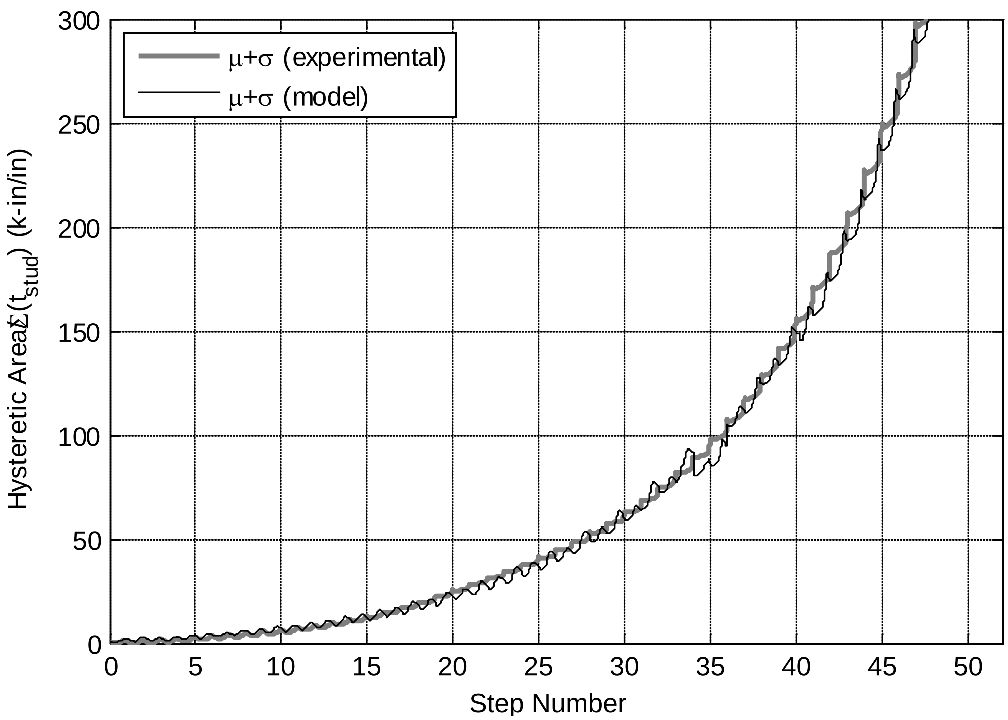

Figure 5-11 Hysteretic area of the mean plus one standard deviation model versus the target mean plus one standard deviation hysteretic area.

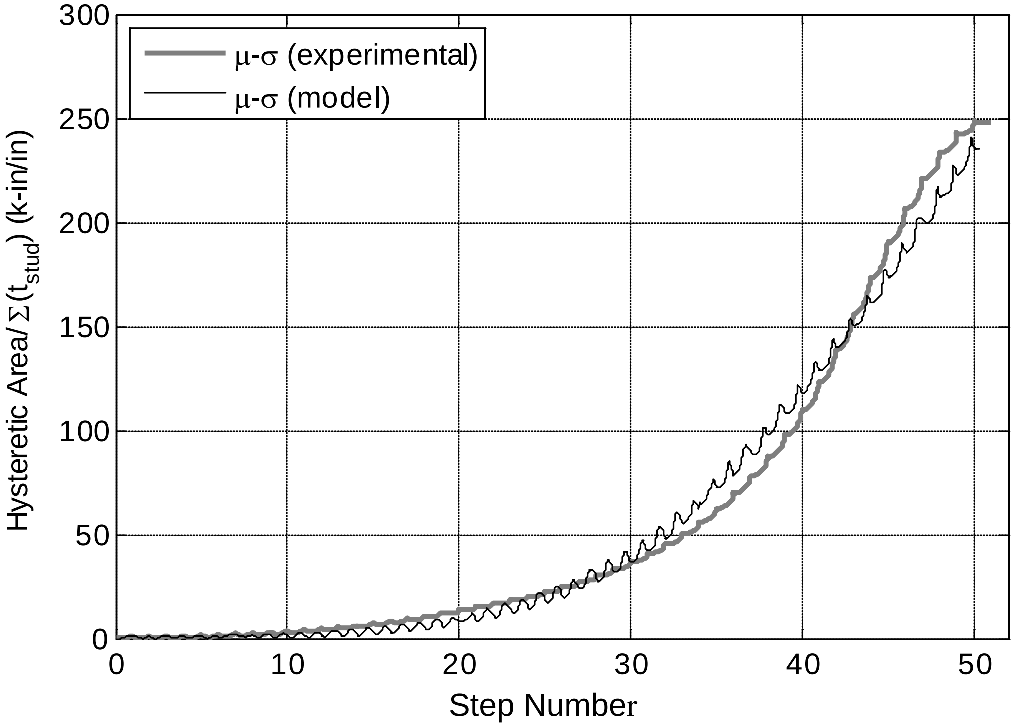

Figure 5-12 Hysteretic area of the mean minus one standard deviation model versus the target mean minus one standard deviation hysteretic area.

5.5 Normalized Model Verification

To assess the variability among the different statistical values of the normalized models, an individual comparison can be made. In Figure 5-13 through Figure 5-18, the model mean (average, μ), mean plus one standard deviation ($\mu+\sigma$) and mean minus one standard deviation ($\mu-\sigma$) are compared against test results for specimen 4 as an example. Comparisons are provided for the hysteretic force-displacement response and the hysteretic energy (area). Complete error metrics assessment will be conducted in the following sections. For this particular specimen, the backbone is best characterized by the mean minus one standard deviation, while the hysteretic area by the mean response. For hysteretic force-displacement response and hysteretic energy comparisons of the responses from each test specimen, refer to the appendices section of the report.

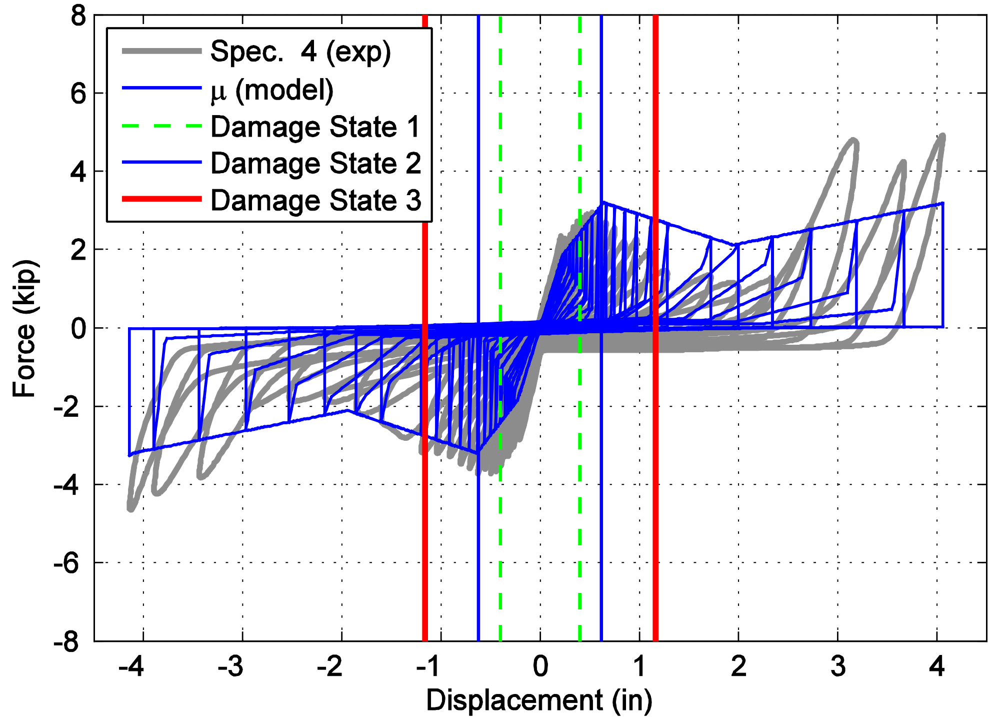

Figure 5-13 Hysteretic behavior of the mean response shown with specimen 4 as an example.

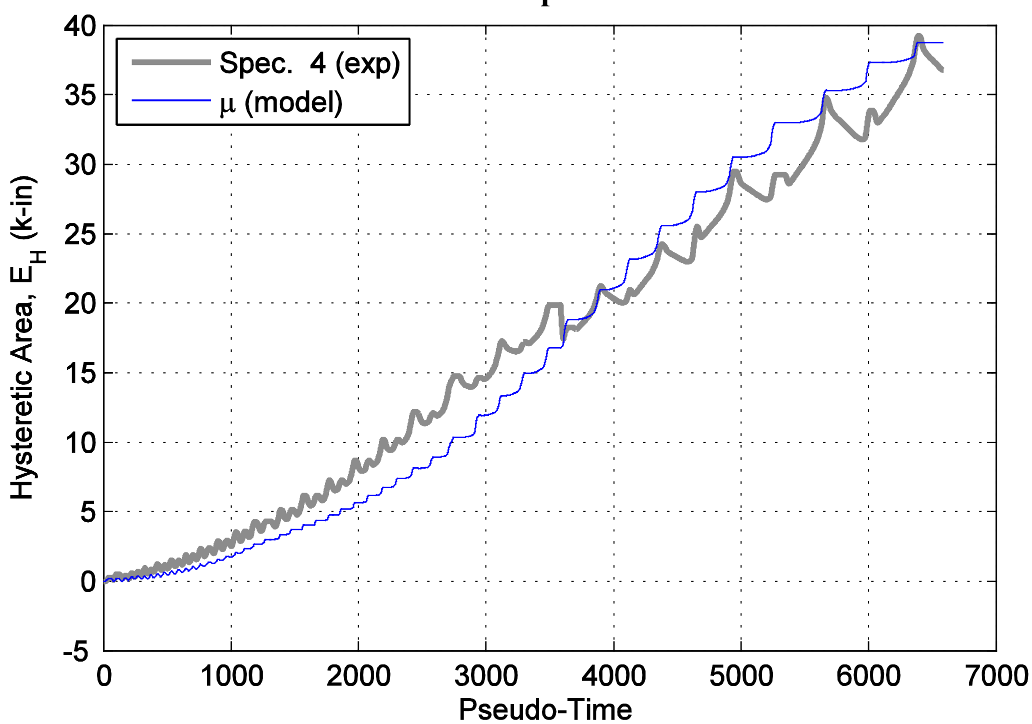

Figure 5-14 Hysteretic area of the mean model with specimen 4 as an example.

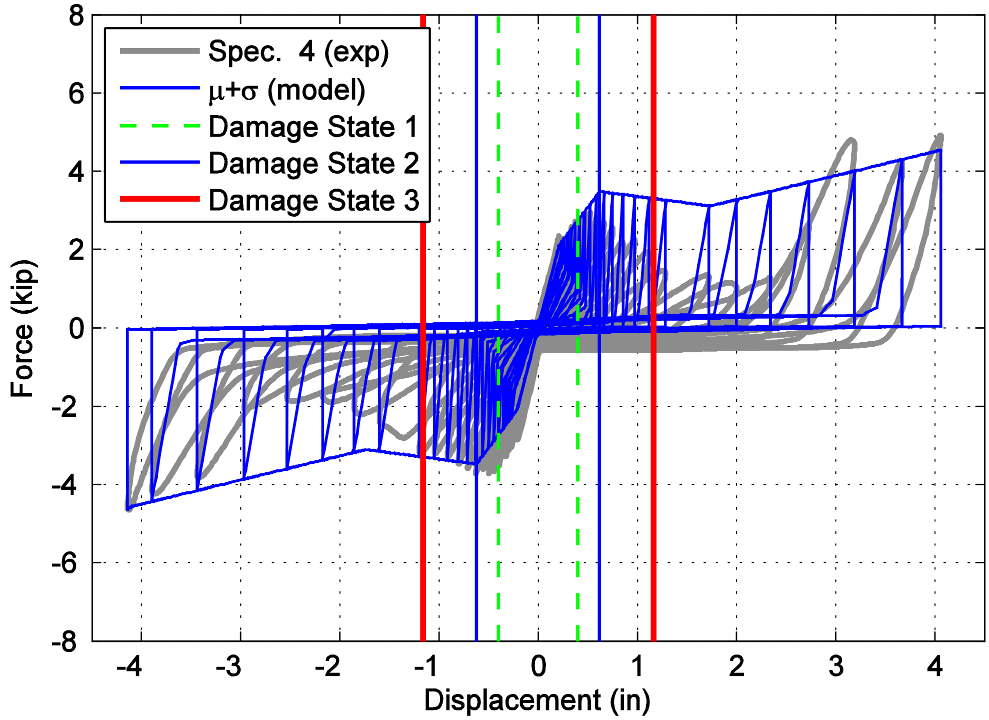

Figure 5-15 Hysteretic behavior of the mean plus one standard deviation response shown with specimen 4 as an example.

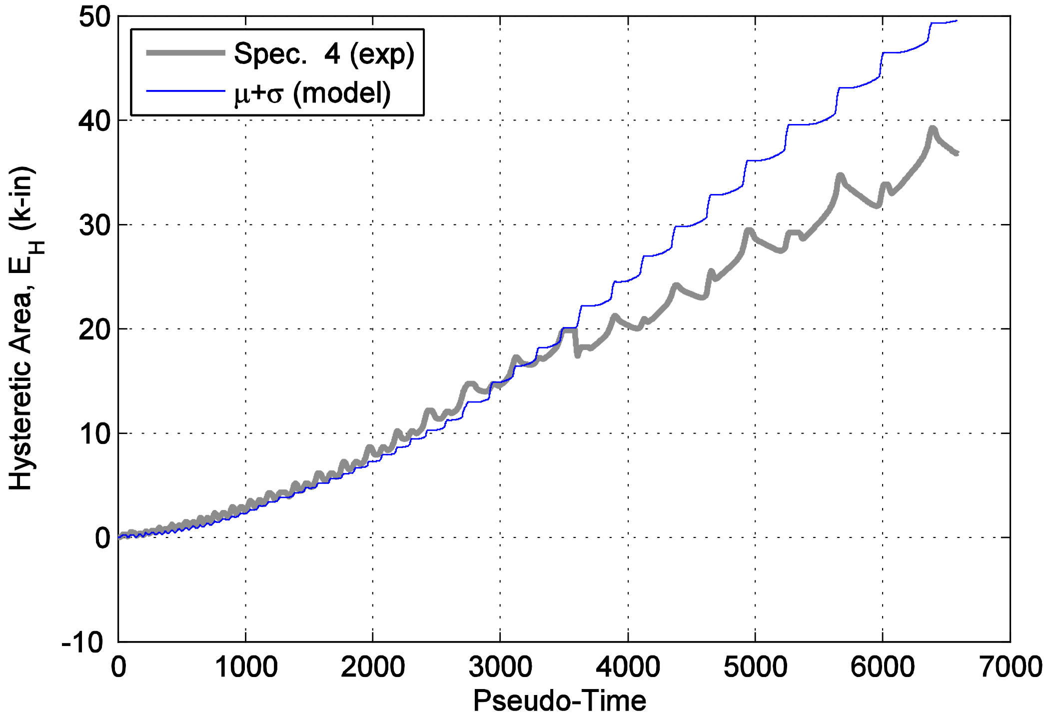

Figure 5-16 Hysteretic area of the mean plus one standard deviation model with specimen 4 as an example.

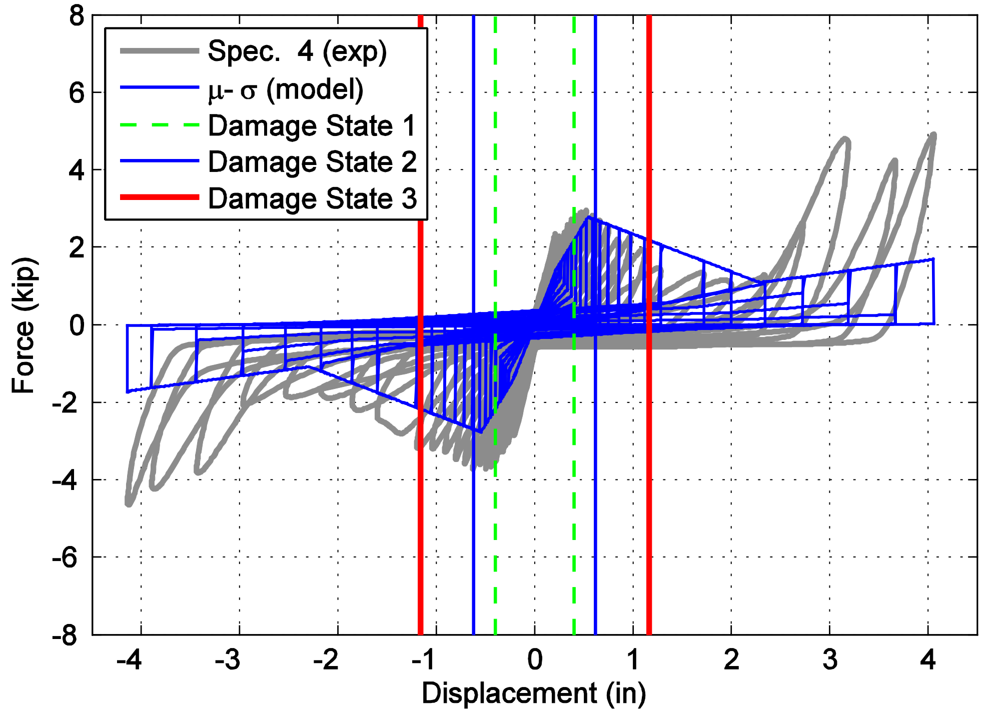

Figure 5-17 Hysteretic behavior of the mean minus one standard deviation response shown with specimen 4 as an example.

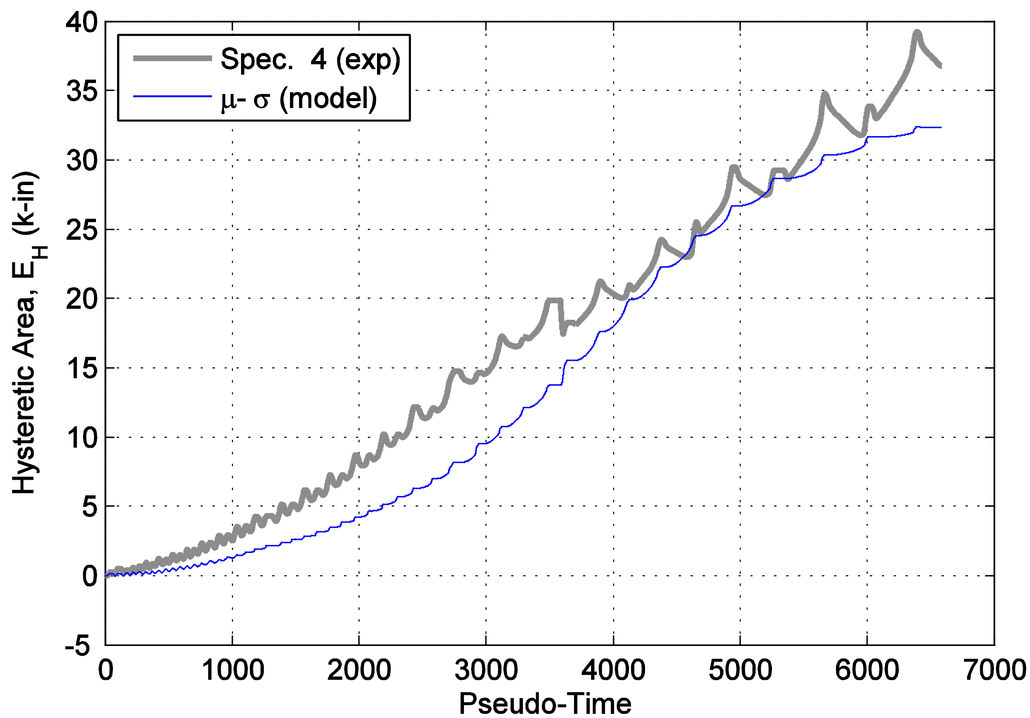

Figure 5-18 Hysteretic area of the mean minus one standard deviation model with specimen 4 as an example.

5.6 Normalized Model Discussion

In the development of the normalized models, a comparison is made between the various statistical levels. The first comparison is made between the various backbones (Table 5-1 and Figure 5-19). In this figure, the mean and plus/minus standard deviations are somewhat similar in their initial stiffness, however their peak and post-peak behavior do vary. The maximum force value also is not at a stable displacement value, identifying that specimens experience their maximum force over a range. The post-peak hardening is noted in all variations, however it is most pronounced in the standard plus a standard deviation model.

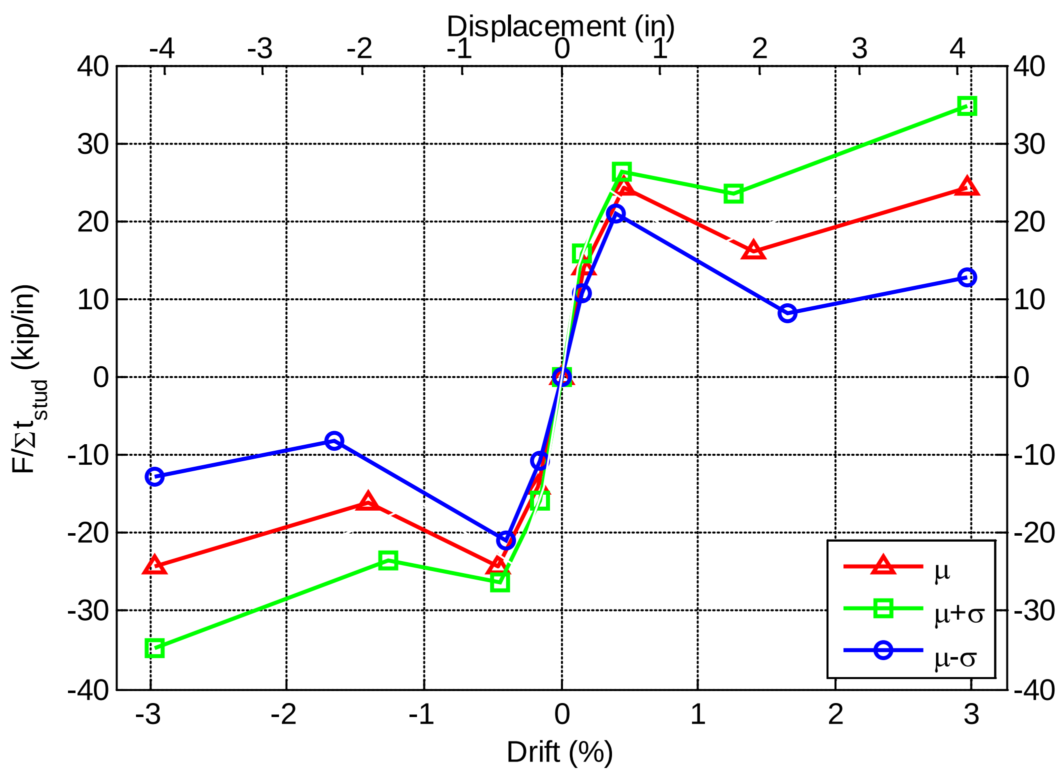

Figure 5-19 Overlay of each subgroup backbones shown demonstrating a large variability.

Table 5-1 Parameters for the normalized partition wall model.

Model	Backbone Points			Unload/Reload	
		Disp (in)	Force/Σt_{stud} (kip/in)	Force	Disp
μ	1	0.225	13.95	0.15	0.4
	2	0.637	24.28	0.01	0.95
	3	1.945	16.04	0.13	0.62
	4	4.100	24.28	0.03	0.97
$\mu+\sigma$	1	0.212	15.92	-0.03	1.1
	2	0.622	26.43	0.01	0.99
	3	1.734	23.61	0.55	0.6
	4	2.338	26.43	0	1
$\mu-\sigma$	1	0.221	10.81	0.15	0.4
	2	0.545	21.07	0.03	0.91
	3	2.291	8.22	0.11	0.89
	4	7.258	21.07	0.07	0.93

The second comparison between the normalized models lies within the calibrated unload and reload parameters which are ratios of force or displacement values in the material model, as described in Figure 4-38. Figures 5-20 and 5-21 identify the numerical values calibrated for force and displacement parameters, respectively. A larger range of selected parameters exist for the force parameters, which indicates more variablity in the force parameters than in the displacement parameters. One note regarding the unload and reload parameters (ratio values)on the mean minus one standard deviation model, f1 and f4 are set at -0.03 and 0.0, respectively. These two parameters do not relate physically to the model or specimen, however they are required numerically to match the hysteretic energy. The displacement parameters have similar values between different statistical variations, indicating less variablity in displacement point selection.

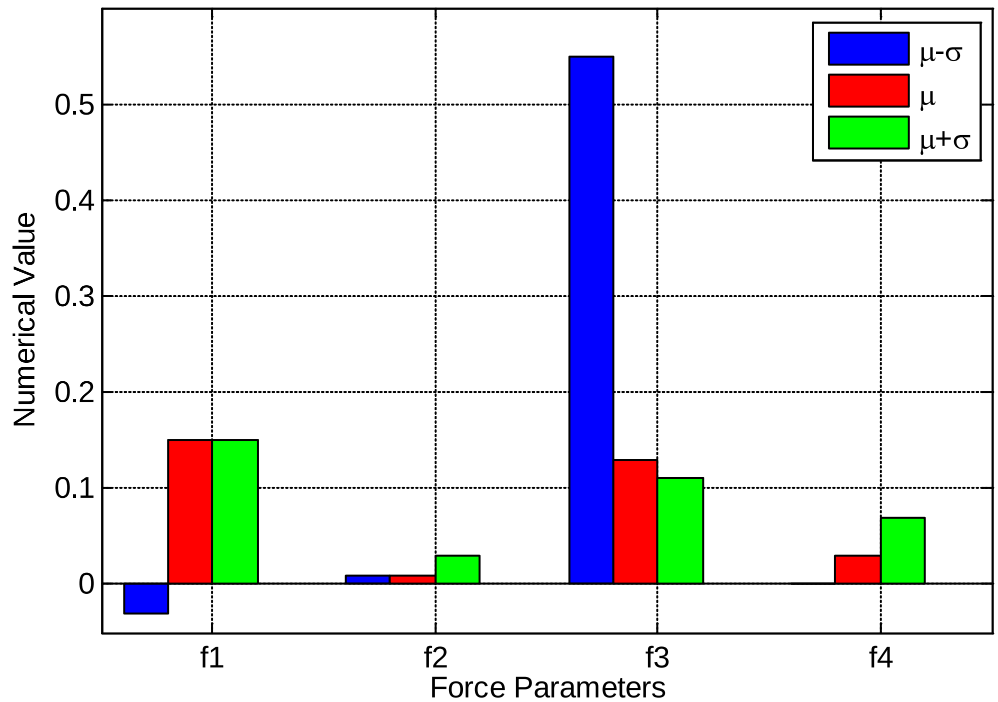

Figure 5-20 Force parameters for each parallel material used for each subgroup. Note the fourth parameter of the mean minus one standard deviation model is zero.

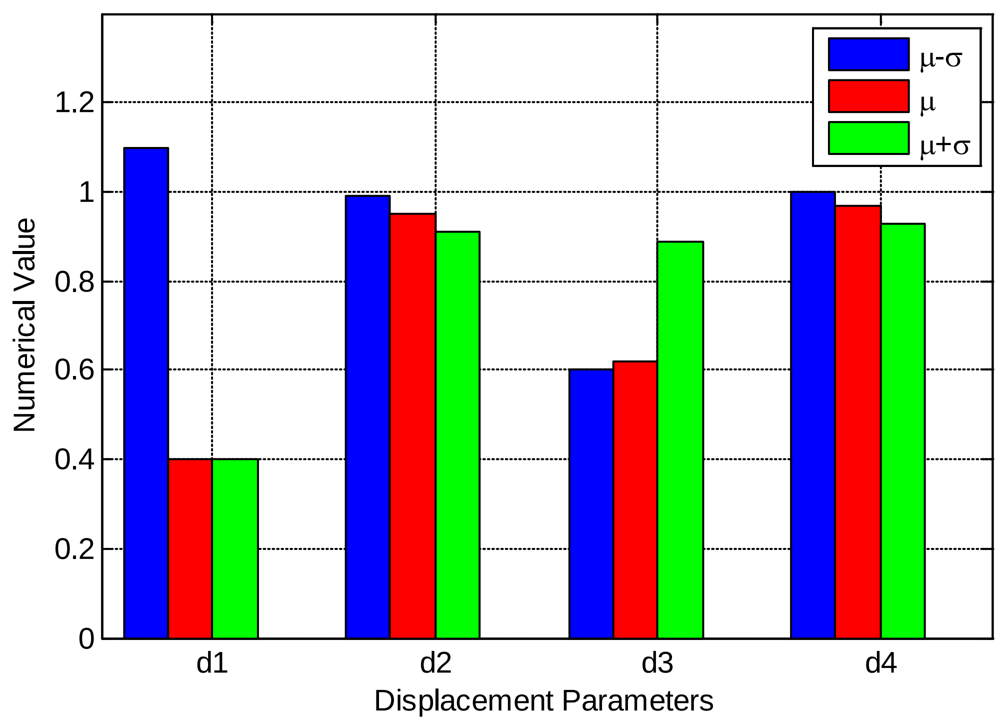

Figure 5-21 Displacement parameters for each parallel material used for each subgroup.

5.7 Concluding Remarks

Herein the development of normalized models and their calibration is presented. Three representative models of mean, mean plus standard deviation, and mean minus standard deviation are calibrated for the considered fully connected specimens. These models are developed with the intention to capture and assess the variability between the specimens. In this attempt of assessing the variability of the partition wall modeling, it is not evident as to which model performs best overall. Thus the analysis of model performance has largely been limited to visual inspection. In order to determine which model most closely captures the experimental behavior a more rigorous error analysis is needed. In the next section, two different error metrics are used to determine which model is most robust while closely capturing the experimental results.

SECTION 6
ERROR METRICS ASSESSMENT

6.1 Introduction

To characterize the model performance, error metrics and individual specimen level comparisons are conducted using all of the developed models. In the previous two sections, the development of four representative subgroup models (1a, 1b, 2a and 2b) and three normalized models for the fully connected walls (μ, $\mu+\sigma$, $\mu-\sigma$) were presented. To justify the use of any of the developed models, particular attention to how successful the models are in the prediction of the experimental behavior must be assessed. In this section, two error metrics are adopted, namely, the average error in maximum force and total half-cycle hysteretic energy. It should be mentioned that these models were implemented in displacement control, therefore displacement error metrics are not meaningful.

6.2 Average Error in Maximum Force

The first error metric is the error associated with the maximum force. This error metric is a measure of how well the particular model backbone estimates the changing strength of the specimen. To illustrate this error metric, specimen 23 is shown as an example. For complete specimen comparisons and error metrics of the remaining specimens and models, see Appendices A -D. In Figure 6-1, the hysteretic behavior of subgroup 2b (institutional fully connected) model is shown along with specimen 23. In this figure, the damage states identified by the experimental team are also overlaid. While this hysteretic plot demonstrates a decent match, it is particularly hard to quantify visually. In order to identify the model's ability to capture the force, the maximum attained force for a given displacement is evaluated. Identifying the maximum force attained throughout the displacement range is similar to comparing the "backbone points". Backbone points are traditionally identified at the turning points associated with a load reversal, whereas in this case the maximum force attained is enveloped at all displacement levels, not just load reversals. Figure 6-2 illustrates the maximum force envelope for both specimen 23 and the 2b subgroup model. This figure highlights how the maximum force obtained is particularly low in the model around specimen attainment of DS_2 and DS_3 and the estimation of the post-peak hardening behavior at larger displacements (approximately 2.5 in) is better in the negative direction in comparison to the positive direction.

Using the maximum force envelope, the residual force difference is calculated as F_{model} - $F_{experimental}$ (Figure 6-3). In this figure for positive displacements, values greater than zero demonstrate that the model is over-predicting the maximum force value attained at a given displacement. Likewise a value less than zero indicates under-prediction. Using the experimentally identified damage states to quantify the model's performance, an average force residual is calculated over each damage state range (i.e. beginning of test, namely: 1) $DS<DS_1$ (no damage), 2) $DS_1 \leq DS < DS_2$ (minor), 3) $DS_2 \leq DS < DS_3$ (moderate) and 4) $DS \geq DS_3$ (severe)). When no damage was noted in the experiment, the average force residual is a mere 0.4 kip (or 5% of the maximum value of the specimen). Comparing the force residuals for the walls when damage occurred, for displacements greater than DS_1, but less than DS_2 (moderate) the average force residual is 1.19 kip (or 15% of the maximum value of the specimen).

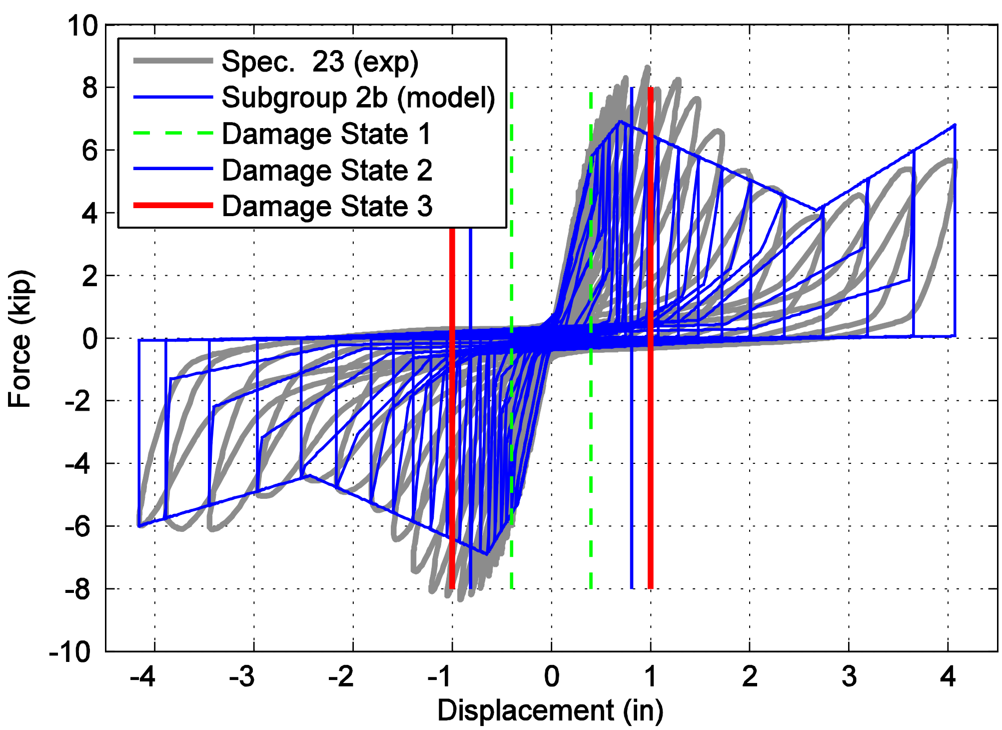

Figure 6-1 Hysteretic overlap comparison between specimen 23 and the 2b subgroup model.

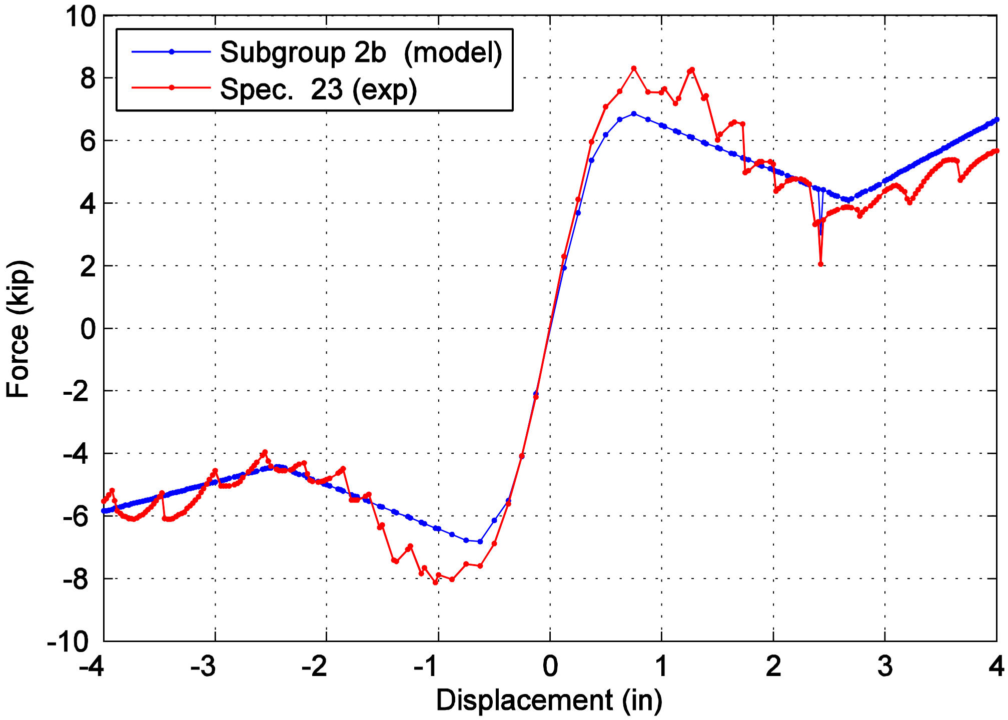

Figure 6-2 Captured maximum force envelope curve for specimen 23 and the 2b subgroup model.

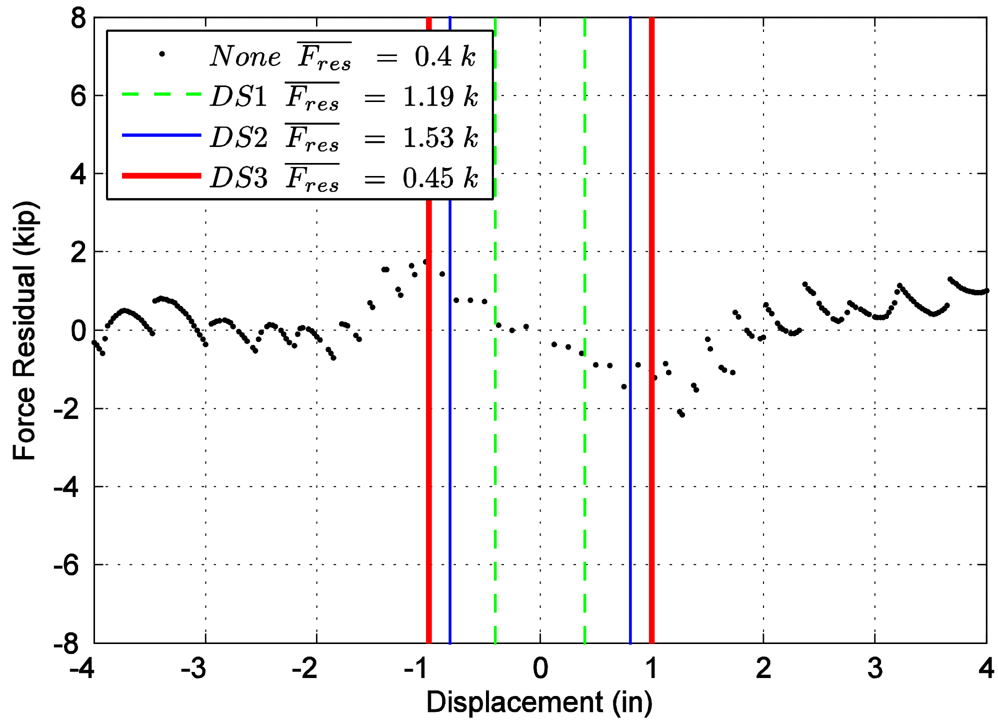

Figure 6-3 Difference in maximum attained force level when comparing specimen 23 and the 2b subgroup model.

For displacements greater than DS_2, but less than DS_3 (severe), the average force residual is 1.53 kip (or 19% of the maximum value of the specimen). For drift levels where damage exceeded DS_3, the average force residual is 0.45 kip (or 6% of the maximum value of the specimen). It is noted that for this test specimen, the maximum force is achieved within DS_1-DS_2 and has a magnitude average force residual of 1.19 kips. Therefore, the percent error is approximately 14% within the windows of DS_1-DS_2. Using this strategy, a modeling assessment is conducted Reference Appendices A - D for complete details on the error metrics as they are conducted for all seven model variations. As one may notice in Appendices A - D, not all damage states are shown. This is either due to the lack of damage state identification in the experiments or two damage states occurring at the same location. When two damage states occur at the same location, i.e. displacement of DS_2 is the displacement of DS_3, DS_3 is used for comparing the error metrics.

6.3 Total Half-Cycle Hysteretic Energy

The second error metric is associated with the hysteretic energy (area under the hysteretic curve). In the model calibration, the cumulative hysteretic energy (Figure 6-4) was used to characterize the unloading parameters (Figure 4-38), describing the relationship between the unloading and reloading. However, the cumulative hysteretic energy does not explicitly demonstrate the model's performance for one individual displacement cycle or load reversal. By evaluating the hysteretic energy on a per half-cycle basis, some bias introduced with the use of one loading protocol can be avoided. To identify the half-cycle energy, the total hysteretic energy is calculated from a zero displacement location to an absolute extremum associated with the peak (target) displacement and then to the immediate next zero crossing. The half-cycle hysteretic energy is then reported versus the target displacement, as demonstrated in Figure 6-5 again for specimen 23. Figure 6-5 shows the target displacement in units of interstory drift (%). In this particular loading protocol, the displacement values are on an upward sweep from 0 to 3% interstory drift, where the negative excursion is slightly larger after the previous positive excursion. As a result, no target drift values are identical.

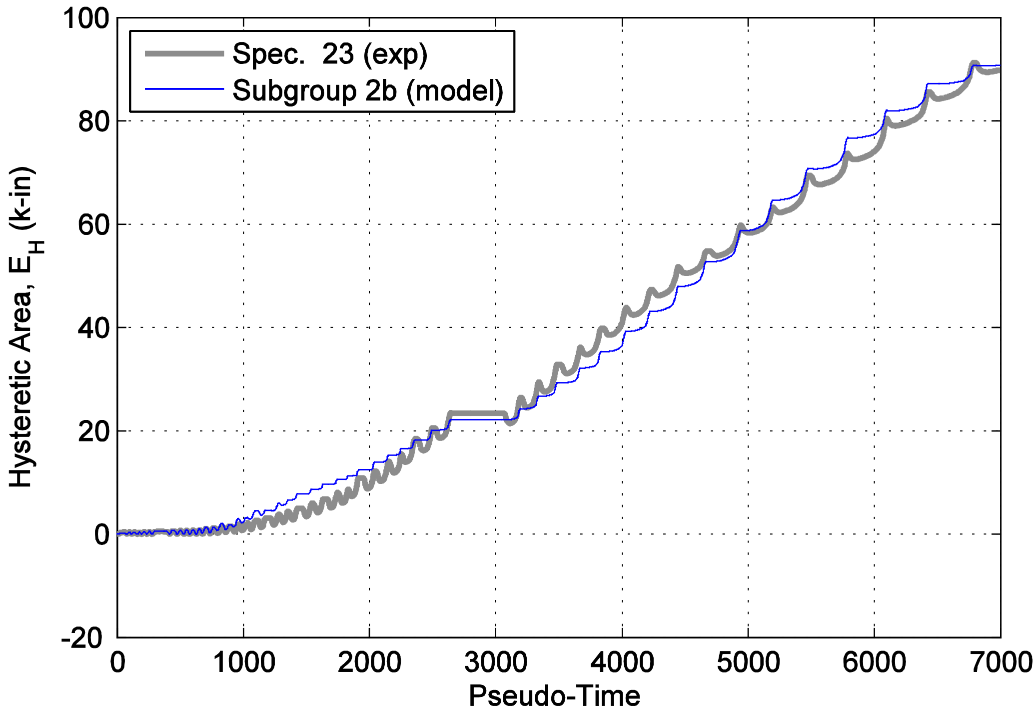

Figure 6-4 Hysteretic energy (area) comparison between specimen 23 and the 2b subgroup model.

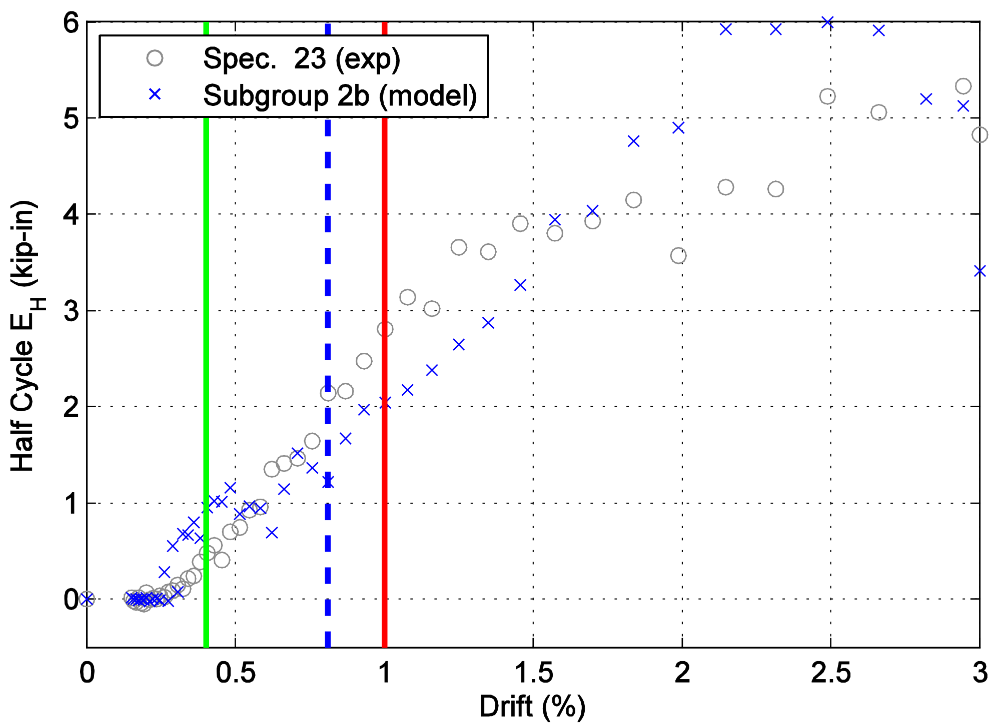

Figure 6-5 Hysteretic energy (area) per half cycle comparison between specimen 23 and the 2b subgroup model shown against maximum achieved drift level.

Using the experimentally identified damage states to quantify the model's performance, the total half-cycle energy residual is calculated over each damage state range. The residual is defined in this case as the total difference in half cycle energy at a target displacement between the experiment and model. The sum is also calculated and reported in the legend, normalized by the cumulative experimental hysteretic energy for the same range, to evaluate the performance over the defined damage level intervals When no damage was noted in the experiment, the normalized (cumulative) half-cycle hysteretic energy is 2.36, approximately 230% higher than what was observed in the physical specimen, due to normalization by a small number. When DS_1 was achieved and before DS_2 onset, the total (cumulative) normalized half-cycle hysteretic energy residual is 0.16. For damage levels between DS_2 and DS_3 and for damage levels greater than DS_3, the normalized (cumulative) half-cycle hysteretic energy residual is 0.29 and 0.01 respectively. It is noted for this text specimen, the maximum difference in target half cycle hysteretic energies is found before DS_1 is achieved. As the specimen progresses the ability of the model to capture the hysteretic model improves. In the calculation of the total half-cycle hysteretic energy residual, the positive and negative signs are retained, as the model can either underestimate (negative values) or overestimate (positive values). Using the normalized half-cycle energy error metric, a modeling assessment will be made further in this section between the subgroup and normalized models. Reference Appendices A - D for complete details on the error metrics.

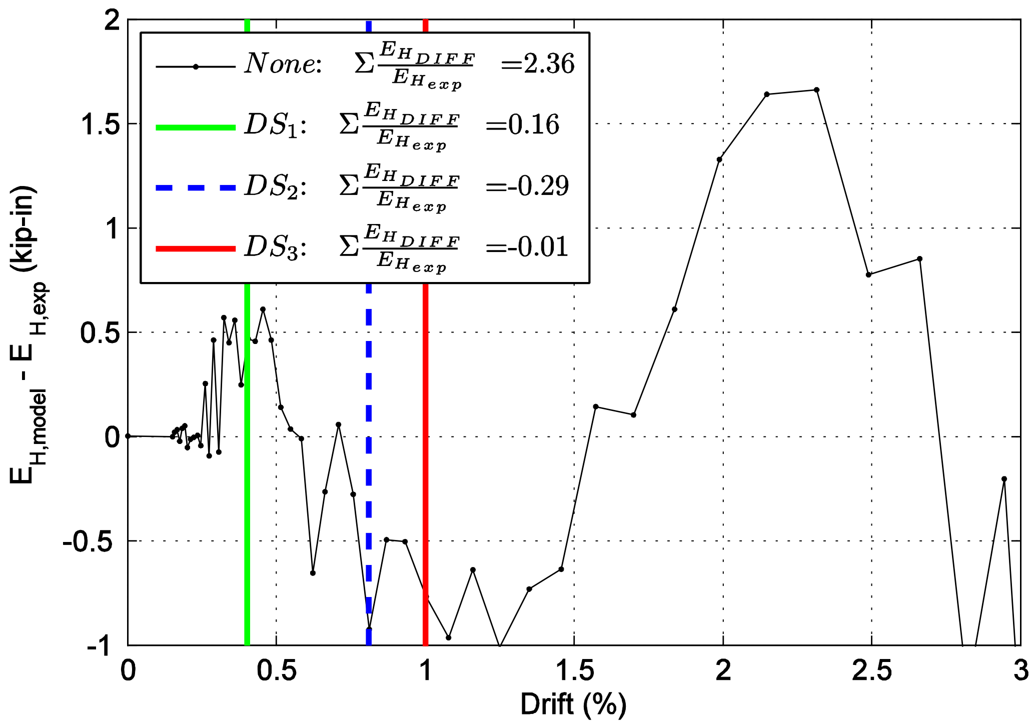

\

Figure 6-6 Difference in hysteretic energy (area) per half cycle comparison for specimen 23.

6.4 Error Metrics and Modeling Assessment

Using the error metrics of residual force and half-cycle hysteretic area, an overall assessment of the model performance for all various types developed is conducted. In Figure 6-7 the overall average force residual between the experiment and the model is shown. The "overall" average is taken in this case as the average of the associated four average force residuals pertaining to each damage interval, 1) DS<DS_1 (no damage), 2) DS_1≤DS<DS_2 (minor), 3) DS_2≤DS<DS_3 (moderate) and 4) DS≥DS_3 (severe). Figures 6-8 and 6-9 demonstrate the average force residuals per particular damage interval. When one compares the various formulations for the subgroup models and the normalized statistical models, it is noted that the mean normalized model performs just as well as the detailed subgroup models. When moderate damage (<DS_2) has occurred to each of the specimens, the mean normalized model performed better, as characterized by a smaller average force residual. The normalized statistical models considering either plus or minus one standard deviation perform generally worse than the average model. In analyzing the plus one standard deviation model for damage exceeding DS_3, it is clear that an overestimation is made due to the post-peak hardening behavior considered, particularly when observing the predictions for specimens 23-28.

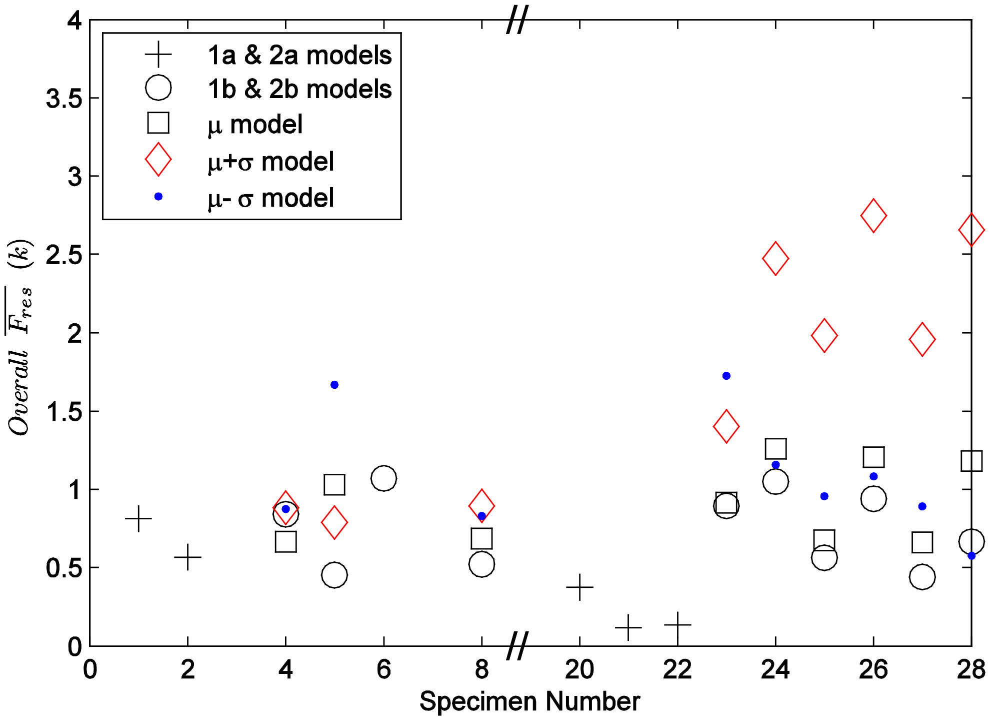

Figure 6-7 Overall average of the average force residual comparing the experimental to the developed models (subgroup, mean, mean plus one standard deviation and mean minus one standard deviation).

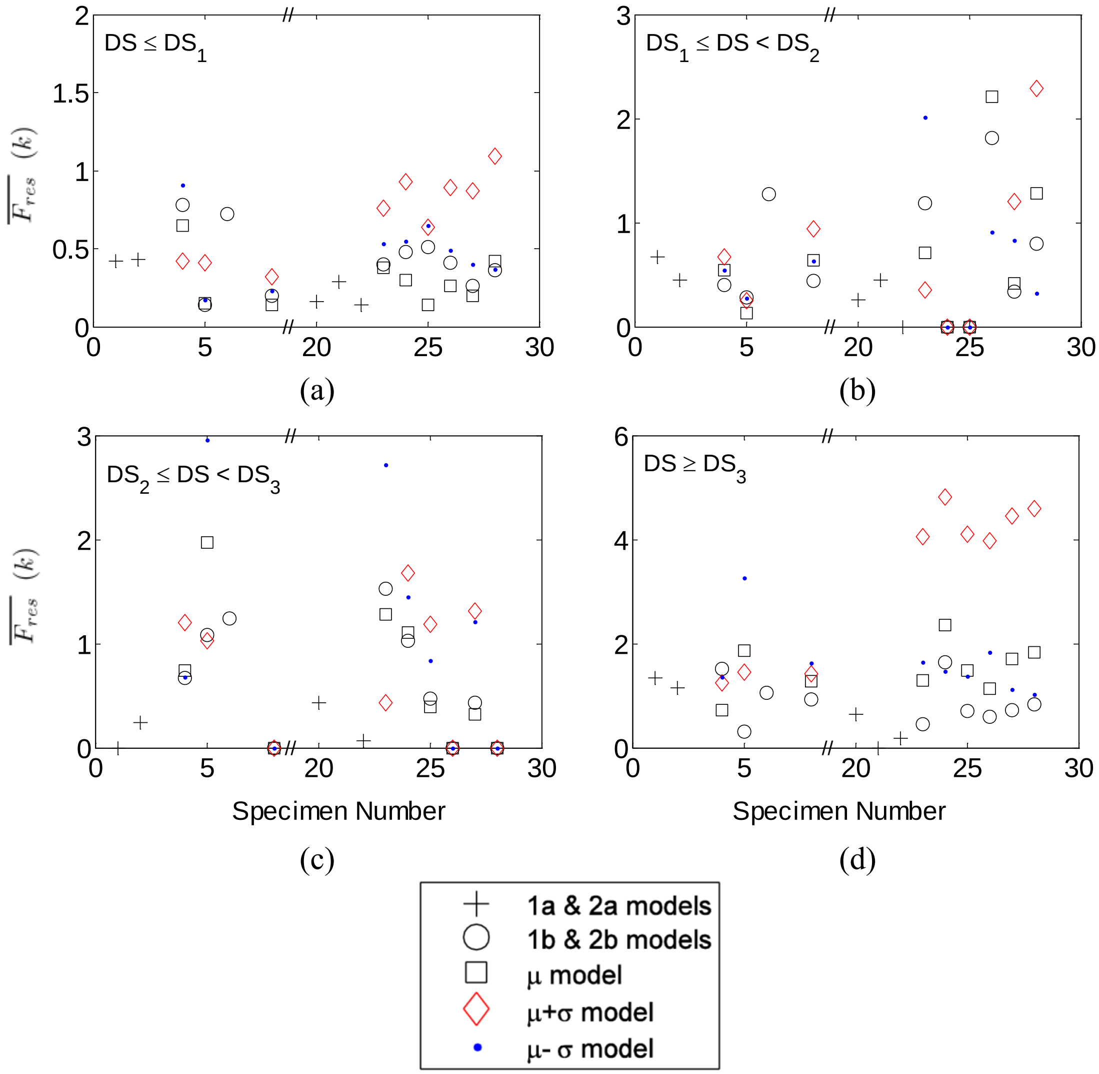

Figure 6-8 Average force residual comparing the experimental to the developed models by damage states: (a) no damage, (b) DS$_1$, (c) DS$_2$ and (d) DS$_3$.

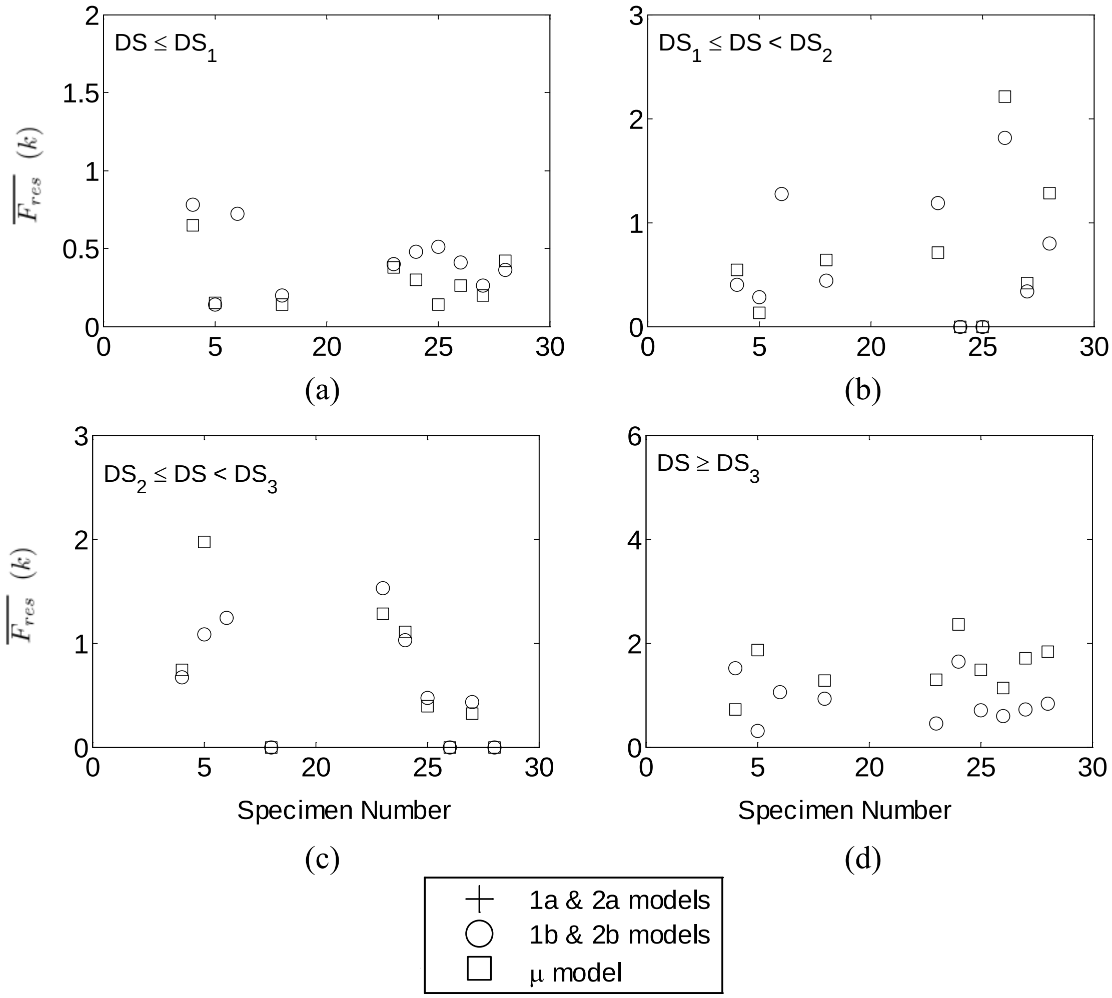

Figure 6-9 Average force residual comparing the experimental to the developed models by damage states: (a) no damage, (b) DS_1, (c) DS_2 and (d) DS_3. Note just the subgroup model and mean model is presented.

In analyzing the second error metric, Figure 6-10 illustrates the overall summation of the difference in half-cycle hysteretic energy for the developed models considering the entire displacement range. In addition, Figures 6-11 and 6-12 illustrate the difference in half-cycle hysteretic energy for the developed models on a per damage interval. When one compares the various formulations for the subgroup models and the normalized statistical models, it is noted that the average statistical model performs almost as well as the detailed subgroup models. When moderate damage has occurred to each of the specimens (DS_1 to DS_2), the mean normalized statistical model actually (μ) performs better for a few specimens. The mean normalized statistical model (μ) overestimates the half-cycle hysteretic energy for displacement values greater than DS_3.

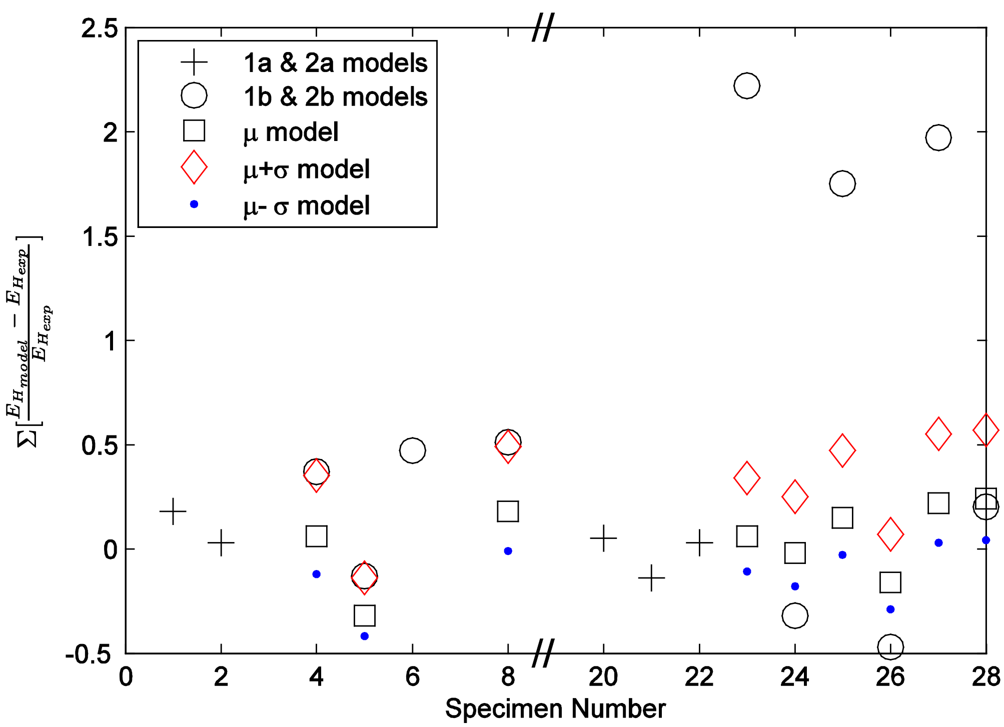

Figure 6-10 Overall residual in half-cycle hysteretic energy comparing the experimental to the developed models (subgroup, mean, mean plus one standard deviation and mean minus one standard deviation).

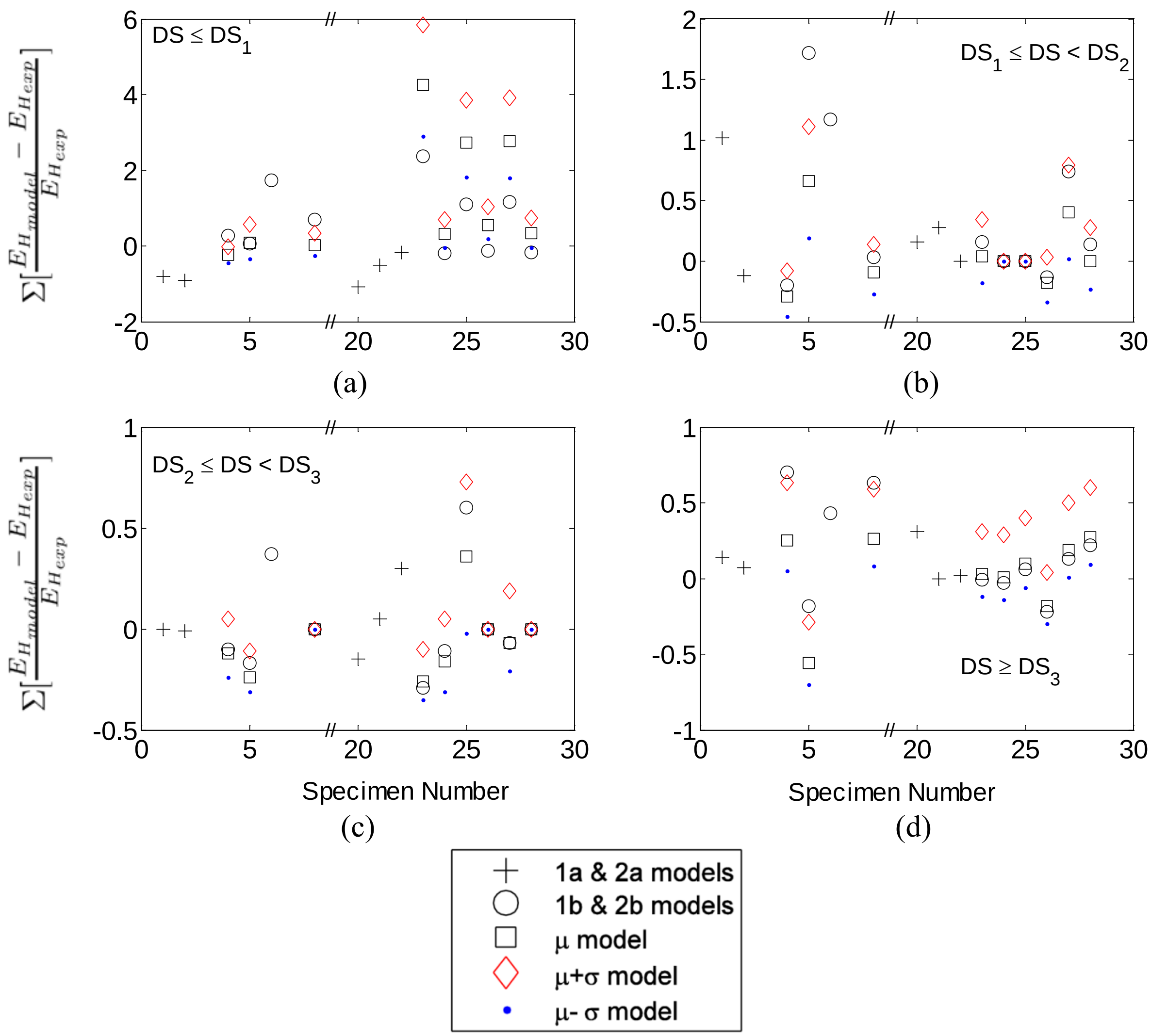

Figure 6-11 Overall residual in half-cycle hysteretic energy comparing the experimental to the developed models by damage states: (a) DS<DS$_1$, (b) DS$_1$≤DS<DS$_2$, (c) DS$_2$≤DS<DS$_3$ and (d) DS≥DS$_3$.

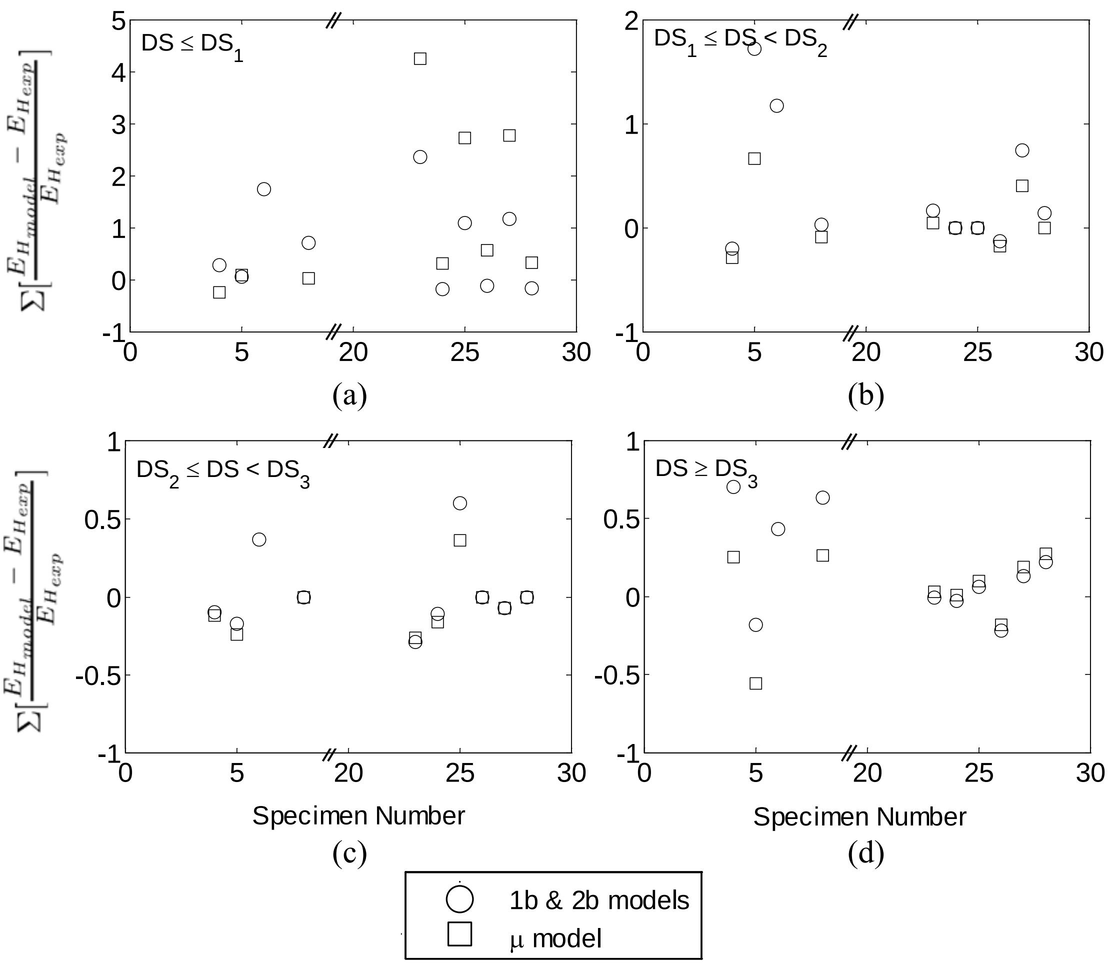

Figure 6-12 Overall residual in half-cycle hysteretic energy comparing the experimental to the developed models by damage states: (a) DS<DS_1, (b) DS_1≤DS<DS_2, (c) DS_2≤DS<DS_3 and (d) DS≥DS_3. Note just the subgroup model and mean model is presented.

6.5 Concluding Remarks

A specimen level comparison for each model is conducted for all of the specimens considered in the modeling technique. Using two error metrics of average force residual and overall difference in half-cycle hysteretic energy, performance of each model is assessed. Appendices A – D provide the entire performance evaluation for each model and each wall specimen. Relating the error metrics to observed damage states, a justification can be made for use of either the subgroup or normalized statistical models when considering fully connected partition wall specimens. In terms of the statistical models considering either plus/minus one standard deviation, the performance of the models degrade as expected, nonetheless the effect of the partition walls can be later assessed through its implementation into building models.

SECTION 7
PARTITION WALL IMPLEMENTATION

7.1 Introduction

In this section, the partition wall model is now implemented into larger numerical models of buildings, with the goal of evaluating the partition wall impact on the building dynamic characteristics and producing the response of the partition wall itself to earthquake motions imparted on the building. The later data are useful for generating fragility plots of the building-partition wall system. The first issue explored is how the partition wall is implemented in the building model. To integrate the lumped partition wall into a large building model, scaling the partition wall model characteristics is needed to account for walls of different lengths. In this work due to its broader coverage, the preferred partition wall model type is the normalized model (statistical mean value). Appendix E presents the procedure as used in this implementation of the partition wall model in OpenSees.

7.2 Partition Wall Implementation within a Building Model

The model as implemented is envisioned to be utilized with beam and beam-column elements in a finite element context. The typical configuration for example as shown in Figure 7-1, where the partition wall is connected to the structural model, spanning the beam midpoints between adjacent floor levels using slaved degrees-of-freedom (equalDOF command) simulating rigid members. The boundary conditions for the intersections at the beam midpoints for the fully connected partition wall models are modeled by restraining the two lateral displacement and one rotational degrees of freedom at both the top and bottom nodes (Figure 7-1) for a two dimensional model. This simplistic model allows for the partition wall to be lumped at the story mid-height and bay width, neglecting any torsional effect if placed in a three dimensional model. The force-displacement relations of the implemented walls are shown in Figure 7-2 and Figure 7-3.

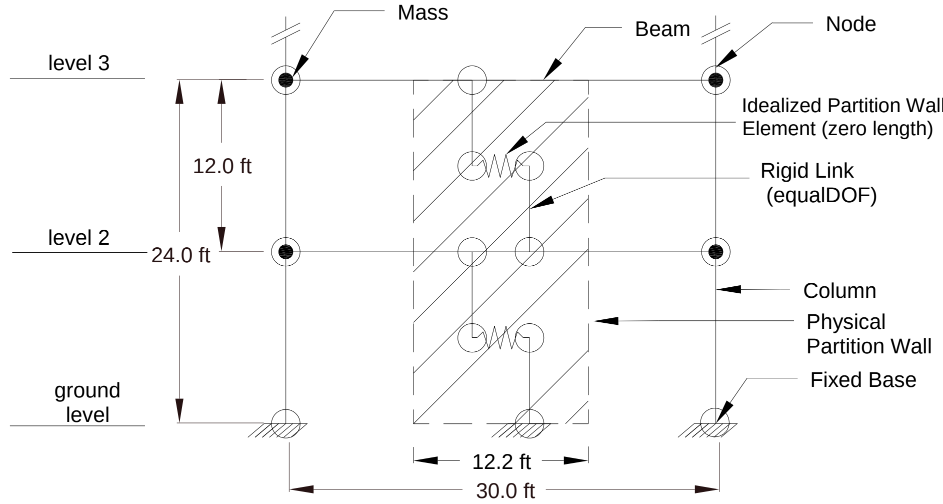

Figure 7-1 Partition wall implementation between two adjacent story levels.
In this example, a 12.2 ft wall is placed within a bay width of 30 ft.

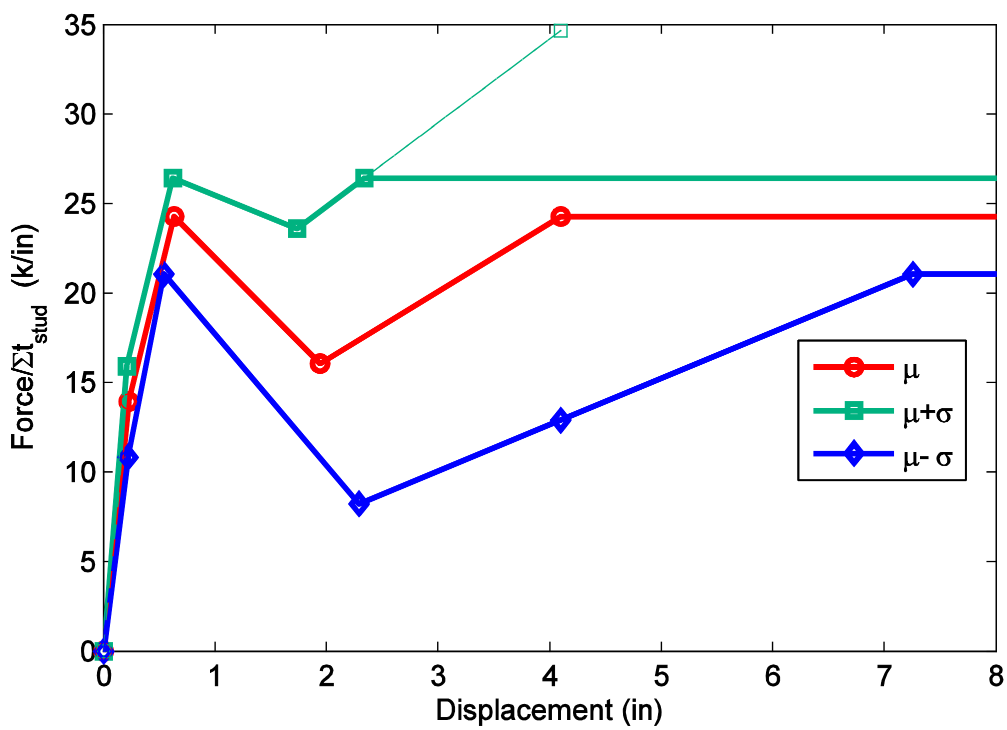

Figure 7-2 Backbone of the normalized partition wall model as implemented in OpenSees.

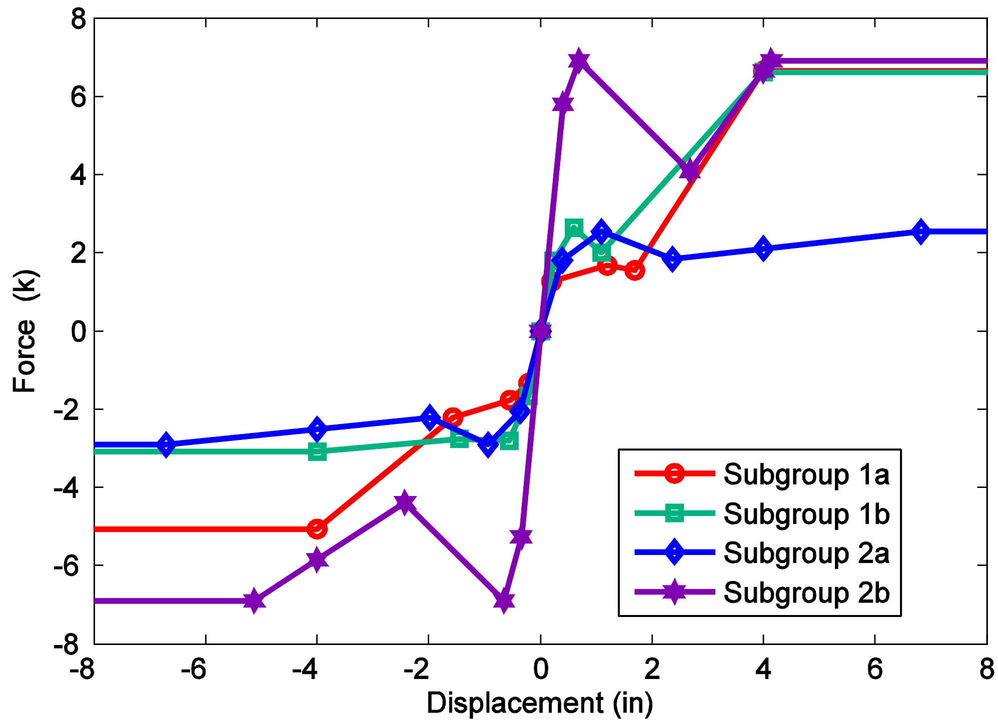

Figure 7-3 Backbone of the Subgroup type partition wall model as implemented in OpenSees.

7.3 Scaling Rules and Recommended Wall Lengths

After the walls are placed between the building floor levels, the actual length of the partition wall to be carried by a given frame bay in the building model needs to be determined. One method to determine representative wall lengths is based on partition indices. French and Xu (2010) determined partition indices by analyzing three model building blueprints and compared their findings to that proposed in ATC-58 (ATC, 2009). The partition index is a takeoff quantity defined as the total lineal feet of partition walls per floor divided by the floor area ($L/L^2 = 1/L$). To explore the full range of partition wall lengths, commonly observed, herein the upper and lower bound values are utilized.

Knowing the details of each of the building plans, the corresponding partition wall lengths are estimated assuming the walls are proportional to the building geometry and the tributary area of an interior frame. Using these partition indices results, two partition wall lengths L_{min} and L_{max} are calculated. The scaling of the partition walls is primarily based on the number of studs for a given partition wall configuration, which is a linear relation of the wall length (Figure 7-4).

Considering an example building suite, the corresponding maximum and minimum values for partition lengths are demonstrated in Table 7-1).

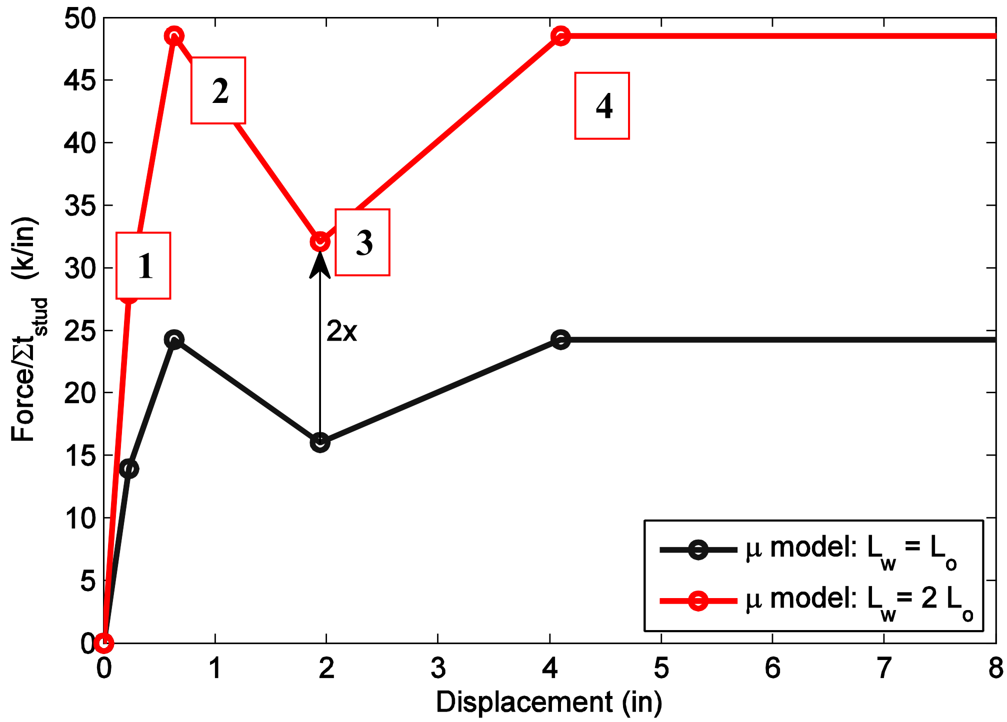

Figure 7-4 Example of partition wall scaling when the target wall is twice the length of the original wall with twice the number of vertical studs in the lateral direction. The four marked points highlight the points considered for scaling walls of different lengths.

7.3.1 Stiffness

The initial stiffness is directly controlled through the first backbone point of the model. When walls are scaled for different lengths, the number of studs considered when using the normalized partition wall model will adjust the initial stiffness accordingly. Recall Figure 5-1 shows the experimental backbones prior to conducting normalization. In this figure, it is clearly visible that the institutional specimens are stiffer and stronger. However, when normalizing the strength by the thickness of the studs, the backbones collapse to similar values as shown in Figure 5-2. This observation supports use of a simple linear scaling according to the number of studs along a wall length to calculate the initial stiffness of the partition walls model.

Table 7-1 Partition wall indices for each building and corresponding wall lengths.

Building Type[6]	**Partition Wall Characteristics**		
	Classification[7]	*Partition Index (1/ft) [lower bound, upper bound]*[8]	*Number of Walls and Length (ft)*
RC-2	1	0.07 0.13	56 ft 104 ft
RC-4	1	0.07 0.13	56 ft 104 ft
RC-8	1	0.07 0.13	56 ft 104 ft
RC-12	1	0.07 0.13	56 ft 104 ft
RC-20	1	0.07 0.13	56 ft 104 ft
ST-3	1	0.07 0.13	50 ft 94ft
ST-9	1	0.07 0.13	63 ft 117 ft
ST-20	1	0.07 0.13	25 ft 48 ft
ST-3	2	0.06 0.14	43 ft 101 ft

7.3.2 Maximum Force (Yielding)

The maximum force obtained by the walls, the 2nd backbone point, is demonstrated in Figure 5-1. Once again, Figure 5-2 normalizes this quantity for the stud thickness without introducing any additional scatter in the data up until the yielding point. Since no significant difference is noted for the displacement occurrences it is justifiable to idealize in a linear fashion the maximum force by the total number of studs for a given partition wall length.

---

[6] Refer to table 7-2 for building details, RC-X is a reinforced concrete building with X number of stories, and ST-X is a steel building with X number of stories. ST-3H is a three story steel hospital building.
[7] Classification is defined by building occupancy, 1 refers to office and 2 refers to hospital usage.
[8] Partition index values were obtained by French and Xu (2010).

7.3.3 Post-Yield Degradation

The post-peak behavior (backbone point 3) of the partition wall system is not well behaved for most of the tested partition wall systems. Degradation of the wall load carry capacity does occur for displacement values in excess of the maximum force. However whether this degradation continues or experiences a post-peak hardening is ill-defined and is demonstrated by comparing the differences between the mean and standard deviation variants of the model. Since no better method can be determined to assess the post-yield degradation, it is assumed to be linearly scaled by the total number of studs for a given partition wall length. This is considered reasonable, conservative, and consistent with experimental observations given the lack of information regarding the behavior in this region of response.

7.3.4 Post-Yield Hardening and Capping Force

Post-yield hardening characterized by 4^{th} backbone point is largely governed by the damage characteristics of the specimens. The post-yield hardening is envisioned to physically occur if the gap between the ceiling and drywall panel, or return wall and drywall panel, closes. This post-yield hardening does not always occur, but this physical behavior is realistic and observed in two specimens without the presence of return walls, namely specimens 5 and 6. Consequently this behavior is not neglected in the model. This post-yield hardening has not been considered in previous studies (Davies, 2009 and Restrepo and Lang, 2011).

Herein capping force is selected as the force value when the partition wall specimens are pushed beyond the testing limit of 3% interstory drift. This maximum force is capped at the yield force to assure that undue excess strength is not realized by the model (note the mean plus one standard deviation model in Figure 7-2). However this capping force limitation is not placed on the developed subgroup models, because force values greater than the yield strength were observed in the experiments. Consequently the maximum force value obtained in the subgroup models experiments are set as the capping force for these models (1a and 1b). These maximum force values obtained in the subgroup 1a and 1b may reach the physical limit in which the gypsum experiences crushing.

7.3.5 Limitation in Wall Length

In the scaling of partition walls for different lengths, this method is most ideal for walls near the same length as those tested (H/L is approximately 1). The failure mode of extremely long walls may change, and this is an important feature to consider in future experimental setups. However when one considers the total length of walls, it should be noted that the partition index is defined as the sum of all individual walls rather than the length of a single wall. Many partition walls of smaller lengths, as tested, would combine in series. Many walls on the same floor in series would be justified for use in the linearly scaling method by the number of vertical studs in the lateral direction.

7.4 Example Building Suite Considered

To demonstrate the partition wall implementation and study its impact on buildings, a suite of buildings with a range of characteristics (floor heights, construction types, occupancies, periods, etc.) is selected and modeled in OpenSees. The proposed suite of building model includes nine buildings (Table 7-2). These nine buildings are either steel or reinforced concrete style construction, have either an occupancy use of general office or hospital; and range from 2-20 stories in height. These building models details are presented in Table 7-2. Within each building model, the interior partition wall characteristics will be varied due to the different possible configurations in practice. The first 5 buildings, concrete special moment frames were developed in a study by Wood et al. (2009) denoted as RC-X (i.e. RC-2, RC-4, etc.), a three-story steel hospital is a redesigned SAC building by Wieser (2011) denoted as S-3H, and the last three buildings are sample buildings taken from the 1999 SAC Steel Project (Gupta et al., 1999) denoted as S-X (S-3, S-9 and S-20).

Table 7-2 Suite of buildings considered. (RC = reinforced concrete. NS=north-south direction, EW=east-west direction)

Building	Design Code	Occupancy/Use	Number of Stories	Floor Plan		Story Heights			Design Accelerations		Site Classification (ASCE 7-05)	Period
				NS	EW	First (ft)	Second (ft)	Upper (ft)	S_s (g)	S_1 (g)		T_1 (s)
RC-2	IBC 2006, ACI 318-08	Office Bldg	2	5 @ 30ft	5 @ 30ft	12.0	12.0	12.0	2.00	0.77	C	0.24
RC-4	IBC 2006, ACI 318-08	Office Bldg	4	5 @ 30ft	5 @ 30ft	12.0	12.0	12.0	2.00	0.77	C	0.47
RC-8	IBC 2006, ACI 318-08	Office Bldg	8	5 @ 30ft	5 @ 30ft	12.0	12.0	12.0	2.00	0.77	C	0.89
RC-12	IBC 2006, ACI 318-08	Office Bldg	12	5 @ 30ft	5 @ 30ft	12.0	12.0	12.0	2.00	0.77	C	1.33
RC-20	IBC 2006, ACI 318-08	Office Bldg	20	5 @ 30ft	5 @ 30ft	12.0	12.0	12.0	2.00	0.77	C	2.07
S-3H	IBC 2006	Hospital	3	4 @ 30ft	6 @ 30ft	20.0	16.0	16.0	1.508	0.75	D	0.28
Building	Design Code	Occupancy/Use	Number of Stories	Floor Plan		Story Heights			Seismic Design		Site Classification (UBC 1994)	Period
				NS	EW	First (ft)	Second (ft)	Upper (ft)	Zone	Effective PGA (g)		T_1 (s)
S-3	UBC 1994	Office Bldg	3	4 @ 30ft	6 @ 30ft	13.0	13.0	13.0	4	0.40	s2	0.34
S-9	UBC 1994	Office Bldg	9	5 @ 30ft	5 @ 30ft	12.0	18.0	13.0	4	0.40	s2	0.82
S-20	UBC 1994	Office Bldg	20	5 @ 20ft	6 @ 20ft	24.0	18.0	13.0	4	0.40	s2	1.79

7.5 Sample Building Sensitivity

To quickly gather a sense of the sensitivity in the partition wall placement in various buildings considered in the example building suite, an eigenvalue analysis is conducted. In the eigenvalue analysis, the parameters collected and compared are the modal frequencies (periods) and mass participation estimates for the first four modes, when appropriate. Table 7-3 through Table 7-11 display the period and mass participation estimates for the first four modes by building type. In each table, the periods and mass participation estimates are shown for bare structure (no wall) and the short and long wall placements considering each of the normalized models: mean, mean minus one standard deviation, and mean plus one standard deviation. Furthermore to simplify the comparison, two normalized parameters are calculated demonstrating the dynamic shift when considering the addition of partition walls to the bare frame system (no wall) in equations 7-1 and 7-2:

$$T_i^* = \frac{T_i^n}{T_i^{bare}} \tag{7-1}$$

$$MP_i^* = \frac{MP_i^n}{MP_i^{bare}} \tag{7-2}$$

where the period of the structure with the wall is divided by the period of structure without any wall (bare frame) placements in the ith mode. In addition, the mass participation of the structure with the wall is divided by the mass participation of structure without any wall placements in the ith mode. The illustration of these normalized parameters is shown in Figure 7-5 through Figure 7-13. As expected, when the wall length is increased, the vibration period of the building decreases. Similarly, when one considers use of the mean minus a standard deviation, the dynamic shift on the building is reduced, as the strength and the stiffness of the wall is reduced in the modeling formulation. This statement holds true as well when considering the mean plus a standard deviations, as the dynamic shift is increased due to a greater stiffness and strength of the partition wall. However the degree to which this dynamic shift occurs is most influenced by length of the wall rather than which of the normalized walls are used. The greatest period shift is found in the three story hospital, which is the only building model which considered use of institutional partition walls (group 2). The shift is on the order of 14% when considering the longest wall and the mean plus one standard deviation representative model. The smallest period shift is found in the 20 story steel model (SAC building) almost an obscure effect, due to the reduced wall lengths. The largest change in the mass participation is noted in RC-9, where the second mode is increased by approximately 40%. However, this change in mass participation is not a significant change because the bare structure has a mass participation in the second mode of 0.4% and this increased to 0.6%, demonstrating one disadvantage of the selected normalized parameter.

Table 7-3 Modal periods and mass participation sensitivity for RC-2.

			Average		Minus Std		Plus Std	
	Mode	No wall	56 ft	104 ft	56 ft	104 ft	56 ft	104 ft
Period (s)	1	0.203	0.196	0.192	0.198	0.194	0.195	0.190
	2	0.051	0.050	0.050	0.050	0.050	0.050	0.050
MP (%)	1	0.843	0.846	0.848	0.845	0.847	0.846	0.849
	2	0.157	0.154	0.152	0.155	0.153	0.154	0.151

Table 7-4 Modal periods and mass participation sensitivity for RC-4.

			Average		Minus Std		Plus Std	
	Mode	No wall	56 ft	104 ft	56 ft	104 ft	56 ft	104 ft
Period (s)	1	0.419	0.400	0.387	0.403	0.393	0.396	0.381
	2	0.116	0.113	0.111	0.114	0.112	0.113	0.110
	3	0.056	0.056	0.055	0.056	0.055	0.055	0.055
	4	0.037	0.037	0.037	0.037	0.037	0.037	0.037
MP (%)	1	0.792	0.797	0.800	0.796	0.799	0.798	0.801
	2	0.140	0.137	0.135	0.137	0.136	0.136	0.134
	3	0.053	0.052	0.051	0.052	0.052	0.052	0.051
	4	0.015	0.015	0.014	0.015	0.014	0.014	0.014

Table 7-5 Modal periods and mass participation sensitivity for RC-8.

			Average		Minus Std		Plus Std	
	Mode	No wall	56 ft	104 ft	56 ft	104 ft	56 ft	104 ft
Period (s)	1	0.784	0.748	0.724	0.755	0.735	0.742	0.714
	2	0.241	0.233	0.226	0.234	0.229	0.231	0.224
	3	0.126	0.122	0.120	0.123	0.121	0.122	0.119
	4	0.079	0.077	0.076	0.078	0.077	0.077	0.076
MP (%)	1	0.784	0.787	0.789	0.787	0.788	0.788	0.790
	2	0.106	0.105	0.105	0.106	0.105	0.105	0.105
	3	0.043	0.042	0.041	0.042	0.042	0.042	0.041
	4	0.027	0.026	0.026	0.026	0.026	0.026	0.026

Table 7-6 Modal periods and mass participation sensitivity for RC-12.

			Average		Minus Std		Plus Std	
	Mode	No wall	56 ft	104 ft	56 ft	104 ft	56 ft	104 ft
Period (s)	1	1.190	1.137	1.101	1.147	1.117	1.127	1.086
	2	0.380	0.364	0.353	0.367	0.358	0.361	0.349
	3	0.207	0.199	0.194	0.201	0.196	0.198	0.191
	4	0.134	0.130	0.127	0.131	0.128	0.129	0.126
MP (%)	1	0.778	0.779	0.780	0.779	0.779	0.779	0.780
	2	0.097	0.098	0.099	0.098	0.098	0.098	0.099
	3	0.040	0.040	0.039	0.040	0.040	0.040	0.039
	4	0.024	0.023	0.023	0.023	0.023	0.023	0.023

Table 7-7 Modal periods and mass participation sensitivity for RC-20.

	Mode	No wall	Average		Minus Std		Plus Std	
			56 ft	104 ft	56 ft	104 ft	56 ft	104 ft
Period (s)	1	2.067	1.984	1.929	1.999	1.953	1.969	1.907
	2	0.710	0.672	0.649	0.679	0.659	0.666	0.639
	3	0.394	0.372	0.358	0.376	0.364	0.368	0.353
	4	0.262	0.250	0.242	0.252	0.245	0.247	0.238
MP (%)	1	0.738	0.740	0.740	0.739	0.740	0.740	0.740
	2	0.131	0.132	0.133	0.132	0.133	0.132	0.134
	3	0.027	0.027	0.027	0.027	0.027	0.027	0.027
	4	0.030	0.029	0.029	0.029	0.029	0.029	0.029

Table 7-8 Modal periods and mass participation sensitivity for S-3.

	Mode	No wall	Average		Minus Std		Plus Std	
			50 ft	94 ft	50 ft	94 ft	50 ft	94 ft
Period (s)	1	0.343	0.328	0.317	0.331	0.322	0.325	0.313
	2	0.119	0.114	0.111	0.115	0.112	0.113	0.109
	3	0.071	0.069	0.068	0.070	0.069	0.069	0.067
MP (%)	1	0.868	0.873	0.876	0.872	0.875	0.874	0.878
	2	0.081	0.077	0.075	0.078	0.076	0.077	0.075
	3	0.031	0.030	0.029	0.030	0.029	0.030	0.028

Table 7-9 Modal periods and mass participation sensitivity for S-3H.

	Mode	No wall	Average		Minus Std		Plus Std	
			43 ft	101 ft	43 ft	101 ft	43 ft	101 ft
Period (s)	1	0.280	0.263	0.246	0.266	0.252	0.259	0.241
	2	0.082	0.079	0.075	0.079	0.076	0.078	0.074
	3	0.042	0.041	0.040	0.041	0.041	0.041	0.040
	4	0.000	0.000	0.000	0.000	0.000	0.000	0.000
MP (%)	1	0.903	0.906	0.908	0.905	0.907	0.906	0.909
	2	0.056	0.054	0.053	0.055	0.053	0.054	0.053
	3	0.020	0.019	0.018	0.019	0.019	0.019	0.018

Table 7-10 Modal periods and mass participation sensitivity for S-9.

	Mode	No wall	Average		Minus Std		Plus Std	
			63 ft	117 ft	56 ft	104 ft	56 ft	104 ft
Period (s)	1	0.820	0.783	0.757	0.790	0.768	0.776	0.746
	2	0.286	0.272	0.262	0.275	0.267	0.270	0.258
	3	0.168	0.160	0.154	0.161	0.156	0.158	0.152
	4	0.115	0.110	0.107	0.111	0.108	0.109	0.106
MP (%)	1	0.880	0.878	0.877	0.879	0.878	0.878	0.876
	2	0.004	0.005	0.006	0.005	0.006	0.005	0.006
	3	0.087	0.085	0.084	0.085	0.085	0.085	0.084
	4	0.010	0.009	0.008	0.009	0.009	0.009	0.008

Table 7-11 Modal periods and mass participation sensitivity for S-20.

	Mode	No wall	Average		Minus Std		Plus Std	
			25 ft	48 ft	25 ft	48 ft	25 ft	48 ft
Period (s)	1	1.397	1.387	1.378	1.389	1.382	1.385	1.374
	2	0.413	0.408	0.404	0.409	0.406	0.407	0.402
	3	0.217	0.214	0.211	0.214	0.212	0.213	0.210
	4	0.151	0.149	0.147	0.149	0.147	0.148	0.146
MP (%)	1	0.738	0.737	0.736	0.737	0.736	0.737	0.735
	2	0.164	0.166	0.167	0.166	0.167	0.166	0.168
	3	0.042	0.042	0.043	0.042	0.043	0.042	0.043
	4	0.016	0.016	0.016	0.016	0.016	0.016	0.017

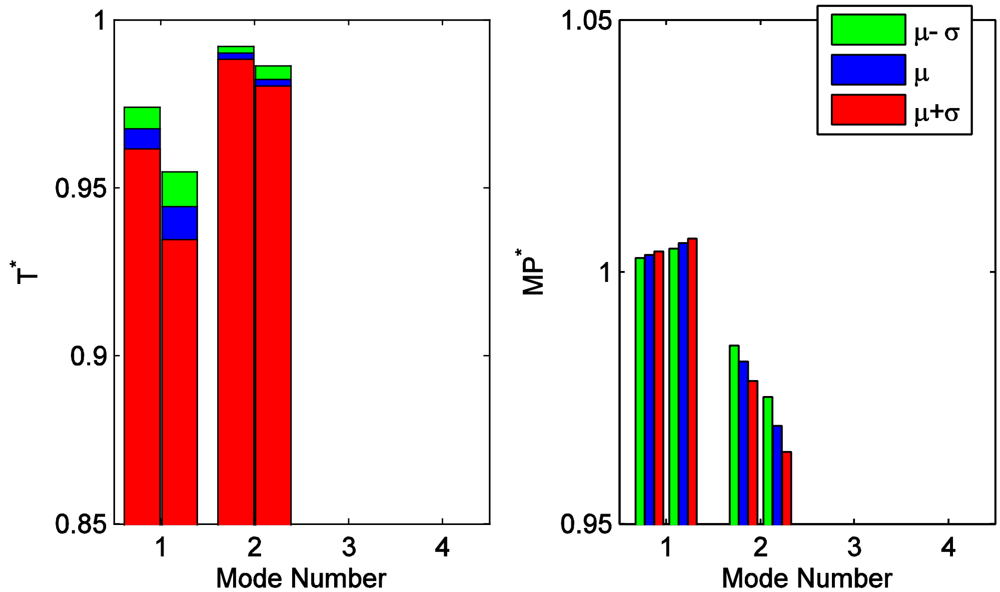

Figure 7-5 Normalized plots demonstrating period and mass participations sensitivities for RC-2.

Note in the period illustration, the right and left bars refer to the short and long wall lengths. Similarly for the mass participations, the immediate three bars to the right and left refer to the short and long wall lengths, for each statistical level.

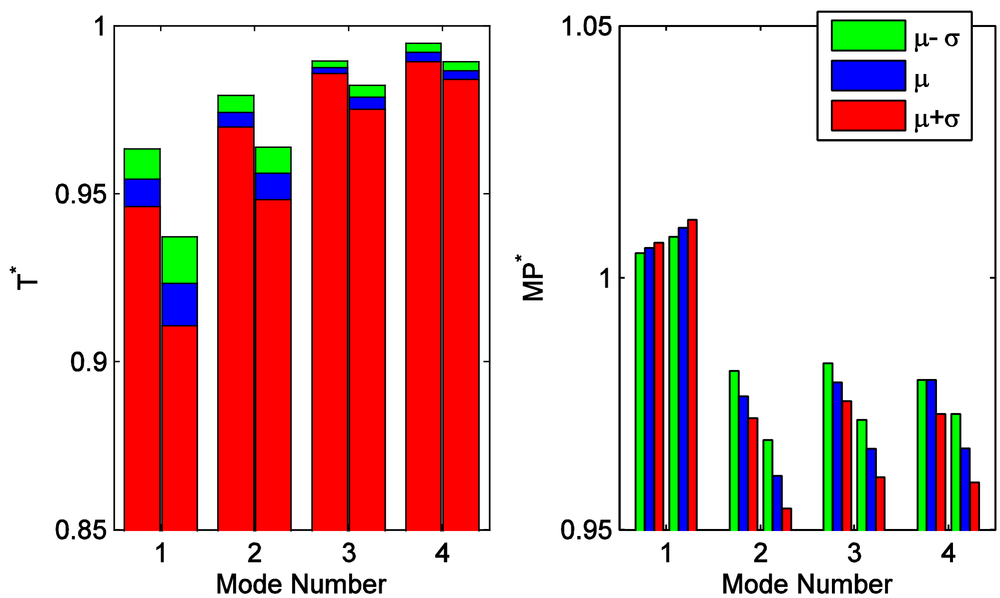

Figure 7-6 Normalized plots demonstrating period and mass participations sensitivities for RC-4.

Note in the period illustration, the right and left bars refer to the short and long wall lengths. Similarly for the mass participations, the immediate three bars to the right and left refer to the short and long wall lengths, for each statistical level.

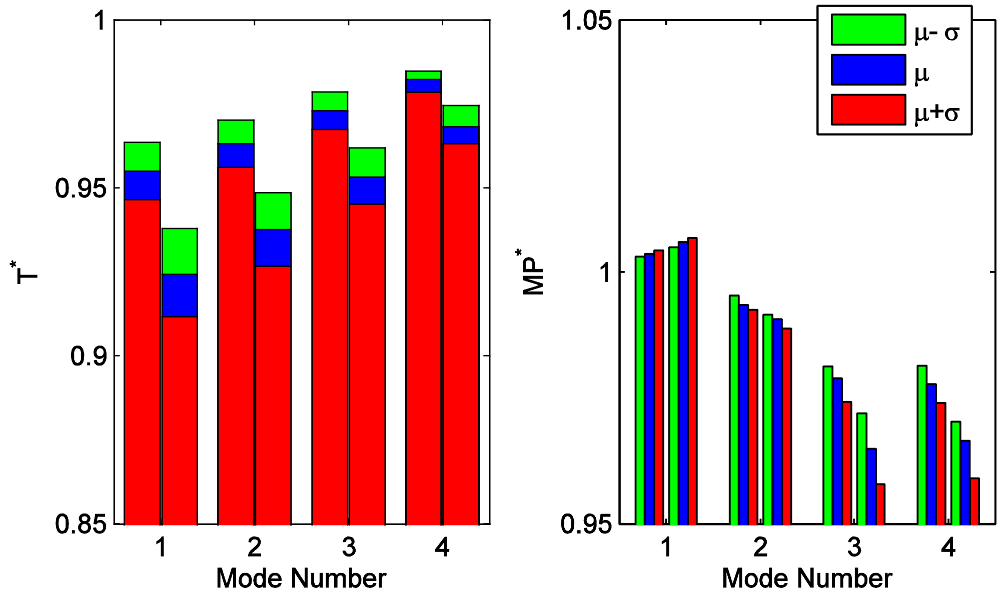

Figure 7-7 Normalized plots demonstrating period and mass participations sensitivities for RC-8.

Note in the period illustration, the right and left bars refer to the short and long wall lengths. Similarly for the mass participations, the immediate three bars to the right and left refer to the short and long wall lengths, for each statistical level.

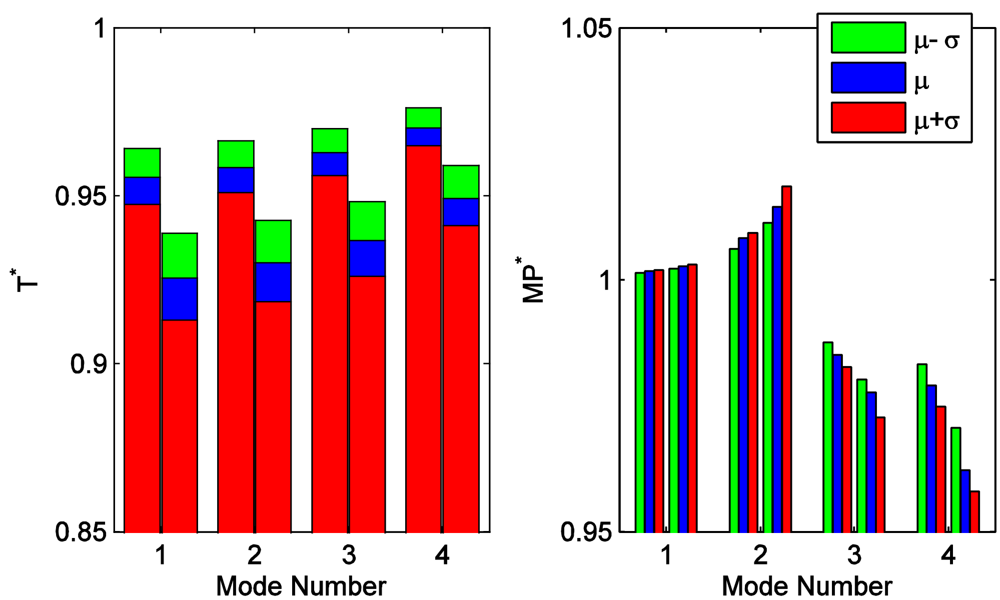

Figure 7-8 Normalized plots demonstrating period and mass participations sensitivities for RC-12.

Note in the period illustration, the right and left bars refer to the short and long wall lengths. Similarly for the mass participations, the immediate three bars to the right and left refer to the short and long wall lengths, for each statistical level.

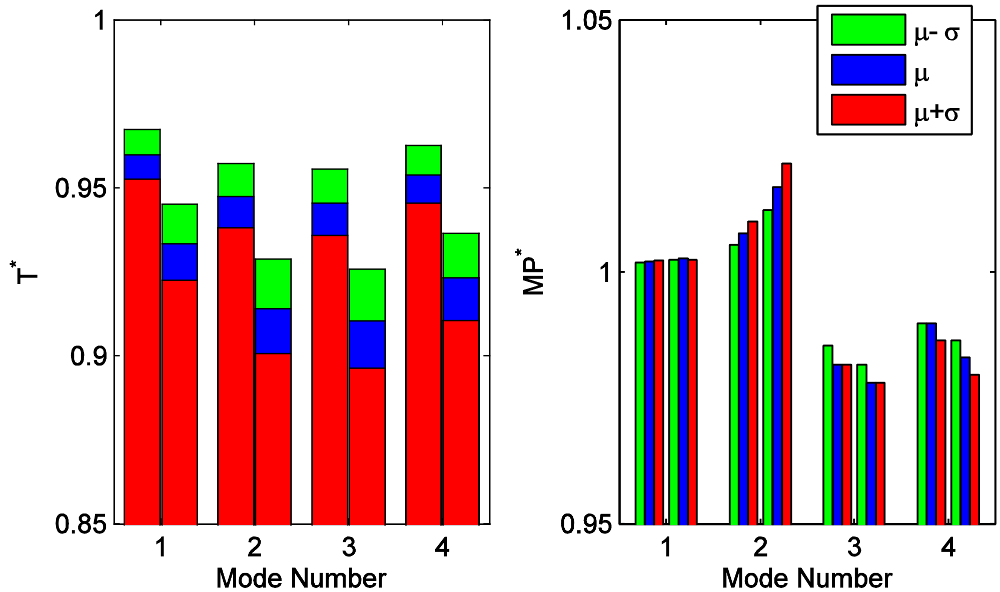

Figure 7- 9 Normalized plots demonstrating period and mass participations sensitivities for RC-20.

Note in the period illustration, the right and left bars refer to the short and long wall lengths. Similarly for the mass participations, the immediate three bars to the right and left refer to the short and long wall lengths, for each statistical level.

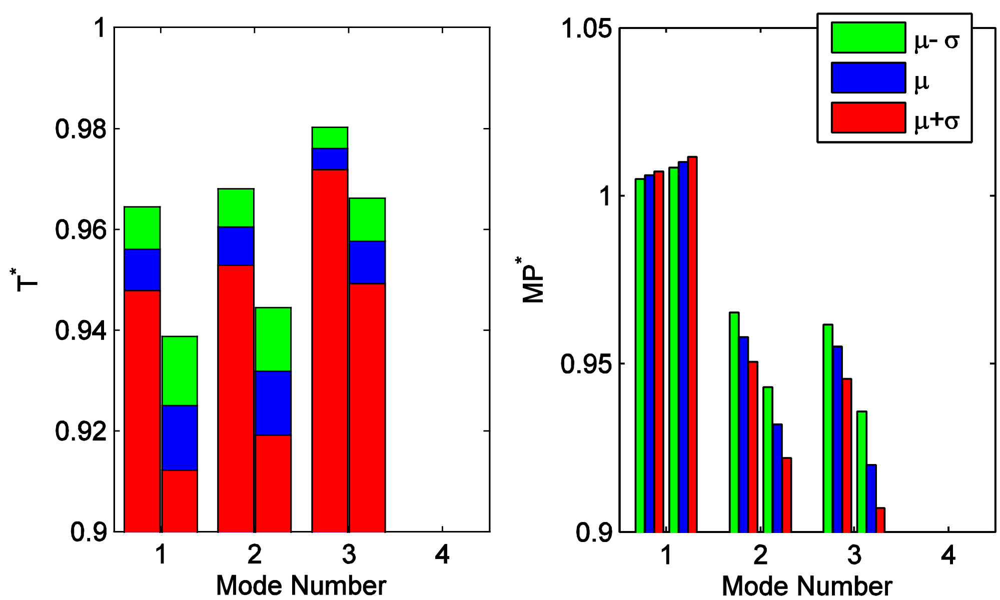

Figure 7-10 Normalized plots demonstrating period and mass participations sensitivities for S-3.

Note in the period illustration, the right and left bars refer to the short and long wall lengths. Similarly for the mass participations, the immediate three bars to the right and left refer to the short and long wall lengths, for each statistical level.

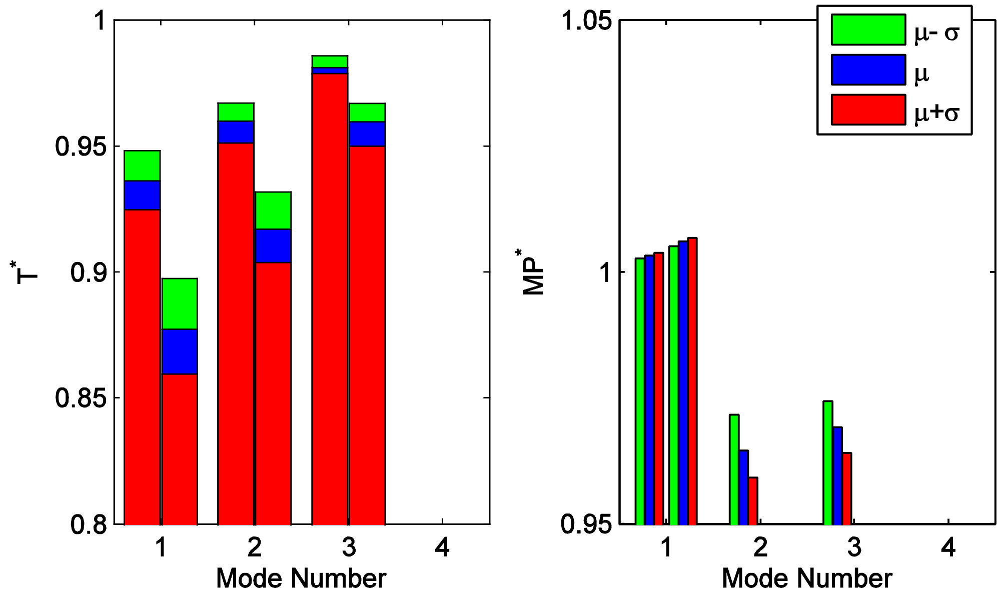

Figure 7-11 Normalized plots demonstrating period and mass participations sensitivities for S-3H.

Note in the period illustration, the right and left bars refer to the short and long wall lengths. Similarly for the mass participations, the immediate three bars to the right and left refer to the short and long wall lengths, for each statistical level.

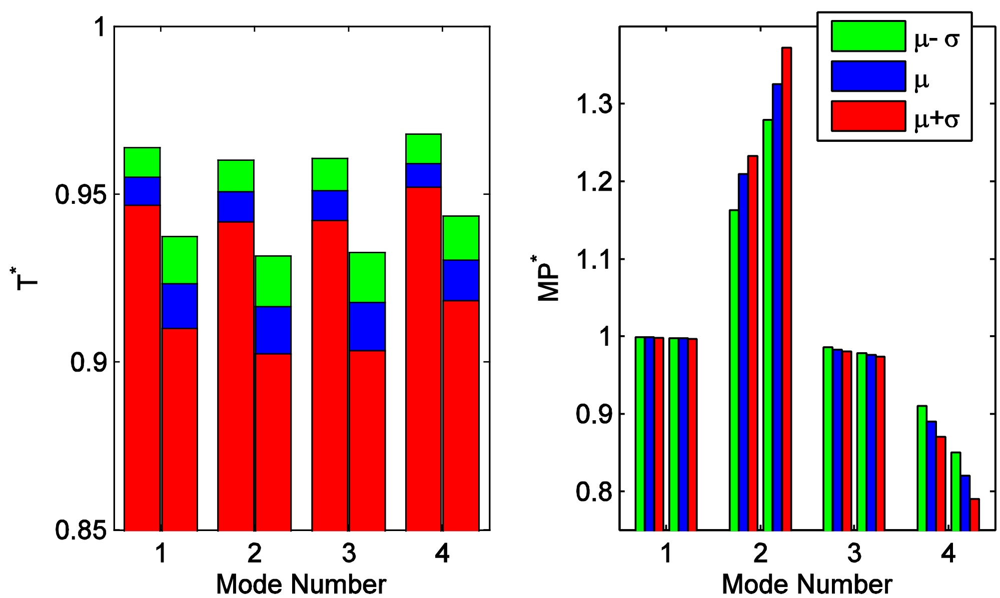

Figure 7-12 Normalized plots demonstrating period and mass participations sensitivities for S-9.

Note in the period illustration, the right and left bars refer to the short and long wall lengths. Similarly for the mass participations, the immediate three bars to the right and left refer to the short and long wall lengths, for each statistical level.

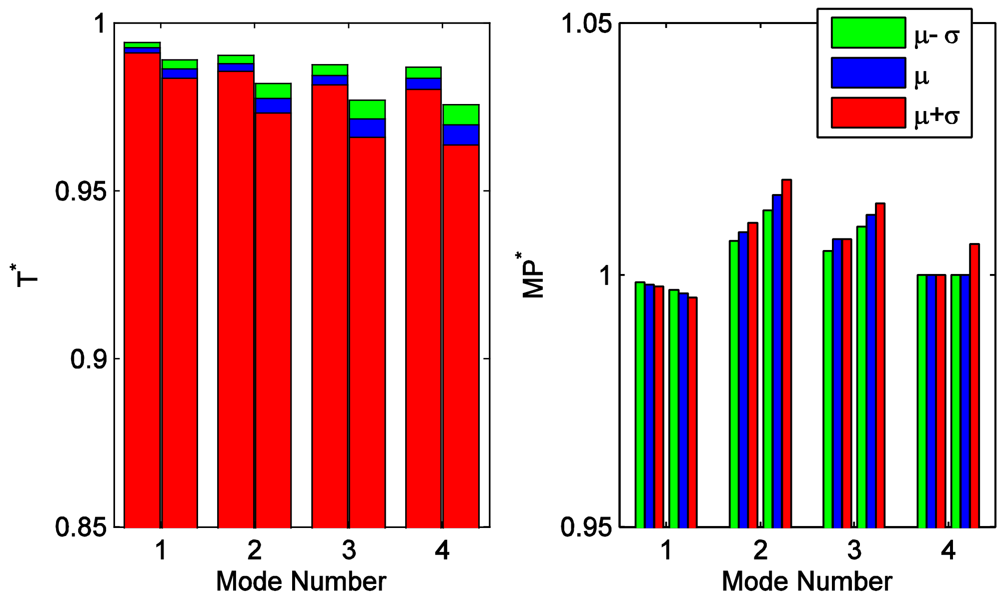

Figure 7-13 Normalized plots demonstrating period and mass participations sensitivities for S-20.

Note in the period illustration, the right and left bars refer to the short and long wall lengths. Similarly for the mass participations, the immediate three bars to the right and left refer to the short and long wall lengths, for each statistical level.

7.6 Implementation Conclusion and Further Studies

In this section, the model implementation is explored. Model implementation whereby the partition wall spans two adjacent floor beams is illustrated. Using the developed models, rules for scaling of the partition walls of different lengths are required and detailed. The scaling of the partition walls is based on the number of vertical studs for a known partition wall type. However this type of linear scaling should not be adopted for walls of considerable lengths, which may experience a change of failure mode and significant behavioral change is anticipated. Knowledge of the behavior of partition walls of various lengths must be explored in future experiments.

Using the normalized partition wall models, an example suite of buildings is considered to understand the dynamic sensitivity when one considers wall placement. Nine representative building models considering both concrete and steel moment frame structures are demonstrated with various partition wall placements. Knowing the dynamic shifts introduced by inclusion of the partition wall is critical in the model assessment for future studies. The follow-up report to this study documents the fragility development of these buildings in an uncoupled (no partition walls) and coupled (with partition walls) analyses.

SECTION 8
CONCLUSIONS

8.1 Motivation and Scope of Work

In numerous earthquakes, the damage to nonstructural components and systems (NCSs) has exceeded the cost of structural damage in buildings. NCSs within buildings may have complicated configurations and connections to a building making them susceptible to earthquake damage. The majority of NCSs are placed or distributed throughout a building, and therefore not subjected to the ground motion generated by the earthquake, but rather to an amplified and filtered motion transmitted by the building. NCSs can affect the building performance after a seismic event and they are capable of causing serious injuries or death (e.g. Filiatrault et al., 2002).

In practice, NCSs are diverse, however this report focuses on a portion of a larger study whereby one widely used nonstructural system representing significant investment, namely, the ceiling-piping-partition (CPP) system, is studied. A major component of this three piece subsystem is the partition wall subsystem. The focus herein is on the development and calibration of a numerical model for capturing the in-plane seismic response of full-height partition walls. Prior to this effort, a detailed 50 specimen test program was conducted at the State University of New York, University at Buffalo (Davies, 2009). Using these experimental results, a partition wall modeling scheme is outlined. It should be noted that the most common partition wall subsystem utilized in the United States for buildings other than houses is the metal stud-gypsum board type (Figure 8-1), and therefore this is the type of material and construction considered herein.

8.2 Model Summary

The platform selected to model the partition walls is Open System for Earthquake Engineering Simulation (OpenSees) (Mazzoni et al., 2009). OpenSees is an open-source simulation and modeling software platform developed by the Pacific Earthquake Engineering Research (PEER) Center. The partition wall is developed as a lumped model, which is discretized using a zero-length element coupled with the pinching4 material. *Pinching4* is a uniaxial material model that allows for a “pinched” load-deformation response with an optional degradation contribution. To represent the experimental specimens, this *pinching4* material is used in a parallel configuration providing better control of the unload and reload parameters as a function of the displacement range. Robust performance of the model is sought across the drift levels associated with three commonly observed damage states of minor, moderate and major.

Figure 8-1 Example usage of light-gauge steel studding and gypsum board system during construction.

In the use of the material, the partition wall is characterized as a simple uniaxial spring. This spring is implemented only in the in-plane direction whereas the out–of-plane behavior of the partition walls is not characterized numerically herein. The out-of-plane behavior of the walls is approximately 10% of the in-plane partition wall stiffness and therefore negligible when considered their placement in potential building models.

Two different classes of models were developed: subgroup and normalized models. The four subgroup models are: 1) 1a commercial partial connection, 2) 1b commercial full connection, 3) 2a institutional partial connection and 4) 2b institutional full connection. Each of these models are based the mean response of the specimens within the subgroup. To simplify the modeling approach, subgroups 1b and 2b are combined into a normalized model and the variability in model response, as compared with the experiment, evaluated. Subgroups 1a and 2a, corresponding to partially connected specimens, are not considered for the normalized models due to different mechanisms developed during testing. Three different normalized partition wall models are developed: 1) mean (μ), 2) mean plus one standard deviation ($\mu+\sigma$) and 3) mean minus one standard deviation ($\mu-\sigma$). The chosen backbone force-displacement points and the unload and reloading parameters for each set of models are shown in Tables 4-1 and 5-1.

8.3 Model Use and Future Work

The developed models are evaluated using two error metrics in section 6, force residual and difference in half cycle energy. For a fully connected specimen, use of the normalized mean model is shown to represent the partition wall subsystem well. For a partially connected partition wall, the subgroup model 1b or 2b (commercial or institutional) would represent this partition wall subsystem. In the end either representation provides for fruitful assessment of the walls behavior, particularly within the drift ratios of interest, i.e. those linked with physical damage states of interest to qualify for repair or replacement of the wall. Using these developed models, guidelines for implementation within OpenSees are presented in Section 7. The sensitivity of including partition walls within numerical building models are demonstrated in terms of period and modal participation changes in Section 7. The greatest period shift is observed in a model of a three-story hospital, which is the only building model which considered use of institutional partition walls (group 2). In a follow-up report, the building models with partition walls are subjected to suite of nonlinear time history analyses to develop fragility functions representing the various damage levels.

SECTION 9
REFERENCES

American Concrete Institute. (2008) "*Building code requirements for structural concrete." ACI 318-08*, Farmington Hills, Michigan.

Arnold, A.E., Uang, C.M., Filiatrault, A. (2003). *Cyclic Behavior and Repair of Stucco and Gypsum Sheathed Woodframe Walls: Phase I.* Report No. SSRP 2002/07, Department of Structural Engineering, University of California, San Diego, La Jolla, CA.

Arnold, A.E., Uang, C.M., Filiatrault, A. (2005). *Cyclic Behavior and Repair of Stucco and Gypsum Sheathed Woodframe Walls: Phase II.* Report No. SSRP 2003/02, Department of Structural Engineering, University of California, San Diego, La Jolla, CA.

ASCE 7-05. (2006). *Minimum Design Loads for Buildings and Other Structures*. American Society of Civil Engineers: Reston, VA.

Applied Technology Council. (2009). *ATC-58 50% Draft. Guidelines for Seismic Performance Assessment of Buildings.* Redwood City, CA,

Baird, A., Diaferia, R., Palermo, A. and Pampanin, S. (2011). "Parametric Investigation of Seismic Interaction between Precast Concrete Cladding Systems and Moment Resisting Frames." *ASCE Structures Congress 2011:* 1286-1297.

Bersofsky, A. (2004). *A Seismic Performance Evaluation of Gypsum Wallboard Partitions.* MS Thesis, Department of Structural Engineering, University of California, San Diego, La Jolla, CA.

Building Seismic Safety Council (BSSC), (2000). *Standard and Commentary for the Seismic Rehabilitation of Buildings, FEMA-356*, Federal Emergency Management Agency, Washington, D.C

Carr, A.J. (2005). *Computer Program RUAUMOKO*. Department of Civil Engineering, University of Canterbury, Christchurch, New Zealand.

Davies, R. D. (2009). *Seismic Evaluation, Parameterization, and Effect of Light-Frame Steel Studded Gypsum Partition Walls.* MS Thesis, Department of Civil, Structural and Environmental Engineering, University at Buffalo, State University of New York (SUNY).

Dinehart, D.W. and Shenton, H.W. (2000). “Model for Dynamic Analysis of Wood Frame Shear Walls.” *ASCE Journal of Engineering Mechanics*, 126(9): 899-908.

Earthquake Engineering Research Institute (EERI) (2010a). *The El Mayor Cucapah, Baja California Earthquake April 4, 2010. An EERI Reconnaissance Report 2010-02*. Meneses, J. (ed), Oakland, California.

Earthquake Engineering Research Institute (EERI) (2010b). *Learning from Earthquakes: The M_w 8.8 Chile Earthquake of February 27, 2010. EERI Special Earthquake Report – June 2010.* Oakland, California.

Filiatrault, A., Christopoulos, C., and Stearns, C. (2002). *Guidelines, Specifications, and Seismic Performance Characterization of Nonstructural Building Components and Equipment*. PEER Report 2002/05. Pacific Earthquake Engineering Research Center, College of Engineering, UC Berkeley.

Folz, B and Filiatrault, A. (2001). “Cyclic Analysis of Wood Shear Walls.” *ASCE Journal of Structural Engineering,* 127(4): 433-441.

Folz, B and Filiatrault, A. (2004a). “Seismic Analysis of Woodframe Structures. I: Model Formulation.” *ASCE Journal of Structural Engineering,* 130(9): 1353-1360.

Folz, B and Filiatrault, A. (2004b). “Seismic Analysis of Woodframe Structures. I: Model Implementation and Verification.” *ASCE Journal of Structural Engineering,* 130(9): 1361-1370.

French, S. and Xu, J. (2010). Internal project correspondent. Not published.

Fülöp, L.A. and Dubina, D. (2004a). “Performance of Wall-Stud Cold-Formed Shear Panels Under Monotonic and Cyclic Loading Part II; Numerical Modelling and Performance Analysis.” *Thin-Walled Structures, 42(2): 339-349.*

Fülöp, L.A. and Dubina, D. (2004b). “Performance of Wall-Stud Cold-Formed Shear Panels Under Monotonic and Cyclic Loading Part I; Experimental Research.” *Thin-Walled Structures,* 42(2): 321-338.

Gupta, A. and Krawinkler, H. (1999). *Seismic Demands for Performance Evaluation of Steel Moment Resisting Frame Structures (SAC Task 5.4.3). Report No. 132,* Department of Civil and Environmental Engineering, Stanford University.

Ibarra, L.F., Medina, R.A., and Krawinkler, H. (2004). “Hysteretic Models that Incorporate Strength and Stiffness Deterioration.” *Earthquake Engineering and Structural Dynamics, 34(12): 1489-1511.*

International Code Council, ICC. (2006). *International building code 2006*. International Code Council, Falls Church, Va.

International Conference of Building Officials. (1994). *Uniform Building Code 1994.* Whittier, CA.

Judd, J.P. and Fonseca, F.S. (2005). “Analytical model for Sheathing-to Framing Connections in Wood Shear Walls and Diaphragms.” *ASCE Journal of Structural Engineering,* 131(2): 345-352.

Kanvinde, A.M. and Deierlein, G.G. (2006). “Analytical Models for the Seismic Performance of Gypsum Drywall Partitions.” *Earthquake Spectra.* 22(2): 391-411

Krawinkler, H., Parisi, F., Ibarra, L. Ayoub, A. and Medina, R. (2000). *Development of a testing protocol for wood frame structures*, Report No. W-02, CUREE, Richmond, California.

Lang, A.F. and Restrepo, J.I. (2007). *Seismic Performance Evaluation of Gypsum Wallbaord Partitions. Structural Systems Research Program Report* SSRP 2007/07, University of California, San Diego, La Jolla, CA.

Lee, T.H., Kato, M., Tomohiro, M., Suita, K., and Nakashima, M. (2007). "Seismic performance evaluation of non-structural components: Drywall partitions." *Earthquake Engineering and Structural Dynamics*, 36(3): 367-382.

Mazzoni, S., McKenna, F., Scott, M. H., and Fenves, G. L., (2009). *Open System for Engineering Simulation User-Command-Language Manual*, version 2.0, Pacific Earthquake Engineering Research Center, University of California, Berkeley. <http://opensees.berkeley.edu/>.

Memari, A.M., Kasal, B., Manbeck, H.B., and Adams, A.R. (2008). *Experimental Cyclic Racking Evaluation of Light-frame Wood Stud and Steel Stud Wall Systems*. University Park: The Pennsylvania Housing Research Center.

Mosqueda, G., Retamales, R., Filiatrault, A., and Reinhorn, A.M. (2009). “Testing Facility for Experimental Evaluation of Nonstructural Components under Full-scale Floor Motions,” *Journal of The Structural Design of Tall Buildings*, Wiley, 18(4): 387-404.

NAHB Research Center, Inc. (1997). *Monotonic Tests of Cold-Formed Steel Shear Walls with Openings*. The American Iron and Steel Institute Washington, DC.

NEES Nonstructural Project (2012). *Simulation of the Seismic Performance of Nonstructural Systems.* Accessed May 1, 2012. http://www.nees-nonstructural.org/.

Pang, W.C., Rosowsky, D.V., Pei, S., and van de Lindt, J.W. (2007). “Evolutionary Parameter Hysteretic Model for Shear Walls.” *ASCE Journal of Structural Engineering,* 133(8): 1118-1129.

Restrepo, J.I. and Lang, A.F. (2011). “Study of Loading Protocols in Light Gage Stud Partition Walls” *Earthquake Spectra, 27(4): 1169-1185.*

Restrepo, J.I. and Bersofsky, A.M. (2010). “Performance Characteristics of Light Gage Steel Stud Partition Walls” *Thin-Walled Structures* 49(2): 317-324.

Retamales, R., Mosqueda, G., Filiatrault, A., and Reinhorn, A. (2008). *New Experimental Capabilities and Loading Protocols for Seismic Qualification and Fragility Assessment of Nonstructural Components.* MCEER Technical Report 08-0026, University at Buffalo, State University of New York (SUNY).

Serrette, R., Encalada, J., Juadines, M., and Nguyen H. (1997). "Static Racking Behavior of Plywood, OSB, Gypsum, and FiberBond Walls with Metal Framing," *ASCE Journal of Structural Engineering*, 123(8): 1079-1086.

SSMA. Steel Stud Manufactures Association. (2010). *Product Technical Information. SSMA PTIC rev 12/2010*. Accessed November 2010.http://www.ssma.com/documents/ ssmatechcatalog.pdf>

Stewart, W.G. (1987). *The Seismic Design of Plywood Sheathed Shear-Walls*. PhD Thesis, University of Canterbury, Christchurch, New Zealand.

Structural Engineering Association of Southern California (SEAOSC). (2001). *Report of A Testing Program of Light-Framed Walls with Wood-Sheathed Shear Panels.* University of California, Irvine, Irvine, California.

Taghavi, S. and Miranda, E. (2003). *Response Assessment of Nonstructural Building Elements*. PEER Report 2003/05. Pacific Earthquake Engineering Research Center, College of Engineering, UC Berkeley.

Van de Lindt, J.W. and Walz, M.A. (2003). "Development and Application of Wood Shear Wall Reliability Model." *ASCE Journal of Structural Engineering, 129(3): 405-413.*

Villaverde, R. (2009). *Fundamental Concepts of Earthquake Engineering.* CRC Press, Boca Raton, FL.

Wieser, J. (2011). *Assessment of Floor Accelerations in Yielding Buildings.* MS Thesis, Department of Civil and Environmental Engineering, University of Nevada, Reno.

Wood, R.L.; Hutchinson, T.C. and Hoehler, M.S. (2009). "Cyclic Load and Crack Protocol for Anchored Nonstructural Components and Systems," *Structural Systems Research Program Report* SSRP 2009/12, University of California, San Diego, La Jolla, CA.

MCEER Technical Reports

MCEER publishes technical reports on a variety of subjects written by authors funded through MCEER. These reports are available from both MCEER Publications and the National Technical Information Service (NTIS). Requests for reports should be directed to MCEER Publications, MCEER, University at Buffalo, State University of New York, 133A Ketter Hall, Buffalo, New York 14260. Reports can also be requested through NTIS, P.O. Box 1425, Springfield, Virginia 22151. NTIS accession numbers are shown in parenthesis, if available.

NCEER-87-0001 "First-Year Program in Research, Education and Technology Transfer," 3/5/87, (PB88-134275, A04, MF-A01).

NCEER-87-0002 "Experimental Evaluation of Instantaneous Optimal Algorithms for Structural Control," by R.C. Lin, T.T. Soong and A.M. Reinhorn, 4/20/87, (PB88-134341, A04, MF-A01).

NCEER-87-0003 "Experimentation Using the Earthquake Simulation Facilities at University at Buffalo," by A.M. Reinhorn and R.L. Ketter, not available.

NCEER-87-0004 "The System Characteristics and Performance of a Shaking Table," by J.S. Hwang, K.C. Chang and G.C. Lee, 6/1/87, (PB88-134259, A03, MF-A01). This report is available only through NTIS (see address given above).

NCEER-87-0005 "A Finite Element Formulation for Nonlinear Viscoplastic Material Using a Q Model," by O. Gyebi and G. Dasgupta, 11/2/87, (PB88-213764, A08, MF-A01).

NCEER-87-0006 "Symbolic Manipulation Program (SMP) - Algebraic Codes for Two and Three Dimensional Finite Element Formulations," by X. Lee and G. Dasgupta, 11/9/87, (PB88-218522, A05, MF-A01).

NCEER-87-0007 "Instantaneous Optimal Control Laws for Tall Buildings Under Seismic Excitations," by J.N. Yang, A. Akbarpour and P. Ghaemmaghami, 6/10/87, (PB88-134333, A06, MF-A01). This report is only available through NTIS (see address given above).

NCEER-87-0008 "IDARC: Inelastic Damage Analysis of Reinforced Concrete Frame - Shear-Wall Structures," by Y.J. Park, A.M. Reinhorn and S.K. Kunnath, 7/20/87, (PB88-134325, A09, MF-A01). This report is only available through NTIS (see address given above).

NCEER-87-0009 "Liquefaction Potential for New York State: A Preliminary Report on Sites in Manhattan and Buffalo," by M. Budhu, V. Vijayakumar, R.F. Giese and L. Baumgras, 8/31/87, (PB88-163704, A03, MF-A01). This report is available only through NTIS (see address given above).

NCEER-87-0010 "Vertical and Torsional Vibration of Foundations in Inhomogeneous Media," by A.S. Veletsos and K.W. Dotson, 6/1/87, (PB88-134291, A03, MF-A01). This report is only available through NTIS (see address given above).

NCEER-87-0011 "Seismic Probabilistic Risk Assessment and Seismic Margins Studies for Nuclear Power Plants," by Howard H.M. Hwang, 6/15/87, (PB88-134267, A03, MF-A01). This report is only available through NTIS (see address given above).

NCEER-87-0012 "Parametric Studies of Frequency Response of Secondary Systems Under Ground-Acceleration Excitations," by Y. Yong and Y.K. Lin, 6/10/87, (PB88-134309, A03, MF-A01). This report is only available through NTIS (see address given above).

NCEER-87-0013 "Frequency Response of Secondary Systems Under Seismic Excitation," by J.A. HoLung, J. Cai and Y.K. Lin, 7/31/87, (PB88-134317, A05, MF-A01). This report is only available through NTIS (see address given above).

NCEER-87-0014 "Modelling Earthquake Ground Motions in Seismically Active Regions Using Parametric Time Series Methods," by G.W. Ellis and A.S. Cakmak, 8/25/87, (PB88-134283, A08, MF-A01). This report is only available through NTIS (see address given above).

NCEER-87-0015 "Detection and Assessment of Seismic Structural Damage," by E. DiPasquale and A.S. Cakmak, 8/25/87, (PB88-163712, A05, MF-A01). This report is only available through NTIS (see address given above).

NCEER-87-0016 "Pipeline Experiment at Parkfield, California," by J. Isenberg and E. Richardson, 9/15/87, (PB88-163720, A03, MF-A01). This report is available only through NTIS (see address given above).

NCEER-87-0017 "Digital Simulation of Seismic Ground Motion," by M. Shinozuka, G. Deodatis and T. Harada, 8/31/87, (PB88-155197, A04, MF-A01). This report is available only through NTIS (see address given above).

NCEER-87-0018 "Practical Considerations for Structural Control: System Uncertainty, System Time Delay and Truncation of Small Control Forces," J.N. Yang and A. Akbarpour, 8/10/87, (PB88-163738, A08, MF-A01). This report is only available through NTIS (see address given above).

NCEER-87-0019 "Modal Analysis of Nonclassically Damped Structural Systems Using Canonical Transformation," by J.N. Yang, S. Sarkani and F.X. Long, 9/27/87, (PB88-187851, A04, MF-A01).

NCEER-87-0020 "A Nonstationary Solution in Random Vibration Theory," by J.R. Red-Horse and P.D. Spanos, 11/3/87, (PB88-163746, A03, MF-A01).

NCEER-87-0021 "Horizontal Impedances for Radially Inhomogeneous Viscoelastic Soil Layers," by A.S. Veletsos and K.W. Dotson, 10/15/87, (PB88-150859, A04, MF-A01).

NCEER-87-0022 "Seismic Damage Assessment of Reinforced Concrete Members," by Y.S. Chung, C. Meyer and M. Shinozuka, 10/9/87, (PB88-150867, A05, MF-A01). This report is available only through NTIS (see address given above).

NCEER-87-0023 "Active Structural Control in Civil Engineering," by T.T. Soong, 11/11/87, (PB88-187778, A03, MF-A01).

NCEER-87-0024 "Vertical and Torsional Impedances for Radially Inhomogeneous Viscoelastic Soil Layers," by K.W. Dotson and A.S. Veletsos, 12/87, (PB88-187786, A03, MF-A01).

NCEER-87-0025 "Proceedings from the Symposium on Seismic Hazards, Ground Motions, Soil-Liquefaction and Engineering Practice in Eastern North America," October 20-22, 1987, edited by K.H. Jacob, 12/87, (PB88-188115, A23, MF-A01). This report is available only through NTIS (see address given above).

NCEER-87-0026 "Report on the Whittier-Narrows, California, Earthquake of October 1, 1987," by J. Pantelic and A. Reinhorn, 11/87, (PB88-187752, A03, MF-A01). This report is available only through NTIS (see address given above).

NCEER-87-0027 "Design of a Modular Program for Transient Nonlinear Analysis of Large 3-D Building Structures," by S. Srivastav and J.F. Abel, 12/30/87, (PB88-187950, A05, MF-A01). This report is only available through NTIS (see address given above).

NCEER-87-0028 "Second-Year Program in Research, Education and Technology Transfer," 3/8/88, (PB88-219480, A04, MF-A01).

NCEER-88-0001 "Workshop on Seismic Computer Analysis and Design of Buildings With Interactive Graphics," by W. McGuire, J.F. Abel and C.H. Conley, 1/18/88, (PB88-187760, A03, MF-A01). This report is only available through NTIS (see address given above).

NCEER-88-0002 "Optimal Control of Nonlinear Flexible Structures," by J.N. Yang, F.X. Long and D. Wong, 1/22/88, (PB88-213772, A06, MF-A01).

NCEER-88-0003 "Substructuring Techniques in the Time Domain for Primary-Secondary Structural Systems," by G.D. Manolis and G. Juhn, 2/10/88, (PB88-213780, A04, MF-A01).

NCEER-88-0004 "Iterative Seismic Analysis of Primary-Secondary Systems," by A. Singhal, L.D. Lutes and P.D. Spanos, 2/23/88, (PB88-213798, A04, MF-A01).

NCEER-88-0005 "Stochastic Finite Element Expansion for Random Media," by P.D. Spanos and R. Ghanem, 3/14/88, (PB88-213806, A03, MF-A01).

NCEER-88-0006 "Combining Structural Optimization and Structural Control," by F.Y. Cheng and C.P. Pantelides, 1/10/88, (PB88-213814, A05, MF-A01).

NCEER-88-0007 "Seismic Performance Assessment of Code-Designed Structures," by H.H-M. Hwang, J-W. Jaw and H-J. Shau, 3/20/88, (PB88-219423, A04, MF-A01). This report is only available through NTIS (see address given above).

NCEER-88-0008 "Reliability Analysis of Code-Designed Structures Under Natural Hazards," by H.H-M. Hwang, H. Ushiba and M. Shinozuka, 2/29/88, (PB88-229471, A07, MF-A01). This report is only available through NTIS (see address given above).

NCEER-88-0009 "Seismic Fragility Analysis of Shear Wall Structures," by J-W Jaw and H.H-M. Hwang, 4/30/88, (PB89-102867, A04, MF-A01).

NCEER-88-0010 "Base Isolation of a Multi-Story Building Under a Harmonic Ground Motion - A Comparison of Performances of Various Systems," by F-G Fan, G. Ahmadi and I.G. Tadjbakhsh, 5/18/88, (PB89-122238, A06, MF-A01). This report is only available through NTIS (see address given above).

NCEER-88-0011 "Seismic Floor Response Spectra for a Combined System by Green's Functions," by F.M. Lavelle, L.A. Bergman and P.D. Spanos, 5/1/88, (PB89-102875, A03, MF-A01).

NCEER-88-0012 "A New Solution Technique for Randomly Excited Hysteretic Structures," by G.Q. Cai and Y.K. Lin, 5/16/88, (PB89-102883, A03, MF-A01).

NCEER-88-0013 "A Study of Radiation Damping and Soil-Structure Interaction Effects in the Centrifuge," by K. Weissman, supervised by J.H. Prevost, 5/24/88, (PB89-144703, A06, MF-A01).

NCEER-88-0014 "Parameter Identification and Implementation of a Kinematic Plasticity Model for Frictional Soils," by J.H. Prevost and D.V. Griffiths, not available.

NCEER-88-0015 "Two- and Three- Dimensional Dynamic Finite Element Analyses of the Long Valley Dam," by D.V. Griffiths and J.H. Prevost, 6/17/88, (PB89-144711, A04, MF-A01).

NCEER-88-0016 "Damage Assessment of Reinforced Concrete Structures in Eastern United States," by A.M. Reinhorn, M.J. Seidel, S.K. Kunnath and Y.J. Park, 6/15/88, (PB89-122220, A04, MF-A01). This report is only available through NTIS (see address given above).

NCEER-88-0017 "Dynamic Compliance of Vertically Loaded Strip Foundations in Multilayered Viscoelastic Soils," by S. Ahmad and A.S.M. Israil, 6/17/88, (PB89-102891, A04, MF-A01).

NCEER-88-0018 "An Experimental Study of Seismic Structural Response With Added Viscoelastic Dampers," by R.C. Lin, Z. Liang, T.T. Soong and R.H. Zhang, 6/30/88, (PB89-122212, A05, MF-A01). This report is available only through NTIS (see address given above).

NCEER-88-0019 "Experimental Investigation of Primary - Secondary System Interaction," by G.D. Manolis, G. Juhn and A.M. Reinhorn, 5/27/88, (PB89-122204, A04, MF-A01).

NCEER-88-0020 "A Response Spectrum Approach For Analysis of Nonclassically Damped Structures," by J.N. Yang, S. Sarkani and F.X. Long, 4/22/88, (PB89-102909, A04, MF-A01).

NCEER-88-0021 "Seismic Interaction of Structures and Soils: Stochastic Approach," by A.S. Veletsos and A.M. Prasad, 7/21/88, (PB89-122196, A04, MF-A01). This report is only available through NTIS (see address given above).

NCEER-88-0022 "Identification of the Serviceability Limit State and Detection of Seismic Structural Damage," by E. DiPasquale and A.S. Cakmak, 6/15/88, (PB89-122188, A05, MF-A01). This report is available only through NTIS (see address given above).

NCEER-88-0023 "Multi-Hazard Risk Analysis: Case of a Simple Offshore Structure," by B.K. Bhartia and E.H. Vanmarcke, 7/21/88, (PB89-145213, A05, MF-A01).

NCEER-88-0024 "Automated Seismic Design of Reinforced Concrete Buildings," by Y.S. Chung, C. Meyer and M. Shinozuka, 7/5/88, (PB89-122170, A06, MF-A01). This report is available only through NTIS (see address given above).

NCEER-88-0025 "Experimental Study of Active Control of MDOF Structures Under Seismic Excitations," by L.L. Chung, R.C. Lin, T.T. Soong and A.M. Reinhorn, 7/10/88, (PB89-122600, A04, MF-A01).

NCEER-88-0026 "Earthquake Simulation Tests of a Low-Rise Metal Structure," by J.S. Hwang, K.C. Chang, G.C. Lee and R.L. Ketter, 8/1/88, (PB89-102917, A04, MF-A01).

NCEER-88-0027 "Systems Study of Urban Response and Reconstruction Due to Catastrophic Earthquakes," by F. Kozin and H.K. Zhou, 9/22/88, (PB90-162348, A04, MF-A01).

NCEER-88-0028 "Seismic Fragility Analysis of Plane Frame Structures," by H.H-M. Hwang and Y.K. Low, 7/31/88, (PB89-131445, A06, MF-A01).

NCEER-88-0029 "Response Analysis of Stochastic Structures," by A. Kardara, C. Bucher and M. Shinozuka, 9/22/88, (PB89-174429, A04, MF-A01).

NCEER-88-0030 "Nonnormal Accelerations Due to Yielding in a Primary Structure," by D.C.K. Chen and L.D. Lutes, 9/19/88, (PB89-131437, A04, MF-A01).

NCEER-88-0031 "Design Approaches for Soil-Structure Interaction," by A.S. Veletsos, A.M. Prasad and Y. Tang, 12/30/88, (PB89-174437, A03, MF-A01). This report is available only through NTIS (see address given above).

NCEER-88-0032 "A Re-evaluation of Design Spectra for Seismic Damage Control," by C.J. Turkstra and A.G. Tallin, 11/7/88, (PB89-145221, A05, MF-A01).

NCEER-88-0033 "The Behavior and Design of Noncontact Lap Splices Subjected to Repeated Inelastic Tensile Loading," by V.E. Sagan, P. Gergely and R.N. White, 12/8/88, (PB89-163737, A08, MF-A01).

NCEER-88-0034 "Seismic Response of Pile Foundations," by S.M. Mamoon, P.K. Banerjee and S. Ahmad, 11/1/88, (PB89-145239, A04, MF-A01).

NCEER-88-0035 "Modeling of R/C Building Structures With Flexible Floor Diaphragms (IDARC2)," by A.M. Reinhorn, S.K. Kunnath and N. Panahshahi, 9/7/88, (PB89-207153, A07, MF-A01).

NCEER-88-0036 "Solution of the Dam-Reservoir Interaction Problem Using a Combination of FEM, BEM with Particular Integrals, Modal Analysis, and Substructuring," by C-S. Tsai, G.C. Lee and R.L. Ketter, 12/31/88, (PB89-207146, A04, MF-A01).

NCEER-88-0037 "Optimal Placement of Actuators for Structural Control," by F.Y. Cheng and C.P. Pantelides, 8/15/88, (PB89-162846, A05, MF-A01).

NCEER-88-0038 "Teflon Bearings in Aseismic Base Isolation: Experimental Studies and Mathematical Modeling," by A. Mokha, M.C. Constantinou and A.M. Reinhorn, 12/5/88, (PB89-218457, A10, MF-A01). This report is available only through NTIS (see address given above).

NCEER-88-0039 "Seismic Behavior of Flat Slab High-Rise Buildings in the New York City Area," by P. Weidlinger and M. Ettouney, 10/15/88, (PB90-145681, A04, MF-A01).

NCEER-88-0040 "Evaluation of the Earthquake Resistance of Existing Buildings in New York City," by P. Weidlinger and M. Ettouney, 10/15/88, not available.

NCEER-88-0041 "Small-Scale Modeling Techniques for Reinforced Concrete Structures Subjected to Seismic Loads," by W. Kim, A. El-Attar and R.N. White, 11/22/88, (PB89-189625, A05, MF-A01).

NCEER-88-0042 "Modeling Strong Ground Motion from Multiple Event Earthquakes," by G.W. Ellis and A.S. Cakmak, 10/15/88, (PB89-174445, A03, MF-A01).

NCEER-88-0043 "Nonstationary Models of Seismic Ground Acceleration," by M. Grigoriu, S.E. Ruiz and E. Rosenblueth, 7/15/88, (PB89-189617, A04, MF-A01).

NCEER-88-0044 "SARCF User's Guide: Seismic Analysis of Reinforced Concrete Frames," by Y.S. Chung, C. Meyer and M. Shinozuka, 11/9/88, (PB89-174452, A08, MF-A01).

NCEER-88-0045 "First Expert Panel Meeting on Disaster Research and Planning," edited by J. Pantelic and J. Stoyle, 9/15/88, (PB89-174460, A05, MF-A01).

NCEER-88-0046 "Preliminary Studies of the Effect of Degrading Infill Walls on the Nonlinear Seismic Response of Steel Frames," by C.Z. Chrysostomou, P. Gergely and J.F. Abel, 12/19/88, (PB89-208383, A05, MF-A01).

NCEER-88-0047 "Reinforced Concrete Frame Component Testing Facility - Design, Construction, Instrumentation and Operation," by S.P. Pessiki, C. Conley, T. Bond, P. Gergely and R.N. White, 12/16/88, (PB89-174478, A04, MF-A01).

NCEER-89-0001 "Effects of Protective Cushion and Soil Compliancy on the Response of Equipment Within a Seismically Excited Building," by J.A. HoLung, 2/16/89, (PB89-207179, A04, MF-A01).

NCEER-89-0002 "Statistical Evaluation of Response Modification Factors for Reinforced Concrete Structures," by H.H-M. Hwang and J-W. Jaw, 2/17/89, (PB89-207187, A05, MF-A01).

NCEER-89-0003 "Hysteretic Columns Under Random Excitation," by G-Q. Cai and Y.K. Lin, 1/9/89, (PB89-196513, A03, MF-A01).

NCEER-89-0004 "Experimental Study of `Elephant Foot Bulge' Instability of Thin-Walled Metal Tanks," by Z-H. Jia and R.L. Ketter, 2/22/89, (PB89-207195, A03, MF-A01).

NCEER-89-0005 "Experiment on Performance of Buried Pipelines Across San Andreas Fault," by J. Isenberg, E. Richardson and T.D. O'Rourke, 3/10/89, (PB89-218440, A04, MF-A01). This report is available only through NTIS (see address given above).

NCEER-89-0006 "A Knowledge-Based Approach to Structural Design of Earthquake-Resistant Buildings," by M. Subramani, P. Gergely, C.H. Conley, J.F. Abel and A.H. Zaghw, 1/15/89, (PB89-218465, A06, MF-A01).

NCEER-89-0007 "Liquefaction Hazards and Their Effects on Buried Pipelines," by T.D. O'Rourke and P.A. Lane, 2/1/89, (PB89-218481, A09, MF-A01).

NCEER-89-0008 "Fundamentals of System Identification in Structural Dynamics," by H. Imai, C-B. Yun, O. Maruyama and M. Shinozuka, 1/26/89, (PB89-207211, A04, MF-A01).

NCEER-89-0009 "Effects of the 1985 Michoacan Earthquake on Water Systems and Other Buried Lifelines in Mexico," by A.G. Ayala and M.J. O'Rourke, 3/8/89, (PB89-207229, A06, MF-A01).

NCEER-89-R010 "NCEER Bibliography of Earthquake Education Materials," by K.E.K. Ross, Second Revision, 9/1/89, (PB90-125352, A05, MF-A01). This report is replaced by NCEER-92-0018.

NCEER-89-0011 "Inelastic Three-Dimensional Response Analysis of Reinforced Concrete Building Structures (IDARC-3D), Part I - Modeling," by S.K. Kunnath and A.M. Reinhorn, 4/17/89, (PB90-114612, A07, MF-A01). This report is available only through NTIS (see address given above).

NCEER-89-0012 "Recommended Modifications to ATC-14," by C.D. Poland and J.O. Malley, 4/12/89, (PB90-108648, A15, MF-A01).

NCEER-89-0013 "Repair and Strengthening of Beam-to-Column Connections Subjected to Earthquake Loading," by M. Corazao and A.J. Durrani, 2/28/89, (PB90-109885, A06, MF-A01).

NCEER-89-0014 "Program EXKAL2 for Identification of Structural Dynamic Systems," by O. Maruyama, C-B. Yun, M. Hoshiya and M. Shinozuka, 5/19/89, (PB90-109877, A09, MF-A01).

NCEER-89-0015 "Response of Frames With Bolted Semi-Rigid Connections, Part I - Experimental Study and Analytical Predictions," by P.J. DiCorso, A.M. Reinhorn, J.R. Dickerson, J.B. Radziminski and W.L. Harper, 6/1/89, not available.

NCEER-89-0016 "ARMA Monte Carlo Simulation in Probabilistic Structural Analysis," by P.D. Spanos and M.P. Mignolet, 7/10/89, (PB90-109893, A03, MF-A01).

NCEER-89-P017 "Preliminary Proceedings from the Conference on Disaster Preparedness - The Place of Earthquake Education in Our Schools," Edited by K.E.K. Ross, 6/23/89, (PB90-108606, A03, MF-A01).

NCEER-89-0017 "Proceedings from the Conference on Disaster Preparedness - The Place of Earthquake Education in Our Schools," Edited by K.E.K. Ross, 12/31/89, (PB90-207895, A012, MF-A02). This report is available only through NTIS (see address given above).

NCEER-89-0018 "Multidimensional Models of Hysteretic Material Behavior for Vibration Analysis of Shape Memory Energy Absorbing Devices, by E.J. Graesser and F.A. Cozzarelli, 6/7/89, (PB90-164146, A04, MF-A01).

NCEER-89-0019 "Nonlinear Dynamic Analysis of Three-Dimensional Base Isolated Structures (3D-BASIS)," by S. Nagarajaiah, A.M. Reinhorn and M.C. Constantinou, 8/3/89, (PB90-161936, A06, MF-A01). This report has been replaced by NCEER-93-0011.

NCEER-89-0020 "Structural Control Considering Time-Rate of Control Forces and Control Rate Constraints," by F.Y. Cheng and C.P. Pantelides, 8/3/89, (PB90-120445, A04, MF-A01).

NCEER-89-0021 "Subsurface Conditions of Memphis and Shelby County," by K.W. Ng, T-S. Chang and H-H.M. Hwang, 7/26/89, (PB90-120437, A03, MF-A01).

NCEER-89-0022 "Seismic Wave Propagation Effects on Straight Jointed Buried Pipelines," by K. Elhmadi and M.J. O'Rourke, 8/24/89, (PB90-162322, A10, MF-A02).

NCEER-89-0023 "Workshop on Serviceability Analysis of Water Delivery Systems," edited by M. Grigoriu, 3/6/89, (PB90-127424, A03, MF-A01).

NCEER-89-0024 "Shaking Table Study of a 1/5 Scale Steel Frame Composed of Tapered Members," by K.C. Chang, J.S. Hwang and G.C. Lee, 9/18/89, (PB90-160169, A04, MF-A01).

NCEER-89-0025 "DYNA1D: A Computer Program for Nonlinear Seismic Site Response Analysis - Technical Documentation," by Jean H. Prevost, 9/14/89, (PB90-161944, A07, MF-A01). This report is available only through NTIS (see address given above).

NCEER-89-0026 "1:4 Scale Model Studies of Active Tendon Systems and Active Mass Dampers for Aseismic Protection," by A.M. Reinhorn, T.T. Soong, R.C. Lin, Y.P. Yang, Y. Fukao, H. Abe and M. Nakai, 9/15/89, (PB90-173246, A10, MF-A02). This report is available only through NTIS (see address given above).

NCEER-89-0027 "Scattering of Waves by Inclusions in a Nonhomogeneous Elastic Half Space Solved by Boundary Element Methods," by P.K. Hadley, A. Askar and A.S. Cakmak, 6/15/89, (PB90-145699, A07, MF-A01).

NCEER-89-0028 "Statistical Evaluation of Deflection Amplification Factors for Reinforced Concrete Structures," by H.H.M. Hwang, J-W. Jaw and A.L. Ch'ng, 8/31/89, (PB90-164633, A05, MF-A01).

NCEER-89-0029 "Bedrock Accelerations in Memphis Area Due to Large New Madrid Earthquakes," by H.H.M. Hwang, C.H.S. Chen and G. Yu, 11/7/89, (PB90-162330, A04, MF-A01).

NCEER-89-0030 "Seismic Behavior and Response Sensitivity of Secondary Structural Systems," by Y.Q. Chen and T.T. Soong, 10/23/89, (PB90-164658, A08, MF-A01).

NCEER-89-0031 "Random Vibration and Reliability Analysis of Primary-Secondary Structural Systems," by Y. Ibrahim, M. Grigoriu and T.T. Soong, 11/10/89, (PB90-161951, A04, MF-A01).

NCEER-89-0032 "Proceedings from the Second U.S. - Japan Workshop on Liquefaction, Large Ground Deformation and Their Effects on Lifelines, September 26-29, 1989," Edited by T.D. O'Rourke and M. Hamada, 12/1/89, (PB90-209388, A22, MF-A03).

NCEER-89-0033 "Deterministic Model for Seismic Damage Evaluation of Reinforced Concrete Structures," by J.M. Bracci, A.M. Reinhorn, J.B. Mander and S.K. Kunnath, 9/27/89, (PB91-108803, A06, MF-A01).

NCEER-89-0034 "On the Relation Between Local and Global Damage Indices," by E. DiPasquale and A.S. Cakmak, 8/15/89, (PB90-173865, A05, MF-A01).

NCEER-89-0035 "Cyclic Undrained Behavior of Nonplastic and Low Plasticity Silts," by A.J. Walker and H.E. Stewart, 7/26/89, (PB90-183518, A10, MF-A01).

NCEER-89-0036 "Liquefaction Potential of Surficial Deposits in the City of Buffalo, New York," by M. Budhu, R. Giese and L. Baumgrass, 1/17/89, (PB90-208455, A04, MF-A01).

NCEER-89-0037 "A Deterministic Assessment of Effects of Ground Motion Incoherence," by A.S. Veletsos and Y. Tang, 7/15/89, (PB90-164294, A03, MF-A01).

NCEER-89-0038 "Workshop on Ground Motion Parameters for Seismic Hazard Mapping," July 17-18, 1989, edited by R.V. Whitman, 12/1/89, (PB90-173923, A04, MF-A01).

NCEER-89-0039 "Seismic Effects on Elevated Transit Lines of the New York City Transit Authority," by C.J. Costantino, C.A. Miller and E. Heymsfield, 12/26/89, (PB90-207887, A06, MF-A01).

NCEER-89-0040 "Centrifugal Modeling of Dynamic Soil-Structure Interaction," by K. Weissman, Supervised by J.H. Prevost, 5/10/89, (PB90-207879, A07, MF-A01).

NCEER-89-0041 "Linearized Identification of Buildings With Cores for Seismic Vulnerability Assessment," by I-K. Ho and A.E. Aktan, 11/1/89, (PB90-251943, A07, MF-A01).

NCEER-90-0001 "Geotechnical and Lifeline Aspects of the October 17, 1989 Loma Prieta Earthquake in San Francisco," by T.D. O'Rourke, H.E. Stewart, F.T. Blackburn and T.S. Dickerman, 1/90, (PB90-208596, A05, MF-A01).

NCEER-90-0002 "Nonnormal Secondary Response Due to Yielding in a Primary Structure," by D.C.K. Chen and L.D. Lutes, 2/28/90, (PB90-251976, A07, MF-A01).

NCEER-90-0003 "Earthquake Education Materials for Grades K-12," by K.E.K. Ross, 4/16/90, (PB91-251984, A05, MF-A05). This report has been replaced by NCEER-92-0018.

NCEER-90-0004 "Catalog of Strong Motion Stations in Eastern North America," by R.W. Busby, 4/3/90, (PB90-251984, A05, MF-A01).

NCEER-90-0005 "NCEER Strong-Motion Data Base: A User Manual for the GeoBase Release (Version 1.0 for the Sun3)," by P. Friberg and K. Jacob, 3/31/90 (PB90-258062, A04, MF-A01).

NCEER-90-0006 "Seismic Hazard Along a Crude Oil Pipeline in the Event of an 1811-1812 Type New Madrid Earthquake," by H.H.M. Hwang and C-H.S. Chen, 4/16/90, (PB90-258054, A04, MF-A01).

NCEER-90-0007 "Site-Specific Response Spectra for Memphis Sheahan Pumping Station," by H.H.M. Hwang and C.S. Lee, 5/15/90, (PB91-108811, A05, MF-A01).

NCEER-90-0008 "Pilot Study on Seismic Vulnerability of Crude Oil Transmission Systems," by T. Ariman, R. Dobry, M. Grigoriu, F. Kozin, M. O'Rourke, T. O'Rourke and M. Shinozuka, 5/25/90, (PB91-108837, A06, MF-A01).

NCEER-90-0009 "A Program to Generate Site Dependent Time Histories: EQGEN," by G.W. Ellis, M. Srinivasan and A.S. Cakmak, 1/30/90, (PB91-108829, A04, MF-A01).

NCEER-90-0010 "Active Isolation for Seismic Protection of Operating Rooms," by M.E. Talbott, Supervised by M. Shinozuka, 6/8/9, (PB91-110205, A05, MF-A01).

NCEER-90-0011 "Program LINEARID for Identification of Linear Structural Dynamic Systems," by C-B. Yun and M. Shinozuka, 6/25/90, (PB91-110312, A08, MF-A01).

NCEER-90-0012 "Two-Dimensional Two-Phase Elasto-Plastic Seismic Response of Earth Dams," by A.N. Yiagos, Supervised by J.H. Prevost, 6/20/90, (PB91-110197, A13, MF-A02).

NCEER-90-0013 "Secondary Systems in Base-Isolated Structures: Experimental Investigation, Stochastic Response and Stochastic Sensitivity," by G.D. Manolis, G. Juhn, M.C. Constantinou and A.M. Reinhorn, 7/1/90, (PB91-110320, A08, MF-A01).

NCEER-90-0014 "Seismic Behavior of Lightly-Reinforced Concrete Column and Beam-Column Joint Details," by S.P. Pessiki, C.H. Conley, P. Gergely and R.N. White, 8/22/90, (PB91-108795, A11, MF-A02).

NCEER-90-0015 "Two Hybrid Control Systems for Building Structures Under Strong Earthquakes," by J.N. Yang and A. Danielians, 6/29/90, (PB91-125393, A04, MF-A01).

NCEER-90-0016 "Instantaneous Optimal Control with Acceleration and Velocity Feedback," by J.N. Yang and Z. Li, 6/29/90, (PB91-125401, A03, MF-A01).

NCEER-90-0017 "Reconnaissance Report on the Northern Iran Earthquake of June 21, 1990," by M. Mehrain, 10/4/90, (PB91-125377, A03, MF-A01).

NCEER-90-0018 "Evaluation of Liquefaction Potential in Memphis and Shelby County," by T.S. Chang, P.S. Tang, C.S. Lee and H. Hwang, 8/10/90, (PB91-125427, A09, MF-A01).

NCEER-90-0019 "Experimental and Analytical Study of a Combined Sliding Disc Bearing and Helical Steel Spring Isolation System," by M.C. Constantinou, A.S. Mokha and A.M. Reinhorn, 10/4/90, (PB91-125385, A06, MF-A01). This report is available only through NTIS (see address given above).

NCEER-90-0020 "Experimental Study and Analytical Prediction of Earthquake Response of a Sliding Isolation System with a Spherical Surface," by A.S. Mokha, M.C. Constantinou and A.M. Reinhorn, 10/11/90, (PB91-125419, A05, MF-A01).

NCEER-90-0021 "Dynamic Interaction Factors for Floating Pile Groups," by G. Gazetas, K. Fan, A. Kaynia and E. Kausel, 9/10/90, (PB91-170381, A05, MF-A01).

NCEER-90-0022 "Evaluation of Seismic Damage Indices for Reinforced Concrete Structures," by S. Rodriguez-Gomez and A.S. Cakmak, 9/30/90, PB91-171322, A06, MF-A01).

NCEER-90-0023 "Study of Site Response at a Selected Memphis Site," by H. Desai, S. Ahmad, E.S. Gazetas and M.R. Oh, 10/11/90, (PB91-196857, A03, MF-A01).

NCEER-90-0024 "A User's Guide to Strongmo: Version 1.0 of NCEER's Strong-Motion Data Access Tool for PCs and Terminals," by P.A. Friberg and C.A.T. Susch, 11/15/90, (PB91-171272, A03, MF-A01).

NCEER-90-0025 "A Three-Dimensional Analytical Study of Spatial Variability of Seismic Ground Motions," by L-L. Hong and A.H.-S. Ang, 10/30/90, (PB91-170399, A09, MF-A01).

NCEER-90-0026 "MUMOID User's Guide - A Program for the Identification of Modal Parameters," by S. Rodriguez-Gomez and E. DiPasquale, 9/30/90, (PB91-171298, A04, MF-A01).

NCEER-90-0027 "SARCF-II User's Guide - Seismic Analysis of Reinforced Concrete Frames," by S. Rodriguez-Gomez, Y.S. Chung and C. Meyer, 9/30/90, (PB91-171280, A05, MF-A01).

NCEER-90-0028 "Viscous Dampers: Testing, Modeling and Application in Vibration and Seismic Isolation," by N. Makris and M.C. Constantinou, 12/20/90 (PB91-190561, A06, MF-A01).

NCEER-90-0029 "Soil Effects on Earthquake Ground Motions in the Memphis Area," by H. Hwang, C.S. Lee, K.W. Ng and T.S. Chang, 8/2/90, (PB91-190751, A05, MF-A01).

NCEER-91-0001 "Proceedings from the Third Japan-U.S. Workshop on Earthquake Resistant Design of Lifeline Facilities and Countermeasures for Soil Liquefaction, December 17-19, 1990," edited by T.D. O'Rourke and M. Hamada, 2/1/91, (PB91-179259, A99, MF-A04).

NCEER-91-0002 "Physical Space Solutions of Non-Proportionally Damped Systems," by M. Tong, Z. Liang and G.C. Lee, 1/15/91, (PB91-179242, A04, MF-A01).

NCEER-91-0003 "Seismic Response of Single Piles and Pile Groups," by K. Fan and G. Gazetas, 1/10/91, (PB92-174994, A04, MF-A01).

NCEER-91-0004 "Damping of Structures: Part 1 - Theory of Complex Damping," by Z. Liang and G. Lee, 10/10/91, (PB92-197235, A12, MF-A03).

NCEER-91-0005 "3D-BASIS - Nonlinear Dynamic Analysis of Three Dimensional Base Isolated Structures: Part II," by S. Nagarajaiah, A.M. Reinhorn and M.C. Constantinou, 2/28/91, (PB91-190553, A07, MF-A01). This report has been replaced by NCEER-93-0011.

NCEER-91-0006 "A Multidimensional Hysteretic Model for Plasticity Deforming Metals in Energy Absorbing Devices," by E.J. Graesser and F.A. Cozzarelli, 4/9/91, (PB92-108364, A04, MF-A01).

NCEER-91-0007 "A Framework for Customizable Knowledge-Based Expert Systems with an Application to a KBES for Evaluating the Seismic Resistance of Existing Buildings," by E.G. Ibarra-Anaya and S.J. Fenves, 4/9/91, (PB91-210930, A08, MF-A01).

NCEER-91-0008 "Nonlinear Analysis of Steel Frames with Semi-Rigid Connections Using the Capacity Spectrum Method," by G.G. Deierlein, S-H. Hsieh, Y-J. Shen and J.F. Abel, 7/2/91, (PB92-113828, A05, MF-A01).

NCEER-91-0009 "Earthquake Education Materials for Grades K-12," by K.E.K. Ross, 4/30/91, (PB91-212142, A06, MF-A01). This report has been replaced by NCEER-92-0018.

NCEER-91-0010 "Phase Wave Velocities and Displacement Phase Differences in a Harmonically Oscillating Pile," by N. Makris and G. Gazetas, 7/8/91, (PB92-108356, A04, MF-A01).

NCEER-91-0011 "Dynamic Characteristics of a Full-Size Five-Story Steel Structure and a 2/5 Scale Model," by K.C. Chang, G.C. Yao, G.C. Lee, D.S. Hao and Y.C. Yeh," 7/2/91, (PB93-116648, A06, MF-A02).

NCEER-91-0012 "Seismic Response of a 2/5 Scale Steel Structure with Added Viscoelastic Dampers," by K.C. Chang, T.T. Soong, S-T. Oh and M.L. Lai, 5/17/91, (PB92-110816, A05, MF-A01).

NCEER-91-0013 "Earthquake Response of Retaining Walls; Full-Scale Testing and Computational Modeling," by S. Alampalli and A-W.M. Elgamal, 6/20/91, not available.

NCEER-91-0014 "3D-BASIS-M: Nonlinear Dynamic Analysis of Multiple Building Base Isolated Structures," by P.C. Tsopelas, S. Nagarajaiah, M.C. Constantinou and A.M. Reinhorn, 5/28/91, (PB92-113885, A09, MF-A02).

NCEER-91-0015 "Evaluation of SEAOC Design Requirements for Sliding Isolated Structures," by D. Theodossiou and M.C. Constantinou, 6/10/91, (PB92-114602, A11, MF-A03).

NCEER-91-0016 "Closed-Loop Modal Testing of a 27-Story Reinforced Concrete Flat Plate-Core Building," by H.R. Somaprasad, T. Toksoy, H. Yoshiyuki and A.E. Aktan, 7/15/91, (PB92-129980, A07, MF-A02).

NCEER-91-0017 "Shake Table Test of a 1/6 Scale Two-Story Lightly Reinforced Concrete Building," by A.G. El-Attar, R.N. White and P. Gergely, 2/28/91, (PB92-222447, A06, MF-A02).

NCEER-91-0018 "Shake Table Test of a 1/8 Scale Three-Story Lightly Reinforced Concrete Building," by A.G. El-Attar, R.N. White and P. Gergely, 2/28/91, (PB93-116630, A08, MF-A02).

NCEER-91-0019 "Transfer Functions for Rigid Rectangular Foundations," by A.S. Veletsos, A.M. Prasad and W.H. Wu, 7/31/91, not available.

NCEER-91-0020 "Hybrid Control of Seismic-Excited Nonlinear and Inelastic Structural Systems," by J.N. Yang, Z. Li and A. Danielians, 8/1/91, (PB92-143171, A06, MF-A02).

NCEER-91-0021 "The NCEER-91 Earthquake Catalog: Improved Intensity-Based Magnitudes and Recurrence Relations for U.S. Earthquakes East of New Madrid," by L. Seeber and J.G. Armbruster, 8/28/91, (PB92-176742, A06, MF-A02).

NCEER-91-0022 "Proceedings from the Implementation of Earthquake Planning and Education in Schools: The Need for Change - The Roles of the Changemakers," by K.E.K. Ross and F. Winslow, 7/23/91, (PB92-129998, A12, MF-A03).

NCEER-91-0023 "A Study of Reliability-Based Criteria for Seismic Design of Reinforced Concrete Frame Buildings," by H.H.M. Hwang and H-M. Hsu, 8/10/91, (PB92-140235, A09, MF-A02).

NCEER-91-0024 "Experimental Verification of a Number of Structural System Identification Algorithms," by R.G. Ghanem, H. Gavin and M. Shinozuka, 9/18/91, (PB92-176577, A18, MF-A04).

NCEER-91-0025 "Probabilistic Evaluation of Liquefaction Potential," by H.H.M. Hwang and C.S. Lee," 11/25/91, (PB92-143429, A05, MF-A01).

NCEER-91-0026 "Instantaneous Optimal Control for Linear, Nonlinear and Hysteretic Structures - Stable Controllers," by J.N. Yang and Z. Li, 11/15/91, (PB92-163807, A04, MF-A01).

NCEER-91-0027 "Experimental and Theoretical Study of a Sliding Isolation System for Bridges," by M.C. Constantinou, A. Kartoum, A.M. Reinhorn and P. Bradford, 11/15/91, (PB92-176973, A10, MF-A03).

NCEER-92-0001 "Case Studies of Liquefaction and Lifeline Performance During Past Earthquakes, Volume 1: Japanese Case Studies," Edited by M. Hamada and T. O'Rourke, 2/17/92, (PB92-197243, A18, MF-A04).

NCEER-92-0002 "Case Studies of Liquefaction and Lifeline Performance During Past Earthquakes, Volume 2: United States Case Studies," Edited by T. O'Rourke and M. Hamada, 2/17/92, (PB92-197250, A20, MF-A04).

NCEER-92-0003 "Issues in Earthquake Education," Edited by K. Ross, 2/3/92, (PB92-222389, A07, MF-A02).

NCEER-92-0004 "Proceedings from the First U.S. - Japan Workshop on Earthquake Protective Systems for Bridges," Edited by I.G. Buckle, 2/4/92, (PB94-142239, A99, MF-A06).

NCEER-92-0005 "Seismic Ground Motion from a Haskell-Type Source in a Multiple-Layered Half-Space," A.P. Theoharis, G. Deodatis and M. Shinozuka, 1/2/92, not available.

NCEER-92-0006 "Proceedings from the Site Effects Workshop," Edited by R. Whitman, 2/29/92, (PB92-197201, A04, MF-A01).

NCEER-92-0007 "Engineering Evaluation of Permanent Ground Deformations Due to Seismically-Induced Liquefaction," by M.H. Baziar, R. Dobry and A-W.M. Elgamal, 3/24/92, (PB92-222421, A13, MF-A03).

NCEER-92-0008 "A Procedure for the Seismic Evaluation of Buildings in the Central and Eastern United States," by C.D. Poland and J.O. Malley, 4/2/92, (PB92-222439, A20, MF-A04).

NCEER-92-0009 "Experimental and Analytical Study of a Hybrid Isolation System Using Friction Controllable Sliding Bearings," by M.Q. Feng, S. Fujii and M. Shinozuka, 5/15/92, (PB93-150282, A06, MF-A02).

NCEER-92-0010 "Seismic Resistance of Slab-Column Connections in Existing Non-Ductile Flat-Plate Buildings," by A.J. Durrani and Y. Du, 5/18/92, (PB93-116812, A06, MF-A02).

NCEER-92-0011 "The Hysteretic and Dynamic Behavior of Brick Masonry Walls Upgraded by Ferrocement Coatings Under Cyclic Loading and Strong Simulated Ground Motion," by H. Lee and S.P. Prawel, 5/11/92, not available.

NCEER-92-0012 "Study of Wire Rope Systems for Seismic Protection of Equipment in Buildings," by G.F. Demetriades, M.C. Constantinou and A.M. Reinhorn, 5/20/92, (PB93-116655, A08, MF-A02).

NCEER-92-0013 "Shape Memory Structural Dampers: Material Properties, Design and Seismic Testing," by P.R. Witting and F.A. Cozzarelli, 5/26/92, (PB93-116663, A05, MF-A01).

NCEER-92-0014 "Longitudinal Permanent Ground Deformation Effects on Buried Continuous Pipelines," by M.J. O'Rourke, and C. Nordberg, 6/15/92, (PB93-116671, A08, MF-A02).

NCEER-92-0015 "A Simulation Method for Stationary Gaussian Random Functions Based on the Sampling Theorem," by M. Grigoriu and S. Balopoulou, 6/11/92, (PB93-127496, A05, MF-A01).

NCEER-92-0016 "Gravity-Load-Designed Reinforced Concrete Buildings: Seismic Evaluation of Existing Construction and Detailing Strategies for Improved Seismic Resistance," by G.W. Hoffmann, S.K. Kunnath, A.M. Reinhorn and J.B. Mander, 7/15/92, (PB94-142007, A08, MF-A02).

NCEER-92-0017 "Observations on Water System and Pipeline Performance in the Limón Area of Costa Rica Due to the April 22, 1991 Earthquake," by M. O'Rourke and D. Ballantyne, 6/30/92, (PB93-126811, A06, MF-A02).

NCEER-92-0018 "Fourth Edition of Earthquake Education Materials for Grades K-12," Edited by K.E.K. Ross, 8/10/92, (PB93-114023, A07, MF-A02).

NCEER-92-0019 "Proceedings from the Fourth Japan-U.S. Workshop on Earthquake Resistant Design of Lifeline Facilities and Countermeasures for Soil Liquefaction," Edited by M. Hamada and T.D. O'Rourke, 8/12/92, (PB93-163939, A99, MF-E11).

NCEER-92-0020 "Active Bracing System: A Full Scale Implementation of Active Control," by A.M. Reinhorn, T.T. Soong, R.C. Lin, M.A. Riley, Y.P. Wang, S. Aizawa and M. Higashino, 8/14/92, (PB93-127512, A06, MF-A02).

NCEER-92-0021 "Empirical Analysis of Horizontal Ground Displacement Generated by Liquefaction-Induced Lateral Spreads," by S.F. Bartlett and T.L. Youd, 8/17/92, (PB93-188241, A06, MF-A02).

NCEER-92-0022 "IDARC Version 3.0: Inelastic Damage Analysis of Reinforced Concrete Structures," by S.K. Kunnath, A.M. Reinhorn and R.F. Lobo, 8/31/92, (PB93-227502, A07, MF-A02).

NCEER-92-0023 "A Semi-Empirical Analysis of Strong-Motion Peaks in Terms of Seismic Source, Propagation Path and Local Site Conditions, by M. Kamiyama, M.J. O'Rourke and R. Flores-Berrones, 9/9/92, (PB93-150266, A08, MF-A02).

NCEER-92-0024 "Seismic Behavior of Reinforced Concrete Frame Structures with Nonductile Details, Part I: Summary of Experimental Findings of Full Scale Beam-Column Joint Tests," by A. Beres, R.N. White and P. Gergely, 9/30/92, (PB93-227783, A05, MF-A01).

NCEER-92-0025 "Experimental Results of Repaired and Retrofitted Beam-Column Joint Tests in Lightly Reinforced Concrete Frame Buildings," by A. Beres, S. El-Borgi, R.N. White and P. Gergely, 10/29/92, (PB93-227791, A05, MF-A01).

NCEER-92-0026 "A Generalization of Optimal Control Theory: Linear and Nonlinear Structures," by J.N. Yang, Z. Li and S. Vongchavalitkul, 11/2/92, (PB93-188621, A05, MF-A01).

NCEER-92-0027 "Seismic Resistance of Reinforced Concrete Frame Structures Designed Only for Gravity Loads: Part I - Design and Properties of a One-Third Scale Model Structure," by J.M. Bracci, A.M. Reinhorn and J.B. Mander, 12/1/92, (PB94-104502, A08, MF-A02).

NCEER-92-0028 "Seismic Resistance of Reinforced Concrete Frame Structures Designed Only for Gravity Loads: Part II - Experimental Performance of Subassemblages," by L.E. Aycardi, J.B. Mander and A.M. Reinhorn, 12/1/92, (PB94-104510, A08, MF-A02).

NCEER-92-0029 "Seismic Resistance of Reinforced Concrete Frame Structures Designed Only for Gravity Loads: Part III - Experimental Performance and Analytical Study of a Structural Model," by J.M. Bracci, A.M. Reinhorn and J.B. Mander, 12/1/92, (PB93-227528, A09, MF-A01).

NCEER-92-0030 "Evaluation of Seismic Retrofit of Reinforced Concrete Frame Structures: Part I - Experimental Performance of Retrofitted Subassemblages," by D. Choudhuri, J.B. Mander and A.M. Reinhorn, 12/8/92, (PB93-198307, A07, MF-A02).

NCEER-92-0031 "Evaluation of Seismic Retrofit of Reinforced Concrete Frame Structures: Part II - Experimental Performance and Analytical Study of a Retrofitted Structural Model," by J.M. Bracci, A.M. Reinhorn and J.B. Mander, 12/8/92, (PB93-198315, A09, MF-A03).

NCEER-92-0032 "Experimental and Analytical Investigation of Seismic Response of Structures with Supplemental Fluid Viscous Dampers," by M.C. Constantinou and M.D. Symans, 12/21/92, (PB93-191435, A10, MF-A03). This report is available only through NTIS (see address given above).

NCEER-92-0033 "Reconnaissance Report on the Cairo, Egypt Earthquake of October 12, 1992," by M. Khater, 12/23/92, (PB93-188621, A03, MF-A01).

NCEER-92-0034 "Low-Level Dynamic Characteristics of Four Tall Flat-Plate Buildings in New York City," by H. Gavin, S. Yuan, J. Grossman, E. Pekelis and K. Jacob, 12/28/92, (PB93-188217, A07, MF-A02).

NCEER-93-0001 "An Experimental Study on the Seismic Performance of Brick-Infilled Steel Frames With and Without Retrofit," by J.B. Mander, B. Nair, K. Wojtkowski and J. Ma, 1/29/93, (PB93-227510, A07, MF-A02).

NCEER-93-0002 "Social Accounting for Disaster Preparedness and Recovery Planning," by S. Cole, E. Pantoja and V. Razak, 2/22/93, (PB94-142114, A12, MF-A03).

NCEER-93-0003 "Assessment of 1991 NEHRP Provisions for Nonstructural Components and Recommended Revisions," by T.T. Soong, G. Chen, Z. Wu, R-H. Zhang and M. Grigoriu, 3/1/93, (PB93-188639, A06, MF-A02).

NCEER-93-0004 "Evaluation of Static and Response Spectrum Analysis Procedures of SEAOC/UBC for Seismic Isolated Structures," by C.W. Winters and M.C. Constantinou, 3/23/93, (PB93-198299, A10, MF-A03).

NCEER-93-0005 "Earthquakes in the Northeast - Are We Ignoring the Hazard? A Workshop on Earthquake Science and Safety for Educators," edited by K.E.K. Ross, 4/2/93, (PB94-103066, A09, MF-A02).

NCEER-93-0006 "Inelastic Response of Reinforced Concrete Structures with Viscoelastic Braces," by R.F. Lobo, J.M. Bracci, K.L. Shen, A.M. Reinhorn and T.T. Soong, 4/5/93, (PB93-227486, A05, MF-A02).

NCEER-93-0007 "Seismic Testing of Installation Methods for Computers and Data Processing Equipment," by K. Kosar, T.T. Soong, K.L. Shen, J.A. HoLung and Y.K. Lin, 4/12/93, (PB93-198299, A07, MF-A02).

NCEER-93-0008 "Retrofit of Reinforced Concrete Frames Using Added Dampers," by A. Reinhorn, M. Constantinou and C. Li, not available.

NCEER-93-0009 "Seismic Behavior and Design Guidelines for Steel Frame Structures with Added Viscoelastic Dampers," by K.C. Chang, M.L. Lai, T.T. Soong, D.S. Hao and Y.C. Yeh, 5/1/93, (PB94-141959, A07, MF-A02).

NCEER-93-0010 "Seismic Performance of Shear-Critical Reinforced Concrete Bridge Piers," by J.B. Mander, S.M. Waheed, M.T.A. Chaudhary and S.S. Chen, 5/12/93, (PB93-227494, A08, MF-A02).

NCEER-93-0011 "3D-BASIS-TABS: Computer Program for Nonlinear Dynamic Analysis of Three Dimensional Base Isolated Structures," by S. Nagarajaiah, C. Li, A.M. Reinhorn and M.C. Constantinou, 8/2/93, (PB94-141819, A09, MF-A02).

NCEER-93-0012 "Effects of Hydrocarbon Spills from an Oil Pipeline Break on Ground Water," by O.J. Helweg and H.H.M. Hwang, 8/3/93, (PB94-141942, A06, MF-A02).

NCEER-93-0013 "Simplified Procedures for Seismic Design of Nonstructural Components and Assessment of Current Code Provisions," by M.P. Singh, L.E. Suarez, E.E. Matheu and G.O. Maldonado, 8/4/93, (PB94-141827, A09, MF-A02).

NCEER-93-0014 "An Energy Approach to Seismic Analysis and Design of Secondary Systems," by G. Chen and T.T. Soong, 8/6/93, (PB94-142767, A11, MF-A03).

NCEER-93-0015 "Proceedings from School Sites: Becoming Prepared for Earthquakes - Commemorating the Third Anniversary of the Loma Prieta Earthquake," Edited by F.E. Winslow and K.E.K. Ross, 8/16/93, (PB94-154275, A16, MF-A02).

NCEER-93-0016 "Reconnaissance Report of Damage to Historic Monuments in Cairo, Egypt Following the October 12, 1992 Dahshur Earthquake," by D. Sykora, D. Look, G. Croci, E. Karaesmen and E. Karaesmen, 8/19/93, (PB94-142221, A08, MF-A02).

NCEER-93-0017 "The Island of Guam Earthquake of August 8, 1993," by S.W. Swan and S.K. Harris, 9/30/93, (PB94-141843, A04, MF-A01).

NCEER-93-0018 "Engineering Aspects of the October 12, 1992 Egyptian Earthquake," by A.W. Elgamal, M. Amer, K. Adalier and A. Abul-Fadl, 10/7/93, (PB94-141983, A05, MF-A01).

NCEER-93-0019 "Development of an Earthquake Motion Simulator and its Application in Dynamic Centrifuge Testing," by I. Krstelj, Supervised by J.H. Prevost, 10/23/93, (PB94-181773, A-10, MF-A03).

NCEER-93-0020 "NCEER-Taisei Corporation Research Program on Sliding Seismic Isolation Systems for Bridges: Experimental and Analytical Study of a Friction Pendulum System (FPS)," by M.C. Constantinou, P. Tsopelas, Y-S. Kim and S. Okamoto, 11/1/93, (PB94-142775, A08, MF-A02).

NCEER-93-0021 "Finite Element Modeling of Elastomeric Seismic Isolation Bearings," by L.J. Billings, Supervised by R. Shepherd, 11/8/93, not available.

NCEER-93-0022 "Seismic Vulnerability of Equipment in Critical Facilities: Life-Safety and Operational Consequences," by K. Porter, G.S. Johnson, M.M. Zadeh, C. Scawthorn and S. Eder, 11/24/93, (PB94-181765, A16, MF-A03).

NCEER-93-0023 "Hokkaido Nansei-oki, Japan Earthquake of July 12, 1993, by P.I. Yanev and C.R. Scawthorn, 12/23/93, (PB94-181500, A07, MF-A01).

NCEER-94-0001 "An Evaluation of Seismic Serviceability of Water Supply Networks with Application to the San Francisco Auxiliary Water Supply System," by I. Markov, Supervised by M. Grigoriu and T. O'Rourke, 1/21/94, (PB94-204013, A07, MF-A02).

NCEER-94-0002 "NCEER-Taisei Corporation Research Program on Sliding Seismic Isolation Systems for Bridges: Experimental and Analytical Study of Systems Consisting of Sliding Bearings, Rubber Restoring Force Devices and Fluid Dampers," Volumes I and II, by P. Tsopelas, S. Okamoto, M.C. Constantinou, D. Ozaki and S. Fujii, 2/4/94, (PB94-181740, A09, MF-A02 and PB94-181757, A12, MF-A03).

NCEER-94-0003 "A Markov Model for Local and Global Damage Indices in Seismic Analysis," by S. Rahman and M. Grigoriu, 2/18/94, (PB94-206000, A12, MF-A03).

NCEER-94-0004 "Proceedings from the NCEER Workshop on Seismic Response of Masonry Infills," edited by D.P. Abrams, 3/1/94, (PB94-180783, A07, MF-A02).

NCEER-94-0005 "The Northridge, California Earthquake of January 17, 1994: General Reconnaissance Report," edited by J.D. Goltz, 3/11/94, (PB94-193943, A10, MF-A03).

NCEER-94-0006 "Seismic Energy Based Fatigue Damage Analysis of Bridge Columns: Part I - Evaluation of Seismic Capacity," by G.A. Chang and J.B. Mander, 3/14/94, (PB94-219185, A11, MF-A03).

NCEER-94-0007 "Seismic Isolation of Multi-Story Frame Structures Using Spherical Sliding Isolation Systems," by T.M. Al-Hussaini, V.A. Zayas and M.C. Constantinou, 3/17/94, (PB94-193745, A09, MF-A02).

NCEER-94-0008 "The Northridge, California Earthquake of January 17, 1994: Performance of Highway Bridges," edited by I.G. Buckle, 3/24/94, (PB94-193851, A06, MF-A02).

NCEER-94-0009 "Proceedings of the Third U.S.-Japan Workshop on Earthquake Protective Systems for Bridges," edited by I.G. Buckle and I. Friedland, 3/31/94, (PB94-195815, A99, MF-A06).

NCEER-94-0010 "3D-BASIS-ME: Computer Program for Nonlinear Dynamic Analysis of Seismically Isolated Single and Multiple Structures and Liquid Storage Tanks," by P.C. Tsopelas, M.C. Constantinou and A.M. Reinhorn, 4/12/94, (PB94-204922, A09, MF-A02).

NCEER-94-0011 "The Northridge, California Earthquake of January 17, 1994: Performance of Gas Transmission Pipelines," by T.D. O'Rourke and M.C. Palmer, 5/16/94, (PB94-204989, A05, MF-A01).

NCEER-94-0012 "Feasibility Study of Replacement Procedures and Earthquake Performance Related to Gas Transmission Pipelines," by T.D. O'Rourke and M.C. Palmer, 5/25/94, (PB94-206638, A09, MF-A02).

NCEER-94-0013 "Seismic Energy Based Fatigue Damage Analysis of Bridge Columns: Part II - Evaluation of Seismic Demand," by G.A. Chang and J.B. Mander, 6/1/94, (PB95-18106, A08, MF-A02).

NCEER-94-0014 "NCEER-Taisei Corporation Research Program on Sliding Seismic Isolation Systems for Bridges: Experimental and Analytical Study of a System Consisting of Sliding Bearings and Fluid Restoring Force/Damping Devices," by P. Tsopelas and M.C. Constantinou, 6/13/94, (PB94-219144, A10, MF-A03).

NCEER-94-0015 "Generation of Hazard-Consistent Fragility Curves for Seismic Loss Estimation Studies," by H. Hwang and J-R. Huo, 6/14/94, (PB95-181996, A09, MF-A02).

NCEER-94-0016 "Seismic Study of Building Frames with Added Energy-Absorbing Devices," by W.S. Pong, C.S. Tsai and G.C. Lee, 6/20/94, (PB94-219136, A10, A03).

NCEER-94-0017 "Sliding Mode Control for Seismic-Excited Linear and Nonlinear Civil Engineering Structures," by J. Yang, J. Wu, A. Agrawal and Z. Li, 6/21/94, (PB95-138483, A06, MF-A02).

NCEER-94-0018 "3D-BASIS-TABS Version 2.0: Computer Program for Nonlinear Dynamic Analysis of Three Dimensional Base Isolated Structures," by A.M. Reinhorn, S. Nagarajaiah, M.C. Constantinou, P. Tsopelas and R. Li, 6/22/94, (PB95-182176, A08, MF-A02).

NCEER-94-0019 "Proceedings of the International Workshop on Civil Infrastructure Systems: Application of Intelligent Systems and Advanced Materials on Bridge Systems," Edited by G.C. Lee and K.C. Chang, 7/18/94, (PB95-252474, A20, MF-A04).

NCEER-94-0020 "Study of Seismic Isolation Systems for Computer Floors," by V. Lambrou and M.C. Constantinou, 7/19/94, (PB95-138533, A10, MF-A03).

NCEER-94-0021 "Proceedings of the U.S.-Italian Workshop on Guidelines for Seismic Evaluation and Rehabilitation of Unreinforced Masonry Buildings," Edited by D.P. Abrams and G.M. Calvi, 7/20/94, (PB95-138749, A13, MF-A03).

NCEER-94-0022 "NCEER-Taisei Corporation Research Program on Sliding Seismic Isolation Systems for Bridges: Experimental and Analytical Study of a System Consisting of Lubricated PTFE Sliding Bearings and Mild Steel Dampers," by P. Tsopelas and M.C. Constantinou, 7/22/94, (PB95-182184, A08, MF-A02).

NCEER-94-0023 "Development of Reliability-Based Design Criteria for Buildings Under Seismic Load," by Y.K. Wen, H. Hwang and M. Shinozuka, 8/1/94, (PB95-211934, A08, MF-A02).

NCEER-94-0024 "Experimental Verification of Acceleration Feedback Control Strategies for an Active Tendon System," by S.J. Dyke, B.F. Spencer, Jr., P. Quast, M.K. Sain, D.C. Kaspari, Jr. and T.T. Soong, 8/29/94, (PB95-212320, A05, MF-A01).

NCEER-94-0025 "Seismic Retrofitting Manual for Highway Bridges," Edited by I.G. Buckle and I.F. Friedland, published by the Federal Highway Administration (PB95-212676, A15, MF-A03).

NCEER-94-0026 "Proceedings from the Fifth U.S.-Japan Workshop on Earthquake Resistant Design of Lifeline Facilities and Countermeasures Against Soil Liquefaction," Edited by T.D. O'Rourke and M. Hamada, 11/7/94, (PB95-220802, A99, MF-E08).

NCEER-95-0001 "Experimental and Analytical Investigation of Seismic Retrofit of Structures with Supplemental Damping: Part 1 - Fluid Viscous Damping Devices," by A.M. Reinhorn, C. Li and M.C. Constantinou, 1/3/95, (PB95-266599, A09, MF-A02).

NCEER-95-0002 "Experimental and Analytical Study of Low-Cycle Fatigue Behavior of Semi-Rigid Top-And-Seat Angle Connections," by G. Pekcan, J.B. Mander and S.S. Chen, 1/5/95, (PB95-220042, A07, MF-A02).

NCEER-95-0003 "NCEER-ATC Joint Study on Fragility of Buildings," by T. Anagnos, C. Rojahn and A.S. Kiremidjian, 1/20/95, (PB95-220026, A06, MF-A02).

NCEER-95-0004 "Nonlinear Control Algorithms for Peak Response Reduction," by Z. Wu, T.T. Soong, V. Gattulli and R.C. Lin, 2/16/95, (PB95-220349, A05, MF-A01).

NCEER-95-0005 "Pipeline Replacement Feasibility Study: A Methodology for Minimizing Seismic and Corrosion Risks to Underground Natural Gas Pipelines," by R.T. Eguchi, H.A. Seligson and D.G. Honegger, 3/2/95, (PB95-252326, A06, MF-A02).

NCEER-95-0006 "Evaluation of Seismic Performance of an 11-Story Frame Building During the 1994 Northridge Earthquake," by F. Naeim, R. DiSulio, K. Benuska, A. Reinhorn and C. Li, not available.

NCEER-95-0007 "Prioritization of Bridges for Seismic Retrofitting," by N. Basöz and A.S. Kiremidjian, 4/24/95, (PB95-252300, A08, MF-A02).

NCEER-95-0008 "Method for Developing Motion Damage Relationships for Reinforced Concrete Frames," by A. Singhal and A.S. Kiremidjian, 5/11/95, (PB95-266607, A06, MF-A02).

NCEER-95-0009 "Experimental and Analytical Investigation of Seismic Retrofit of Structures with Supplemental Damping: Part II - Friction Devices," by C. Li and A.M. Reinhorn, 7/6/95, (PB96-128087, A11, MF-A03).

NCEER-95-0010 "Experimental Performance and Analytical Study of a Non-Ductile Reinforced Concrete Frame Structure Retrofitted with Elastomeric Spring Dampers," by G. Pekcan, J.B. Mander and S.S. Chen, 7/14/95, (PB96-137161, A08, MF-A02).

NCEER-95-0011 "Development and Experimental Study of Semi-Active Fluid Damping Devices for Seismic Protection of Structures," by M.D. Symans and M.C. Constantinou, 8/3/95, (PB96-136940, A23, MF-A04).

NCEER-95-0012 "Real-Time Structural Parameter Modification (RSPM): Development of Innervated Structures," by Z. Liang, M. Tong and G.C. Lee, 4/11/95, (PB96-137153, A06, MF-A01).

NCEER-95-0013 "Experimental and Analytical Investigation of Seismic Retrofit of Structures with Supplemental Damping: Part III - Viscous Damping Walls," by A.M. Reinhorn and C. Li, 10/1/95, (PB96-176409, A11, MF-A03).

NCEER-95-0014 "Seismic Fragility Analysis of Equipment and Structures in a Memphis Electric Substation," by J-R. Huo and H.H.M. Hwang, 8/10/95, (PB96-128087, A09, MF-A02).

NCEER-95-0015 "The Hanshin-Awaji Earthquake of January 17, 1995: Performance of Lifelines," Edited by M. Shinozuka, 11/3/95, (PB96-176383, A15, MF-A03).

NCEER-95-0016 "Highway Culvert Performance During Earthquakes," by T.L. Youd and C.J. Beckman, available as NCEER-96-0015.

NCEER-95-0017 "The Hanshin-Awaji Earthquake of January 17, 1995: Performance of Highway Bridges," Edited by I.G. Buckle, 12/1/95, not available.

NCEER-95-0018 "Modeling of Masonry Infill Panels for Structural Analysis," by A.M. Reinhorn, A. Madan, R.E. Valles, Y. Reichmann and J.B. Mander, 12/8/95, (PB97-110886, MF-A01, A06).

NCEER-95-0019 "Optimal Polynomial Control for Linear and Nonlinear Structures," by A.K. Agrawal and J.N. Yang, 12/11/95, (PB96-168737, A07, MF-A02).

NCEER-95-0020 "Retrofit of Non-Ductile Reinforced Concrete Frames Using Friction Dampers," by R.S. Rao, P. Gergely and R.N. White, 12/22/95, (PB97-133508, A10, MF-A02).

NCEER-95-0021 "Parametric Results for Seismic Response of Pile-Supported Bridge Bents," by G. Mylonakis, A. Nikolaou and G. Gazetas, 12/22/95, (PB97-100242, A12, MF-A03).

NCEER-95-0022 "Kinematic Bending Moments in Seismically Stressed Piles," by A. Nikolaou, G. Mylonakis and G. Gazetas, 12/23/95, (PB97-113914, MF-A03, A13).

NCEER-96-0001 "Dynamic Response of Unreinforced Masonry Buildings with Flexible Diaphragms," by A.C. Costley and D.P. Abrams," 10/10/96, (PB97-133573, MF-A03, A15).

NCEER-96-0002 "State of the Art Review: Foundations and Retaining Structures," by I. Po Lam, not available.

NCEER-96-0003 "Ductility of Rectangular Reinforced Concrete Bridge Columns with Moderate Confinement," by N. Wehbe, M. Saiidi, D. Sanders and B. Douglas, 11/7/96, (PB97-133557, A06, MF-A02).

NCEER-96-0004 "Proceedings of the Long-Span Bridge Seismic Research Workshop," edited by I.G. Buckle and I.M. Friedland, not available.

NCEER-96-0005 "Establish Representative Pier Types for Comprehensive Study: Eastern United States," by J. Kulicki and Z. Prucz, 5/28/96, (PB98-119217, A07, MF-A02).

NCEER-96-0006 "Establish Representative Pier Types for Comprehensive Study: Western United States," by R. Imbsen, R.A. Schamber and T.A. Osterkamp, 5/28/96, (PB98-118607, A07, MF-A02).

NCEER-96-0007 "Nonlinear Control Techniques for Dynamical Systems with Uncertain Parameters," by R.G. Ghanem and M.I. Bujakov, 5/27/96, (PB97-100259, A17, MF-A03).

NCEER-96-0008 "Seismic Evaluation of a 30-Year Old Non-Ductile Highway Bridge Pier and Its Retrofit," by J.B. Mander, B. Mahmoodzadegan, S. Bhadra and S.S. Chen, 5/31/96, (PB97-110902, MF-A03, A10).

NCEER-96-0009 "Seismic Performance of a Model Reinforced Concrete Bridge Pier Before and After Retrofit," by J.B. Mander, J.H. Kim and C.A. Ligozio, 5/31/96, (PB97-110910, MF-A02, A10).

NCEER-96-0010 "IDARC2D Version 4.0: A Computer Program for the Inelastic Damage Analysis of Buildings," by R.E. Valles, A.M. Reinhorn, S.K. Kunnath, C. Li and A. Madan, 6/3/96, (PB97-100234, A17, MF-A03).

NCEER-96-0011 "Estimation of the Economic Impact of Multiple Lifeline Disruption: Memphis Light, Gas and Water Division Case Study," by S.E. Chang, H.A. Seligson and R.T. Eguchi, 8/16/96, (PB97-133490, A11, MF-A03).

NCEER-96-0012 "Proceedings from the Sixth Japan-U.S. Workshop on Earthquake Resistant Design of Lifeline Facilities and Countermeasures Against Soil Liquefaction, Edited by M. Hamada and T. O'Rourke, 9/11/96, (PB97-133581, A99, MF-A06).

NCEER-96-0013 "Chemical Hazards, Mitigation and Preparedness in Areas of High Seismic Risk: A Methodology for Estimating the Risk of Post-Earthquake Hazardous Materials Release," by H.A. Seligson, R.T. Eguchi, K.J. Tierney and K. Richmond, 11/7/96, (PB97-133565, MF-A02, A08).

NCEER-96-0014 "Response of Steel Bridge Bearings to Reversed Cyclic Loading," by J.B. Mander, D-K. Kim, S.S. Chen and G.J. Premus, 11/13/96, (PB97-140735, A12, MF-A03).

NCEER-96-0015 "Highway Culvert Performance During Past Earthquakes," by T.L. Youd and C.J. Beckman, 11/25/96, (PB97-133532, A06, MF-A01).

NCEER-97-0001 "Evaluation, Prevention and Mitigation of Pounding Effects in Building Structures," by R.E. Valles and A.M. Reinhorn, 2/20/97, (PB97-159552, A14, MF-A03).

NCEER-97-0002 "Seismic Design Criteria for Bridges and Other Highway Structures," by C. Rojahn, R. Mayes, D.G. Anderson, J. Clark, J.H. Hom, R.V. Nutt and M.J. O'Rourke, 4/30/97, (PB97-194658, A06, MF-A03).

NCEER-97-0003 "Proceedings of the U.S.-Italian Workshop on Seismic Evaluation and Retrofit," Edited by D.P. Abrams and G.M. Calvi, 3/19/97, (PB97-194666, A13, MF-A03).

NCEER-97-0004 "Investigation of Seismic Response of Buildings with Linear and Nonlinear Fluid Viscous Dampers," by A.A. Seleemah and M.C. Constantinou, 5/21/97, (PB98-109002, A15, MF-A03).

NCEER-97-0005 "Proceedings of the Workshop on Earthquake Engineering Frontiers in Transportation Facilities," edited by G.C. Lee and I.M. Friedland, 8/29/97, (PB98-128911, A25, MR-A04).

NCEER-97-0006 "Cumulative Seismic Damage of Reinforced Concrete Bridge Piers," by S.K. Kunnath, A. El-Bahy, A. Taylor and W. Stone, 9/2/97, (PB98-108814, A11, MF-A03).

NCEER-97-0007 "Structural Details to Accommodate Seismic Movements of Highway Bridges and Retaining Walls," by R.A. Imbsen, R.A. Schamber, E. Thorkildsen, A. Kartoum, B.T. Martin, T.N. Rosser and J.M. Kulicki, 9/3/97, (PB98-108996, A09, MF-A02).

NCEER-97-0008 "A Method for Earthquake Motion-Damage Relationships with Application to Reinforced Concrete Frames," by A. Singhal and A.S. Kiremidjian, 9/10/97, (PB98-108988, A13, MF-A03).

NCEER-97-0009 "Seismic Analysis and Design of Bridge Abutments Considering Sliding and Rotation," by K. Fishman and R. Richards, Jr., 9/15/97, (PB98-108897, A06, MF-A02).

NCEER-97-0010 "Proceedings of the FHWA/NCEER Workshop on the National Representation of Seismic Ground Motion for New and Existing Highway Facilities," edited by I.M. Friedland, M.S. Power and R.L. Mayes, 9/22/97, (PB98-128903, A21, MF-A04).

NCEER-97-0011 "Seismic Analysis for Design or Retrofit of Gravity Bridge Abutments," by K.L. Fishman, R. Richards, Jr. and R.C. Divito, 10/2/97, (PB98-128937, A08, MF-A02).

NCEER-97-0012 "Evaluation of Simplified Methods of Analysis for Yielding Structures," by P. Tsopelas, M.C. Constantinou, C.A. Kircher and A.S. Whittaker, 10/31/97, (PB98-128929, A10, MF-A03).

NCEER-97-0013 "Seismic Design of Bridge Columns Based on Control and Repairability of Damage," by C-T. Cheng and J.B. Mander, 12/8/97, (PB98-144249, A11, MF-A03).

NCEER-97-0014 "Seismic Resistance of Bridge Piers Based on Damage Avoidance Design," by J.B. Mander and C-T. Cheng, 12/10/97, (PB98-144223, A09, MF-A02).

NCEER-97-0015 "Seismic Response of Nominally Symmetric Systems with Strength Uncertainty," by S. Balopoulou and M. Grigoriu, 12/23/97, (PB98-153422, A11, MF-A03).

NCEER-97-0016 "Evaluation of Seismic Retrofit Methods for Reinforced Concrete Bridge Columns," by T.J. Wipf, F.W. Klaiber and F.M. Russo, 12/28/97, (PB98-144215, A12, MF-A03).

NCEER-97-0017 "Seismic Fragility of Existing Conventional Reinforced Concrete Highway Bridges," by C.L. Mullen and A.S. Cakmak, 12/30/97, (PB98-153406, A08, MF-A02).

NCEER-97-0018 "Loss Asssessment of Memphis Buildings," edited by D.P. Abrams and M. Shinozuka, 12/31/97, (PB98-144231, A13, MF-A03).

NCEER-97-0019 "Seismic Evaluation of Frames with Infill Walls Using Quasi-static Experiments," by K.M. Mosalam, R.N. White and P. Gergely, 12/31/97, (PB98-153455, A07, MF-A02).

NCEER-97-0020 "Seismic Evaluation of Frames with Infill Walls Using Pseudo-dynamic Experiments," by K.M. Mosalam, R.N. White and P. Gergely, 12/31/97, (PB98-153430, A07, MF-A02).

NCEER-97-0021 "Computational Strategies for Frames with Infill Walls: Discrete and Smeared Crack Analyses and Seismic Fragility," by K.M. Mosalam, R.N. White and P. Gergely, 12/31/97, (PB98-153414, A10, MF-A02).

NCEER-97-0022 "Proceedings of the NCEER Workshop on Evaluation of Liquefaction Resistance of Soils," edited by T.L. Youd and I.M. Idriss, 12/31/97, (PB98-155617, A15, MF-A03).

MCEER-98-0001 "Extraction of Nonlinear Hysteretic Properties of Seismically Isolated Bridges from Quick-Release Field Tests," by Q. Chen, B.M. Douglas, E.M. Maragakis and I.G. Buckle, 5/26/98, (PB99-118838, A06, MF-A01).

MCEER-98-0002 "Methodologies for Evaluating the Importance of Highway Bridges," by A. Thomas, S. Eshenaur and J. Kulicki, 5/29/98, (PB99-118846, A10, MF-A02).

MCEER-98-0003 "Capacity Design of Bridge Piers and the Analysis of Overstrength," by J.B. Mander, A. Dutta and P. Goel, 6/1/98, (PB99-118853, A09, MF-A02).

MCEER-98-0004 "Evaluation of Bridge Damage Data from the Loma Prieta and Northridge, California Earthquakes," by N. Basoz and A. Kiremidjian, 6/2/98, (PB99-118861, A15, MF-A03).

MCEER-98-0005 "Screening Guide for Rapid Assessment of Liquefaction Hazard at Highway Bridge Sites," by T. L. Youd, 6/16/98, (PB99-118879, A06, not available on microfiche).

MCEER-98-0006 "Structural Steel and Steel/Concrete Interface Details for Bridges," by P. Ritchie, N. Kauhl and J. Kulicki, 7/13/98, (PB99-118945, A06, MF-A01).

MCEER-98-0007 "Capacity Design and Fatigue Analysis of Confined Concrete Columns," by A. Dutta and J.B. Mander, 7/14/98, (PB99-118960, A14, MF-A03).

MCEER-98-0008 "Proceedings of the Workshop on Performance Criteria for Telecommunication Services Under Earthquake Conditions," edited by A.J. Schiff, 7/15/98, (PB99-118952, A08, MF-A02).

MCEER-98-0009 "Fatigue Analysis of Unconfined Concrete Columns," by J.B. Mander, A. Dutta and J.H. Kim, 9/12/98, (PB99-123655, A10, MF-A02).

MCEER-98-0010 "Centrifuge Modeling of Cyclic Lateral Response of Pile-Cap Systems and Seat-Type Abutments in Dry Sands," by A.D. Gadre and R. Dobry, 10/2/98, (PB99-123606, A13, MF-A03).

MCEER-98-0011 "IDARC-BRIDGE: A Computational Platform for Seismic Damage Assessment of Bridge Structures," by A.M. Reinhorn, V. Simeonov, G. Mylonakis and Y. Reichman, 10/2/98, (PB99-162919, A15, MF-A03).

MCEER-98-0012 "Experimental Investigation of the Dynamic Response of Two Bridges Before and After Retrofitting with Elastomeric Bearings," by D.A. Wendichansky, S.S. Chen and J.B. Mander, 10/2/98, (PB99-162927, A15, MF-A03).

MCEER-98-0013 "Design Procedures for Hinge Restrainers and Hinge Sear Width for Multiple-Frame Bridges," by R. Des Roches and G.L. Fenves, 11/3/98, (PB99-140477, A13, MF-A03).

MCEER-98-0014 "Response Modification Factors for Seismically Isolated Bridges," by M.C. Constantinou and J.K. Quarshie, 11/3/98, (PB99-140485, A14, MF-A03).

MCEER-98-0015 "Proceedings of the U.S.-Italy Workshop on Seismic Protective Systems for Bridges," edited by I.M. Friedland and M.C. Constantinou, 11/3/98, (PB2000-101711, A22, MF-A04).

MCEER-98-0016 "Appropriate Seismic Reliability for Critical Equipment Systems: Recommendations Based on Regional Analysis of Financial and Life Loss," by K. Porter, C. Scawthorn, C. Taylor and N. Blais, 11/10/98, (PB99-157265, A08, MF-A02).

MCEER-98-0017 "Proceedings of the U.S. Japan Joint Seminar on Civil Infrastructure Systems Research," edited by M. Shinozuka and A. Rose, 11/12/98, (PB99-156713, A16, MF-A03).

MCEER-98-0018 "Modeling of Pile Footings and Drilled Shafts for Seismic Design," by I. PoLam, M. Kapuskar and D. Chaudhuri, 12/21/98, (PB99-157257, A09, MF-A02).

MCEER-99-0001 "Seismic Evaluation of a Masonry Infilled Reinforced Concrete Frame by Pseudodynamic Testing," by S.G. Buonopane and R.N. White, 2/16/99, (PB99-162851, A09, MF-A02).

MCEER-99-0002 "Response History Analysis of Structures with Seismic Isolation and Energy Dissipation Systems: Verification Examples for Program SAP2000," by J. Scheller and M.C. Constantinou, 2/22/99, (PB99-162869, A08, MF-A02).

MCEER-99-0003 "Experimental Study on the Seismic Design and Retrofit of Bridge Columns Including Axial Load Effects," by A. Dutta, T. Kokorina and J.B. Mander, 2/22/99, (PB99-162877, A09, MF-A02).

MCEER-99-0004 "Experimental Study of Bridge Elastomeric and Other Isolation and Energy Dissipation Systems with Emphasis on Uplift Prevention and High Velocity Near-source Seismic Excitation," by A. Kasalanati and M. C. Constantinou, 2/26/99, (PB99-162885, A12, MF-A03).

MCEER-99-0005 "Truss Modeling of Reinforced Concrete Shear-flexure Behavior," by J.H. Kim and J.B. Mander, 3/8/99, (PB99-163693, A12, MF-A03).

MCEER-99-0006 "Experimental Investigation and Computational Modeling of Seismic Response of a 1:4 Scale Model Steel Structure with a Load Balancing Supplemental Damping System," by G. Pekcan, J.B. Mander and S.S. Chen, 4/2/99, (PB99-162893, A11, MF-A03).

MCEER-99-0007 "Effect of Vertical Ground Motions on the Structural Response of Highway Bridges," by M.R. Button, C.J. Cronin and R.L. Mayes, 4/10/99, (PB2000-101411, A10, MF-A03).

MCEER-99-0008 "Seismic Reliability Assessment of Critical Facilities: A Handbook, Supporting Documentation, and Model Code Provisions," by G.S. Johnson, R.E. Sheppard, M.D. Quilici, S.J. Eder and C.R. Scawthorn, 4/12/99, (PB2000-101701, A18, MF-A04).

MCEER-99-0009 "Impact Assessment of Selected MCEER Highway Project Research on the Seismic Design of Highway Structures," by C. Rojahn, R. Mayes, D.G. Anderson, J.H. Clark, D'Appolonia Engineering, S. Gloyd and R.V. Nutt, 4/14/99, (PB99-162901, A10, MF-A02).

MCEER-99-0010 "Site Factors and Site Categories in Seismic Codes," by R. Dobry, R. Ramos and M.S. Power, 7/19/99, (PB2000-101705, A08, MF-A02).

MCEER-99-0011 "Restrainer Design Procedures for Multi-Span Simply-Supported Bridges," by M.J. Randall, M. Saiidi, E. Maragakis and T. Isakovic, 7/20/99, (PB2000-101702, A10, MF-A02).

MCEER-99-0012 "Property Modification Factors for Seismic Isolation Bearings," by M.C. Constantinou, P. Tsopelas, A. Kasalanati and E. Wolff, 7/20/99, (PB2000-103387, A11, MF-A03).

MCEER-99-0013 "Critical Seismic Issues for Existing Steel Bridges," by P. Ritchie, N. Kauhl and J. Kulicki, 7/20/99, (PB2000-101697, A09, MF-A02).

MCEER-99-0014 "Nonstructural Damage Database," by A. Kao, T.T. Soong and A. Vender, 7/24/99, (PB2000-101407, A06, MF-A01).

MCEER-99-0015 "Guide to Remedial Measures for Liquefaction Mitigation at Existing Highway Bridge Sites," by H.G. Cooke and J. K. Mitchell, 7/26/99, (PB2000-101703, A11, MF-A03).

MCEER-99-0016 "Proceedings of the MCEER Workshop on Ground Motion Methodologies for the Eastern United States," edited by N. Abrahamson and A. Becker, 8/11/99, (PB2000-103385, A07, MF-A02).

MCEER-99-0017 "Quindío, Colombia Earthquake of January 25, 1999: Reconnaissance Report," by A.P. Asfura and P.J. Flores, 10/4/99, (PB2000-106893, A06, MF-A01).

MCEER-99-0018 "Hysteretic Models for Cyclic Behavior of Deteriorating Inelastic Structures," by M.V. Sivaselvan and A.M. Reinhorn, 11/5/99, (PB2000-103386, A08, MF-A02).

MCEER-99-0019 "Proceedings of the 7th U.S.- Japan Workshop on Earthquake Resistant Design of Lifeline Facilities and Countermeasures Against Soil Liquefaction," edited by T.D. O'Rourke, J.P. Bardet and M. Hamada, 11/19/99, (PB2000-103354, A99, MF-A06).

MCEER-99-0020 "Development of Measurement Capability for Micro-Vibration Evaluations with Application to Chip Fabrication Facilities," by G.C. Lee, Z. Liang, J.W. Song, J.D. Shen and W.C. Liu, 12/1/99, (PB2000-105993, A08, MF-A02).

MCEER-99-0021 "Design and Retrofit Methodology for Building Structures with Supplemental Energy Dissipating Systems," by G. Pekcan, J.B. Mander and S.S. Chen, 12/31/99, (PB2000-105994, A11, MF-A03).

MCEER-00-0001 "The Marmara, Turkey Earthquake of August 17, 1999: Reconnaissance Report," edited by C. Scawthorn; with major contributions by M. Bruneau, R. Eguchi, T. Holzer, G. Johnson, J. Mander, J. Mitchell, W. Mitchell, A. Papageorgiou, C. Scaethorn, and G. Webb, 3/23/00, (PB2000-106200, A11, MF-A03).

MCEER-00-0002 "Proceedings of the MCEER Workshop for Seismic Hazard Mitigation of Health Care Facilities," edited by G.C. Lee, M. Ettouney, M. Grigoriu, J. Hauer and J. Nigg, 3/29/00, (PB2000-106892, A08, MF-A02).

MCEER-00-0003 "The Chi-Chi, Taiwan Earthquake of September 21, 1999: Reconnaissance Report," edited by G.C. Lee and C.H. Loh, with major contributions by G.C. Lee, M. Bruneau, I.G. Buckle, S.E. Chang, P.J. Flores, T.D. O'Rourke, M. Shinozuka, T.T. Soong, C-H. Loh, K-C. Chang, Z-J. Chen, J-S. Hwang, M-L. Lin, G-Y. Liu, K-C. Tsai, G.C. Yao and C-L. Yen, 4/30/00, (PB2001-100980, A10, MF-A02).

MCEER-00-0004 "Seismic Retrofit of End-Sway Frames of Steel Deck-Truss Bridges with a Supplemental Tendon System: Experimental and Analytical Investigation," by G. Pekcan, J.B. Mander and S.S. Chen, 7/1/00, (PB2001-100982, A10, MF-A02).

MCEER-00-0005 "Sliding Fragility of Unrestrained Equipment in Critical Facilities," by W.H. Chong and T.T. Soong, 7/5/00, (PB2001-100983, A08, MF-A02).

MCEER-00-0006 "Seismic Response of Reinforced Concrete Bridge Pier Walls in the Weak Direction," by N. Abo-Shadi, M. Saiidi and D. Sanders, 7/17/00, (PB2001-100981, A17, MF-A03).

MCEER-00-0007 "Low-Cycle Fatigue Behavior of Longitudinal Reinforcement in Reinforced Concrete Bridge Columns," by J. Brown and S.K. Kunnath, 7/23/00, (PB2001-104392, A08, MF-A02).

MCEER-00-0008 "Soil Structure Interaction of Bridges for Seismic Analysis," I. PoLam and H. Law, 9/25/00, (PB2001-105397, A08, MF-A02).

MCEER-00-0009 "Proceedings of the First MCEER Workshop on Mitigation of Earthquake Disaster by Advanced Technologies (MEDAT-1), edited by M. Shinozuka, D.J. Inman and T.D. O'Rourke, 11/10/00, (PB2001-105399, A14, MF-A03).

MCEER-00-0010 "Development and Evaluation of Simplified Procedures for Analysis and Design of Buildings with Passive Energy Dissipation Systems, Revision 01," by O.M. Ramirez, M.C. Constantinou, C.A. Kircher, A.S. Whittaker, M.W. Johnson, J.D. Gomez and C. Chrysostomou, 11/16/01, (PB2001-105523, A23, MF-A04).

MCEER-00-0011 "Dynamic Soil-Foundation-Structure Interaction Analyses of Large Caissons," by C-Y. Chang, C-M. Mok, Z-L. Wang, R. Settgast, F. Waggoner, M.A. Ketchum, H.M. Gonnermann and C-C. Chin, 12/30/00, (PB2001-104373, A07, MF-A02).

MCEER-00-0012 "Experimental Evaluation of Seismic Performance of Bridge Restrainers," by A.G. Vlassis, E.M. Maragakis and M. Saiid Saiidi, 12/30/00, (PB2001-104354, A09, MF-A02).

MCEER-00-0013 "Effect of Spatial Variation of Ground Motion on Highway Structures," by M. Shinozuka, V. Saxena and G. Deodatis, 12/31/00, (PB2001-108755, A13, MF-A03).

MCEER-00-0014 "A Risk-Based Methodology for Assessing the Seismic Performance of Highway Systems," by S.D. Werner, C.E. Taylor, J.E. Moore, II, J.S. Walton and S. Cho, 12/31/00, (PB2001-108756, A14, MF-A03).

MCEER-01-0001 "Experimental Investigation of P-Delta Effects to Collapse During Earthquakes," by D. Vian and M. Bruneau, 6/25/01, (PB2002-100534, A17, MF-A03).

MCEER-01-0002 "Proceedings of the Second MCEER Workshop on Mitigation of Earthquake Disaster by Advanced Technologies (MEDAT-2)," edited by M. Bruneau and D.J. Inman, 7/23/01, (PB2002-100434, A16, MF-A03).

MCEER-01-0003 "Sensitivity Analysis of Dynamic Systems Subjected to Seismic Loads," by C. Roth and M. Grigoriu, 9/18/01, (PB2003-100884, A12, MF-A03).

MCEER-01-0004 "Overcoming Obstacles to Implementing Earthquake Hazard Mitigation Policies: Stage 1 Report," by D.J. Alesch and W.J. Petak, 12/17/01, (PB2002-107949, A07, MF-A02).

MCEER-01-0005 "Updating Real-Time Earthquake Loss Estimates: Methods, Problems and Insights," by C.E. Taylor, S.E. Chang and R.T. Eguchi, 12/17/01, (PB2002-107948, A05, MF-A01).

MCEER-01-0006 "Experimental Investigation and Retrofit of Steel Pile Foundations and Pile Bents Under Cyclic Lateral Loadings," by A. Shama, J. Mander, B. Blabac and S. Chen, 12/31/01, (PB2002-107950, A13, MF-A03).

MCEER-02-0001 "Assessment of Performance of Bolu Viaduct in the 1999 Duzce Earthquake in Turkey" by P.C. Roussis, M.C. Constantinou, M. Erdik, E. Durukal and M. Dicleli, 5/8/02, (PB2003-100883, A08, MF-A02).

MCEER-02-0002 "Seismic Behavior of Rail Counterweight Systems of Elevators in Buildings," by M.P. Singh, Rildova and L.E. Suarez, 5/27/02. (PB2003-100882, A11, MF-A03).

MCEER-02-0003 "Development of Analysis and Design Procedures for Spread Footings," by G. Mylonakis, G. Gazetas, S. Nikolaou and A. Chauncey, 10/02/02, (PB2004-101636, A13, MF-A03, CD-A13).

MCEER-02-0004 "Bare-Earth Algorithms for Use with SAR and LIDAR Digital Elevation Models," by C.K. Huyck, R.T. Eguchi and B. Houshmand, 10/16/02, (PB2004-101637, A07, CD-A07).

MCEER-02-0005 "Review of Energy Dissipation of Compression Members in Concentrically Braced Frames," by K.Lee and M. Bruneau, 10/18/02, (PB2004-101638, A10, CD-A10).

MCEER-03-0001 "Experimental Investigation of Light-Gauge Steel Plate Shear Walls for the Seismic Retrofit of Buildings" by J. Berman and M. Bruneau, 5/2/03, (PB2004-101622, A10, MF-A03, CD-A10).

MCEER-03-0002 "Statistical Analysis of Fragility Curves," by M. Shinozuka, M.Q. Feng, H. Kim, T. Uzawa and T. Ueda, 6/16/03, (PB2004-101849, A09, CD-A09).

MCEER-03-0003 "Proceedings of the Eighth U.S.-Japan Workshop on Earthquake Resistant Design f Lifeline Facilities and Countermeasures Against Liquefaction," edited by M. Hamada, J.P. Bardet and T.D. O'Rourke, 6/30/03, (PB2004-104386, A99, CD-A99).

MCEER-03-0004 "Proceedings of the PRC-US Workshop on Seismic Analysis and Design of Special Bridges," edited by L.C. Fan and G.C. Lee, 7/15/03, (PB2004-104387, A14, CD-A14).

MCEER-03-0005 "Urban Disaster Recovery: A Framework and Simulation Model," by S.B. Miles and S.E. Chang, 7/25/03, (PB2004-104388, A07, CD-A07).

MCEER-03-0006 "Behavior of Underground Piping Joints Due to Static and Dynamic Loading," by R.D. Meis, M. Maragakis and R. Siddharthan, 11/17/03, (PB2005-102194, A13, MF-A03, CD-A00).

MCEER-04-0001 "Experimental Study of Seismic Isolation Systems with Emphasis on Secondary System Response and Verification of Accuracy of Dynamic Response History Analysis Methods," by E. Wolff and M. Constantinou, 1/16/04 (PB2005-102195, A99, MF-E08, CD-A00).

MCEER-04-0002 "Tension, Compression and Cyclic Testing of Engineered Cementitious Composite Materials," by K. Kesner and S.L. Billington, 3/1/04, (PB2005-102196, A08, CD-A08).

MCEER-04-0003 "Cyclic Testing of Braces Laterally Restrained by Steel Studs to Enhance Performance During Earthquakes," by O.C. Celik, J.W. Berman and M. Bruneau, 3/16/04, (PB2005-102197, A13, MF-A03, CD-A00).

MCEER-04-0004 "Methodologies for Post Earthquake Building Damage Detection Using SAR and Optical Remote Sensing: Application to the August 17, 1999 Marmara, Turkey Earthquake," by C.K. Huyck, B.J. Adams, S. Cho, R.T. Eguchi, B. Mansouri and B. Houshmand, 6/15/04, (PB2005-104888, A10, CD-A00).

MCEER-04-0005 "Nonlinear Structural Analysis Towards Collapse Simulation: A Dynamical Systems Approach," by M.V. Sivaselvan and A.M. Reinhorn, 6/16/04, (PB2005-104889, A11, MF-A03, CD-A00).

MCEER-04-0006 "Proceedings of the Second PRC-US Workshop on Seismic Analysis and Design of Special Bridges," edited by G.C. Lee and L.C. Fan, 6/25/04, (PB2005-104890, A16, CD-A00).

MCEER-04-0007 "Seismic Vulnerability Evaluation of Axially Loaded Steel Built-up Laced Members," by K. Lee and M. Bruneau, 6/30/04, (PB2005-104891, A16, CD-A00).

MCEER-04-0008 "Evaluation of Accuracy of Simplified Methods of Analysis and Design of Buildings with Damping Systems for Near-Fault and for Soft-Soil Seismic Motions," by E.A. Pavlou and M.C. Constantinou, 8/16/04, (PB2005-104892, A08, MF-A02, CD-A00).

MCEER-04-0009 "Assessment of Geotechnical Issues in Acute Care Facilities in California," by M. Lew, T.D. O'Rourke, R. Dobry and M. Koch, 9/15/04, (PB2005-104893, A08, CD-A00).

MCEER-04-0010 "Scissor-Jack-Damper Energy Dissipation System," by A.N. Sigaher-Boyle and M.C. Constantinou, 12/1/04 (PB2005-108221).

MCEER-04-0011 "Seismic Retrofit of Bridge Steel Truss Piers Using a Controlled Rocking Approach," by M. Pollino and M. Bruneau, 12/20/04 (PB2006-105795).

MCEER-05-0001 "Experimental and Analytical Studies of Structures Seismically Isolated with an Uplift-Restraint Isolation System," by P.C. Roussis and M.C. Constantinou, 1/10/05 (PB2005-108222).

MCEER-05-0002 "A Versatile Experimentation Model for Study of Structures Near Collapse Applied to Seismic Evaluation of Irregular Structures," by D. Kusumastuti, A.M. Reinhorn and A. Rutenberg, 3/31/05 (PB2006-101523).

MCEER-05-0003 "Proceedings of the Third PRC-US Workshop on Seismic Analysis and Design of Special Bridges," edited by L.C. Fan and G.C. Lee, 4/20/05, (PB2006-105796).

MCEER-05-0004 "Approaches for the Seismic Retrofit of Braced Steel Bridge Piers and Proof-of-Concept Testing of an Eccentrically Braced Frame with Tubular Link," by J.W. Berman and M. Bruneau, 4/21/05 (PB2006-101524).

MCEER-05-0005 "Simulation of Strong Ground Motions for Seismic Fragility Evaluation of Nonstructural Components in Hospitals," by A. Wanitkorkul and A. Filiatrault, 5/26/05 (PB2006-500027).

MCEER-05-0006 "Seismic Safety in California Hospitals: Assessing an Attempt to Accelerate the Replacement or Seismic Retrofit of Older Hospital Facilities," by D.J. Alesch, L.A. Arendt and W.J. Petak, 6/6/05 (PB2006-105794).

MCEER-05-0007 "Development of Seismic Strengthening and Retrofit Strategies for Critical Facilities Using Engineered Cementitious Composite Materials," by K. Kesner and S.L. Billington, 8/29/05 (PB2006-111701).

MCEER-05-0008 "Experimental and Analytical Studies of Base Isolation Systems for Seismic Protection of Power Transformers," by N. Murota, M.Q. Feng and G-Y. Liu, 9/30/05 (PB2006-111702).

MCEER-05-0009 "3D-BASIS-ME-MB: Computer Program for Nonlinear Dynamic Analysis of Seismically Isolated Structures," by P.C. Tsopelas, P.C. Roussis, M.C. Constantinou, R. Buchanan and A.M. Reinhorn, 10/3/05 (PB2006-111703).

MCEER-05-0010 "Steel Plate Shear Walls for Seismic Design and Retrofit of Building Structures," by D. Vian and M. Bruneau, 12/15/05 (PB2006-111704).

MCEER-05-0011 "The Performance-Based Design Paradigm," by M.J. Astrella and A. Whittaker, 12/15/05 (PB2006-111705).

MCEER-06-0001 "Seismic Fragility of Suspended Ceiling Systems," H. Badillo-Almaraz, A.S. Whittaker, A.M. Reinhorn and G.P. Cimellaro, 2/4/06 (PB2006-111706).

MCEER-06-0002 "Multi-Dimensional Fragility of Structures," by G.P. Cimellaro, A.M. Reinhorn and M. Bruneau, 3/1/06 (PB2007-106974, A09, MF-A02, CD A00).

MCEER-06-0003 "Built-Up Shear Links as Energy Dissipators for Seismic Protection of Bridges," by P. Dusicka, A.M. Itani and I.G. Buckle, 3/15/06 (PB2006-111708).

MCEER-06-0004 "Analytical Investigation of the Structural Fuse Concept," by R.E. Vargas and M. Bruneau, 3/16/06 (PB2006-111709).

MCEER-06-0005 "Experimental Investigation of the Structural Fuse Concept," by R.E. Vargas and M. Bruneau, 3/17/06 (PB2006-111710).

MCEER-06-0006 "Further Development of Tubular Eccentrically Braced Frame Links for the Seismic Retrofit of Braced Steel Truss Bridge Piers," by J.W. Berman and M. Bruneau, 3/27/06 (PB2007-105147).

MCEER-06-0007 "REDARS Validation Report," by S. Cho, C.K. Huyck, S. Ghosh and R.T. Eguchi, 8/8/06 (PB2007-106983).

MCEER-06-0008 "Review of Current NDE Technologies for Post-Earthquake Assessment of Retrofitted Bridge Columns," by J.W. Song, Z. Liang and G.C. Lee, 8/21/06 (PB2007-106984).

MCEER-06-0009 "Liquefaction Remediation in Silty Soils Using Dynamic Compaction and Stone Columns," by S. Thevanayagam, G.R. Martin, R. Nashed, T. Shenthan, T. Kanagalingam and N. Ecemis, 8/28/06 (PB2007-106985).

MCEER-06-0010 "Conceptual Design and Experimental Investigation of Polymer Matrix Composite Infill Panels for Seismic Retrofitting," by W. Jung, M. Chiewanichakorn and A.J. Aref, 9/21/06 (PB2007-106986).

MCEER-06-0011 "A Study of the Coupled Horizontal-Vertical Behavior of Elastomeric and Lead-Rubber Seismic Isolation Bearings," by G.P. Warn and A.S. Whittaker, 9/22/06 (PB2007-108679).

MCEER-06-0012 "Proceedings of the Fourth PRC-US Workshop on Seismic Analysis and Design of Special Bridges: Advancing Bridge Technologies in Research, Design, Construction and Preservation," Edited by L.C. Fan, G.C. Lee and L. Ziang, 10/12/06 (PB2007-109042).

MCEER-06-0013 "Cyclic Response and Low Cycle Fatigue Characteristics of Plate Steels," by P. Dusicka, A.M. Itani and I.G. Buckle, 11/1/06 06 (PB2007-106987).

MCEER-06-0014 "Proceedings of the Second US-Taiwan Bridge Engineering Workshop," edited by W.P. Yen, J. Shen, J-Y. Chen and M. Wang, 11/15/06 (PB2008-500041).

MCEER-06-0015 "User Manual and Technical Documentation for the REDARS^{TM} Import Wizard," by S. Cho, S. Ghosh, C.K. Huyck and S.D. Werner, 11/30/06 (PB2007-114766).

MCEER-06-0016 "Hazard Mitigation Strategy and Monitoring Technologies for Urban and Infrastructure Public Buildings: Proceedings of the China-US Workshops," edited by X.Y. Zhou, A.L. Zhang, G.C. Lee and M. Tong, 12/12/06 (PB2008-500018).

MCEER-07-0001 "Static and Kinetic Coefficients of Friction for Rigid Blocks," by C. Kafali, S. Fathali, M. Grigoriu and A.S. Whittaker, 3/20/07 (PB2007-114767).

MCEER-07-0002 "Hazard Mitigation Investment Decision Making: Organizational Response to Legislative Mandate," by L.A. Arendt, D.J. Alesch and W.J. Petak, 4/9/07 (PB2007-114768).

MCEER-07-0003 "Seismic Behavior of Bidirectional-Resistant Ductile End Diaphragms with Unbonded Braces in Straight or Skewed Steel Bridges," by O. Celik and M. Bruneau, 4/11/07 (PB2008-105141).

MCEER-07-0004 "Modeling Pile Behavior in Large Pile Groups Under Lateral Loading," by A.M. Dodds and G.R. Martin, 4/16/07(PB2008-105142).

MCEER-07-0005 "Experimental Investigation of Blast Performance of Seismically Resistant Concrete-Filled Steel Tube Bridge Piers," by S. Fujikura, M. Bruneau and D. Lopez-Garcia, 4/20/07 (PB2008-105143).

MCEER-07-0006 "Seismic Analysis of Conventional and Isolated Liquefied Natural Gas Tanks Using Mechanical Analogs," by I.P. Christovasilis and A.S. Whittaker, 5/1/07, not available.

MCEER-07-0007 "Experimental Seismic Performance Evaluation of Isolation/Restraint Systems for Mechanical Equipment – Part 1: Heavy Equipment Study," by S. Fathali and A. Filiatrault, 6/6/07 (PB2008-105144).

MCEER-07-0008 "Seismic Vulnerability of Timber Bridges and Timber Substructures," by A.A. Sharma, J.B. Mander, I.M. Friedland and D.R. Allicock, 6/7/07 (PB2008-105145).

MCEER-07-0009 "Experimental and Analytical Study of the XY-Friction Pendulum (XY-FP) Bearing for Bridge Applications," by C.C. Marin-Artieda, A.S. Whittaker and M.C. Constantinou, 6/7/07 (PB2008-105191).

MCEER-07-0010 "Proceedings of the PRC-US Earthquake Engineering Forum for Young Researchers," Edited by G.C. Lee and X.Z. Qi, 6/8/07 (PB2008-500058).

MCEER-07-0011 "Design Recommendations for Perforated Steel Plate Shear Walls," by R. Purba and M. Bruneau, 6/18/07, (PB2008-105192).

MCEER-07-0012 "Performance of Seismic Isolation Hardware Under Service and Seismic Loading," by M.C. Constantinou, A.S. Whittaker, Y. Kalpakidis, D.M. Fenz and G.P. Warn, 8/27/07, (PB2008-105193).

MCEER-07-0013 "Experimental Evaluation of the Seismic Performance of Hospital Piping Subassemblies," by E.R. Goodwin, E. Maragakis and A.M. Itani, 9/4/07, (PB2008-105194).

MCEER-07-0014 "A Simulation Model of Urban Disaster Recovery and Resilience: Implementation for the 1994 Northridge Earthquake," by S. Miles and S.E. Chang, 9/7/07, (PB2008-106426).

MCEER-07-0015 "Statistical and Mechanistic Fragility Analysis of Concrete Bridges," by M. Shinozuka, S. Banerjee and S-H. Kim, 9/10/07, (PB2008-106427).

MCEER-07-0016 "Three-Dimensional Modeling of Inelastic Buckling in Frame Structures," by M. Schachter and AM. Reinhorn, 9/13/07, (PB2008-108125).

MCEER-07-0017 "Modeling of Seismic Wave Scattering on Pile Groups and Caissons," by I. Po Lam, H. Law and C.T. Yang, 9/17/07 (PB2008-108150).

MCEER-07-0018 "Bridge Foundations: Modeling Large Pile Groups and Caissons for Seismic Design," by I. Po Lam, H. Law and G.R. Martin (Coordinating Author), 12/1/07 (PB2008-111190).

MCEER-07-0019 "Principles and Performance of Roller Seismic Isolation Bearings for Highway Bridges," by G.C. Lee, Y.C. Ou, Z. Liang, T.C. Niu and J. Song, 12/10/07 (PB2009-110466).

MCEER-07-0020 "Centrifuge Modeling of Permeability and Pinning Reinforcement Effects on Pile Response to Lateral Spreading," by L.L Gonzalez-Lagos, T. Abdoun and R. Dobry, 12/10/07 (PB2008-111191).

MCEER-07-0021 "Damage to the Highway System from the Pisco, Perú Earthquake of August 15, 2007," by J.S. O'Connor, L. Mesa and M. Nykamp, 12/10/07, (PB2008-108126).

MCEER-07-0022 "Experimental Seismic Performance Evaluation of Isolation/Restraint Systems for Mechanical Equipment – Part 2: Light Equipment Study," by S. Fathali and A. Filiatrault, 12/13/07 (PB2008-111192).

MCEER-07-0023 "Fragility Considerations in Highway Bridge Design," by M. Shinozuka, S. Banerjee and S.H. Kim, 12/14/07 (PB2008-111193).

MCEER-07-0024 "Performance Estimates for Seismically Isolated Bridges," by G.P. Warn and A.S. Whittaker, 12/30/07 (PB2008-112230).

MCEER-08-0001 "Seismic Performance of Steel Girder Bridge Superstructures with Conventional Cross Frames," by L.P. Carden, A.M. Itani and I.G. Buckle, 1/7/08, (PB2008-112231).

MCEER-08-0002 "Seismic Performance of Steel Girder Bridge Superstructures with Ductile End Cross Frames with Seismic Isolators," by L.P. Carden, A.M. Itani and I.G. Buckle, 1/7/08 (PB2008-112232).

MCEER-08-0003 "Analytical and Experimental Investigation of a Controlled Rocking Approach for Seismic Protection of Bridge Steel Truss Piers," by M. Pollino and M. Bruneau, 1/21/08 (PB2008-112233).

MCEER-08-0004 "Linking Lifeline Infrastructure Performance and Community Disaster Resilience: Models and Multi-Stakeholder Processes," by S.E. Chang, C. Pasion, K. Tatebe and R. Ahmad, 3/3/08 (PB2008-112234).

MCEER-08-0005 "Modal Analysis of Generally Damped Linear Structures Subjected to Seismic Excitations," by J. Song, Y-L. Chu, Z. Liang and G.C. Lee, 3/4/08 (PB2009-102311).

MCEER-08-0006 "System Performance Under Multi-Hazard Environments," by C. Kafali and M. Grigoriu, 3/4/08 (PB2008-112235).

MCEER-08-0007 "Mechanical Behavior of Multi-Spherical Sliding Bearings," by D.M. Fenz and M.C. Constantinou, 3/6/08 (PB2008-112236).

MCEER-08-0008 "Post-Earthquake Restoration of the Los Angeles Water Supply System," by T.H.P. Tabucchi and R.A. Davidson, 3/7/08 (PB2008-112237).

MCEER-08-0009 "Fragility Analysis of Water Supply Systems," by A. Jacobson and M. Grigoriu, 3/10/08 (PB2009-105545).

MCEER-08-0010 "Experimental Investigation of Full-Scale Two-Story Steel Plate Shear Walls with Reduced Beam Section Connections," by B. Qu, M. Bruneau, C-H. Lin and K-C. Tsai, 3/17/08 (PB2009-106368).

MCEER-08-0011 "Seismic Evaluation and Rehabilitation of Critical Components of Electrical Power Systems," S. Ersoy, B. Feizi, A. Ashrafi and M. Ala Saadeghvaziri, 3/17/08 (PB2009-105546).

MCEER-08-0012 "Seismic Behavior and Design of Boundary Frame Members of Steel Plate Shear Walls," by B. Qu and M. Bruneau, 4/26/08 . (PB2009-106744).

MCEER-08-0013 "Development and Appraisal of a Numerical Cyclic Loading Protocol for Quantifying Building System Performance," by A. Filiatrault, A. Wanitkorkul and M. Constantinou, 4/27/08 (PB2009-107906).

MCEER-08-0014 "Structural and Nonstructural Earthquake Design: The Challenge of Integrating Specialty Areas in Designing Complex, Critical Facilities," by W.J. Petak and D.J. Alesch, 4/30/08 (PB2009-107907).

MCEER-08-0015 "Seismic Performance Evaluation of Water Systems," by Y. Wang and T.D. O'Rourke, 5/5/08 (PB2009-107908).

MCEER-08-0016 "Seismic Response Modeling of Water Supply Systems," by P. Shi and T.D. O'Rourke, 5/5/08 (PB2009-107910).

MCEER-08-0017 "Numerical and Experimental Studies of Self-Centering Post-Tensioned Steel Frames," by D. Wang and A. Filiatrault, 5/12/08 (PB2009-110479).

MCEER-08-0018 "Development, Implementation and Verification of Dynamic Analysis Models for Multi-Spherical Sliding Bearings," by D.M. Fenz and M.C. Constantinou, 8/15/08 (PB2009-107911).

MCEER-08-0019 "Performance Assessment of Conventional and Base Isolated Nuclear Power Plants for Earthquake Blast Loadings," by Y.N. Huang, A.S. Whittaker and N. Luco, 10/28/08 (PB2009-107912).

MCEER-08-0020 "Remote Sensing for Resilient Multi-Hazard Disaster Response – Volume I: Introduction to Damage Assessment Methodologies," by B.J. Adams and R.T. Eguchi, 11/17/08 (PB2010-102695).

MCEER-08-0021 "Remote Sensing for Resilient Multi-Hazard Disaster Response – Volume II: Counting the Number of Collapsed Buildings Using an Object-Oriented Analysis: Case Study of the 2003 Bam Earthquake," by L. Gusella, C.K. Huyck and B.J. Adams, 11/17/08 (PB2010-100925).

MCEER-08-0022 "Remote Sensing for Resilient Multi-Hazard Disaster Response – Volume III: Multi-Sensor Image Fusion Techniques for Robust Neighborhood-Scale Urban Damage Assessment," by B.J. Adams and A. McMillan, 11/17/08 (PB2010-100926).

MCEER-08-0023 "Remote Sensing for Resilient Multi-Hazard Disaster Response – Volume IV: A Study of Multi-Temporal and Multi-Resolution SAR Imagery for Post-Katrina Flood Monitoring in New Orleans," by A. McMillan, J.G. Morley, B.J. Adams and S. Chesworth, 11/17/08 (PB2010-100927).

MCEER-08-0024 "Remote Sensing for Resilient Multi-Hazard Disaster Response – Volume V: Integration of Remote Sensing Imagery and VIEWS™ Field Data for Post-Hurricane Charley Building Damage Assessment," by J.A. Womble, K. Mehta and B.J. Adams, 11/17/08 (PB2009-115532).

MCEER-08-0025 "Building Inventory Compilation for Disaster Management: Application of Remote Sensing and Statistical Modeling," by P. Sarabandi, A.S. Kiremidjian, R.T. Eguchi and B. J. Adams, 11/20/08 (PB2009-110484).

MCEER-08-0026 "New Experimental Capabilities and Loading Protocols for Seismic Qualification and Fragility Assessment of Nonstructural Systems," by R. Retamales, G. Mosqueda, A. Filiatrault and A. Reinhorn, 11/24/08 (PB2009-110485).

MCEER-08-0027 "Effects of Heating and Load History on the Behavior of Lead-Rubber Bearings," by I.V. Kalpakidis and M.C. Constantinou, 12/1/08 (PB2009-115533).

MCEER-08-0028 "Experimental and Analytical Investigation of Blast Performance of Seismically Resistant Bridge Piers," by S.Fujikura and M. Bruneau, 12/8/08 (PB2009-115534).

MCEER-08-0029 "Evolutionary Methodology for Aseismic Decision Support," by Y. Hu and G. Dargush, 12/15/08.

MCEER-08-0030 "Development of a Steel Plate Shear Wall Bridge Pier System Conceived from a Multi-Hazard Perspective," by D. Keller and M. Bruneau, 12/19/08 (PB2010-102696).

MCEER-09-0001 "Modal Analysis of Arbitrarily Damped Three-Dimensional Linear Structures Subjected to Seismic Excitations," by Y.L. Chu, J. Song and G.C. Lee, 1/31/09 (PB2010-100922).

MCEER-09-0002 "Air-Blast Effects on Structural Shapes," by G. Ballantyne, A.S. Whittaker, A.J. Aref and G.F. Dargush, 2/2/09 (PB2010-102697).

MCEER-09-0003 "Water Supply Performance During Earthquakes and Extreme Events," by A.L. Bonneau and T.D. O'Rourke, 2/16/09 (PB2010-100923).

MCEER-09-0004 "Generalized Linear (Mixed) Models of Post-Earthquake Ignitions," by R.A. Davidson, 7/20/09 (PB2010-102698).

MCEER-09-0005 "Seismic Testing of a Full-Scale Two-Story Light-Frame Wood Building: NEESWood Benchmark Test," by I.P. Christovasilis, A. Filiatrault and A. Wanitkorkul, 7/22/09 (PB2012-102401).

MCEER-09-0006 "IDARC2D Version 7.0: A Program for the Inelastic Damage Analysis of Structures," by A.M. Reinhorn, H. Roh, M. Sivaselvan, S.K. Kunnath, R.E. Valles, A. Madan, C. Li, R. Lobo and Y.J. Park, 7/28/09 (PB2010-103199).

MCEER-09-0007 "Enhancements to Hospital Resiliency: Improving Emergency Planning for and Response to Hurricanes," by D.B. Hess and L.A. Arendt, 7/30/09 (PB2010-100924).

MCEER-09-0008 "Assessment of Base-Isolated Nuclear Structures for Design and Beyond-Design Basis Earthquake Shaking," by Y.N. Huang, A.S. Whittaker, R.P. Kennedy and R.L. Mayes, 8/20/09 (PB2010-102699).

MCEER-09-0009 "Quantification of Disaster Resilience of Health Care Facilities," by G.P. Cimellaro, C. Fumo, A.M Reinhorn and M. Bruneau, 9/14/09 (PB2010-105384).

MCEER-09-0010 "Performance-Based Assessment and Design of Squat Reinforced Concrete Shear Walls," by C.K. Gulec and A.S. Whittaker, 9/15/09 (PB2010-102700).

MCEER-09-0011 "Proceedings of the Fourth US-Taiwan Bridge Engineering Workshop," edited by W.P. Yen, J.J. Shen, T.M. Lee and R.B. Zheng, 10/27/09 (PB2010-500009).

MCEER-09-0012 "Proceedings of the Special International Workshop on Seismic Connection Details for Segmental Bridge Construction," edited by W. Phillip Yen and George C. Lee, 12/21/09 (PB2012-102402).

MCEER-10-0001 "Direct Displacement Procedure for Performance-Based Seismic Design of Multistory Woodframe Structures," by W. Pang and D. Rosowsky, 4/26/10 (PB2012-102403).

MCEER-10-0002 "Simplified Direct Displacement Design of Six-Story NEESWood Capstone Building and Pre-Test Seismic Performance Assessment," by W. Pang, D. Rosowsky, J. van de Lindt and S. Pei, 5/28/10 (PB2012-102404).

MCEER-10-0003 "Integration of Seismic Protection Systems in Performance-Based Seismic Design of Woodframed Structures," by J.K. Shinde and M.D. Symans, 6/18/10 (PB2012-102405).

MCEER-10-0004 "Modeling and Seismic Evaluation of Nonstructural Components: Testing Frame for Experimental Evaluation of Suspended Ceiling Systems," by A.M. Reinhorn, K.P. Ryu and G. Maddaloni, 6/30/10 (PB2012-102406).

MCEER-10-0005 "Analytical Development and Experimental Validation of a Structural-Fuse Bridge Pier Concept," by S. El-Bahey and M. Bruneau, 10/1/10 (PB2012-102407).

MCEER-10-0006 "A Framework for Defining and Measuring Resilience at the Community Scale: The PEOPLES Resilience Framework," by C.S. Renschler, A.E. Frazier, L.A. Arendt, G.P. Cimellaro, A.M. Reinhorn and M. Bruneau, 10/8/10 (PB2012-102408).

MCEER-10-0007 "Impact of Horizontal Boundary Elements Design on Seismic Behavior of Steel Plate Shear Walls," by R. Purba and M. Bruneau, 11/14/10 (PB2012-102409).

MCEER-10-0008 "Seismic Testing of a Full-Scale Mid-Rise Building: The NEESWood Capstone Test," by S. Pei, J.W. van de Lindt, S.E. Pryor, H. Shimizu, H. Isoda and D.R. Rammer, 12/1/10 (PB2012-102410).

MCEER-10-0009 "Modeling the Effects of Detonations of High Explosives to Inform Blast-Resistant Design," by P. Sherkar, A.S. Whittaker and A.J. Aref, 12/1/10 (PB2012-102411).

MCEER-10-0010 "L'Aquila Earthquake of April 6, 2009 in Italy: Rebuilding a Resilient City to Withstand Multiple Hazards," by G.P. Cimellaro, I.P. Christovasilis, A.M. Reinhorn, A. De Stefano and T. Kirova, 12/29/10.

MCEER-11-0001 "Numerical and Experimental Investigation of the Seismic Response of Light-Frame Wood Structures," by I.P. Christovasilis and A. Filiatrault, 8/8/11 (PB2012-102412).

MCEER-11-0002 "Seismic Design and Analysis of a Precast Segmental Concrete Bridge Model," by M. Anagnostopoulou, A. Filiatrault and A. Aref, 9/15/11.

MCEER-11-0003 'Proceedings of the Workshop on Improving Earthquake Response of Substation Equipment," Edited by A.M. Reinhorn, 9/19/11 (PB2012-102413).

MCEER-11-0004 "LRFD-Based Analysis and Design Procedures for Bridge Bearings and Seismic Isolators," by M.C. Constantinou, I. Kalpakidis, A. Filiatrault and R.A. Ecker Lay, 9/26/11.

MCEER-11-0005 "Experimental Seismic Evaluation, Model Parameterization, and Effects of Cold-Formed Steel-Framed Gypsum Partition Walls on the Seismic Performance of an Essential Facility," by R. Davies, R. Retamales, G. Mosqueda and A. Filiatrault, 10/12/11.

MCEER-11-0006 "Modeling and Seismic Performance Evaluation of High Voltage Transformers and Bushings," by A.M. Reinhorn, K. Oikonomou, H. Roh, A. Schiff and L. Kempner, Jr., 10/3/11.

MCEER-11-0007 "Extreme Load Combinations: A Survey of State Bridge Engineers," by G.C. Lee, Z. Liang, J.J. Shen and J.S. O'Connor, 10/14/11.

MCEER-12-0001 "Simplified Analysis Procedures in Support of Performance Based Seismic Design," by Y.N. Huang and A.S. Whittaker.

MCEER-12-0002 "Seismic Protection of Electrical Transformer Bushing Systems by Stiffening Techniques," by M. Koliou, A. Filiatrault, A.M. Reinhorn and N. Oliveto, 6/1/12.

MCEER-12-0003 "Post-Earthquake Bridge Inspection Guidelines," by J.S. O'Connor and S. Alampalli, 6/8/12.

MCEER-12-0004 "Integrated Design Methodology for Isolated Floor Systems in Single-Degree-of-Freedom Structural Fuse Systems," by S. Cui, M. Bruneau and M.C. Constantinou, 6/13/12.

MCEER-12-0005 "Characterizing the Rotational Components of Earthquake Ground Motion," by D. Basu, A.S. Whittaker and M.C. Constantinou, 6/15/12.

MCEER-12-0006 "Bayesian Fragility for Nonstructural Systems," by C.H. Lee and M.D. Grigoriu, 9/12/12.

MCEER-12-0007 "A Numerical Model for Capturing the In-Plane Seismic Response of Interior Metal Stud Partition Walls," by R.L. Wood and T.C. Hutchinson, 9/12/12.

MCEER

EARTHQUAKE ENGINEERING TO EXTREME EVENTS

University at Buffalo, The State University of New York

Red Jacket Quadrangle ▪ Buffalo, New York 14261

Phone: (716) 645-3391 ▪ Fax: (716) 645-3399

E-mail: *mceer@buffalo.edu* ▪ WWW Site *http://mceer.buffalo.edu*

University at Buffalo *The State University of New York*

ISSN 1520-295X